JUSTUS-LIEBIG-
UNIVERSITÄT
GIESSEN

Investigating the Metabolome of *Schistosoma mansoni* by High-Resolution Mass Spectrometry Imaging

Cumulative Dissertation

by

Patrik Kadesch

prepared at the

Institute of Inorganic and Analytical Chemistry

for the Degree of

Doctor rerum naturalium (*Dr. rer. nat.*)

Justus Liebig University

Giessen, 2021

Table of contents

List of Abbreviations

Abbreviation	Explanation
(AP-S)MALDI	(Atmospheric Pressure Scanning Microprobe) Matrix Assisted Laser Desorption/Ionization
(D)ESI	(Desorption) Electrospray Ionization
(HR)MS	(High Resolution) Mass Spectrometry
(L)PC	(Lyso) Phosphatidylcholine
(L)PE	(Lyso) Phosphatidylethanolamine
(M)ANOVA	(Multiple-Class) Analysis Of Variance
(U)HPLC	(Ultra) High Performance Liquid Chromatography
Cer	Ceramide
CID	Collision Induced Dissociation
CMC	Carboxymethylcellulose
C-trap	C-Shaped Ion Trap
DDA	Data-Dependent Acquisition
DG	Diglyceride
FA	Fatty Acid
FDR	False-Discovery-Rate
FFPE	Formalin Fixation and Paraffin Embedded
FT-ICR	Fourier-Transform Ion Cyclotron Resonance Mass Spectrometer
GC	Gas Chromatography
HETE	Hydroxyeicosatetraenoic Acid
IL	Interleukin
IUPAC	International Union of Pure and Applied Chemistry
LC	Liquid Chromatography
LSD	Light Scattering Detector
m/*z*	Mass-To-Charge Number
MS	Mass Spectrometry
MS^2	Tandem Mass Spectrometry
MSI	Mass Spectrometry Imaging
NTDs	Neglected Tropical Diseases
OCT	Optimal Cutting Temperature
PAF	Platelet Activation Factor
PCA	Principle Component Analysis
PI	Phosphatidylinositol
PLA	Phospholipase A
PS	Phosphatidylserine
PUFA	Polyunsaturated Fatty Acid
PZQ	Praziquantel
QqQ	Triple Quadrupole Mass Spectrometer
RGB	Red, Green and Blue
RGB	Red-Green-Blue
ROI	Region-Of-Interest
ROS	Reactive Oxygen Species
S. mansoni	*Schistosoma mansoni*
SM	Sphingomyelin
TG	Triglyceride
TH2	T-Helper Cell Type 2
TIC	Total Ion Current
TLR	Toll-Like Receptor
ToF	Time of Flight

List of Publications

This thesis is based on the following publications in peer-reviewed journals

Publication 1

Kadesch, Patrik; Quack, Thomas; Gerbig, Stefanie; Grevelding, Christoph G.; Spengler, Bernhard; Lipid Topography in *Schistosoma mansoni* Cryosections, Revealed by Microembedding and High-Resolution Atmospheric-Pressure Matrix-Assisted Laser Desorption/Ionization (MALDI) Mass Spectrometry Imaging, Analytical Chemistry **2019**, 91 (7), pp 4520-4528.

Publication 2

Kadesch, Patrik; Quack, Thomas; Gerbig, Stefanie; Grevelding, Christoph G.; Spengler, Bernhard; Tissue- and sex-specific lipidomic analysis of *Schistosoma mansoni* using high-resolution atmospheric pressure scanning microprobe matrix-assisted laser desorption/ionization mass spectrometry imaging, PLOS Neglected Tropical Diseases **2020**, 14(5), e0008145

Statement in Lieu of an Oath

I declare that I have completed this dissertation single-handedly without the unauthorized help of a second party and only with the assistance acknowledged therein. I have appropriately acknowledged and cited all text passages that are derived verbatim from or are based on the content of published work of others, and all information relating to verbal communications. I consent to the use of an anti-plagiarism software to check my thesis. I have abided by the principles of good scientific conduct laid down in the charter of the Justus Liebig University Giessen „Satzung der Justus-Liebig-Universität Gießen zur Sicherung guter wissenschaftlicher Praxis“ in carrying out the investigations described in the dissertation.

_____

Date, Signature

First referee: Prof. Dr. Bernhard Spengler

Second referee: Prof. Dr. Christoph G. Grevelding

Day of oral exam:

Abstract

Neglected tropical diseases (NTD) are a burden to one billion humans in the (sub-)tropics and poverty-related regions, worldwide. Schistosomiasis, caused by the parasitic flatworm *Schistosoma mansoni*, is one of those NTDs. The disease is currently spreading because of climate change and migration, exposing approximately 700 million people to the risk of infection. Therefore, novel strategies are required to prevent infection and to eliminate the worm burden. One promising drug target is the surface (tegument) of adult male and female schistosome worms. Schistosomes live in constant pairing contact, established via the teguments of male and female, as a prerequisite for egg production. Living in the blood stream, they are also in contact with the host's immune system and therefore require immune evasion, moderated by the outer tegument. Lipids are one major class of constituents of the tegument, but limited information is available on its exact biochemical composition. The abundance and spatial distribution of lipids is therefore of high interest. MS is the technique of choice to answer this research question, as it allows multiplexed lipid detection in a nontargeted analysis approach. AP-SMALDI MSI is capable of delivering high spatial resolution in the micrometer range. Due to the small size of *Schistosoma* (approximately 500 µm in length), this high lateral resolution is essential to resolve detailed structures within the worms. In addition, this technique requires low sample quantities, and recent instrumental advances enable analysis of 3D-surfaces.

We utilized MSI to investigate and characterize the spatial distribution of lipids on the surface of adult schistosome worms in comparison to their inner tissue. However, there are no suitable protocols available for production of the necessary cryosections and analysis by MSI. To overcome this limitation, different embedding protocols, like the classical embedding in cryomolds were tested and modified, e.g. by centrifugation steps for improved planarity. However, embedded worms were lacking planar orientation and sections were not intact after cutting. Also, the tissue was partially disrupted during this process, leading to poor section quality. Finally, a microembedding approach was developed, which uses small quantities of gelatin and represents a high-precision approach. This protocol allowed preparing consecutive high-quality cryosections of a mating worm couple. MS ion images of intact couples revealed differences between male and female in metabolites and lipids. Detailed structures observed from light microscopic images were retained in ion images at 10 µm and 5 µm spatial resolution. To further investigate putative isobaric interferences, on-tissue tandem mass spectrometry imaging (MS^2I) was utilized to trace characteristic lipid fragments across the tissue and to demonstrate the high sensitivity of the setup even at a lateral resolution < 10 µm. This work was summarized in publication one and enabled the investigation of surface in comparison to the inner tissue of schistosomes.

High-resolution MSI of male and female surfaces and couple sections was conducted. An LC-MS/MS-based data repository in combination with unsupervised ion image annotation using the "Metaspace" software was employed for lipid assignment. Multivariate statistical analysis of MSI data by hierarchical clustering revealed deviating signal intensities of lipids on surface vs inner tissue of the worm. PC and specific PE signals were enhanced inside the worm, while SM, PS, LPC and other PE lipids were more abundant on the surface. These findings were in accordance with literature, but enhanced the compositional information from lipid class level to lipid species level. In addition, for PEs, the number of carbon atoms in the fatty acyl chains was found to be decreased on the surface in comparison to the inner tissue. Differences between male and female surface compositions were observed as well. Several sex-specific TGs were found, which differed in numbers of fatty acid carbon atoms and double bonds. For the first time, differences in lipid composition were found between male

and female *S. mansoni* worms. Now a broad toolbox of preparative and data interpretation workflows is available to the scientific community, adaptable to a variety of research issues.

Chapter I - Synopsis

Introduction and Motivation

Mass spectrometry (MS) has become a valuable tool in natural sciences over the past decades. For the nontargeted analysis of biomolecules, MS is currently the technique of choice applicable to the detection of a vast variety of molecules simultaneously as it allows identification, quantitation with high sample throughput. Since its invention in 1994,[1] MALDI MS imaging (MSI) has become an emerging technique, allowing for the investigation of the spatial distribution of biomolecules in a wide variety of tissues which is of high interest for the life sciences.[2-4] Matrix-assisted laser desorption/ionization (MALDI) MSI is the most promising technique for MS imaging, as it is capable of analyzing the distribution of unfragmented biomolecules with a high spatial resolution of typically 5-10 µm[5-10] down to 1.4 µm,[11] and recent advances in instrumentation enable 3D-surface analysis.[7] However, protocols and applications for the most recent technical advances are very sparse yet.

Neglected tropical diseases (NTD), endemic to (sub-)tropical and poverty related regions, are threatening millions of people worldwide. This brings the human pathogen *Schistosoma mansoni*, causing schistosomiasis, also known as bilharzia, into research focus.[12] Schistosomes are parasitic flatworms (trematodes or blood flukes) which have developed two different sexes. Male worms are up to 1 cm long and several-hundred micrometer thick, while the female can be longer but thinner. Research should concentrate on understanding this parasitic disease on a fundamental, biological level in order to develop strategies to counteract spreading and severe impairments associated with this disease. It is known that the tegumental surface of schistosomes comprises a wide variety of lipids, which is expected to be of high biological importance,[13] since the parasite resides in venules and is therefore in constant, direct contact with the host. Therefore, permanent interaction between the immune systems of both, host and pathogen, occurs. The schistosome surface comprises mostly lipids. Host-derived lipids are acquired and subsequently modified by the parasite to obtain specialized lipids, expected to be crucial for its survival.[13] However, knowledge on the exact composition is limited and thus the picture is far from complete for understanding the function of individual key components. For nontargeted, spatial analysis of lipids in such small schistosomes, high-resolution 3D-surface atmospheric pressure scanning microprobe MALDI (AP-SMALDI) MSI is the technique of choice. One major advantage of the technique is that MS and MSI analyses require low sample quantities.[7] Therefore, the biological model system *S. mansoni* is ideally suited for investigating the spatial distribution of lipids on the surface compared to the worm inner tissues by MSI.

The anatomical structure of adult schistosome worms is complex as they comprise a number of organs. Amongst those, the sexual organs are of high interest as they are key for reproduction. The preparation of tissue sections is required to access these inner organs of the sub-millimeter-sized worms. However, there was no protocol available to obtain longitudinal sections, in which the shape and structure of adult worms is preserved and which is also compatible with MSI. Additionally, tissue sections are a pre-requisite for characterizing the tegumental surface in comparison to the inner structure of the worms. Therefore, the first step of our work was to develop a sectioning procedure which is compatible with MSI and which enables the preparation of longitudinal tissue sections,

allowing to allocate single organs and to investigate paired couples. This work was described in publication number one. To put this information into biological context, the surface of previously coupled male and female worms was compared to signals from the worms' inner tissues in biological triplicates. After data acquisition, unsupervised annotation and subsequent MS^2-based identification, a self-developed multivariate statistical analysis workflow was employed for data reduction and classification of ion signals into biological groups. Differentially abundant lipid signals were found for surface and inner worm tissues across several lipid classes. In addition, differences between male and female surfaces were found, mostly regarding triglyceride (TG) lipids. Our findings were in line with published literature but enhance the knowledge on lipid species level enabling tailored research on lipid drug targets. This work was described in publication number two.

Mass Spectrometry

Mass spectrometry is a technique applied to ions, determining the mass-to-charge-number (*m*/*z*) ratio. In a mass spectrum, the signal intensity is plotted against the *m*/*z* ratio, resulting in peaks. Besides the qualitative information, the signal intensity is proportional to the concentration, thus simultaneously enabling quantification. Based on the accurate mass, compound structures can be assigned using databases, based on ppm-range mass accuracy. One of the most important values in MS is the calculation of mass resolution (*R*), determining the peak width of a signal (*m*) for example at half-maximum ($\Delta m_{50\%}$), according to Equation 1. This number is a measure to describe the separability of two peaks by a mass spectrometer.

$$R = \frac{m/z}{\Delta m/z_{50\%}}$$

Equation 1: Calculation of mass resolution from an MS peak. Mass resolution (*R*), mass-to-charge-number ratio (*m/z*) and half-maximum peak width ($\Delta m/z_{50\%}$).[14]

Another important parameter, especially to estimate the probability of true-positive database assignment, is mass accuracy ($\Delta m/m$). Equation 2 describes the deviation of observed mass ($m_{obs.}$) from theoretical mass ($m_{th.}$) relative to the theoretical mass. Mass accuracy is typically reported in parts-per-million (*ppm*).

$$\Delta m/m = \frac{m_{obs.} - m_{th.}}{m_{th.}}$$

Equation 2: Calculation of mass accuracy from empirical and theoretical values. Mass accuracy ($\Delta m/m$), observed ($m_{obs.}$) and theoretical mass ($m_{th.}$).[15]

Besides solely relying on exact mass determination and database assignments, identification can be conducted by performing fragmentation experiments and comparing fragmentation spectra to those of authentic standards. The most common fragmentation mechanism is collision-induced dissociation (CID). An ion package of a small *m*/*z* range, typically belonging to only one substance, is isolated as the precursor. Collisions are induced by introduction of an inert gas at elevated pressure and subsequent acceleration of the ions, ultimately leading to dissociation into product ions. Depending on substance class, characteristic fragment ions occur, which serve for structure elucidation and thus identification.

A wide variety of mass spectrometers is available for mass analysis. The most common mass analyzers are (triple-)quadrupole (QqQ), time of flight (ToF), fourier-transform ion cyclotron resonance (FT-ICR) and orbital trapping instruments. The relative numbers of

publications reporting the use of these four mass spectrometer types are shown Figure 1. To date, predominantly ToF-analyzers are used. However, market share decreases because of the newly developed orbitrap instruments. In the early 2000s, the use of QqQ increased and since 2011 remained constant. FT-ICR mass analyzers, as first commercial and widespread high-resolution MS instruments, were extensively used in the 90s. However, the market share decreased in the 2000s and is relatively constant since 2010. The latest MS technology are the orbitrap instruments. After introduction of commercial instruments in 2005, the market share increased each year. Most likely, many researchers replaced ToF and FT-ICR instruments by orbitrap instruments as they offer high mass resolving power and accuracy at adequate scan speeds and require fewer resources than FT-ICR instruments.

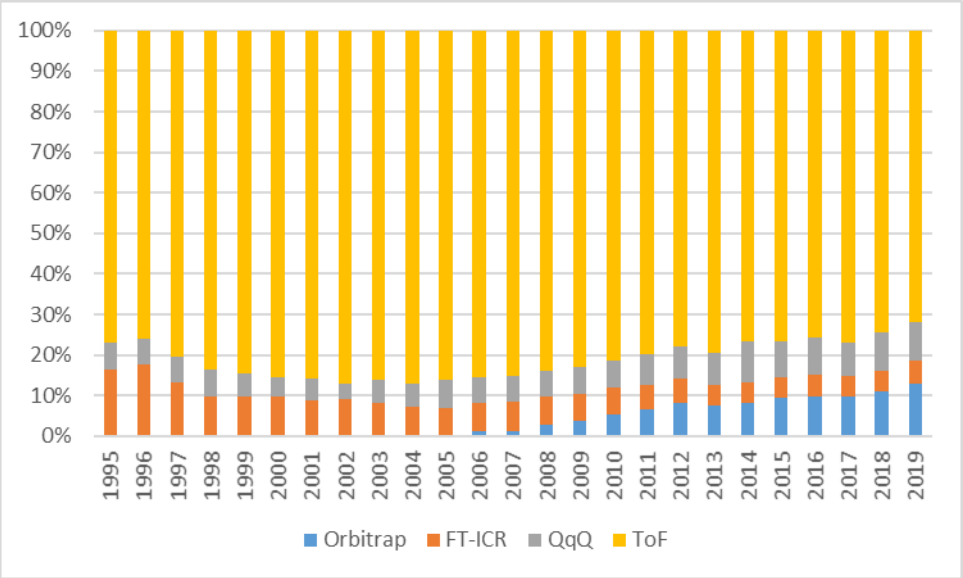

Figure 1: Mass analyzers used in scientific literature per webofknowledge.com-database search published between 1995 and April 2019.

MALDI for analysis of large biomolecules by use of an organic matrix was described by Karas and Hillenkamp in 1988.[16] An organic matrix, nicotinic acid, was used for controlled energy uptake and soft desorption of biomolecules, allowing desorption and ionization of proteins above 10 kDa by an ultraviolet laser system.[16] Because of the "soft" ionization character of MALDI, intact quasi-molecular ions can be observed, similar to electrospray ionization (ESI).[16-18] Nowadays, organic matrices are widely used by the MALDI community with the most prominent matrix being 2,5-dihydroxybenzoic acid.[19]

In MALDI, the matrix serves to dilute and spatially separate the analytes.[20] Laser-generated photons are absorbed by the matrix, leading to transition into the gas-phase of both, matrix and analyte.[20] To date, the most prominent model for MALDI is the so-called "lucky-survivor model".[20] Upon laser irradiation, negatively and positively charged ions in different charge states and neutral particles are obtained.[20] In the MALDI-plume, emitted with high initial velocity and velocity spread, neutralization occurs upon rapid recombination of particles, proportional to charge state.[20] Singly charged ion species are the "lucky survivors" of this process.[20]

Fenn *et al.* published the concept of ESI for analysis of (large) biomolecules in 1989.[21] Nowadays, ESI is one of the most commonly used ionization techniques in bioanalysis worldwide.[22] ESI is a spray ionization method in which a substance is transferred from liquid-neutral to gaseous-ionized state.[17,21] The "soft" ionization character of ESI leads to intact

quasi-molecular ions, compared to more “hard” ionization techniques prone to analyte fragmentation.[21] The benefit over classical soft ionization techniques is that ESI can be operated *ex vacuo*, under ambient conditions.[21] This enables in-line coupling of liquid chromatography (LC) to MS, as is commonly used in bioanalysis.[17,22]

In ESI, a liquid analyte-containing solution is pumped through a stainless steel capillary at microliter-per-minute flow rates. An electrostatic field of several kV/mm is applied between capillary and MS-inlet.[17,21] Excess charge at the needle tip leads to formation of fine, charged droplets because of Coulomb forces induced by the electric field.[21] At elevated temperatures in the MS interface region, solvent evaporates from the fine droplets until the surface charge density exceeds the Rayleigh limit and Coulomb explosion/repulsion leads to smaller daughter droplets.[21] A series of this cascades yields quasi-molecular ions suitable for detection by MS.[21]

In 2000, Makarov published the concept of an electrostatic axially-harmonic orbital trapping mass analyzer, also known as orbitrap.[23] Coupling to an ESI ion source was published in 2003, which opened the field for commercial success and widespread use by the scientific community.[24-26] The orbitrap consists of a spindle-like inner electrode and a split, barrel-like outer electrode.[23] Ions are trapped in an electric field induced between inner and outer electrode, forcing ions to orbit on stable trajectories around the central electrode.[23] Oscillation in axial direction induces an electric current at the split, outer electrode.[23] A frequency spectrum is obtained by time-domain transient and subsequent Fourier-transformation.[23,25] The mass-to-charge dependency of the axial oscillation frequency (ω) is described in Equation 3.[23] Obtained mass spectra show characteristics of a high mass resolving power above 100,000 at *m*/*z* 200 in combination with a high mass accuracy in the lower ppm range.[25]

$$\omega = \left(\frac{kq}{m}\right)^{1/2}$$

Equation 3: Description of ion motion in an orbitrap. Axial oscillation frequency (ω), axial restoring force (k), charge (q) and mass of an ion (m).[23,27]

Well-controlled ion injection into the orbitrap is key to obtain high mass resolving power and accuracy.[25] First versions used electrostatic lenses to guide ions into the orbitrap, demanding discontinuous ion supply.[23,25] Implementation of a linear quadrupole ion trap or C-trap, a C-shaped linear ion trap, allowed collection of dense ion packages prior to HRMS analysis.[25] Ejection of the ion package in nanosecond pulses forces the ions onto more stable trajectories.[25] The accumulation of ion packages does not only increase sensitivity but also leads to an increase in mass resolving power and higher dynamic range, because of fewer axial dephasing.[25] Additionally, by implementation of a “lock mass” function, recalibration of mass spectra to ubiquitous contaminants on the fly, sub-ppm mass accuracy can be obtained.[28] Solely based on MS^1 spectra, database assignments are a valuable tool for assigning molecular structures to *m*/*z* values. However, only MS^2 experiments enable reliable compound identification. This feature was not available for orbitrap mass spectrometers. To overcome this limitation, an octapole collision cell was implemented at the back end of the C-trap.[29] Fragmentation experiments enable the aforementioned reliable identification of biomolecular compounds, especially because of FT orbitrap performance characteristics available in MS^2.[29] To date, the setup described here is state-of-the-art and globally used by the bioanalytical community.[26]

Mass Spectrometry Imaging

Classical biological techniques such as (immuno-)staining are either very unspecific or are tailored for recognition of one particular analyte or class.[2,30,31] Knowledge of the sample composition concerning target-molecules is required prior to investigation.[2,4,31,32] In addition, production of customized, novel antibodies for immunostaining is time consuming and typically requires animal experiments.[33] In contrast, MSI is able to detect a large variety of biomolecules in a complex sample, label-free and multiplexed.[2] To investigate the spatial distribution of unknown substances, a wide variety of MSI[1] tools are available.[30,32,34]

The most common MSI ionization techniques are MALDI and desorption electrospray ionization (DESI).[4] The ionization process in DESI is taking advantage of electrospray ionization.[35] An electrospray, consisting of primary, charged solvent droplets is directed towards the sample surface, where analyte molecules are dissolved and desorbed.[35] Secondary charged and analyte-containing droplets are attracted by the MS inlet because of an electric field.[35] The benefit of DESI is that multiple charging is obtained and no matrix has to be added.[35] The spatial resolution is less than one millimeter,[36] with a minimum of 35 µm.[37] MALDI on the other hand has a spatial resolution of 5-10 µm,[2,3] but only singly charged ions are obtained.[20] By combination with ToF MS, analysis of large biomolecules such as proteins or glycans becomes feasible.[2,3] However, the extended mass range of ToF instruments comes at the cost of reduced mass resolving power and accuracy, indispensable when investigating complex small molecules such as lipids. This limitation can be overcome by coupling the ionization source to either FT ICR or orbitrap mass spectrometers.[5,31] Ion packages are collected for each pixel prior to HRMS analysis, requiring ion trapping. The C-shaped linear ion trap is the most efficient commercialized ion trap for that purpose.[25,38] To date, the C-trap is only available for orbitrap mass spectrometers. The ion yield obtained by MALDI from very small spots is rather low. Therefore, at high spatial resolution, orbitrap mass analyzers are the instruments of choice.

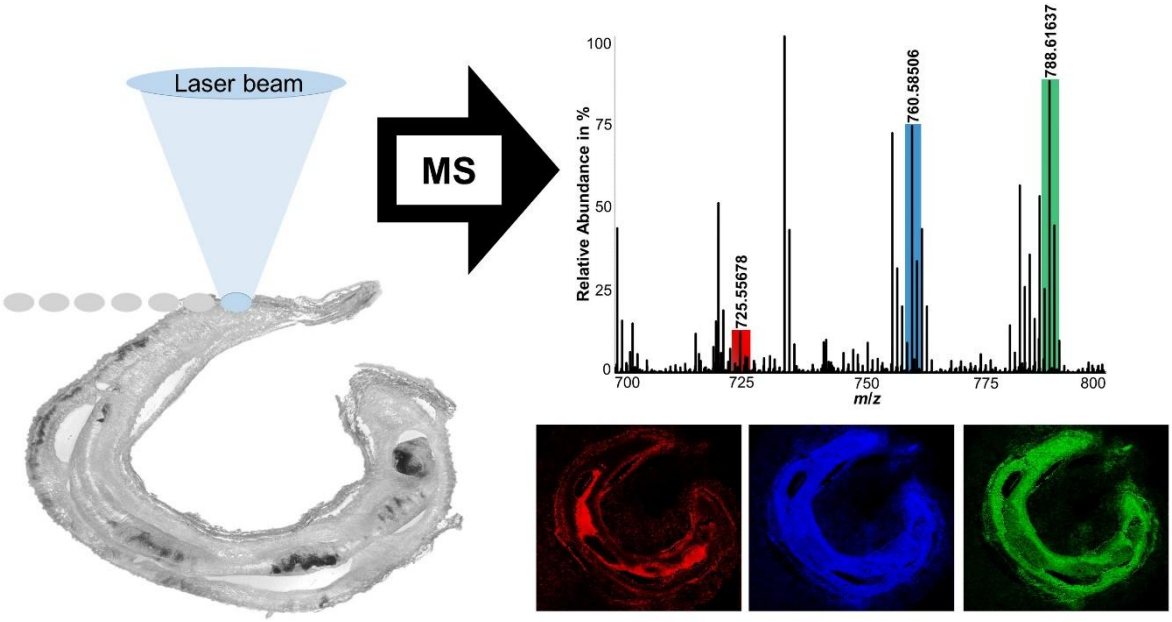

Figure 2: MALDI MSI operating principle. The sample is scanned in a pixel-by-pixel workflow where matrix/analyte co-crystals are desorbed/ionized by a pulsed UV laser beam, generating one mass spectrum per pixel. MS ion images are formed, displaying semi-quantitative analyte distributions in regions of interest.

For MSI, the sample area of interest is divided into pixels. The surface is probed by recording one mass spectrum per pixel in a pixel-by-pixel-type workflow. Thereafter, images are constructed by combining spatial x,y- and mass spectrometric *m*/*z*-information. The signal intensity is usually depicted by a color-scale or brightness gradient to visualize the spatial abundance of one *m*/*z*-signal. Upon overlay of the three native color channels, red, green and blue (RGB), overlays can be constructed losslessly. The workflow of MSI is shown for MALDI in Figure 2. Depending on the biological question, tissue, e.g. organs, are cut into cryosections with thicknesses in the lower micrometer-range.[31] For sectioning of fragile samples, several embedding methods are available.[31] After drying of the sample in a desiccator, the sample is coated with matrix by either spraying or sublimation.[2,3,11,31] The surface is analyzed by the MALDI probe pixel by pixel.[1] Images are then generated for different analytes and subsequently interpreted.[1-3,31]

The pixel size in MALDI MSI is typically in the range of 20-50 µm.[2,3,6] Recent technical advances enabled to reach laser spot sizes down to 5-10 µm,[5-10] and even 1 µm.[11,39] The focal depth of the laser is inversely proportional to the laser focus, which is especially relevant at high spatial resolution. Sample topography can thus lead to changes in spot size, affecting fluence and therefore changes in the MALDI desorption and ionization process and signal intensity.[7,20] Topography-related measurement artifacts can be reduced by use of a laser based, triangulation autofocusing system, enabling analysis of non-flat surfaces.[7] However, the MALDI process in most instruments is taking place under vacuum conditions, therefore demanding appropriate sample preparation according to volatility of analyte and matrix.[16,20] This limitation can be overcome by use of an atmospheric-pressure MALDI source (AP-SMALDI).[2,5,31] AP-SMALDI is well suited for analysis of small molecules such as lipids, saccharides, peptides and drug molecules.[2,5,7,31] Coupled to an orbitrap mass spectrometer, this system allows for studying biological specimen with high resolution and high accuracy in mass and space.

Data evaluation is one of the key steps defining the experimental outcome. Most experimental settings use MSI at MS^1 level to determine the distribution of compounds.[2-4,31] Signal annotation then solely relies on database assignments. For large datasets and non-targeted analysis, this process requires extensive human resources, because annotations need to be verified according to factors such as spatial distribution, possible adducts, mass accuracy or isotope ratios. Metaspace, a recently published online repository, allows for unsupervised database annotations of high-resolution MSI data (metaspace2020.eu).[40] Metabolite annotation is controlled by false-discovery-rate (FDR) based bioinformatics, scoring each signal to the measures ρ_{chaos}, rating the randomness of an ion image signal distribution, $\rho_{spectral}$, for matching spectral isotope ratios, and $\rho_{spatial}$, rating the co-localization of putative isotopologues.[40] In sum, these signals represent the metabolite-signal match (MSM) score.[40] After scoring against an *in silico* decoy database, containing unexpected/not meaningful adducts, such as heavy metals, an FDR-score value is obtained to rate the probability of false-positive assignment.[40] Commonly used metabolite and lipid-containing databases are Lipid Maps (Lipidomics Gateway, lipidmaps.org),[41,42] SwissLipids (a knowledge resource for lipids and their biology, swisslipids.org)[43] and the Human Metabolome Database (HMDB, hmdb.ca).[44-47] However, these databases are often limited to known metabolites. This limitation can be overcome by generating a home-built database from MS^2 experiments, allowing reliable identification. In case of MALDI, in particular at high spatial resolution, however, the resulting ion population is relatively low. This is especially problematic in MS^2-experiments, where, again, many ions are lost during transfer and

fragmentation. MS^2 imaging (MS^2I) experiments may help to overcome this issue. MS^2I is not feasible for samples that are analyzed with highest lateral resolution or for experiments with very low amount of sample material. Research has been conducted towards smart methods for data-dependent acquisition (DDA) in MSI.[48] However, commercial solutions are not available to the MSI community yet. Currently, this limitation is partially overcome by building up home-built, custom databases, e.g. by performing extraction and LC-MS^2 experiments complementarily.

Lipid Assignment and Identification

According to International Union of Pure and Applied Chemistry (IUPAC), lipids are defined as "substances of biological origin [...] soluble in nonpolar solvents".[50] Biochemically, lipids can be defined as "a chemically diverse group of compounds, the common and defining feature of which is their insolubility in water".[51]

This non-stringent IUPAC definition has been described more precisely in a classification system, which is referred to as Lipid Maps terminology.[49,52,53] Structural features are the basis for a hierarchical classification system.[43,49] An example for hierarchical classification of one phosphatidylcholine is shown in Table 1. In Figure 3, a putative phosphatidylcholine ether head group is shown for correlation with lipid hierarchy. At category level, the only information on the lipid is that phosphate is bonded, by definition, to a glycerol backbone in sn-3 position, depicted in orange and blue in Figure 3. The head group is defined further on main class level as glycerophosphocholine, corresponding to orange, blue and green structures, shown in Figure 3. The substituents at sn-1 and sn-2 position (see Figure 3) are defined at sub-class level, in this case as esters (here, in Figure 3, an ester in sn-1 position and an ether in sn-2 position) and thus phosphatidylcholine (PC). At species level, the fatty acid sum composition is known as number of carbon atoms in the fatty acyl chains. The fatty acid composition is depicted as number of carbon atoms and number of double bonds separated by a colon. Therefore, PC (34:1) represents a phosphatidylcholine with the fatty acyl substituents comprising 34 carbon atoms and one double bond. Information on fatty acid chain lengths is obtained at molecular subspecies level e.g. PC (16:0_18:1). Sn-positions of fatty acyl substituents are defined at structural subspecies level as sn-1/sn-2 e.g. PC (16:0/18:1). Information on the double bond is added on isomeric subspecies level. The double bond position and configuration for aforementioned example could be PC (16:0/18:1(9Z)), which means that the double bond is located at carbon number 9 starting from acid group and has *cis* (Z) configuration. Most standard lipids can be categorized using this classification system.

Table 1: Hierarchical classification system of lipids (example taken from SwissLipids.org).[49]

Hierarchy level	Example
Category	Glycerophospholipid
Main class	Glycerophosphocholine
Sub class	Phosphatidylcholine (PC)
Species	PC (34:1)
Molecular subspecies	PC (16:0_18:1)
Structural subspecies	PC (16:0/18:1)
Isomeric subspecies	PC (16:0/18:1(9Z))

Despite lipids comprising only a very limited elemental complexity (consisting only of C, H, N, O, P and S), isobaric variants are challenging to the field. Instead of fatty acids, ethers can occur at sn-1/-2 positions. A PC plasmalogen at sn-2 is depicted in Figure 3, as one representative of ether lipids, with the double bond being at $\Delta 1$ position. The MS toolbox for identification of sn-isomers or even double bond elucidation in lipids, to date is relatively sparse and reliable lipid assignment/identification is complicated. Lipids, down to isomeric subspecies level, however, are important for a variety of endogenous functions, e.g. influencing membrane packaging/arrangement[54] or arrangement of lipid-protein complexes.[55] Therefore, improved MS methods are required in the future to further investigate lipid isomers.

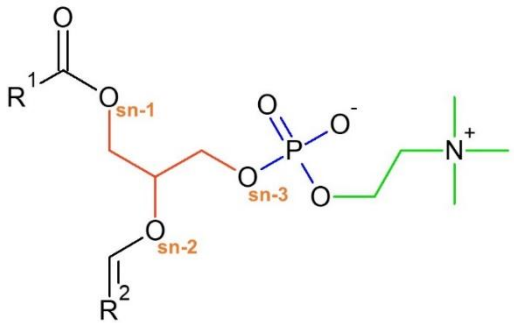

Figure 3: Generic phosphatidylcholine ether. Glycerol (red), phosphate group (blue) and tertiary ethanol amine (green) forming the phosphatidylcholine backbone. Alkyl ester in sn-1 position and alkenyl ether in sn-2 position. Substituents R^1 and R^2 with variable alkyl chain length.

MSI typically relies on differentiation of compounds solely based on MS^1 data. However, the lipid adducts lyso-phosphatidylethanolamine (LPE) (18:1) as sodium adduct (*m*/*z* 502.2904) and the protonated molecule of LPE (20:4) (*m*/*z* 502.2928) require a mass resolving power of >210,000 for signal separation and a mass accuracy better than ± 2 ppm for correct assignment. Commercial orbitrap instruments are not able to deliver this resolution in this *m*/*z*-range. Database assignments are therefore prone to misinterpretation.[56] This limitation can partially be overcome by using more reliable databases. Such databases can be derived from e.g. top-down lipidomic techniques, where a precursor, an intact lipid ion, is selected and fragmented, yielding characteristic fragments for identification of head group and nonpolar substituents.

Fragmentation experiments are essential for reliable identification. Common mass spectrometric approaches use either direct infusion techniques, referred to as *shotgun* approach,[57] or separation by chromatography prior to MS analysis.[58,59] Both approaches require extraction of lipids by use of (non-)polar organic solvents. The most common methods for extraction use a combination of methanol and water and either chloroform[60] or methyl-tert-butyl ether.[61] The underlying assumption is that all analytes are extracted quantitatively. This is an intrinsic problem, because model systems for a more detailed investigation of extraction processes are lacking. It has been observed, that, after tedious method optimization, lipids can be extracted almost quantitatively.[61] Non-quantitative extraction may result in extraction bias throughout different analyte classes, leading to over-/underestimation of abundance. This issue was addressed by the microbial-research community regarding extraction of e.g. DNA,[62] lipids[63,64] and proteins,[65] and subsequent high-throughput analysis. Non-quantitative extraction may lead to unintentional falsification of results, putatively altering experimental outcome and therefore affecting biological interpretation. To shed light on the severity of such effects further systematic investigation

are required in the future to help to develop strategies for estimating and counteracting extraction bias.

Mass spectrometry is widely accepted as a suitable method for comprehensive analysis of lipids. For absolute quantitation, typically a set of stable isotope-labelled internal standards is used.[66] Lipids are defined by a wide variety of physico-chemical properties such as polarity and solubility. Therefore, differences in ionization efficiency occur which become increasingly challenging throughout lipid hierarchy and require even more elaborate experimental designs for enabling comprehensive analysis.[66] This is already complex in *shotgun*-lipidomics and becomes even more difficult when separation techniques such as LC are used.[67] For quantification, multiple standards are needed to overcome limitations derived from differences in retention time, otherwise hindering absolute quantitation.[67,68] However, lipid studies are often solely limited to descriptive findings, whereas biochemical, mechanistic studies of e.g. individual lipids are relatively sparse and often specific to one particular organism. Another general problem is the sheer amount of data generated throughout all 'omics disciplines. One promising attempt to cope with the data is to use extensive bioinformatic strategies to combine 'omics data and to apply known biological pathways as a template.[69,70] By combining information e.g. from transcriptomic, proteomic and metabolomic datasets using a dimensionality-reduction approach, it is possible to deduce putative mechanistic linkages, which then require further investigation and verification *in vivo*.[70]

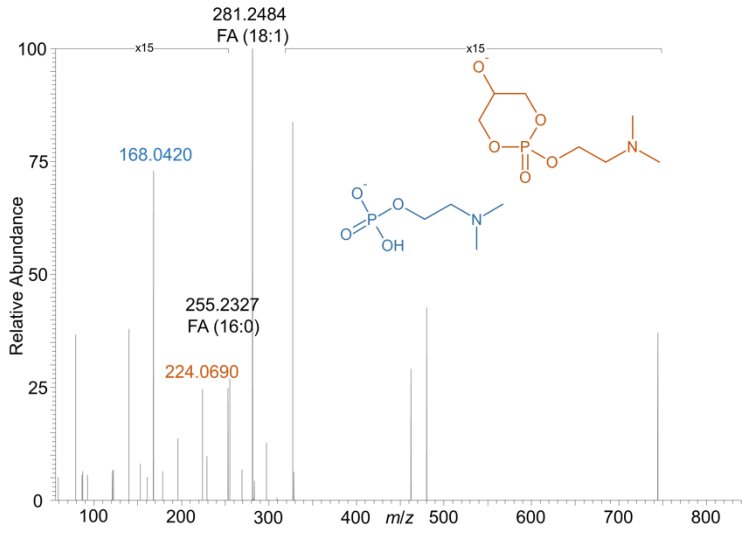

Figure 4: Fragment spectrum of precursor *m/z* 804.564 acquired in negative-ion polarity by higher-collisional dissociation (HCD). Data interpretation was conducted by Lipid Data Analyzer.[71,72] The signal was identified as PC (16:0_18:1) based on fatty acyl (*m/z* 255.2327, *Δ*m/m= 1.0 ppm and *m/z* 281.2484, *Δ*m/m= 0.7 ppm) and characteristic PC head group fragments (at *m/z* 168.0420, *Δ*m/m= 6.6 ppm and *m/z* 224.0690, *Δ*m/m= 1.5 ppm).[73,74]

One classical way, as was done in this work, is to acquire data for nontargeted analysis by data-dependent-acquisition (DDA), where precursors are selected and fragmented according to pre-defined criteria in dependency of analytes of interest. The subsequent data interpretation utilizes fragmentation-rule-based algorithms for reliable identification *in silico*. An example for a fragment spectrum acquired in negative-ion polarity is shown in Figure 4. Experimentally, the precursor ion at *m/z* 804.564 was isolated in an isolation window of ± 0.5 Da and fragmented by HCD. *In silico*, Lipid Data Analyzer (LDA) identified the compound as PC (16:0_18:1). Fragments of the fatty acyl (FA) substituent can be observed in the spectrum (black numbering). The FA (16:0) is shown at *m/z* 255.2327, while FA (18:1)

appears at *m*/*z* 281.2484. The head group can be identified according to characteristic fragments at *m*/*z* 168.0420 and *m*/*z* 224.0690.[73,74] All characteristic fragments, required for identification, were detected.

Schistosomiasis

The three most prominent *Schistosoma* species are *S. japonicum*, *S. mansoni*, and *S. haematobium*, which inhabit the mesenteric veins of gut and bladder of their hosts, respectively.[12,75] In the venous system the adult male and female worms reside in a mated state, producing approximately 300 eggs per day.[12] Maturation of the female requires constant direct pairing contact with the male, resulting in fertility and egg production.[12] Therefore, intervention in the male-female interaction is ideally suited for disrupting the life cycle chemotherapeutically. Approximately 50% of the eggs reach the gut lumen and are excreted via feces. Residing eggs may reach the liver or spleen where they are trapped.[12] On the other hand, parasitic miracidia hedge from excreted eggs upon contact with water to close the life-cycle.[12] The sex of the worm is already defined at that stage.[76,77] Specific intermediate sweet water snail hosts of the genus *Biomphalaria* are infected and production of multiple generations of cercaria occurs.[12] Vertebrate-infective cercaria are released upon light exposure and fresh-water contact.[12] This vertebrate-infective state penetrates the skin of e.g. *homo sapiens* and loses the tail, which was previously required for motility in water.[12] The parasites utilize the blood stream to reach the host lungs, where adulteration of schistosomula to mature flatworms occurs.[12] Pairing contact between sexually immature male and female is established between dorsal tegument of the female and the ventral tegument of the male, also called the gynaecophoric canal.[12] Sexual adulteration of the female is initiated and maintained during permanent pairing contact with the male and is a reversible process.[12] The pairing status of a female can be assessed visually by phenotype, because its size increases as a result of pairing-stimulated vitelline cell production.[12] The mated couple utilizes passive transport to reach the mesenteric veins of the hosts gut.[12] Also, oral and ventral suckers can be utilized for active movement. For successful reproduction, spermatozoids are produced in the males' testes and released towards the female. Taken up by the female, spermatozoids can be stored to later fertilize oocytes. For composite egg production, an oocyte is surrounded with multiple vitelline cells in the ootype. The female releases composite eggs to close the life cycle.

Schistosomes occur in (sub-)tropical areas and are endemic to Africa, the Middle East, South America and Southeast Asia, but first cases have been reported in Europe already.[12,75] Approximately 220 million people suffer from schistosomiasis worldwide, 50% of which are treated annually.[75] Prevalence and endemic spread are expected in this century due to global warming.[78,79] The major problem of schistosomiasis is that the host immune system typically reacts to trapped eggs by granuloma formation and ultimately calcification.[12] Depending on the worm burden and immune competence, schistosomiasis can lead to lethal liver cirrhosis if not treated in time.[12] The only chemotherapeutic treatment available is Praziquantel (PZQ), commonly used in mass drug administration for temporarily eliminating the worm burden of human communities in endemic areas.[75,80] Patients often live in poverty with limited access to sanitation and clean water and are thus prone to contemporary reinfection.[12,75,80] The World Health Organization classified schistosomiasis as a "neglected tropical disease", to raise awareness to this devastating disease and for focusing research to develop novel treatments and countermeasures.[75] One prerequisite for developing novel strategies is knowledge of fundamental biology e.g. to identify key metabolites, essential for the parasite's survival.

Mass Spectrometric Investigations of Lipids in Adult *Schistosoma mansoni*

A number of studies have been conducted describing the abundance of lipids in adult *S. mansoni* worms using mass spectrometry. In 1998, a first study used high performance liquid chromatography (HPLC), coupled to a light scattering detector (LSD) to investigate phospholipids from tegument and worm carcasses of *S. mansoni* worms.[13] Fractions of PC and PE were collected and quantified by the LSD.[13] Subsequently, lipids were identified according to characteristic head group fragments and digestion by phospholipase A2 (PLA2) for structure elucidation of sn-positional isomers.[13] Extracts of whole worm *versus* tegumental fragments prepared by a protocol by Dyer and Blight revealed enrichment of saturated and unsaturated PC in the tegument. In addition, ether-linked species of PC and PE were described in adult *S. mansoni* for the first time. PC-O were discussed to be putative precursors of platelet activation factor (PAF), known for the ability to modulate immune host cells and to act pro-inflammatoryly.[13] However, PE-O was found to be highly enriched in the tegument.[13] Also, parasite-initiated elongation of host-derived lipids was observed.[13] The biological importance of unsaturated PC and plasmalogen species has been discussed with regards to increased resistance against reactive oxygen species (ROS), as sequestered by neutrophils and macrophages, and resistance against the host immune system.[13] Finally, the authors propose fatty acid (FA) (20:1) as possible second messenger for signal transduction from tegument to worm body, because of its high abundance throughout different lipid species in the tegument.[13] In 2008, a study based on HPLC-MS was conducted, extensively describing PC, PE, PS and PI in *S. mansoni*, compared to hamster blood.[81] Overall, 400 phospholipids were quantified in both, positive- and negative-ion mode.[81] Very long-chain FA substituents, containing more than 20 carbon atoms, were observed for PC, PE and PS in the worms, but were absent in the host.[81] Thereby it was confirmed that *S. mansoni* is able to elongate host-derived FAs.[81] The authors proposed that schistosomes either comprise specific trans-acylases for elongation of fatty acids in phospholipids or a distinct DG-pool for phospholipid synthesis.[81] In 2014, rapid identification and quantitation of lipids was enabled using an Orbitrap instrument (Thermo Fisher Scientific, Bremen), which is able to acquire high-resolution mass spectra. The Orbitrap significantly increased throughput and sensitivity. Thereby detailed lipidomic investigations of *S. mansoni* became feasible. One study combined MALDI MSI and ESI-HRMS to distinguish different Brazilian strains, and males and females.[82] Glycerophospholipids, DG and TG were investigated on whole worm couples.[82] The authors claim to have localized structural organs such as tegument, oral and ventral sucker, digestive system and reproductive organs.[82] However, according to anatomy of adult schistosomes, the locations of the reproductive system shown in either MS ion image or microscopic image, match the authors' assignments,[82] but could also be attributed to topography-related artifacts. More abundant signals were mostly detected in males,[82] because the female resides in the gynaecophoric canal of the male and thus cannot be reached solely by MALDI. From principle component analysis (PCA), markers for different strains were obtained and most belonged to the classes of TG and PC.[82] The class of TG was found exclusively in males.[82] The literature suggests that free FA are stored as TG, because catabolism through β-oxidation cannot occur in schistosomes.[82] Only one signal (*m*/*z* 825) could be attributed to females.[82] Another study by the same group in 2015 used MALDI MSI to distinguish males and females, determining the distribution of lipids and investigate the effect of PZQ on males compared to females.[83] Differences between males and females were found from raw data.[83] After PZQ treatment in mice, the phospholipid profile of male and female *S. mansoni* worms was altered.[83] The authors conclude that molecular pathways are affected differently in both sexes.[83] The location of PS was attributed

to oral and ventral sucker and the reproductive system.[83] Another HPLC-MS study investigated PC, PS, PE and PI as lyso and diacyl species in whole worms, tegument and hamster blood.[84] PC and PS were found to be different in the tegument compared to whole worm.[83] The findings show PS to be more abundant on the tegumental surface[84] and are in contradiction to studies by Ferreira *et al* from 2015.[83] Additionally, the tegument was found to be enriched in lyso species, which the authors thought to be involved in host-parasite interaction.[84] However, to test this hypothesis, the authors attempted to detect lyso species from extracts of incubation medium *in vitro* and from blood *in vivo*, but were not able to detect such lyso species.[84] For the first time, a peculiar double-bond position at *Δ*5 was described in PC (34:1) for schistosomes, not detectable in the host.[84] No differences in PE and PI were observed between surface and worm body.[84] The authors suggest that schistosomes comprise molecular mechanisms to selectively enrich their tegument in certain glycerophospholipids.[84] Recently, a comprehensive lipidome analysis, covering the whole life cycle and excretory products, was conducted using LC-MS and gas chromatography (GC) coupled with MS.[85] A database containing 350 lipids and bioactive molecules was established and deposited for further use.[85] The three predominant species, present throughout the whole life cycle were PC (34:1), PC (36:1) and PC (36:2).[85] The lipid profile of whole worms and eggs was found to be similar.[85] Immunomodulatoryly relevant compounds, such as polyunsaturated fatty acids were found, but in both stages, with lower abundance in adult worms.[85] To cover functional aspects, *S. mansoni*-derived PS-fractions were added to dendritic cells, inducing anti-inflammatory TH2 and interleukin 10 (IL-10)-producing T-cells by activation of toll-like receptor 2 (TLR2).[85] Arachidonic acid-derived 15-hydroxyeicosatetraenoic acid (15-HETE) was hypothesized to play a role in host-parasite interaction.[85] Altogether, the resulting database serves as a starting point for further identification of immunomodulatory lipids.[85] Lipids are speculated to play a key role in protection of the parasite from the host's immune system and extensive modulation thereof. However, further studies are required to confirm findings of this study and to prove the proposed interaction hypotheses.

Atmospheric Pressure Matrix Assisted Laser Desorption/Ionization Mass Spectrometry Imaging of Biological Tissues (Publication 1)

MALDI MSI is commonly applied to a large variety of biological samples.[2] For investigation of e.g. animal organs, it is necessary to prepare micrometer-thin tissue sections prior to matrix application.[2,5] Typically this is achieved by cutting fresh-frozen tissue in a cryotome and subsequent mounting on a glass slide.[5] Thereby, the inner substructure of organs becomes accessible by MSI and additionally a planar surface is obtained allowing to record MS images at high spatial resolution of ≤ 20 µm.[11] For smaller specimens, however, direct sectioning often is not possible. This limitation can be overcome by use of embedding material prior to cutting. One commonly used embedding agent in histology is 'optimal cutting temperature' (OCT) compound. The use of OCT is not recommended in mass spectrometry because contained glycols and resins cause severe ion suppression effects in MALDI.[31] Another common procedure utilizes fixation by formalin (methanol and water containing formaldehyde solution) and subsequent embedding in paraffin (FFPE) to preserve the sample, enabling storage under ambient conditions over a long period of time.[86] This FFPE procedure is commonly used in clinical routine after surgical removal of tissues to enable assessments by pathologists and for generation of large tissue libraries e.g. in oncology. This protocol is not compatible with MALDI, because embedding and deparaffinization require xylene, leading to delocalization and removal of many lipid classes.[87,88] Nevertheless, there

are few substances available for embedding, compatible with MSI. Carboxymethylcellulose (CMC) can be used as 2 %-5 % aqueous solution and has been successfully applied to specimens as small as *Anopheles stephensi* mosquitoes.[89,90] Gelatin allowed cryosectioning of the cerebral ganglia of the freshwater snail *Lymnaea stagnalis* and subsequent MALDI MSI was conducted.[34] To investigate the effect of an eye drop preservative in a rabbit model system, eyes were embedded in aqueous tragacanth gum solution before cryosectioning.[91] However, embedding agents need to be selected, formulated and optimized, depending on sample and analytical question.

For small, micrometer-sized tissue samples, a variety of specialized protocols is available. To investigate the whole-body of *Caenorhabditis elegans*, a freeze-cracking method was applied to enable studies by MALDI MSI.[92] Additionally, the signal intensity in the mass range of phospholipids increased, compared to direct analysis of the surface.[92] For investigation of the fruit fly, *Drosophila melanogaster* was embedded in CMC.[90] The protocol was later adapted to the use of gelatin solution,[93] allowing to cut 20 µm thick tissue sections for molecular investigations by MALDI MSI.[90,93] Modifying this protocol by adding an ethanol series for water removal prior to embedding in either CMC or gelatin also successfully gave longitudinal cryosections and additionally allowed preparation of *D. melanogaster* brain sections.[94] Besides increasing the tissue stability by an ethanol series, a variety of chemical fixation techniques is available such as formalin fixation without paraffin embedding. Another fixative is glutaraldehyde (1,5-pentanedial) which reacts with amino groups, leading to cross-linking of proteins and thus increasing solidity. Glutaraldehyde has been useful for preparing sections of bovine eye balls and analysis by MSI.[95] A severe decrease in sphingo- and phospholipids was observed, likely because of high glutaraldehyde concentration and long incubation time, ultimately leading to quantitative protein cross-links, hindering extraction and ionization by MALDI.[95] However, when decreasing the amount of fixative and reducing the time of exposure, even single cells can be fixed, allowing detection of carbohydrates, nucleic acids and lipids.[96] Therefore, glutaraldehyde is a promising candidate for sample preservation, compatible with MSI.

Mass Spectrometry Imaging of Adult *Schistosoma mansoni* Parasites

To access inner organs and investigate male and female *in copula*, artifact-free tissue sections of paired couples were required. *S. mansoni* worms are approximately 8-11 mm long and 500 µm thick. Therefore, direct cutting is not possible and application of embedding techniques is required. Gelatin was chosen for embedding, which is most fluidic at elevated temperatures and still flexible under ambient conditions. The content of gelatin was varied to find the best compromise between fluidity and solidity at –20 °C and –30 °C. The optimum was found at an aqueous solution of 8 %.

Classical cryomold embedding gave longitudinal sections, but severe artifacts and fissures of tissue were observed. The yield of tissue sections was solely based on chance. To increase the probability to obtain sections with desired orientation, a centrifugation step was added prior to freezing the sample. Thereby, section quality was improved and worm orientation was visually assessable. Nevertheless, tissue fissures were observed and anatomical structures were not determined. This limitation was overcome by using a miniaturized sample holder and microliter amounts of embedding agent.

Two consecutive sections of a *S. mansoni* couple were obtained and scanned with MALDI MSI with high spatial resolution of 10 µm and 5 µm, respectively. Differences in lipid composition were visible between male and female. In addition, structural features were

preserved and organs such as the gut were visible in the ion images. Structures were more detailed at 5 µm pixel size. However, doubling the lateral resolution quadruples the number of pixels and therefore recording time.

Differences in lipid composition between both sexes are visualized in Figure 5. MSI was conducted with high resolution in mass and space of 240,000 and 5 µm, respectively. The MS ion signal shown in Figure 5A at *m/z* 782.5674 is one representative example for equally distributed signals between male and female. Based on accurate mass, this signal can be assigned to isobaric ions of either PE(37:1) or PC(34:1) as sodium adduct when compared to the human metabolome database (HMDB).[44-47] A signal at *m/z* 810.5988, which is more abundant in the male, is shown in green in Figure 5B. Assignment according to HMDB[44-47] led to PE(39:1) or PC(36:1) as sodiated species. The red ion channel shown in Figure 5C corresponds to either PE(39:2) or PC(36:2) as sodiated molecule. This signal shows an increased signal intensity in some parts of the female. The red-green-blue (RGB) overlay in Figure 5D was obtained by combining Figure 5A-C. Differences between male and female and heterogeneities within each individual become even more obvious. Some structural features can be assigned to organs when compared to the digital light microscopic image in Figure 5E. For instance the gut of male and female can be recognized and shows the characteristic, meander-like shape (see white arrows in Figure 5D).

Putative isobaric interferences may lead to wrong annotations when relying solely on MS^1-data. Fragmentation experiments directly from tissue are required for reliable identification by MALDI, to eliminate hypothetical isobaric bias. In addition, these MS^2I experiments were conducted as a proof-of-concept study, to demonstrate adequate sensitivity of the method. This allows to identify substances on tissue according to characteristic fragment mass. For

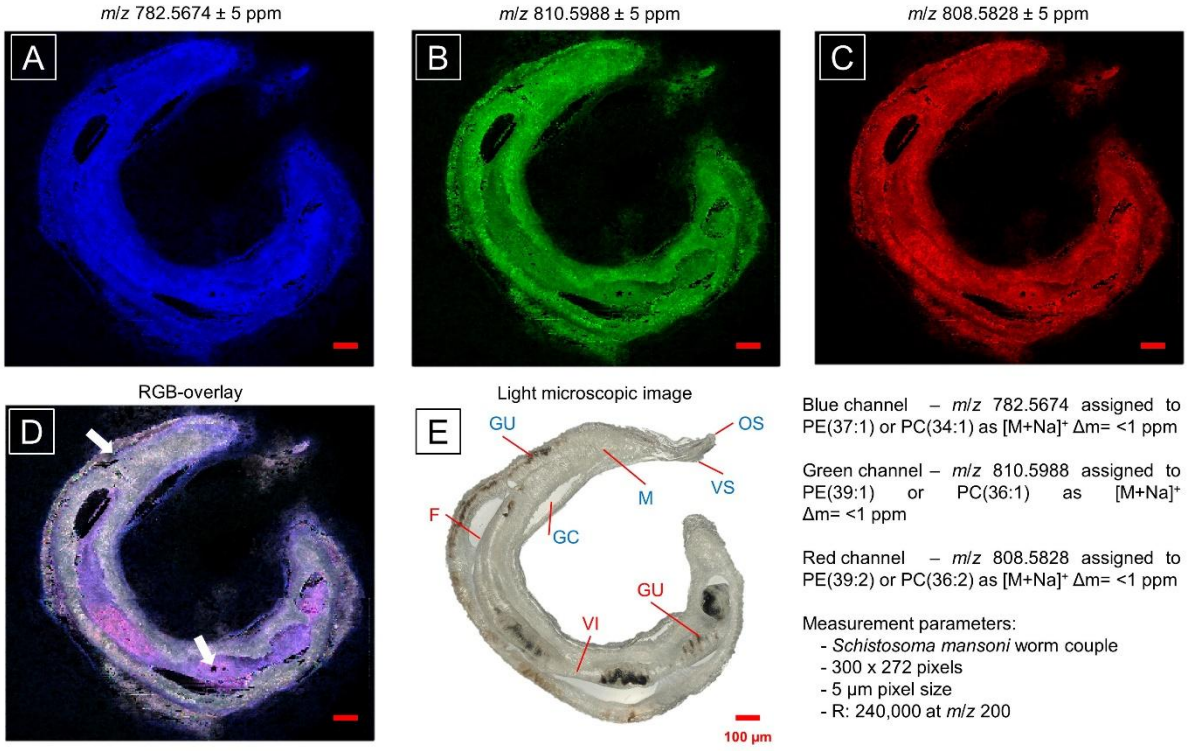

Figure 5: MS ion images of a *S. mansoni* paired couple. A - blue ion channel, equally distributed between male and female. B - green ion channel more abundant in the male. C - red ion channel with increased signal intensity in the inner part of the worm. D - red-green-blue overlay. E - digital light microscopic image. All images are to scale. The scale bars are 100 µm.

instance, the ion at *m*/*z* 808.5828 (in Figure 5C) was identified by MS^2I on-tissue. All fragments were exclusive to PC and no fragments indicated the presence of PE. Additionally, such fragments can be traced across the whole tissue, giving the opportunity to discover differential distributions of otherwise indiscriminable, isobaric fragments.

A sample preparation method has been successfully developed, allowing reproducible production of tissue sections, subsequent data acquisition by high resolution MSI and finally detailed evaluation of the data. Thereby, this first publication sets the methodical fundamentals, enabling studies in a biological context by comparing surface *versus* inner worm tissues as shown in the second publication.

Mass Spectrometry Imaging - Characterizing the Spatial Distribution of Lipids in Adult *Schistosoma mansoni* Parasites (Publication 2)

The description of a biological system requires extensive planning, determining the later experimental outcome. In case of *S. mansoni*, where the tegumental surface is in constant, direct contact with the host, the unique lipid composition has been reported previously.[84,97,98] Some investigations of the tegument were based on immunohistochemistry, failing to give information on the lipid-species level. More detailed studies of lipid species, however, were based on (LC-)ESI-MS, lacking spatial information and requiring extraction of lipids. This procedure is especially error prone, because the tegument is only nanometer-thick in contrast to a few hundred micrometer-thick worm carcass, therefore containing several orders of magnitude more lipid material.[13,84,97,99],In another study, the surface was analyzed by MSI, but no tissue sections were prepared.[82] However, reliable tegument studies by MSI were enabled by our group only recently, by implementation of a laser triangulation autofocusing system, especially important at high lateral resolution,[7] and a method allowing to prepare longitudinal cryosections of schistosome worms.[100]

A strategy for data evaluation and interpretation is of utmost importance, because of the large data file size obtained per specimen, especially for high-resolution MSI. Our study attempted to describe the differences between tegumental surface and worm body tissue. Additionally, it was aimed to describe differences in surface lipids between male and female. To solve this issue efficiently, tissue sections of paired *S. mansoni* worm couples were prepared, harboring metabolic information of both, male and female in the paired state. This enabled comparison to the surface of paired, but freshly separated *S. mansoni* worms. Separation just prior to chemical fixation was desired to yield worms with known pairing history and thus reduce putative, but expected, differences derived from the unpaired state. The distribution of lipids on the surface of male and female worms was determined by MSI. Analysis of each class, tissue sections of couples on the one hand and male and female surfaces on the other hand, in biological triplicates has set the fundamentals for multivariate statistical analysis. After unsupervised MALDI MSI signal annotation by Metaspace and subsequent comparison to a homebuilt LC-MS^2 database, one region of interest (ROI) was defined per biological sample. ROIs were defined based on one representative ion image, displaying the tissue, brought to superposition with a digital light microscopic image of the tissue. The afore-created mass list of all identified lipids was used for exporting mean signal intensity, to obtain one intensity value for each *m*/*z*-value per ROI.

Multivariate Statistical Analysis

The data evaluation process in MSI typically includes visual impressions by the operator. This is an error prone procedure, as it is based on subjective criteria and requires a lot of

time to compare and select images of interest. To overcome this limitation, multivariate statistical analysis is a powerful tool to speed-up this process as it allows investigation of all signals simultaneously and according to objective measures, ultimately representing a more robust signal classification approach. Gaussian distribution of signal intensities during one experiment is assumed for all signals, which is a prerequisite for usage of most statistic models. In MSI, statistical analysis is a tool towards more objective data interpretation. In perspective, statistical analysis can be used to decrease the time required for data analysis and interpretation. Nevertheless, the visual impression after statistics gives ultimate proof over the success of this model, categorized into true-positive, true-negative, false-positive and false-negative.

The putative normal distribution of all signals obtained by MS is visualized in Figure 6 in blue. Normalization of each signal intensity, in MSI to the total ion current (TIC), leads to an increased probability density, assimilating the signal intensities of all *m*/*z* values (see Figure 6). However, the mean remains constant. Also, the area under the curve is still normalized to 1, representing the sum of all possible outcomes.

The Z-score (z_i) is a statistical transformation system. Within one measurement, the deviation of signal intensity (x_i) of each observed *m*/*z* value from the mean signal intensity ($\bar{x}$) is calculated relative to the standard deviation (σ), assuming normal distribution. The Z-score can be calculated according to Equation 4. However, outliers or highly abundant signals may lead to falsification of the Z-score when applied to a mass spectrum. This issue can be partially overcome by using the median ($\bar{x}_{med}$), which is thought to be less error prone.

$$z_i = \frac{x_i - \bar{x}}{\sigma}$$

Equation 4: Calculation of the Z-score. Z-score (z_i), observed value (x_i), mean ($\bar{x}$) and standard deviation (σ).[101]

In MSI, signal intensities are highly heterogeneous across all signals. Based on abundance and ionization efficiency this becomes especially problematic for lower-abundant signals such as DG. The inequality in signal intensity of distinct *m*/*z* values is adjusted by applying the Z-score to one measurement. First, signal intensities are now normalized to the same scale and are thus comparable within and between measurements. Second, this brings values statistically slightly closer to each other within one measurement. Obtained scores

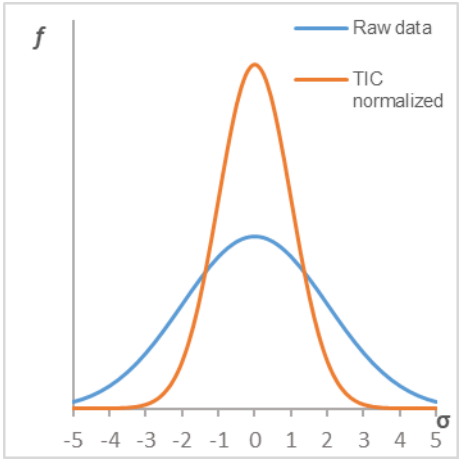

Figure 6: Gaussian distributions. Standard deviation (σ) and probability density (*f*). A (TIC) normalization increases the density of the normal distribution. The mean is constant. The area under each curve is 1.

can be further processed for analysis of variance (ANOVA). Variations of ANOVA model systems are usually based on variance and test parameters to unravel (linear) correlations between observed values, here signal intensity of biological groups.

For comparison of biological groups, multiple-class ANOVA (MANOVA) can be used for finding differences, e.g. based on signal intensity. The means, calculated from distinct biological classes, for instance, are tested for inequality. The means differ from each other if the test turns positive with a yes-type reply. However, it has been determined that there is a difference, but not how it is manifested, e.g. if a signal is more/less abundant. MANOVA enables testing of multiple dependent variables. For MSI data, this could be transferred to different isotopologues, which give multiple signals and always occur in the same ratio e.g. ^{12}C, ^{13}C, $^{13}C_2$ etc. Overall, MANOVA is a useful tool to answer multiple research questions simultaneously,[102] e.g. differences in signal intensities for acquired replicates, and is therefore well suited for evaluation in untargeted analyses of data such as those obtained by MSI.

Post hoc analysis comprises multiple statistical testing algorithms. The aforementioned ANOVA is the basis for every *post hoc* test to discover differences between biological groups. For MS data this allows to rate a signal as either equally, more or less abundant. The significance of a finding is usually FDR controlled and based on *p*-value, the probability that the observed value can be explained by the null hypothesis. However, for MSI data, *post hoc* tests are reasonable to calculate differences more objectively and thus narrow-down the signals to be assessed visually for data evaluation. Using significantly different signals for performing MANOVA prior to *post hoc* testing may serve as an additional quality control procedure.

Hierarchical clustering is a powerful tool for the classification of signals based on similarity. Similarity is described mathematically according to e.g. Euclidean distance, as used by the "Perseus" program. The Euclidean distance can be calculated by Equation 5 and expresses the distance between two points, e.g. in signal intensity. In hierarchical clustering, similarity is also quantifiable by a dendrogram in which the similarity and order in which clusters were

$$d(p,q) = \sqrt{\sum_{i=1}^{n}(q_i - p_i)^2}$$

Equation 5: Euclidean distance calculated from Cartesian coordinates. Euclidean distance (*d*), two coordinates (*p* and *q*) and number of data points observed (*n*).[103]

built, can be visualized. Multiple restarts serve to compensate the starting point problem, because clustering starts from the first value in a matrix and during statistical processing the first value can be random, otherwise leading to irreproducible clustering. The dendrogram displays quantitative differences between signals according to the lengths of the branches.

Signal-intensity-based categorization of lipids has been proven to simplify data analysis and speed up the evaluation process for large data file sizes. However, one of the limitations to be overcome is finding the ideal FDR threshold value when performing MANOVA and *post hoc* tests or hierarchical clustering. This setting was observed to heavily influence the amount of true/false-positive/negative results. After reaching a certain threshold, the classification system yields many more signals to be significantly different but many of these signals are false-positives, observed from MS images. Further optimization and more adequate mathematical procedures may help to balance true/false-positives/negatives.

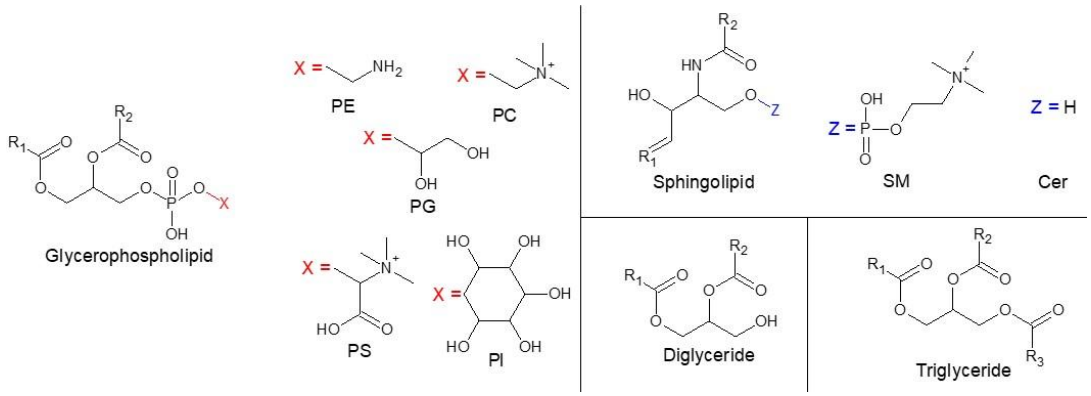

Figure 7: Structures of lipids, analyzed by LC-MS. Phosphatidyl-glyceride (PG), -ethanolamine (PE), -choline (PC), -serine (PS) and -inositole (PI). Sphingolipids of sphingomyelin (SM) and ceramide (CE). $R_1/R_2/R_3$: fatty acid substituent in sn-1/sn-2-position, and sn-3-position in case of triglyceride (TG).

Characterizing the Lipids on the Tegumental Surface of Adult Schistosomes Compared to Inner Worm Tissues

We attempted to characterize the surface in comparison to the inner tissue of adult *S. mansoni* worms by high resolution MSI. Biological triplicates of freshly separated intact males and females and sections of paired couples were subjected to MSI analyses. Signals obtained by MSI were automatically assigned, based on Metaspace online repository using SwissLipids database.[40,43] In parallel, a lipid database was generated based on LC-MS of whole worm extracts. Comparing annotations by Metaspace[40] to a homebuilt MS^2-based database gave more confidence in assigned lipid structures. The head groups of all lipid classes covered in this study are shown in Figure 7. Lipid signals were categorized in an unsupervised fashion into either tissue or surface, or male/female surface-specific, as well as unspecific signals using a self-established multivariate statistical analysis approach. MS images of such categorized signals were assessed visually for correct categorization. Examples for visually correct category assignment are shown in Figure 8, showing the digital light microscopic images for reference in Figure 8A. Males (M) are marked blue and females (F) in red, with direct surface analysis on the left (Figure 8A) and tissue sections on the right (of Figure 8A). An overlay of two ions in a red-green (RG) superposition is shown in Figure 8B. The green signal at *m*/*z* 753.5881 was classified to be more abundant on the surface and represents SM (d36:1) as the sodiated molecular ion species. The outlines of the worms in cross sections are visible as well, but are absent in the worm body. The MS ion at *m*/*z* 832.5827 is shown in red and was identified as PC (40:7) as the protonated molecule. The red ion channel is more abundant in the inner tissues of the worm and cannot be seen on the surface. Therefore, the multivariate statistical data analysis workflow appears to be a valid procedure for unsupervised signal classification and was verified by visual assessment.

Differences in lipid composition were investigated regarding their abundance on the lipid class level. In total, the signals found to be more abundant on the surface comprised 27 SM, 10 PS, 9 PE, 3 LPC and 1 PC species, while signals that are more abundant in tissue sections were 20 PE, 20 PC and 1 LPC species. It has been reported that SM are exclusive to the surface[97] and that surface-associated PS are involved in host-pathogen interaction.[84] Also, differences in PC were previously found between both tissues.[84] Therefore, our findings are well in accordance with literature.

The class of PE was further compared on the lipid species level by plotting the number of carbon atoms in the fatty acyl chains *versus* the number of double bonds. The mean number

of carbon atoms decreased from *n* = 40 in the inner worm tissues to *n* = 37 on the surface. These findings are in contrast to literature, where no differences in PE were detected using outdated low-resolution, triple quadrupole mass spectrometry.[84] However, the experimental conditions in MSI are quasi *in situ* because they do not require lipid extraction. In addition, instrumental improvements were made in the past years, boosting sensitivity and accuracy of analytical methods. Therefore, our findings are reasonable and expected to be authentic true-positive findings.

Applying computational comparison of male *versus* female surface based on the same dataset revealed sex-specific maker signals. From the MS ion images, signals appeared to be almost exclusive to either sex, thus being highly specific. Analysis on the lipid class level revealed marker signals for females comprising 7 LPC, 6 PC, 4 TG, 3 PE, 3 SM and 1 Cer species, while 18 TG, 1 PS, 1 SM and 1 PC species were more abundant on the tegument of males. The compound classes of LPC, SM and Cer are known to play a role in signal transduction and may thus also be involved in male-female signal transduction.[104,105] Looking further into the number of double bonds and number of carbon atoms in the fatty acyl chains of TG gave mean compositions of (50:1) and (58:5) in female and male respectively. This is assumed to affect a decrease in membrane fluidity of the male and thus enhance flexibility. It can be hypothesized that TGs serve as repositories for precursors to prepare schistosome-specific lipids such as phospholipids.[106]

Differences between worm surfaces and the inner tissues were found by MALDI MSI.#### Computational data analysis comprising Z-scoring, *post hoc* testing and hierarchical clustering was optimized successfully to reveal higher/lower abundant signals for the different biological groups. One major advantage over classical LC-MS-based methods is that the MSI workflow is significantly closer to *in situ* conditions. In sum, our findings based

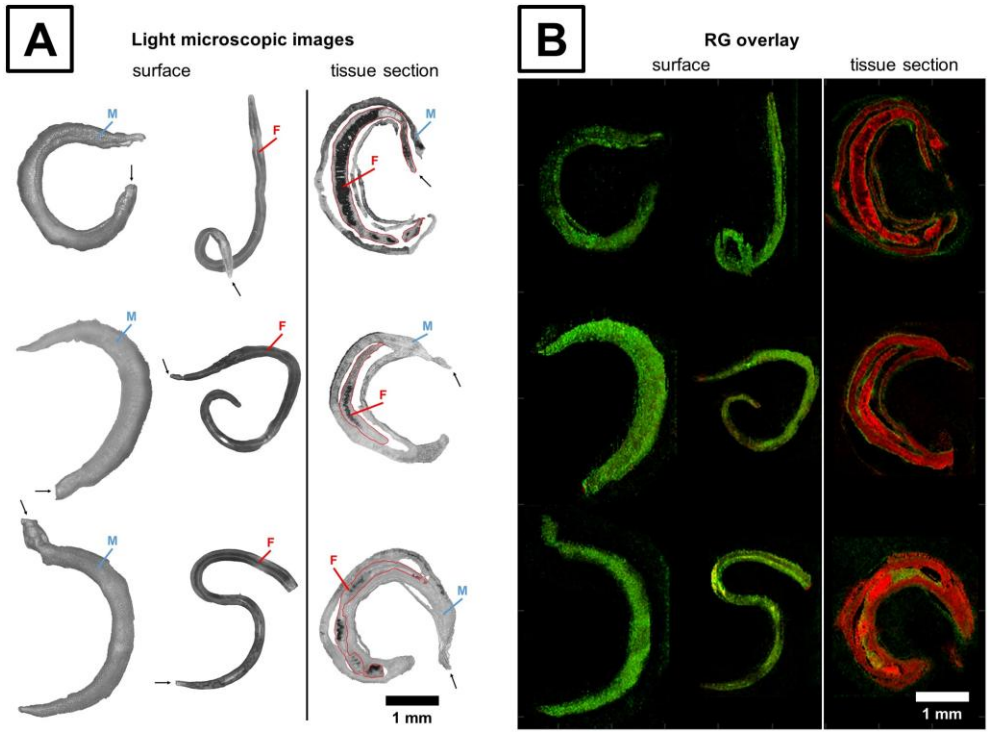

Figure 8: Multimodal imaging of *S. mansoni* worms of surfaces of males (M) and females (F) as well as cryosections of mated couples. A - digital light microscopic image. Black arrows indicate the anterior end. B - RG overlay of two MS ion images categorized upregulated on the surface (in green at *m/z* 753.5881 ±3 ppm assigned to SM (d36:1) as $[M+Na]^+$ with *Δ*m/m ≤ 1 ppm) and worm tissue section (in red at *m/z* 832.5827 ±3 ppm assigned to PC (40:7) as $[M+H]^+$ with *Δ*m/m ≤ 1 ppm). All images to scale.

on MSI are supported by literature, and conclusive findings were previously obtained by classical lipidomic techniques. The developed workflow has the potential to be adapted to a variety of other research questions. More advanced algorithms may lead to a more reliable classification as false-positive/negative findings need to be balanced manually by adjusting the FDR.

Conclusions and Future Perspectives

High-resolution 3D-surface AP-MALDI MSI was applied to the detection of a variety of small biomolecules in sections of *S. mansoni* parasites. A method was developed to prepare longitudinal cryosections of tiny, adult worms which is compatible with MSI and MS^2I experiments at high spatial resolution of 5 µm and 10 µm. MSI in combination with multivariate statistical analysis enabled the assessment of differentially abundant lipids on the surface and in inner worm tissue, and on surfaces of males and females, respectively. The results are in line with literature but enhance the knowledge on surface composition at the lipid species level. For the first time, male and female were distinguished on the metabolic level by MSI. In sum, the developed tools can be further adapted to a large variety of other bioorganisms and analytical problems.

Now, that the toolboxes are available to our workgroup and to the scientific community, a variety of follow-up studies are possible. Cutting of small objects by microembedding is now used extensively by the group e.g. for cutting *Drosophila melanogaster* embryos or even *D. melanogaster* brains. To characterize the inner tissues and organs of schistosomes, an organ isolation protocol can be used to harvest reproductive organs and built up a metabolic organ atlas for *S. mansoni*.[107] In perspective, this could help to interpret complex MSI data obtained from sections and gain in-depth knowledge about biological processes when combined with other 'omics data. To come one step closer to the goal of developing anti-schistosomal drugs, the distribution of a variety of active pharmaceutical ingredients can be tested *in vitro*. Investigations by MSI gather the potential to unravel mechanisms of uptake, metabolization and drug targets, possible sites of molecular interaction, e.g. starting with the gold-standard PZQ and going on to promising candidates such as Imatinib.[12,108] MSI analysis on the metabolic level can be a valuable tool to get hints on key molecular pathways involved in maturation from virgin to pairing-experienced worms.[77] Hindering the maturation and thus egg production can be a major goal for developing novel therapeutics to prevent devastating pathology. However, typically eggs get trapped in venules of the liver where they cause severe inflammation, because the hosts' immune system is unable to degrade eggs timely. In addition to granuloma formation, schistosomiasis bears greater risk to develop hepatocellular carcinoma.[109] MSI could be used here to visualize lipids and metabolites in hepatocytes, linked to tumor genesis. In sum, we initiated all these steps, potentially leading to many follow-up projects.

Now that the surface of *S. mansoni* has been described, additional genera of schistosomes could be investigated such as *S. japonicum*, *S. haematobium* or *S. mekongi*, for instance. This is especially important because these species are endemic to different geographical and host-anatomical areas. *S. japonicum* for example resides in the venous complex of the bladder. In addition, the severity of pathology is different across strains.

In the context of understanding biochemical pathways or interactions on the molecular level, fundamental knowledge is lacking on role and function of individual lipids and specific lipid classes, especially in *S. mansoni* parasites. Further studies should be conducted to shed light on molecular mechanisms. Especially enzymes seem to play an important role in

schistosomes, because *de novo* synthesis of certain fatty acids is not possible. Nevertheless, schistosomes developed an extraordinary lipid biology, for instance very-long chain fatty acids, odd-chain fatty acids or uncommon double-bond positional isomers.[13,81,110,111] Substrates and enzymes catalyzing formation of such lipids are usually unknown. Since MS investigations can locate the presence of such unusual lipids, first hints towards their formation can be obtained using the methods developed and applied during this thesis.

References

(1) Spengler, B.; Hubert, M.; Kaufmann, R. MALDI Ion Imaging and Biological Ion Imaging with a new Scanning UV-Laser Microprobe. 42nd Annual Conf. On Mass Spectrom. and Allied Topics 1994, 1041.

(2) Spengler, B. Mass Spectrometry Imaging of Biomolecular Information. Analytical Chemistry 2015, 87, 64-82.

(3) Paine, M. R. L.; Kooijman, P. C.; Fisher, G. L.; Heeren, R. M. A.; Fernandez, F. M.; Ellis, S. R. Visualizing molecular distributions for biomaterials applications with mass spectrometry imaging: a review. Journal of Materials Chemistry B 2017, 5, 7444-7460.

(4) Amstalden van Hove, E. R.; Smith, D. F.; Heeren, R. M. A. A concise review of mass spectrometry imaging. Journal of Chromatography A 2010, 1217, 3946-3954.

(5) Koestler, M.; Kirsch, D.; Hester, A.; Leisner, A.; Guenther, S.; Spengler, B. A high-resolution scanning microprobe matrix-assisted laser desorption/ionization ion source for imaging analysis on an ion trap/Fourier transform ion cyclotron resonance mass spectrometer. Rapid communications in mass spectrometry : RCM 2008, 22, 3275-3285.

(6) Ogrinc Potočnik, N.; Porta, T.; Becker, M.; Heeren, R. M. A.; Ellis, S. R. Use of advantageous, volatile matrices enabled by next-generation high-speed matrix-assisted laser desorption/ionization time-of-flight imaging employing a scanning laser beam. Rapid Communications in Mass Spectrometry 2015, 29, 2195-2203.

(7) Kompauer, M.; Heiles, S.; Spengler, B. Autofocusing MALDI mass spectrometry imaging of tissue sections and 3D chemical topography of nonflat surfaces. Nature Methods 2017, 14, 1156-1158.

(8) Soltwisch, J.; Kettling, H.; Vens-Cappell, S.; Wiegelmann, M.; Müthing, J.; Dreisewerd, K. Mass spectrometry imaging with laser-induced postionization. Science (New York, N.Y.) 2015, 348, 211-215.

(9) Kettling, H.; Vens-Cappell, S.; Soltwisch, J.; Pirkl, A.; Haier, J.; Müthing, J.; Dreisewerd, K. MALDI Mass Spectrometry Imaging of Bioactive Lipids in Mouse Brain with a Synapt G2-S Mass Spectrometer Operated at Elevated Pressure: Improving the Analytical Sensitivity and the Lateral Resolution to Ten Micrometers. Analytical Chemistry 2014, 86, 7798-7805.

(10) Korte, A. R.; Yandeau-Nelson, M. D.; Nikolau, B. J.; Lee, Y. J. Subcellular-level resolution MALDI-MS imaging of maize leaf metabolites by MALDI-linear ion trap-Orbitrap mass spectrometer. Analytical and bioanalytical chemistry 2015, 407, 2301-2309.

(11) Kompauer, M.; Heiles, S.; Spengler, B. Atmospheric pressure MALDI mass spectrometry imaging of tissues and cells at 1.4-μm lateral resolution. Nature Methods 2017, 14, 90-96.

(12) McManus, D. P.; Dunne, D. W.; Sacko, M.; Utzinger, J.; Vennervald, B. J.; Zhou, X.-N. Schistosomiasis. Nature Reviews Disease Primers 2018, 4, 13.

(13) Brouwers, J. F. H. M.; Gadella, B. M.; van Golde, L. M. G.; Tielens, A. G. M. Quantitative analysis of phosphatidylcholine molecular species using HPLC and light scattering detection. Journal of Lipid Research 1998, 39, 344-353.

(14) Marshall, A. G.; Hendrickson, C. L.; Shi, S. D.-H. Peer reviewed: scaling ms plateaus with high-resolution FT-ICRMS. Analytical Chemistry 2002, 74, 252-259.

(15) Brenton, A. G.; Godfrey, A. R. Accurate Mass Measurement: Terminology and Treatment of Data. Journal of the American Society for Mass Spectrometry 2010, 21, 1821-1835.

(16) Karas, M.; Hillenkamp, F. Laser desorption ionization of proteins with molecular masses exceeding 10,000 daltons. Analytical Chemistry 1988, 60, 2299-2301.

(17) Fenn, J. B.; Mann, M.; Meng, C. K.; Wong, S. F.; Whitehouse, C. M. Electrospray ionization–principles and practice. Mass Spectrometry Reviews 1990, 9, 37-70.

(18) El-Aneed, A.; Cohen, A.; Banoub, J. Mass Spectrometry, Review of the Basics: Electrospray, MALDI, and Commonly Used Mass Analyzers. Applied Spectroscopy Reviews 2009, 44, 210-230.

(19) Strupat, K.; Karas, M.; Hillenkamp, F. 2,5-Dihydroxybenzoic acid: a new matrix for laser desorption—ionization mass spectrometry. International Journal of Mass Spectrometry and Ion Processes 1991, 111, 89-102.

(20) Karas, M.; Glückmann, M.; Schäfer, J. Ionization in matrix-assisted laser desorption/ionization: singly charged molecular ions are the lucky survivors. Journal of Mass Spectrometry 2000, 35, 1-12.

(21) Fenn, J.; Mann, M.; Meng, C.; Wong, S.; Whitehouse, C. Electrospray ionization for mass spectrometry of large biomolecules. Science (New York, N.Y.) 1989, 246, 64-71.

(22) Jemal, M. High-throughput quantitative bioanalysis by LC/MS/MS. Biomedical Chromatography 2000, 14, 422-429.

(23) Makarov, A. Electrostatic Axially Harmonic Orbital Trapping: A High-Performance Technique of Mass Analysis. Analytical Chemistry 2000, 72, 1156-1162.

(24) Hardman, M.; Makarov, A. A. Interfacing the Orbitrap Mass Analyzer to an Electrospray Ion Source. Analytical Chemistry 2003, 75, 1699-1705.

(25) Perry, R. H.; Cooks, R. G.; Noll, R. J. Orbitrap mass spectrometry: Instrumentation, ion motion and applications. Mass Spectrometry Reviews 2008, 27, 661-699.

(26) Eliuk, S.; Makarov, A. Evolution of Orbitrap Mass Spectrometry Instrumentation. Annual Review of Analytical Chemistry 2015, 8, 61-80.

(27) Hu, Q.; Noll, R. J.; Li, H.; Makarov, A.; Hardman, M.; Graham Cooks, R. The Orbitrap: a new mass spectrometer. Journal of Mass Spectrometry 2005, 40, 430-443.

(28) Olsen, J. V.; de Godoy, L. M. F.; Li, G.; Macek, B.; Mortensen, P.; Pesch, R.; Makarov, A.; Lange, O.; Horning, S.; Mann, M. Parts per Million Mass Accuracy on an Orbitrap Mass Spectrometer via Lock Mass Injection into a C-trap. Mol Cell Proteomics 2005, 4, 2010-2021.

(29) Olsen, J. V.; Macek, B.; Lange, O.; Makarov, A.; Horning, S.; Mann, M. Higher-energy C-trap dissociation for peptide modification analysis. Nature Methods 2007, 4, 709-712.

(30) Swales, J. G.; Hamm, G.; Clench, M. R.; Goodwin, R. J. Mass spectrometry imaging and its application in pharmaceutical research and development: a concise review. International Journal of Mass Spectrometry 2019, 437, 99-112.

(31) Römpp, A.; Spengler, B. Mass spectrometry imaging with high resolution in mass and space. Histochemistry and Cell Biology 2013, 139, 759-783.

(32) Bodzon-Kulakowska, A.; Suder, P. Imaging mass spectrometry: Instrumentation, applications, and combination with other visualization techniques. Mass Spectrometry Reviews 2016, 35, 147-169.

(33) Bordeaux, J.; Welsh, A. W.; Agarwal, S.; Killiam, E.; Baquero, M. T.; Hanna, J. A.; Anagnostou, V. K.; Rimm, D. L. Antibody validation. BioTechniques 2010, 48, 197-209.

(34) Altelaar, A. F.; van Minnen, J.; Jimenez, C. R.; Heeren, R. M.; Piersma, S. R. Direct molecular imaging of Lymnaea stagnalis nervous tissue at subcellular spatial resolution by mass spectrometry. Anal Chem 2005, 77, 735-741.

(35) Takats, Z.; Wiseman, J. M.; Gologan, B.; Cooks, R. G. Mass spectrometry sampling under ambient conditions with desorption electrospray ionization. Science (New York, N.Y.) 2004, 306, 471-473.

(36) Wiseman, J. M.; Puolitaival, S. M.; Takáts, Z.; Cooks, R. G.; Caprioli, R. M. Mass Spectrometric Profiling of Intact Biological Tissue by Using Desorption Electrospray Ionization. Angewandte Chemie International Edition 2005, 44, 7094-7097.

(37) Campbell, D. I.; Ferreira, C. R.; Eberlin, L. S.; Cooks, R. G. Improved spatial resolution in the imaging of biological tissue using desorption electrospray ionization. Analytical and bioanalytical chemistry 2012, 404, 389-398.

(38) Makarov, A.; Denisov, E.; Kholomeev, A.; Balschun, W.; Lange, O.; Strupat, K.; Horning, S. Performance evaluation of a hybrid linear ion trap/orbitrap mass spectrometer. Analytical chemistry 2006, 78, 2113-2120.

(39) Zavalin, A.; Yang, J.; Hayden, K.; Vestal, M.; Caprioli, R. M. Tissue protein imaging at 1 mum laser spot diameter for high spatial resolution and high imaging speed using transmission geometry MALDI TOF MS. Analytical and bioanalytical chemistry 2015, 407, 2337-2342.

(40) Palmer, A.; Phapale, P.; Chernyavsky, I.; Lavigne, R.; Fay, D.; Tarasov, A.; Kovalev, V.; Fuchser, J.; Nikolenko, S.; Pineau, C.; Becker, M.; Alexandrov, T. FDR-controlled metabolite annotation for high-resolution imaging mass spectrometry. Nature Methods 2016, 14, 57-61.

(41) Fahy, E.; Sud, M.; Cotter, D.; Subramaniam, S. LIPID MAPS online tools for lipid research. Nucleic Acids Research 2007, 35, W606-W612.

(42) Sud, M.; Fahy, E.; Cotter, D.; Brown, A.; Dennis, E. A.; Glass, C. K.; Merrill, A. H., Jr.; Murphy, R. C.; Raetz, C. R.; Russell, D. W.; Subramaniam, S. LMSD: LIPID MAPS structure database. Nucleic Acids Research 2007, 35, D527-532.

(43) Bridge, A.; Gleizes, A.; Niknejad, A.; Aimo, L.; Bougueleret, L.; Hyka-Nouspikel, N.; Xenarios, I.; Kuznetsov, D.; Götz, L.; Liechti, R.; David, F. P. A.; van der Goot, F. G.;

Riezman, H. The SwissLipids knowledgebase for lipid biology. Bioinformatics 2015, 31, 2860-2866.

(44) Wishart, D. S.; Tzur, D.; Knox, C.; Eisner, R.; Guo, A. C.; Young, N.; Cheng, D.; Jewell, K.; Arndt, D.; Sawhney, S.; Fung, C.; Nikolai, L.; Lewis, M.; Coutouly, M.-A.; Forsythe, I.; Tang, P.; Shrivastava, S.; Jeroncic, K.; Stothard, P.; Amegbey, G., et al. HMDB: the Human Metabolome Database. Nucleic Acids Research 2007, 35, D521-526.

(45) Wishart, D. S.; Knox, C.; Guo, A. C.; Eisner, R.; Young, N.; Gautam, B.; Hau, D. D.; Psychogios, N.; Dong, E.; Bouatra, S.; Mandal, R.; Sinelnikov, I.; Xia, J.; Jia, L.; Cruz, J. A.; Lim, E.; Sobsey, C. A.; Shrivastava, S.; Huang, P.; Liu, P., et al. HMDB: a knowledgebase for the human metabolome. Nucleic Acids Research 2009, 37, D603-610.

(46) Wishart, D. S.; Jewison, T.; Guo, A. C.; Wilson, M.; Knox, C.; Liu, Y.; Djoumbou, Y.; Mandal, R.; Aziat, F.; Dong, E.; Bouatra, S.; Sinelnikov, I.; Arndt, D.; Xia, J.; Liu, P.; Yallou, F.; Bjorndahl, T.; Perez-Pineiro, R.; Eisner, R.; Allen, F., et al. HMDB 3.0--The Human Metabolome Database in 2013. Nucleic Acids Research 2013, 41, D801-807.

(47) Wishart, D. S.; Feunang, Y. D.; Marcu, A.; Guo, A. C.; Liang, K.; Vazquez-Fresno, R.; Sajed, T.; Johnson, D.; Li, C.; Karu, N.; Sayeeda, Z.; Lo, E.; Assempour, N.; Berjanskii, M.; Singhal, S.; Arndt, D.; Liang, Y.; Badran, H.; Grant, J.; Serra-Cayuela, A., et al. HMDB 4.0: the human metabolome database for 2018. Nucleic Acids Research 2018, 46, D608-617.

(48) Ellis, S. R.; Paine, M. R. L.; Eijkel, G. B.; Pauling, J. K.; Husen, P.; Jervelund, M. W.; Hermansson, M.; Ejsing, C. S.; Heeren, R. M. A. Automated, parallel mass spectrometry imaging and structural identification of lipids. Nature Methods 2018, 15, 515-518.

(49) Liebisch, G.; Vizcaino, J. A.; Kofeler, H.; Trotzmuller, M.; Griffiths, W. J.; Schmitz, G.; Spener, F.; Wakelam, M. J. Shorthand notation for lipid structures derived from mass spectrometry. Journal of Lipid Research 2013, 54, 1523-1530.

(50) Moss, G. P.; Smith, P. A. S.; Tavernier, D. In Pure and Applied Chemistry; DeGruyter, 1995, pp 1307-1375.

(51) Nelson, D. L.; Cox, M. M.; W.H. Freeman and Company: New York, 2004, pp 343-368.

(52) Fahy, E.; Subramaniam, S.; Brown, H. A.; Glass, C. K.; Merrill, A. H., Jr.; Murphy, R. C.; Raetz, C. R.; Russell, D. W.; Seyama, Y.; Shaw, W.; Shimizu, T.; Spener, F.; van Meer, G.; VanNieuwenhze, M. S.; White, S. H.; Witztum, J. L.; Dennis, E. A. A comprehensive classification system for lipids. Journal of Lipid Research 2005, 46, 839-861.

(53) Fahy, E.; Subramaniam, S.; Murphy, R. C.; Nishijima, M.; Raetz, C. R.; Shimizu, T.; Spener, F.; van Meer, G.; Wakelam, M. J.; Dennis, E. A. Update of the LIPID MAPS comprehensive classification system for lipids. J Lipid Res 2009, 50 Suppl, S9-14.

(54) Martinez-Seara, H.; Róg, T.; Pasenkiewicz-Gierula, M.; Vattulainen, I.; Karttunen, M.; Reigada, R. Effect of Double Bond Position on Lipid Bilayer Properties: Insight through Atomistic Simulations. The Journal of Physical Chemistry B 2007, 111, 11162-11168.

(55) Bolla, J. R.; Agasid, M. T.; Mehmood, S.; Robinson, C. V. Membrane Protein–Lipid Interactions Probed Using Mass Spectrometry. Annual Review of Biochemistry 2019, 88, 85-111.

(56) Fuchs, B.; Bischoff, A.; Süß, R.; Teuber, K.; Schürenberg, M.; Suckau, D.; Schiller, J. Phosphatidylcholines and -ethanolamines can be easily mistaken in phospholipid mixtures: a negative ion MALDI-TOF MS study with 9-aminoacridine as matrix and egg yolk as selected example. Analytical and bioanalytical chemistry 2009, 395, 2479-2487.

(57) Han, X.; Gross, R. W. Shotgun lipidomics: electrospray ionization mass spectrometric analysis and quantitation of cellular lipidomes directly from crude extracts of biological samples. Mass spectrometry reviews 2005, 24, 367-412.

(58) Peterson, B. L.; Cummings, B. S. A review of chromatographic methods for the assessment of phospholipids in biological samples. Biomedical Chromatography 2006, 20, 227-243.

(59) Zhang, A.; Sun, H.; Wang, P.; Han, Y.; Wang, X. Modern analytical techniques in metabolomics analysis. Analyst 2012, 137, 293-300.

(60) Bligh, E. G.; Dyer, W. J. A RAPID METHOD OF TOTAL LIPID EXTRACTION AND PURIFICATION. Canadian Journal of Biochemistry and Physiology 1959, 37, 911-917.

(61) Matyash, V.; Liebisch, G.; Kurzchalia, T. V.; Shevchenko, A.; Schwudke, D. Lipid extraction by methyl-tert-butyl ether for high-throughput lipidomics. Journal of lipid research 2008, 49, 1137-1146.

(62) Feinstein, L. M.; Sul, W. J.; Blackwood, C. B. Assessment of Bias Associated with Incomplete Extraction of Microbial DNA from Soil. Applied and Environmental Microbiology 2009, 75, 5428-5433.

(63) Lesage, V.; Morin, Y.; Rioux, È.; Pomerleau, C.; Ferguson, S. H.; Pelletier, É. Stable isotopes and trace elements as indicators of diet and habitat use in cetaceans: predicting errors related to preservation, lipid extraction, and lipid normalization. Marine Ecology Progress Series 2010, 419, 249-265.

(64) Mintenbeck, K.; Brey, T.; Jacob, U.; Knust, R.; Struck, U. How to account for the lipid effect on carbon stable-isotope ratio (δ13C): sample treatment effects and model bias. Journal of Fish Biology 2008, 72, 815-830.

(65) Leary, D. H.; Hervey, W. J.; Deschamps, J. R.; Kusterbeck, A. W.; Vora, G. J. Which metaproteome? The impact of protein extraction bias on metaproteomic analyses. Molecular and Cellular Probes 2013, 27, 193-199.

(66) Ejsing, C. S.; Sampaio, J. L.; Surendranath, V.; Duchoslav, E.; Ekroos, K.; Klemm, R. W.; Simons, K.; Shevchenko, A. Global analysis of the yeast lipidome by quantitative shotgun mass spectrometry. Proceedings of the National Academy of Sciences 2009, 106, 2136-2141.

(67) Rampler, E.; Coman, C.; Hermann, G.; Sickmann, A.; Ahrends, R.; Koellensperger, G. LILY-lipidome isotope labeling of yeast: in vivo synthesis of 13C labeled reference lipids for quantification by mass spectrometry. Analyst 2017, 142, 1891-1899.

(68) Rampler, E.; Criscuolo, A.; Zeller, M.; El Abiead, Y.; Schoeny, H.; Hermann, G.; Sokol, E.; Cook, K.; Peake, D. A.; Delanghe, B.; Koellensperger, G. A Novel Lipidomics Workflow for Improved Human Plasma Identification and Quantification Using RPLC-MSn Methods and Isotope Dilution Strategies. Analytical Chemistry 2018, 90, 6494-6501.

(69) Pedersen, H. K.; Gudmundsdottir, V.; Nielsen, H. B.; Hyotylainen, T.; Nielsen, T.; Jensen, B. A.; Forslund, K.; Hildebrand, F.; Prifti, E.; Falony, G. Human gut microbes impact host serum metabolome and insulin sensitivity. Nature 2016, 535, 376-381.

(70) Pedersen, H. K.; Forslund, S. K.; Gudmundsdottir, V.; Petersen, A. Ø.; Hildebrand, F.; Hyötyläinen, T.; Nielsen, T.; Hansen, T.; Bork, P.; Ehrlich, S. D.; Brunak, S.; Oresic, M.; Pedersen, O.; Nielsen, H. B. A computational framework to integrate high-throughput '-omics' datasets for the identification of potential mechanistic links. Nature Protocols 2018, 13, 2781-2800.

(71) Hartler, J.; Triebl, A.; Ziegl, A.; Trotzmuller, M.; Rechberger, G. N.; Zeleznik, O. A.; Zierler, K. A.; Torta, F.; Cazenave-Gassiot, A.; Wenk, M. R.; Fauland, A.; Wheelock, C. E.; Armando, A. M.; Quehenberger, O.; Zhang, Q.; Wakelam, M. J. O.; Haemmerle, G.; Spener, F.; Kofeler, H. C.; Thallinger, G. G. Deciphering lipid structures based on platform-independent decision rules. Nature Methods 2017, 14, 1171-1174.

(72) Hartler, J.; Trotzmuller, M.; Chitraju, C.; Spener, F.; Kofeler, H. C.; Thallinger, G. G. Lipid Data Analyzer: unattended identification and quantitation of lipids in LC-MS data. Bioinformatics 2011, 27, 572-577.

(73) Pi, J.; Wu, X.; Feng, Y. Fragmentation patterns of five types of phospholipids by ultra-high-performance liquid chromatography electrospray ionization quadrupole time-of-flight tandem mass spectrometry. Analytical Methods 2016, 8, 1319-1332.

(74) Hsu, F.-F.; Turk, J. Electrospray ionization with low-energy collisionally activated dissociation tandem mass spectrometry of glycerophospholipids: mechanisms of fragmentation and structural characterization. J Chromatogr B Analyt Technol Biomed Life Sci. 2009, 877, 2673-2695.

(75) diseases, W. H. O.-D. o. c. o. n. t., Integrating Neglected Tropical Diseases into Global Health and Development: Fourth WHO report on neglected tropical diseases: Geneva, 2017.

(76) Grevelding, C. G. The female-specific W1 sequence of the Puerto Rican strain of Schistosoma mansoni occurs in both genders of a Liberian strain. Molecular and Biochemical Parasitology 1995, 71, 269-272.

(77) Lu, Z.; Sessler, F.; Holroyd, N.; Hahnel, S.; Quack, T.; Berriman, M.; Grevelding, C. G. Schistosome sex matters: a deep view into gonad-specific and pairing-dependent transcriptomes reveals a complex gender interplay. Scientific Reports 2016, 6, 31150.

(78) Yang, G.-J.; Bergquist, R. Potential Impact of Climate Change on Schistosomiasis: A Global Assessment Attempt. Tropical medicine and infectious disease 2018, 3, 117.

(79) McCreesh, N.; Nikulin, G.; Booth, M. Predicting the effects of climate change on Schistosoma mansoni transmission in eastern Africa. Parasites & Vectors 2015, 8, 4.

(80) Bergquist, R.; Zhou, X.-N.; Rollinson, D.; Reinhard-Rupp, J.; Klohe, K. Elimination of schistosomiasis: the tools required. Infectious Diseases of Poverty 2017, 6, 158.

(81) Retra, K.; Bleijerveld, O. B.; van Gestel, R. A.; Tielens, A. G.; van Hellemond, J. J.; Brouwers, J. F. A simple and universal method for the separation and identification of phospholipid molecular species. Rapid Communications in Mass Spectrometry 2008, 22, 1853-1862.

(82) Ferreira, M. S.; Oliveira, D. N.; Oliveira, R. N.; Allegretti, S. M.; Vercesi, A. E.; Catharino, R. R. Mass spectrometry imaging: a new vision in differentiating Schistosoma mansoni strains. Journal of Mass Spectrometry 2014, 49, 86-92.

(83) Ferreira, M. S.; de Oliveira, R. N.; de Oliveira, D. N.; Esteves, C. Z.; Allegretti, S. M.; Catharino, R. R. Revealing praziquantel molecular targets using mass spectrometry imaging: an expeditious approach applied to Schistosoma mansoni. International journal for parasitology 2015, 45, 385-391.

(84) Retra, K.; deWalick, S.; Schmitz, M.; Yazdanbakhsh, M.; Tielens, A. G. M.; Brouwers, J. F. H. M.; van Hellemond, J. J. The tegumental surface membranes of Schistosoma mansoni are enriched in parasite-specific phospholipid species. International Journal for Parasitology 2015, 45, 629-636.

(85) Giera, M.; Kaisar, M. M.; Derks, R. J.; Steenvoorden, E.; Kruize, Y. C.; Hokke, C. H.; Yazdanbakhsh, M.; Everts, B. The Schistosoma mansoni lipidome: Leads for immunomodulation. Analytica chimica acta 2018, 1037, 107-118.

(86) Fox, C. H.; Johnson, F. B.; Whiting, J.; Roller, P. P. Formaldehyde fixation. Journal of Histochemistry & Cytochemistry 1985, 33, 845-853.

(87) Ly, A.; Buck, A.; Balluff, B.; Sun, N.; Gorzolka, K.; Feuchtinger, A.; Janssen, K.-P.; Kuppen, P. J. K.; van de Velde, C. J. H.; Weirich, G.; Erlmeier, F.; Langer, R.; Aubele, M.; Zitzelsberger, H.; McDonnell, L.; Aichler, M.; Walch, A. High-mass-resolution MALDI mass spectrometry imaging of metabolites from formalin-fixed paraffin-embedded tissue. Nature Protocols 2016, 11, 1428-1443.

(88) Pietrowska, M.; Gawin, M.; Polańska, J.; Widłak, P. Tissue fixed with formalin and processed without paraffin embedding is suitable for imaging of both peptides and lipids by MALDI-IMS. Proteomics 2016, 16, 1670-1677.

(89) Kawamoto, T. Use of a new adhesive film for the preparation of multi-purpose fresh-frozen sections from hard tissues, whole-animals, insects and plants. Archives of histology and cytology 2003, 66, 123-143.

(90) Khalil, S. M.; Rompp, A.; Pretzel, J.; Becker, K.; Spengler, B. Phospholipid Topography of Whole-Body Sections of the Anopheles stephensi Mosquito, Characterized by High-Resolution Atmospheric-Pressure Scanning Microprobe Matrix-Assisted Laser Desorption/Ionization Mass Spectrometry Imaging. Analytical Chemistry 2015, 87, 11309-11316.

(91) Brignole-Baudouin, F.; Desbenoit, N.; Hamm, G.; Liang, H.; Both, J. P.; Brunelle, A.; Fournier, I.; Guerineau, V.; Legouffe, R.; Stauber, J.; Touboul, D.; Wisztorski, M.; Salzet, M.; Laprevote, O.; Baudouin, C. A new safety concern for glaucoma treatment demonstrated by mass spectrometry imaging of benzalkonium chloride distribution in the eye, an experimental study in rabbits. PloS one 2012, 7, e50180.

(92) Hameed, S.; Ikegami, K.; Sugiyama, E.; Matsushita, S.; Kimura, Y.; Hayasaka, T.; Sugiura, Y.; Masaki, N.; Waki, M.; Ohta, I.; Hossen, M. A.; Setou, M. Direct profiling of the phospholipid composition of adult Caenorhabditis elegans using whole-body imaging mass spectrometry. Analytical and bioanalytical chemistry 2015, 407, 7589-7602.

(93) Niehoff, A.-C.; Schulz, J.; Soltwisch, J.; Meyer, S.; Kettling, H.; Sperling, M.; Jeibmann, A.; Dreisewerd, K.; Francesconi, K. A.; Schwerdtle, T.; Karst, U. Imaging by Elemental and Molecular Mass Spectrometry Reveals the Uptake of an Arsenolipid in the Brain of Drosophila melanogaster. Analytical Chemistry 2016, 88, 5258-5263.

(94) Khalil, S. M.; Pretzel, J.; Becker, K.; Spengler, B. High-resolution AP-SMALDI mass spectrometry imaging of Drosophila melanogaster. International Journal of Mass Spectrometry 2017, 416, 1-19.

(95) Rujoi, M.; Estrada, R.; Yappert, M. C. In situ MALDI-TOF MS regional analysis of neutral phospholipids in lens tissue. Analytical Chemistry 2004, 76, 1657-1663.

(96) Schober, Y.; Guenther, S.; Spengler, B.; Römpp, A. Single cell matrix-assisted laser desorption/ionization mass spectrometry imaging. Analytical Chemistry 2012, 84, 6293-6297.

(97) Redman, C. A.; Kennington, S.; Spathopoulou, T.; Kusel, J. R. Interconversion of sphingomyelin and ceramide in adult Schistosoma mansoni. Molecular and Biochemical Parasitology 1997, 90, 145-153.

(98) Van Hellemond, J. J.; Retra, K.; Brouwers, J. F. H. M.; van Balkom, B. W. M.; Yazdanbakhsh, M.; Shoemaker, C. B.; Tielens, A. G. M. Functions of the tegument of schistosomes: Clues from the proteome and lipidome. International Journal for Parasitology 2006, 36, 691-699.

(99) McLaren, D. J.; Hockley, D. J. Blood flukes have a double outer membrane. Nature 1977, 269, 147-149.

(100) Kadesch, P.; Quack, T.; Gerbig, S.; Grevelding, C. G.; Spengler, B. Lipid Topography in Schistosoma mansoni Cryosections, Revealed by Microembedding and High-Resolution Atmospheric-Pressure Matrix-Assisted Laser Desorption/Ionization (MALDI) Mass Spectrometry Imaging. Analytical Chemistry 2019, 91, 4520-4528.

(101) Jäger, B. P.; Rudolph, P. E. In Statistik : Verstehen durch Experimente mit SAS; De Gruyter: Berlin, 2016, p 398.

(102) Huberty, C. J.; Petoskey, M. D. In Handbook of Applied Multivariate Statistics and Mathematical Modeling, Tinsley, H. E. A.; Brown, S. D., Eds.; Academic Press: San Diego, 2000, pp 183-208.

(103) Anton, H. In Elementary Linear Algebra; Wiley: New York, 2013, p 145.

(104) Meyer zu Heringdorf, D.; Jakobs, K. H. Lysophospholipid receptors: Signalling, pharmacology and regulation by lysophospholipid metabolism. Biochimica et Biophysica Acta (BBA) - Biomembranes 2007, 1768, 923-940.

(105) Spiegel, S.; Foster, D.; Kolesnick, R. Signal transduction through lipid second messengers. Current Opinion in Cell Biology 1996, 8, 159-167.

(106) Bexkens, M. L.; Mebius, M. M.; Houweling, M.; Brouwers, J. F.; Tielens, A. G. M.; van Hellemond, J. J. Schistosoma mansoni does not and cannot oxidise fatty acids, but these are used for biosynthetic purposes instead. International Journal for Parasitology 2019, 49, 647-656.

(107) Hahnel, S.; Lu, Z.; Wilson, R. A.; Grevelding, C. G.; Quack, T. Whole-Organ Isolation Approach as a Basis for Tissue-Specific Analyses in Schistosoma mansoni. PLOS Neglected Tropical Diseases 2013, 7, e2336.

(108) Beckmann, S.; Grevelding, C. Imatinib has a fatal impact on morphology, pairing stability and survival of adult Schistosoma mansoni in vitro. International journal for parasitology 2010, 40, 521-526.

(109) Roderfeld, M.; Padem, S.; Lichtenberger, J.; Quack, T.; Weiskirchen, R.; Longerich, T.; Schramm, G.; Churin, Y.; Irungbam, K.; Tschuschner, A. Schistosoma mansoni Egg–Secreted Antigens Activate Hepatocellular Carcinoma–Associated Transcription Factors c-Jun and STAT3 in Hamster and Human Hepatocytes. Hepatology 2018.

(110) Brouwers, J. F.; Versluis, C.; van Golde, L. M.; Tielens, A. G. 5-Octadecenoic acid: evidence for a novel type of fatty acid modification in schistosomes. The Biochemical journal 1998, 334 (Pt 2), 315-319.

(111) Esch, P.; Heiles, S. Charging and Charge Switching of Unsaturated Lipids and Apolar Compounds Using Paternò-Büchi Reactions. Journal of The American Society for Mass Spectrometry 2018, 29, 1971-1980.

Chapter II - Publication 1

Lipid Topography in *Schistosoma mansoni* Cryosections, Revealed by Microembedding and High-Resolution Atmospheric-Pressure Matrix-Assisted Laser Desorption/Ionization (MALDI) Mass Spectrometry Imaging

Kadesch, Patrik*; Quack, Thomas[#]; Gerbig, Stefanie*; Grevelding, Christoph G.[#]; Spengler, Bernhard*

* Institute of Inorganic and Analytical Chemistry, Justus Liebig University Giessen, Giessen, Germany

[#] Institute of Parasitology, Justus Liebig University Giessen, Giessen, Germany

Analytical Chemistry **2019**, 91 (7), pp 4520-4528

DOI: 10.1021/acs.analchem.8b05440

analytical chemistry

Article

Cite This: *Anal. Chem.* 2019, 91, 4520–4528

pubs.acs.org/ac

Lipid Topography in *Schistosoma mansoni* Cryosections, Revealed by Microembedding and High-Resolution Atmospheric-Pressure Matrix-Assisted Laser Desorption/Ionization (MALDI) Mass Spectrometry Imaging

Patrik Kadesch,[†] Thomas Quack,[‡] Stefanie Gerbig,[†] Christoph G. Grevelding,[‡] and Bernhard Spengler*[,†]

[†]Institute of Inorganic and Analytical Chemistry, Justus Liebig University Giessen, Heinrich-Buff-Ring 17, 35392 Giessen, Germany

[‡]Institute of Parasitology, Justus Liebig University Giessen, BFS, Schubertstrasse 81, 35392 Giessen, Germany

Supporting Information

ABSTRACT: Schistosomes are parasitic platyhelminthes that cause schistosomiasis, which is a life-threatening infectious disease for humans in the tropics and subtropics worldwide. Within the human host, female and male schistosomes develop and pair as a prerequisite for egg production. Part of the eggs get lodged in organs such as the gut, spleen, and liver, where they cause severe inflammatory processes, including liver fibrosis, which is one of the most serious pathological symptoms. High-resolution atmospheric-pressure scanning microprobe matrix-assisted laser desorption/ionization (AP-SMALDI) mass spectrometry imaging (MSI) has been used as a powerful tool to investigate adult schistosomes at the topographic molecular level. An MSI-compatible protocol was developed, covering critical sample preparation steps and focusing on obtaining artifact-free, longitudinal cryosections. Planar, consecutive sections were prepared from ~400 μm thick *S. mansoni* worm couples, comparing several microembedding approaches. High-resolution MSI at both, 10 and 5 μm lateral resolution unraveled anatomical structures and differential abundances of glycerophospholipids and saccharides in females and males. In addition, glycerophospholipids occurred differentially abundant in worm tissues of the female, such as the gut, which is essential for nutrient uptake and subsequent metabolism. Fragment ions of isobaric phospholipids were investigated by on-tissue MS^2 imaging experiments, unambiguously showing isomer-specific ion signals. This study provides a solid basis for investigating schistosome parasites in chemical detail at the whole-worm level by MSI.

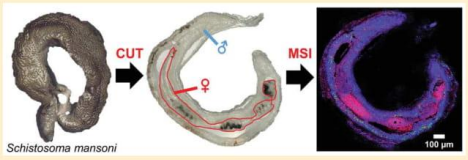

Schistosomiasis, which is also known as bilharzia, is a waterborne disease. Because of limited research budgets and low activity of the pharmaceuticals industry, it has been classified as a "neglected tropical disease" (NTD) by the World Health Organisation (WHO).[1] The disease is endemic in subtropical and tropical areas such as sub-Sahara Africa, the Middle East, parts of Asia and South America, where people often live in poverty and in close contact to the vectors. Currently, ~230 million people worldwide suffer from schistosomiasis, with ~1 billion people at risk, causing more than 200 000 deaths per year.[2] In addition, worm burden is associated with human disabilities or developmental disorders, especially in children. To date, there is no vaccine available[3] and only one drug, praziquantel, that is effective against all schistosome species affecting humans. This limitation justifies the fear of resistance development.[4,5] Because of changing climatic conditions, global trading, and transmigration,[6] the disease is spreading in regions such as South America[7] and Brazil.[8] Recently, even Europe has come into focus, since the first cases were reported from travelers in Corsica (France).[9]

The schistosome vertebrate host, such as *Homo sapiens*, is infected by cercariae, a larval form released by intermediate snail-host species that live in aqueous environments. Upon contact in the water, cecariae penetrate the skin of vertebrate hosts.[2] After transformation into a schistosomulum, the parasite crosses the skin and reaches the bloodstream to migrate via heart and lungs to the liver. Here, the maturation to adult worms occurs.[2] Following pairing, schistosome couples migrate to the mesenteric veins of the gut (*Schistosoma mansoni*; *S. japonicum*) or the venous plexus of the bladder (*S. hematobium*). Schistosomes show two characteristics. First, whereas trematodes are usually hermaphrodites, *Schistosoma spp.* developed sexual dimorphism of adult male and female worms.[2] *In copula*, the female resides within the ventral groove of the male, thereby forming the gynaecophoric canal, resulting in close proximity of female and male syncytial tegument (representing the outer body covering). Second, the development and sexual maturation of the female is strongly dependent on a permanent pairing contact with the male.

Received: November 25, 2018
Accepted: February 26, 2019
Published: February 26, 2019

DOI: 10.1021/acs.analchem.8b05440
Anal. Chem. 2019, 91, 4520–4528

After pairing, *S. mansoni* couples settle in the mesenteric plexus of the gut, where they produce up to 300 eggs per day.[1,2] About half of those eggs reach the gut lumen and are excreted via the feces, whereas the residual eggs are entrained by the bloodstream to different organs, preferentially the liver and spleen, where they get trapped.[1,2] Because of the inability of the host immune system to degrade those eggs, they induce fibrosis and inflammatory processes. This leads to swelling of the inner organs, severe impairments of organ function and, if not treated, conditions such as liver cirrhosis.[2,10] Within the eggs, the first larval stage, the miracidium, develops, which hatches as soon as it comes into contact with light and fresh water. Miracidia specifically infect invertebrate intermediate snail hosts of the genus *Biomphalaria*, in which they undergo an asexual multiplication, resulting in shedding of the second final host-infective larval stage, the cercaria.[11]

Adult *Schistosoma* reveal some characteristic anatomical features such as oral and ventral suckers at their anterior end and tubercles on the dorsal part of the male tegument. The tegument consists of a heptalaminate membrane, two trilaminate membranes,[12] and a proximate cytoplasm.[13] It is involved in uptake and elimination of metabolites and nutrients[12,14,15] and serves as a barrier against the host's immune system.[15−19] Characteristic structures of the male are the testes and the gynaecophoric canal, which represents the contact zone to the female. Specific for the female are the ovary and the vitellarium, generating oocytes and vitelline cells, respectively. Both organs are mandatory for the formation of composite eggs, consisting of fertilized oozysts combined with several vitelline cells. The size of the male varies from 8 mm to 9 mm in length and 350 μm to 500 μm in diameter. The female is ∼350 μm thick and its length can reach up to 11 mm.[20]

It has been demonstrated that atmospheric-pressure scanning microprobe matrix-assisted laser desorption/ionization (AP-SMALDI) mass spectrometry imaging (MSI)[21,22] is a suitable technique for the analysis of such small specimens. MSI provides a platform for label-free, multiplexed analysis that is well-suited for comprehensive chemical characterization, especially of biological samples. In contrast to targeted techniques such as immunostaining, MSI operates in a nontargeted fashion and enables parallel investigation of hundreds of substances. MSI typically requires freshly frozen tissue sections.[23] Specimens are usually freeze-mounted in a cryotome and cut into thin sections without further preparation. However, this procedure only works well for large samples. Depending on the size of the organism, additional sample preparation steps are required. A freeze-cracking procedure was applied to investigate the nematode *Caenorhabditis elegans* (*C. elegans*) to remove the cuticula prior to MSI.[24] An ethanol series was performed to enhance the section quality of *Drosophila melanogaster* brains.[25] For cutting small and heterogeneous organisms such as *Anopheles stephensi* mosquitos,[26,27] direct sectioning is not possible. To overcome this issue, embedding techniques have been applied.[26,27] However, classical formalin-fixation and paraffin-embedding (FFPE), which is the gold standard in histology, is not ideally suited for metabolomic investigations, especially since the lipid profile is partially altered.[28,29] Other polymeric embedding compounds, such as optimal cutting temperature (OCT) medium, are not compatible with MSI either,[30] because they may cause severe ion suppression effects and isobaric interferences. Nevertheless, a few compounds are available for embedding in MSI. Carboxymethyl cellulose (CMC)[26] is typically used as 2%−5% solution in water,[31] while tragacanth gum is used in 10%−20% aqueous solution.[32] Another commonly applied embedding agent is 5% aqueous gelatin.[33] However, typical embedding procedures, especially when using cryomolds, are intended for specimen sizes significantly larger than the samples described here. For small objects in the lower millimeter to micrometer range, it is difficult to define the sectioning plane in a bulk of embedding material. Therefore, alternative techniques and procedures are required.

The AP-SMALDI-MSI[22] workflow usually starts with matrix application by pneumatic spraying[34] or sublimation.[35] Common pixel sizes for MSI analyses are in the range of 20−50 μm.[23,36] In high-resolution imaging experiments, a lateral resolution of 5−10 μm[22,37,38] and even 1.4 μm[34] can be achieved, enabling the investigation of small samples like *S. mansoni*. A complication of such high lateral resolution is that the laser beam must be focused tediously along the *z*-axis. Precise focusing becomes increasingly important for higher lateral resolution, since the depth of focus decreases. Therefore, height variations may lead to artifact formation, because of local defocusing of the laser beam and variation of signal intensities. Recent developments have overcome these problems by profilometry using pixelwise laser triangulation for MALDI[39] or via prescanning the sample with a confocal distance sensor for laser ablation electrospray ionization (LAESI).[40] Thus, it is possible to record high-resolution ion images for complex sample topographies.

Schistosomes are highly evolved biological entities and have developed a characteristic lipid biology. Lipidomic studies generally aim to describe the lipid biology of a system. However, such studies become increasingly difficult with biological complexity and diversity. Schistosomes with their multiple, highly specialized organs, such as the tegument, are therefore composed of different compartments. MS imaging provides outstanding, spatial lipidomic information and can help to unravel either organ-specific or pairing-dependent information. For that, it is mandatory to have sample preparation procedures available to make such structures accessible for MSI analysis.

Lipids are of special interest in *S. mansoni* parasite research,[19] since the worms are not able to synthesize fatty acids and sterols de novo,[41] and some extraordinary lipid species, e.g., Δ5-octadecenoic acid[42] or large quantities of lysophospholipids occur in the tegument.[43] Especially the dorsal male tegument is highly interesting, because it is a special feature of platyhelminths, representing the parasite's frontier for parasite−host interactions.[10,17−19] In former studies, liquid chromatography (LC) was used for the quantitative determination of phosphatidylcholines (PC) and fatty acids derived from these PC precursors, using whole-worm lysates.[44] LC-ESI-MS was used to investigate phospholipids and fatty acid composition in *S. mansoni* from whole worm extracts[45] and the tegument.[43] Previous MSI studies showed that the surface of regionally different *S. mansoni* strains can be distinguished using vacuum MALDI-TOF and infusion ESI-MS.[46] However, the lateral resolution of 50 μm was not sufficient to distinguish anterior and posterior ends. Besides, no inner organs were investigated, since no sections were prepared.

To overcome existing limitations, we aimed to establish a new procedure for detailed MSI analysis. Therefore, we compared multiple embedding protocols, aiming to obtain

DOI: 10.1021/acs.analchem.8b05440
Anal. Chem. 2019, 91, 4520−4528

artifact-free, longitudinal cryosections. To this end, we combined glutaraldehyde fixation and embedding in gelatin to prepare tissue sections from adult *S. mansoni* worms. This method enabled us to prepare technical replicates from a single *S. mansoni* couple. The new protocol for the first time allowed the identification of different metabolites and the detailed visualization of their distribution in *S. mansoni* sections by MSI.

EXPERIMENTAL SECTION

Ethics Statement. Animal experiments were performed in accordance with the European Convention for the Protection of Vertebrate Animals used for experimental and other scientific purposes (ETS No 123; revised Appendix A) and were approved by the Regional Council (Regierungspraesidium) Giessen (V54-19 c 20/15 c GI 18/10).

Sample Preparation. Parasite maintenance was performed as described elsewhere.[47] In brief, Syrian hamsters of the species *Mesocricetus auratus* were infected with *cercariae* of *S. mansoni* (Liberian strain).[47] Adult worms were isolated 42 days post-infection by hepatoportal perfusion.[48] Eggs were extracted from the liver to infect the intermediate snail host *Biomphalaria glabrata* to generate infective cercariae.[47]

Classical Embedding Using Cryomolds. Following perfusion, *S. mansoni* worms were briefly kept in cultivation medium,[47] washed in isotonic NaCl (mass concentration β = 7 g/L; NaCl, p.a. Merck, Darmstadt, Germany) solution, and stored at −80 °C. Aqueous gelatin solution was prepared with a mass concentration of β(gelatin) = 30−120 g/L (water: LC-MS grade, VWR International GmbH, Darmstadt, Germany; gelatin: pharm. Eur., VWR), and heated to 50 °C in a water bath. Disposable cryomolds (Tissue-Tek, Sakura Finetek Germany GmbH, Staufen, Germany) with the dimensions of 15 mm × 15 mm × 5 mm were filled to ∼50% of the volume with gelatin solution and frozen at −20 °C. Thawed *S. mansoni* worms were placed on the frozen gelatin block using a disposable inoculation loop or featherweight forceps. Worms were covered with gelatin solution and frozen at −20 °C for 30 min.

For centrifugation experiments, the worms were placed in aqueous gelatin solution (β = 80 g/L) and centrifuged at 4000*g* for up to 30 min. The cryomolds were frozen at −20 °C to preserve the desired worm orientation. Frozen gelatin blocks were cut into sections 20−40 μm thick, which were then mounted onto glass slides. The glass slides with sections were stored at −80 °C, and sample quality was determined using a digital light microscope (VHX 5000, Keyence, Osaka, Japan) with 250-fold or 1500-fold magnification, using the vendor-based profilometry mode, to obtain three-dimensional (3D) profiles.

Fixation and Microembedding. A 6.7% glutaraldehyde solution (Grade I, Sigma−Aldrich Chemie GmbH, Munich, Germany) was prepared from 20% aqueous glutaraldehyde and phosphate buffered saline (PBS from Gibco, Thermo Fisher Scientific, Bremen, Germany). Fifty microliters (50 μL) of glutaraldehyde solution were deposited on a glass slide. Adult *S. mansoni* males or couples, respectively, were transferred to the fixative using featherweight forceps. A coverslip was applied, and samples were frozen in liquid N_2 and stored at −80 °C until further processing.

Worms were thawed in a desiccator at room temperature. A single worm/couple was transferred to the miniaturized sample holder (stainless steel, d = 6 mm) using featherweight forceps. A quantity of 5−10 μL of 8% gelatin solution (β = 80 g/L) were used to coat the worm. The sample holder was transferred to the cryotome (HM525, Thermo Fisher Scientific) and kept for 30 min before sectioning into specimens 20−40 μm thick. Sections were thaw-mounted on glass slides, and their quality was determined microscopically. Sections of sufficient quality were stored at −80 °C until further analysis.

Matrix Application and Mass Spectrometry Imaging. Samples were thawed in a desiccator at room temperature for 30 min. Microscopic images were recorded prior to matrix application. A quantity of 30 g/L of 2,5-dihydroxybenzoic acid (DHB, for synthesis, Merck) in acetone:water (acetone, LiChrosolv, Merck) 1:1 v/v with 0.1% trifluoroacetic acid (TFA, for spectroscopy, AppliChem GmbH, Darmstadt, Germany) was used as matrix in positive ion mode. An amount of 60−80 μL of matrix solution was applied to each individual sample with a flow rate of 10 μL/min and a rotation of 500 rpm (± 4%), using a SMALDIPrep sprayer (TransMIT GmbH, Giessen, Germany) at a nitrogen pressure of 1 bar.

MSI Setup. An autofocusing AP-SMALDI5 AF ion source[39] (TransMIT GmbH) was coupled to a Q Exactive HF mass spectrometer (Thermo Fisher Scientific (Bremen)). For MS^2 experiments, an AP-SMALDI10 (TransMIT GmbH) was coupled to a Q Exactive mass spectrometer (Thermo Fisher Scientific). The sample was desorbed/ionized by 50 (for MS^2 by 30) UV-laser pulses per pixel at a frequency of 100 Hz (MS^2: 60 Hz). Mass spectra were recorded from m/z 500 to 2000 with a mass resolution of 240 000 at m/z 200 and a mass accuracy of <3 ppm using the lock mass function (m/z 716.12451 = $[5DHB\text{-}4H_2O + NH_4]^+$). The ion injection time was set to 500 ms. S-lens level was set to 100 arbitrary units, and the capillary temperature was 250 °C. The acceleration voltage was set to 3.0 kV (MS^2: 4.3 kV).

For fragmentation experiments, m/z 808.6 ± 0.5 was isolated and fragmented at 20 NCE using higher-energy C-trap collisional dissociation (HCD). MS^2 spectra were recorded from m/z 250 to 1000 with a mass resolution of 140 000 at m/z 200 and a mass accuracy of <5 ppm.

Data Analysis. XCalibur (Thermo Fisher Scientific) was used to display mass spectra. The Mirion[49] software package (v3.2.64.29) was utilized to create ion images. The histogram bin width was set to 0.004 u and the absolute mass variance of spectra was set to 0.005 u. For image generation, each m/z signal was normalized to the total ion current (TIC) of the corresponding pixel (normalized versus native ion images are shown in Figure S1 in the Supporting Information). The LipidMaps database[50] was used to search for putative lipid assignments in combination with a lipidome investigation of *S. mansoni*.[43,45] Database matches for the presented images are shown in Tables S1 and S2 in the Supporting Information. In addition, the Human Metabolome Database (HMDB)[51] was used to annotate small metabolites and to verify database hits found with LipidMaps. ADC/ChemSketch was used to draw chemical structures.

RESULTS AND DISCUSSION

Cryosectioning of *S. mansoni* Worms for MSI. The availability of adequate cryosections is mandatory for investigating the molecular composition by MSI. Because of the small size of adult *S. mansoni* of <10 mm in length and 300−500 μm in diameter, sample embedding was required. MSI-compatible gelatin was used to minimize ion suppression effects during analysis. The content of gelatin varied to adjust

DOI: 10.1021/acs.analchem.8b05440
Anal. Chem. 2019, 91, 4520−4528

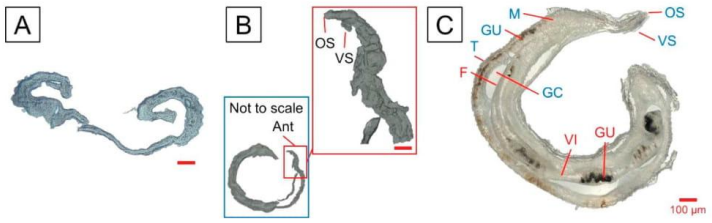

Figure 1. Optical images of longitudinal cryosections of adult *Schistosoma mansoni*: (A) male worm (by classical embedding), (B): male worm (by centrifugation method), and (C) paired couple (by microembedding procedure). [Legend: Ant (anterior end), OS (oral sucker), VS (ventral sucker), M (male), GU (gut), T (tubercles/tegument), GC (gynaecophoric canal), F (female), and VI (vitellarium). Female parts are marked in red, and male parts are marked in blue. Scale bar = 100 μm.]

viscosity in the liquid state and solidity in the solid state, since this is crucial for the embedding as well as the cutting process. Usage of 3% gelatin solution (β = 30 g/L) led to the formation of a liquid film surrounding the tissue section during microscopic evaluation. This could lead to leaking of metabolites from the tissue into the surrounding gelatin, and, therefore, a loss of lateral resolution and formation of measurement artifacts during MSI. A concentration of 12% gelatin (β = 120 g/L) was found to be too high, because it impeded the acquisition of longitudinal worm sections, because it was difficult to define the cutting plane, because of turbidity of the gelatin. Since longitudinal sections were required to facilitate the analysis of inner organs of *S. mansoni*, it was crucial to ensure the correct sectioning plane. In addition, fragmentation of the tissue was observed during cutting when using 12% gelatin. Furthermore, the section coiled up a few seconds after cutting. Finally, the optimal gelatin concentration was determined to be 8% (β = 80 g/L), showing the best performance for both embedding and cutting to generate high-quality longitudinal worm sections. In the following paragraphs, we describe three procedures that were tested for generating high-quality cryosections.

The longitudinal sections allowed investigation of the inner organs of adult worms, as single worms or *in copula*. In Figure 1A, a longitudinal cryosection of a male worm is shown, which was obtained by classical embedding. Here, a gelatin block was frozen in a cryomold, the worm was placed in the middle and was subsequently covered with more gelatin. The tissue appeared in the sections but tissue fragments were observed in the middle part of the specimen. In addition, anterior and posterior ends were indistinguishable. The section could thus not be used to investigate structures or inner organs, as these could not be located in the microscopic images. Furthermore, this sectioning method is time-consuming, since the gelatin block is much larger than the sample and the location of the sample must be determined by careful abrasion of the gelatin block. Placing the worm on the prefrozen gelatin material sometimes resulted in a nonplanar position, since the gelatin did not freeze by forming a flat block, but rather formed a slightly elevated structure in the middle of the cryomold.

Figure 1B shows a section of a male worm, obtained by embedding and centrifugation. This section appeared to be intact. However, we again observed tissue fragmentation, diffuse structures as well as roughness of the surface area. The gynaecophoric canal also showed small fissures in the anterior region. While oral and ventral sucker were clearly visible, the testis structure could not be assigned based on the microscope image. This preparation technique required the handling of large amounts of embedding medium. However, in contrast to the first method using cryomolds, the localization of the worm was easier, since it had been centrifuged to the bottom of the mold. Furthermore, the worm was pressed to the bottom of the mold, which led to a flat orientation. Nonetheless, sample damage during the centrifugation process could not be entirely prevented, and also the flat orientation obtained during centrifugation sometimes changed afterward in the freezing process. In conclusion, this method provided improved section quality but was still not sufficient for MS imaging and organ assignment.

A cryosection obtained by prefixation in glutaraldehyde in combination with microembedding of a paired *S. mansoni* couple is shown in Figure 1C. Similar results were achieved using single male worms (data not shown). Very little tissue disruption was observed, and detailed structures became visible. Male and female worms remained morphologically intact and could be clearly distinguished. In addition, typical features of the male (M), such as oral (OS) and ventral sucker (VS), gut (GU), tubercles/tegument (T), and gynaecophoric canal (GC) were clearly visible. In the female (F), aside from the gut, the vitellarium (VI) also was detectable. While recording the microscopic image, some wrinkling of the tissue section was observed, most likely due to the high water content of the tissue, which evaporates rapidly under the microscope light. The resulting height profile is shown in Figure 2. Nevertheless, it is still possible to measure such sections with high lateral resolution, because varying laser fluences due to

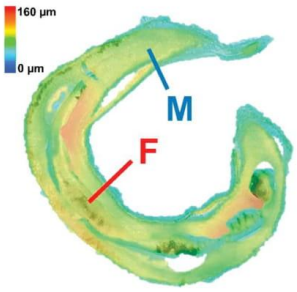

Figure 2. Height profile of a cryosection of the *S. mansoni* couple (male, M and female, F) shown in Figure 1C (recorded via microscope; magnification Rx1500 is required).

DOI: 10.1021/acs.analchem.8b05440
Anal. Chem. 2019, 91, 4520−4528

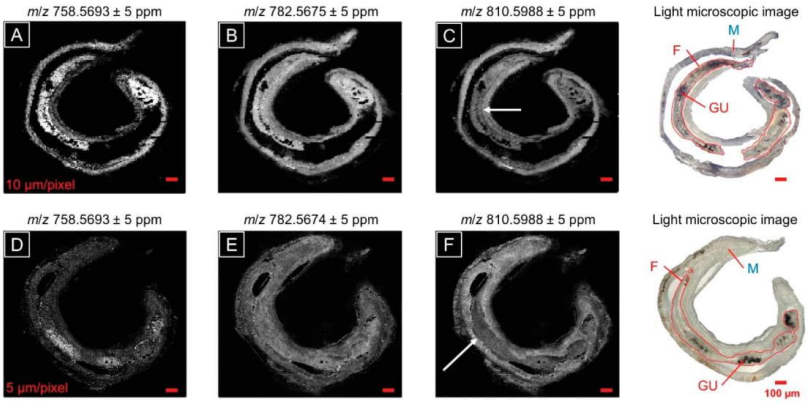

Figure 3. Comparison of a *S. mansoni* couple measured with MSI at 10 μm ((A, B, C) 158 × 148 pixels) and 5 μm ((D, E, F) 300 × 272 pixels) spatial resolution. m/z 758.5693 was assigned to PC(34:2) as $[M + H]^+$ Δm < 1 ppm, m/z 782.5675 to PC(34:1) as $[M + Na]^+$ Δm = 1 ppm and m/z 810.5988 to PC(36:1) as $[M + Na]^+ \Delta m$ = 1 ppm. The light microscopic images show the male (M) and the female (F) with gut (GU). Arrows mark male−female transitions (C, F). All scale bars = 100 μm.

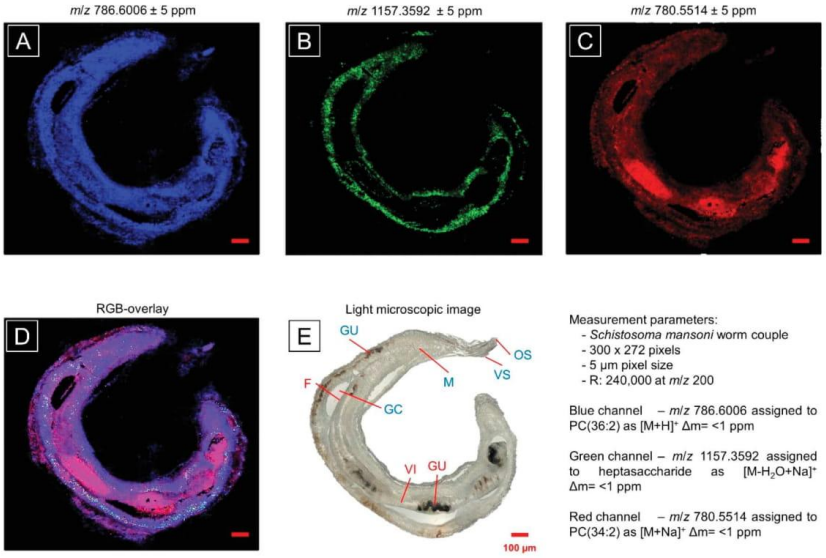

Figure 4. Differential ion distributions in male and female *S. mansoni*. (A) m/z 786.6006 seems to be more abundant in the male. (B) m/z 1157.3592 can be found almost exclusively in the male. (C) m/z 780.5514 is equally distributed in both male and female tissue but is more abundant in proximity of the gut-associated tissues. (D) In the red−green−blue (RGB) overlay, these differences between male and female become more obvious. (E) Light microscopic image shows male (M) with structural features oral (OS) and ventral sucker (VS), gut (GU) and gynaecophoric canal (GC) and female (F) with vitellarium (VI) and gut (GU). Structural annotations are based on the light microscopic image. Scale bar = 100 μm.

uneven surfaces can be compensated by triangulation laser autofocusing.[39]

Fixation of the worms in glutaraldehyde and applying the microembedding procedure resulted in the best section quality. In addition, this procedure required fewer resources, because it was faster and straightforward and required less embedding material and fewer disposables. Moreover, the placement of the worm couple directly on the holder ensured its flat orientation and increased the probability for intact longitudinal sectioning. Up to four consecutive sections of high quality were obtained this way, showing organs and structural features. On average, two sections were obtained per worm specimen. The

DOI: 10.1021/acs.analchem.8b05440
Anal. Chem. 2019, 91, 4520−4528

developed protocol is the first to generate tissue sections from *S. mansoni* worms, which is compatible with MSI.

High-Resolution MS Imaging of Paired *S. mansoni* Worms. Previous MSI studies demonstrated that different *S. mansoni* strains can be discriminated using a combination of vacuum MALDI-MSI and ESI-MS of worm extracts.[46] Surface measurements were performed with a pixel size of 50 μm. However, it was difficult to distinguish anterior and posterior ends from the displayed ion images; inner organs were not analyzed.

In our study, spatially resolved mass spectra of two neighboring tissue sections of *S. mansoni* couples were recorded with step sizes of 10 and 5 μm, using pixel-by-pixel autofocusing. Both sections were analyzed with identical sample preparation conditions and experimental settings. These parameters resulted in image sizes of 158 × 148 and 300 × 272 pixels, acquired with scanning steps of 10 and 5 μm, respectively. The total ion current was similar for both 10 and 5 μm measurements, typically in the range of 10^4 (normalized level). Consequently, MS spectra of similar quality were obtained at both resolutions. Ion images are shown in Figure 3 for step sizes of 10 μm (Figures 3A, 3B, and 3C) and 5 μm (Figures 3D, 3E, and 3F). Both tissue sections were found to be of similar quality, and inner organs could be allocated in the microscopic images of the male (M) and the female (F) (Figure 3). A tissue fragment of the female was lost during matrix application from the section corresponding to Figures 3A, 3B, and 3C (see Figure S2B in the Supporting Information). For nonprocessed microscope images, see Figure S2. Mass signals were assigned based on database search and comparison with published MS^2 data from Retra et al.[43,45] Database hits for all displayed ion images are shown in Table S1 in the Supporting Information. Signal m/z 758.5693 was assigned to PC(34:2) as $[M + H]^+$ with Δm = 1 ppm. Its signal intensity appears to be elevated in the female (Figures 3A and 3D). Evenly abundant signals in male and female were also observed, for example, for m/z 782.5674, which was assigned to PC(34:1) as $[M + Na]^+$ with Δm = 1 ppm (Figures 3B and 3E).[43,45] Several signals were obtained with higher abundance in the male compared to the female, as demonstrated by the signal intensity of m/z 810.5988, assigned to PC(36:1) as $[M + Na]^+$ with Δm = 1 ppm (Figures 3C and 3F).[43,45] Male and female worms could be clearly distinguished based on ion images at both 5 and 10 μm step sizes. In the case of m/z 810.5988, differences between male and female seemed to be more pronounced at quasi-cellular, 5 μm lateral resolution. Structures such as the transition between the female and the male were displayed in more detail with 5 μm resolution (see arrows in Figures 3C and 3F).

Identification of molecular compounds, which are differentially abundant in male and female, is one of the crucial steps to unravel male−female interaction at the molecular level. Especially, the chemical analysis of the female's reproductive system is of high interest, since it fully develops only upon constant pairing contact with the male.[52] Since the intact longitudinal section provides insights into the anatomy of a *S. mansoni* couple, several compounds with distinct topographic distributions in male and female were selected. Ion images of the corresponding m/z values are shown in Figure 4. Annotations were based on accurate mass determination and LipidMaps database hits, in comparison with literature data (see Table S2 in the Supporting Information).[43,45] In Figure 4A, m/z 786.6006 is shown in blue, which was assigned to PC(36:2) as $[M + H]^+$ with a mass deviation of <1 ppm. The signal was evenly distributed in the male and female, but with slightly decreased signal intensities in the female. This may indicate differential lipid metabolism in both sexes. The assigned phosphatidylcholine has been detected previously in *S. mansoni* parasites.[43,45] The ion at m/z 1157.3592 is shown in green and was assigned to the sodium adduct of a heptasaccharide under the loss of water with <1 ppm mass deviation. Since the detection of carbohydrates is an unusual finding compared to phospholipids, we expanded the search for other oligosaccharides to support the assignment. In addition, hexasaccharides and octasaccharides were found, their distributions are shown in Figures S3 and S4 in the Supporting Information, respectively. Ion signals corresponding to small oligosaccharides, for example, a trisaccharide (data not shown), were also found. It is already known from the literature that glucose is taken up via the tegument of *S. mansoni* parasites.[14] *In copula*, the tegumental surface of the female available for glucose uptake is lower, thus giving rise to the assumption that the signal intensity of oligosaccharides might be pronounced in the male. The detected oligosaccharides could be derived from glycogen or amylose, which serve as energy storage. They can be synthesized enzymatically by glycosyltransferases, all required genes and transcripts have been found experimentally in *S. mansoni* (KEGG Enzyme: EC 2.4.1.11 and 2.4.1.18 respectively; pathway: ko00500). The transcriptome shows high activity for the above-mentioned enzymes in adult schistosomes, but significantly elevated activity in the male. This might support higher oligosaccharide signal intensity in the male on the metabolic level.[52] However, detailed assignment of all saccharides requires further studies, since MS^2 experiments were not possible, because of low signal intensities of the saccharides, and current assignments therefore are based solely on accurate mass. The red channel, m/z 780.5514 shows the distribution of sodiated PC(34:2) with a mass deviation of <1 ppm, which was previously found in *S. mansoni*.[43,45] This signal is evenly distributed in female and male tissue, showing an increased signal intensity in the region of gut (GU) and vitellarium (VI). Phosphatidylcholines (PC) are known as membrane lipids[53] and may play a role in germ cell maturation, as it has been observed in male *Macrobrachium rosenbergii*.[54] Note that the detected (phospho)lipids were not limited to the class of phosphatidylcholines; other lipid classes, such as phosphatidylethanolamines, sphingomyelines, diglycerides, triglycerides, etc., also were found.

The red−green−blue (RGB) overlay of the aforementioned ion signals can be found in Figure 4D, each color channel representing one ion signal. The figure shows differences between female and male tissue, the gut-associated tissue (GU) and the vitellarium (VI). An additional RG-overlay using different m/z signals is shown in Figure S5 in the Supporting Information. Unfortunately, parts of the male's head region were subducted in gelatin and, therefore, no lipid signals were recorded in this region.

In summary, we demonstrated MSI analysis of an *S. mansoni* worm couple using high lateral and high mass resolution. Male and female *S. mansoni* could be distinguished based on MS ion images of signals characteristic for or elevated in specific organs like the gut of the female.

High-Resolution MS^2I of Lipids in Adult Male Worms. *S. mansoni* comprise fatty acids and phospholipids with odd chain lengths, adding complexity to structural elucidation and

DOI: 10.1021/acs.analchem.8b05440
Anal. Chem. 2019, 91, 4520−4528

developed protocol is the first to generate tissue sections from *S. mansoni* worms, which is compatible with MSI.

High-Resolution MS Imaging of Paired *S. mansoni* Worms. Previous MSI studies demonstrated that different *S. mansoni* strains can be discriminated using a combination of vacuum MALDI-MSI and ESI-MS of worm extracts.[46] Surface measurements were performed with a pixel size of 50 μm. However, it was difficult to distinguish anterior and posterior ends from the displayed ion images; inner organs were not analyzed.

In our study, spatially resolved mass spectra of two neighboring tissue sections of *S. mansoni* couples were recorded with step sizes of 10 and 5 μm, using pixel-by-pixel autofocusing. Both sections were analyzed with identical sample preparation conditions and experimental settings. These parameters resulted in image sizes of 158 × 148 and 300 × 272 pixels, acquired with scanning steps of 10 and 5 μm, respectively. The total ion current was similar for both 10 and 5 μm measurements, typically in the range of 10^4 (normalized level). Consequently, MS spectra of similar quality were obtained at both resolutions. Ion images are shown in Figure 3 for step sizes of 10 μm (Figures 3A, 3B, and 3C) and 5 μm (Figures 3D, 3E, and 3F). Both tissue sections were found to be of similar quality, and inner organs could be allocated in the microscopic images of the male (M) and the female (F) (Figure 3). A tissue fragment of the female was lost during matrix application from the section corresponding to Figures 3A, 3B, and 3C (see Figure S2B in the Supporting Information). For nonprocessed microscope images, see Figure S2. Mass signals were assigned based on database search and comparison with published MS^2 data from Retra et al.[43,45] Database hits for all displayed ion images are shown in Table S1 in the Supporting Information. Signal m/z 758.5693 was assigned to PC(34:2) as $[M + H]^+$ with Δm = 1 ppm. Its signal intensity appears to be elevated in the female (Figures 3A and 3D). Evenly abundant signals in male and female were also observed, for example, for m/z 782.5674, which was assigned to PC(34:1) as $[M + Na]^+$ with Δm = 1 ppm (Figures 3B and 3E).[43,45] Several signals were obtained with higher abundance in the male compared to the female, as demonstrated by the signal intensity of m/z 810.5988, assigned to PC(36:1) as $[M + Na]^+$ with Δm = 1 ppm (Figures 3C and 3F).[43,45] Male and female worms could be clearly distinguished based on ion images at both 5 and 10 μm step sizes. In the case of m/z 810.5988, differences between male and female seemed to be more pronounced at quasi-cellular, 5 μm lateral resolution. Structures such as the transition between the female and the male were displayed in more detail with 5 μm resolution (see arrows in Figures 3C and 3F).

Identification of molecular compounds, which are differentially abundant in male and female, is one of the crucial steps to unravel male−female interaction at the molecular level. Especially, the chemical analysis of the female's reproductive system is of high interest, since it fully develops only upon constant pairing contact with the male.[52] Since the intact longitudinal section provides insights into the anatomy of a *S. mansoni* couple, several compounds with distinct topographic distributions in male and female were selected. Ion images of the corresponding m/z values are shown in Figure 4. Annotations were based on accurate mass determination and LipidMaps database hits, in comparison with literature data (see Table S2 in the Supporting Information).[43,45] In Figure 4A, m/z 786.6006 is shown in blue, which was assigned to PC(36:2) as $[M + H]^+$ with a mass deviation of <1 ppm. The signal was evenly distributed in the male and female, but with slightly decreased signal intensities in the female. This may indicate differential lipid metabolism in both sexes. The assigned phosphatidylcholine has been detected previously in *S. mansoni* parasites.[43,45] The ion at m/z 1157.3592 is shown in green and was assigned to the sodium adduct of a heptasaccharide under the loss of water with <1 ppm mass deviation. Since the detection of carbohydrates is an unusual finding compared to phospholipids, we expanded the search for other oligosaccharides to support the assignment. In addition, hexasaccharides and octasaccharides were found, their distributions are shown in Figures S3 and S4 in the Supporting Information, respectively. Ion signals corresponding to small oligosaccharides, for example, a trisaccharide (data not shown), were also found. It is already known from the literature that glucose is taken up via the tegument of *S. mansoni* parasites.[14] *In copula*, the tegumental surface of the female available for glucose uptake is lower, thus giving rise to the assumption that the signal intensity of oligosaccharides might be pronounced in the male. The detected oligosaccharides could be derived from glycogen or amylose, which serve as energy storage. They can be synthesized enzymatically by glycosyltransferases, all required genes and transcripts have been found experimentally in *S. mansoni* (KEGG Enzyme: EC 2.4.1.11 and 2.4.1.18 respectively; pathway: ko00500). The transcriptome shows high activity for the above-mentioned enzymes in adult schistosomes, but significantly elevated activity in the male. This might support higher oligosaccharide signal intensity in the male on the metabolic level.[52] However, detailed assignment of all saccharides requires further studies, since MS^2 experiments were not possible, because of low signal intensities of the saccharides, and current assignments therefore are based solely on accurate mass. The red channel, m/z 780.5514 shows the distribution of sodiated PC(34:2) with a mass deviation of <1 ppm, which was previously found in *S. mansoni*.[43,45] This signal is evenly distributed in female and male tissue, showing an increased signal intensity in the region of gut (GU) and vitellarium (VI). Phosphatidylcholines (PC) are known as membrane lipids[53] and may play a role in germ cell maturation, as it has been observed in male *Macrobrachium rosenbergii*.[54] Note that the detected (phospho)lipids were not limited to the class of phosphatidylcholines; other lipid classes, such as phosphatidylethanolamines, sphingomyelines, diglycerides, triglycerides, etc., also were found.

The red−green−blue (RGB) overlay of the aforementioned ion signals can be found in Figure 4D, each color channel representing one ion signal. The figure shows differences between female and male tissue, the gut-associated tissue (GU) and the vitellarium (VI). An additional RG-overlay using different m/z signals is shown in Figure S5 in the Supporting Information. Unfortunately, parts of the male's head region were subducted in gelatin and, therefore, no lipid signals were recorded in this region.

In summary, we demonstrated MSI analysis of an *S. mansoni* worm couple using high lateral and high mass resolution. Male and female *S. mansoni* could be distinguished based on MS ion images of signals characteristic for or elevated in specific organs like the gut of the female.

High-Resolution MS^2I of Lipids in Adult Male Worms. *S. mansoni* comprise fatty acids and phospholipids with odd chain lengths, adding complexity to structural elucidation and

DOI: 10.1021/acs.analchem.8b05440
Anal. Chem. 2019, 91, 4520−4528

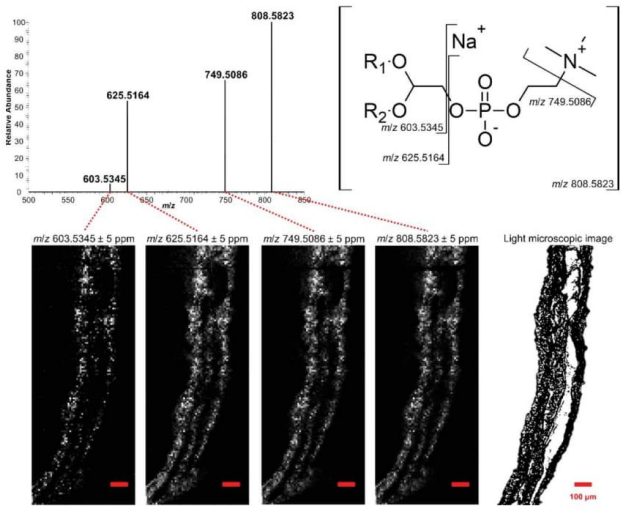

Figure 5. AP-SMALDI MS^2 images of fragment ions from precursor ion m/z 808.5823, obtained with a step size of 10 μm (60 × 150 pixels) from a male *S. mansoni* worm tissue section. Characteristic fragment ions of the phosphatidylcholine residues are displayed in an average spectrum (top left) and are schematically shown in the chemical structure (top right). The fragments are co-localized, as indicated by the MS images in the bottom row.

database searches. To prove MS/MS capabilities directly on tissue and to distinguish isobaric species, the precursor ion at m/z 808.5823, which could be either sodiated PE(39:2) or sodiated PC(36:2), was fragmented, and fragments were detected over the course of the tissue section of 60 by 150 pixels. The resulting ion images of precursor and fragment ions, obtained with 10 μm step size, as well as an average mass spectrum are shown in Figure 5. The product ion signals were found to be co-localized, supporting the assumption that all fragment ions originated from the same precursor. The chemical structure of PC(36:2) is shown in Figure 5 (top row, right side); possible fragmentation sites and the resulting m/z values of the fragment ions are indicated. Fragmentation of the phosphatidylcholine headgroup led to a neutral loss of trimethylamine, observed by transition of m/z 808.5823 to m/z 749.5086, as described in the literature.[55] The signal at m/z 625.5164 was assigned to the loss of $C_2H_5O_4P$ (1,3,2-dioxaphospholane,2-hydroxy-2-oxide) from the ion signal at m/z 749.5086. The neutral loss of $C_2H_4O_4PNa$ can be observed in the transition from m/z 749.5086 to m/z 603.5345. Therefore, the phosphatidylcholine headgroup was identified. All fragments showed a mass deviation of <1 ppm (see Table S3 in the Supporting Information). Consequently, the precursor ion at m/z 808.5823 was assigned to PC(36:2) as a sodium adduct with a mass deviation of <1 ppm. To further confirm the assignment of PC(36:2), we searched the mass spectrum for signals relatable to a PE lipid. No mass signals were observed that could be attributed to PE.

In MS^2I experiments of *S. mansoni* sections, on-tissue fragmentation was used as a tool to discriminate isobaric lipid species such as phosphatidylcholines and phosphatidylethanolamines. Since mass spectra of biological samples are inherently complex, spatially resolved detection of fragment ions adds valuable information about the presence of one or more precursors, highly relevant for avoiding false assignments in unknown samples.

■ CONCLUSION

A new protocol was developed for the preparation of intact longitudinal cryosections of *S. mansoni* worms using glutaraldehyde fixation and microembedding. Its advantage over classical embedding procedures is that the cutting plane can be defined more easily and more precisely, which allows for generation of technical replicates of submillimeter-sized objects. Structural features such as inner organs and the characteristic morphology of paired *Schistosoma* worms were preserved and visualized in MS ion images. The developed fixation and embedding method serves as a template for preparation of other multicellular parasitic and nonparasitic worms. For schistosomes, parasitic trematodes of worldwide importance, this method extends the repertoire of techniques needed in the post-genomic era to unravel functional aspects of schistosome biology, including its reproductive biology. In addition, the procedure can be adapted to nonparasitic close relatives of schistosomes, such as *Planaria*, or even to distinct biological model organisms such as *Drosophila melanogaster* or *Danio rerio* (zebrafish).

High-resolution mass spectrometry imaging was performed in positive ion mode with pixel sizes of 5 and 10 μm, using pixel-by-pixel autofocusing for nonplanar tissue sections with high intermeasurement reproducibility. High-resolution MSI enabled the allocation of ion signals to male and female worms, as well as to inner organs throughout the tissue section, while high mass accuracy allowed for lipid and saccharide assignment. On-tissue MS^2I was used to confirm lipid assignment and to visualize characteristic phosphatidylcholine fragment ions. This method opens a wide perspective for follow-up

DOI: 10.1021/acs.analchem.8b05440
Anal. Chem. 2019, 91, 4520−4528

studies in schistosomes, as well as other small organisms of interest.

■ ASSOCIATED CONTENT

Supporting Information

The Supporting Information is available free of charge on the ACS Publications website at DOI: 10.1021/acs.analchem.8b05440.

Database-assisted annotations of metabolites, native versus TIC-normalized ion images, detailed optical images and MS images of additional metabolites (PDF)

■ AUTHOR INFORMATION

Corresponding Author

*E-mail: Bernhard.spengler@anorg.chemie.uni-giessen.de.

ORCID

Stefanie Gerbig: 0000-0003-1355-4048

Bernhard Spengler: 0000-0003-0179-5653

Notes

The authors declare the following competing financial interest(s): B.S. and C.G.G. are consultants of TransMIT GmbH Giessen.

■ ACKNOWLEDGMENTS

Financial support by the Deutsche Forschungsgemeinschaft (DFG) under Grant Nos. Sp314/13-1 and INST 162/500-1 FUGG and by the State of Hesse, LOEWE Center "DRUID", is gratefully acknowledged. We would like to thank the Promotionskolleg "Bioressourcen und Biotechnologie" of the Technische Hochschule Mittelhessen and Justus Liebig University Giessen for granting a scholarship to P.K. Furthermore, we thank Christina Scheld, Georgette Stovall, and Bianca Kulik for *S. mansoni* maintenance.

■ REFERENCES

(1) *WHO—Integrating Neglected Tropical Diseases into Global Health and Development: Fourth WHO report on neglected tropical diseases*: World Health Organisation: Geneva, Switzerland, 2017.

(2) Colley, D. G.; Bustinduy, A. L.; Secor, W. E.; King, C. H. *Lancet* **2014**, *383*, 2253−2264.

(3) Egesa, M.; Hoffmann, K. F.; Hokke, C. H.; Yazdanbakhsh, M.; Cose, S. *Trends Parasitol.* **2017**, *33*, 918−921.

(4) Vale, N.; Gouveia, M. J.; Rinaldi, G.; Brindley, P. J.; Gärtner, F.; Correia da Costa, J. M. *Antimicrob. Agents Chemother.* **2017**, *61*, DOI: 10.1128/AAC.02582-16

(5) Wiegand, R. E.; Mwinzi, P. N. M.; Montgomery, S. P.; Chan, Y. L.; Andiego, K.; Omedo, M.; Muchiri, G.; Ogutu, M. O.; Rawago, F.; Odiere, M. R.; Karanja, D. M. S.; Secor, W. E. *J. Infect. Dis.* **2017**, *216*, 1425−1433.

(6) Lingscheid, T.; Kurth, F.; Clerinx, J.; Marocco, S.; Trevino, B.; Schunk, M.; Muñoz, J.; Gjørup, I. E.; Jelinek, T.; Develoux, M.; Fry, G.; Jänisch, T.; Schmid, M. L.; Bouchaud, O.; Puente, S.; Zammarchi, L.; Mørch, K.; Björkman, A.; Siikamäki, H.; Neumayr, A.; et al. *Am. J. Trop. Med. Hyg.* **2017**, *97*, 567−574.

(7) Gryseels, B.; Polman, K.; Clerinx, J.; Kestens, L. *Lancet* **2006**, *368*, 1106−1118.

(8) Katz, N. *Acta Trop.* **2008**, *108*, 69−71.

(9) Boissier, J.; Moné, H.; Mitta, G.; Bargues, M. D.; Molyneux, D.; Mas-Coma, S. *Lancet Infect. Dis.* **2015**, *15*, 757−758.

(10) Wilson, M. S.; Mentink-Kane, M. M.; Pesce, J. T.; Ramalingam, T. R.; Thompson, R.; Wynn, T. A. *Immunol. Cell Biol.* **2007**, *85*, 148−154.

(11) Esch, G. W.; Fernandez, J. C. *Am. Midl. Nat.* **1994**, *131*, 209−237.

(12) Hockley, D. J.; McLaren, D. J.; Ward, B. J.; Nermut, M. V. *Tissue Cell* **1975**, *7*, 485−496.

(13) Wilson, R. A.; Barnes, P. E. *Parasitology* **1974**, *68*, 239−258.

(14) Rogers, S. H.; Bueding, E. *Int. J. Parasitol.* **1975**, *5*, 369−371.

(15) Van Hellemond, J. J.; Retra, K.; Brouwers, J. F. H. M.; van Balkom, B. W. M.; Yazdanbakhsh, M.; Shoemaker, C. B.; Tielens, A. G. M. *Int. J. Parasitol.* **2006**, *36*, 691−699.

(16) McLaren, D. J.; Hockley, D. J. *Nature* **1977**, *269*, 147−149.

(17) Maizels, R. M.; Bundy, D. A. P.; Selkirk, M. E.; Smith, D. F.; Anderson, R. M. *Nature* **1993**, *365*, 797.

(18) Pearce, E. J.; MacDonald, A. S. *Nat. Rev. Immunol.* **2002**, *2*, 499−511.

(19) van der Kleij, D.; Yazdanbakhsh, M. *Eur. J. Immunol.* **2003**, *33*, 2953−2963.

(20) Hulstijn, M.; Barros, L. de A.; Neves, R. H.; de Moura, E. G.; Machado-Silva, J. R. *Exp. Parasitol.* **2011**, *129*, 42−47.

(21) Spengler, B.; Hubert, M.; Kaufmann, R. Presented at the *42nd Annual Conference on Mass Spectrometry and Allied Topics*, 1994.

(22) Koestler, M.; Kirsch, D.; Hester, A.; Leisner, A.; Guenther, S.; Spengler, B. *Rapid Commun. Mass Spectrom.* **2008**, *22*, 3275−3285.

(23) Spengler, B. *Anal. Chem.* **2015**, *87*, 64−82.

(24) Hameed, S.; Ikegami, K.; Sugiyama, E.; Matsushita, S.; Kimura, Y.; Hayasaka, T.; Sugiura, Y.; Masaki, N.; Waki, M.; Ohta, I.; Hossen, M. A.; Setou, M. *Anal. Bioanal. Chem.* **2015**, *407*, 7589−7602.

(25) Khalil, S. M.; Pretzel, J.; Becker, K.; Spengler, B. *Int. J. Mass Spectrom.* **2017**, *416*, 1−19.

(26) Khalil, S. M.; Rompp, A.; Pretzel, J.; Becker, K.; Spengler, B. *Anal. Chem.* **2015**, *87*, 11309−11316.

(27) Niehoff, A.-C.; Schulz, J.; Soltwisch, J.; Meyer, S.; Kettling, H.; Sperling, M.; Jeibmann, A.; Dreisewerd, K.; Francesconi, K. A.; Schwerdtle, T.; Karst, U. *Anal. Chem.* **2016**, *88*, 5258−5263.

(28) Ly, A.; Buck, A.; Balluff, B.; Sun, N.; Gorzolka, K.; Feuchtinger, A.; Janssen, K.-P.; Kuppen, P. J. K.; van de Velde, C. J. H.; Weirich, G.; Erlmeier, F.; Langer, R.; Aubele, M.; Zitzelsberger, H.; McDonnell, L.; Aichler, M.; Walch, A. *Nat. Protoc.* **2016**, *11*, 1428.

(29) Pietrowska, M.; Gawin, M.; Polańska, J.; Widłak, P. *Proteomics* **2016**, *16*, 1670−1677.

(30) Römpp, A.; Spengler, B. *Histochem. Cell Biol.* **2013**, *139*, 759−783.

(31) Kawamoto, T. *Arch. Histol. Cytol.* **2003**, *66*, 123−143.

(32) Brignole-Baudouin, F.; Desbenoit, N.; Hamm, G.; Liang, H.; Both, J. P.; Brunelle, A.; Fournier, I.; Guerineau, V.; Legouffe, R.; Stauber, J.; Touboul, D.; Wisztorski, M.; Salzet, M.; Laprevote, O.; Baudouin, C. *PLoS One* **2012**, *7*, No. e50180.

(33) Altelaar, A. F.; van Minnen, J.; Jimenez, C. R.; Heeren, R. M.; Piersma, S. R. *Anal. Chem.* **2005**, *77*, 735−741.

(34) Kompauer, M.; Heiles, S.; Spengler, B. *Nat. Methods* **2017**, *14*, 90.

(35) Hankin, J. A.; Barkley, R. M.; Murphy, R. C. *J. Am. Soc. Mass Spectrom.* **2007**, *18*, 1646−1652.

(36) Paine, M. R. L.; Kooijman, P. C.; Fisher, G. L.; Heeren, R. M. A.; Fernandez, F. M.; Ellis, S. R. *J. Mater. Chem. B* **2017**, *5*, 7444−7460.

(37) Soltwisch, J.; Kettling, H.; Vens-Cappell, S.; Wiegelmann, M.; Muthing, J.; Dreisewerd, K. *Science (Washington, DC, U. S.)* **2015**, *348*, 211−215.

(38) Korte, A. R.; Yandeau-Nelson, M. D.; Nikolau, B. J.; Lee, Y. J. *Anal. Bioanal. Chem.* **2015**, *407*, 2301−2309.

(39) Kompauer, M.; Heiles, S.; Spengler, B. *Nat. Methods* **2017**, *14*, 1156.

(40) Bartels, B.; Kulkarni, P.; Danz, N.; Bocker, S.; Saluz, H. P.; Svatos, A. *RSC Adv.* **2017**, *7*, 9045−9050.

(41) Meyer, F.; Meyer, H.; Bueding, E. *Biochim. Biophys. Acta, Lipids Lipid Metab.* **1970**, *210*, 257−266.

(42) Brouwers, J. F.; Versluis, C.; van Golde, L. M. G.; Tielens, A. G. M. *Biochem. J.* **1998**, *334*, 315−319.

(43) Retra, K.; deWalick, S.; Schmitz, M.; Yazdanbakhsh, M.; Tielens, A. G. M.; Brouwers, J. F. H. M.; van Hellemond, J. J. *Int. J. Parasitol.* **2015**, *45*, 629−636.
(44) Brouwers, J. F. H. M.; Gadella, B. M.; van Golde, L. M. G.; Tielens, A. G. M. *J. Lipid Res.* **1998**, *39*, 344−353.
(45) Retra, K.; Bleijerveld, O. B.; van Gestel, R. A.; Tielens, A. G.; van Hellemond, J. J.; Brouwers, J. F. *Rapid Commun. Mass Spectrom.* **2008**, *22*, 1853−1862.
(46) Ferreira, M. S.; de Oliveira, D. N.; de Oliveira, R. N.; Allegretti, S. M.; Vercesi, A. E.; Catharino, R. R. *J. Mass Spectrom.* **2014**, *49*, 86−92.
(47) Grevelding, C. G. *Mol. Biochem. Parasitol.* **1995**, *71*, 269−272.
(48) Smithers, S. R.; Terry, R. J. *Parasitology* **1965**, *55*, 695−700.
(49) Paschke, C.; Leisner, A.; Hester, A.; Maass, K.; Guenther, S.; Bouschen, W.; Spengler, B. *J. Am. Soc. Mass Spectrom.* **2013**, *24*, 1296−1306.
(50) Fahy, E.; Sud, M.; Cotter, D.; Subramaniam, S. *Nucleic Acids Res.* **2007**, *35*, W606−W612.
(51) Wishart, D. S.; Tzur, D.; Knox, C.; Eisner, R.; Guo, A. C.; Young, N.; Cheng, D.; Jewell, K.; Arndt, D.; Sawhney, S.; Fung, C.; Nikolai, L.; Lewis, M.; Coutouly, M.-A.; Forsythe, I.; Tang, P.; Shrivastava, S.; Jeroncic, K.; Stothard, P.; Amegbey, G.; et al. *Nucleic Acids Res.* **2007**, *35*, D521−D526.
(52) Lu, Z.; Sessler, F.; Holroyd, N.; Hahnel, S.; Quack, T.; Berriman, M.; Grevelding, C. G. *Sci. Rep.* **2016**, *6*, 31150.
(53) van Meer, G.; Voelker, D. R.; Feigenson, G. W. *Nat. Rev. Mol. Cell Biol.* **2008**, *9*, 112−124.
(54) Siangcham, T.; Chansela, P.; Hayasaka, T.; Masaki, N.; Sroyraya, M.; Poljaroen, J.; Suwansa-Ard, S.; Engsusophon, A.; Hanna, P. J.; Sobhon, P.; Setou, M. *PLoS One* **2015**, *10*, No. e0120412.
(55) Han, X.; Gross, R. W. *J. Am. Soc. Mass Spectrom.* **1995**, *6*, 1202−1210.

DOI: 10.1021/acs.analchem.8b05440
Anal. Chem. 2019, 91, 4520−4528

Supplementary Information

Lipid topography in *Schistosoma mansoni* cryosections, revealed by micro-embedding and high-resolution atmospheric-pressure MALDI mass spectrometry imaging

Patrik Kadesch[1], Thomas Quack[2], Stefanie Gerbig[1], Christoph G. Grevelding[2], Bernhard Spengler[1,*]

1: Institute of Inorganic and Analytical Chemistry, Justus Liebig University Giessen, Heinrich-Buff-Ring 17, 35392 Giessen, Germany

2: Institute of Parasitology, Justus Liebig University Giessen, BFS, Schubertstrasse 81, 35392 Giessen, Germany

Table of contents

Supplementary Table 1: Database annotations based on LipidMaps database corresponding to MS images shown in Figure 3.

m/z	Δm to database in ppm	Assignment	Adduct
758.5693	1	PC(34:2)* PC(O-34:3(OH)) PC(P-34:2(OH)) PE(37:2) PE(P-37:2(OH))	$[M+H]^+$
		PC(34:1(OH)) PE(37:1(OH)) PS(O-36:1) PS(P-36:0)	$[M+H_2O+H]^+$
		PA(39:3)	$[M+NH_4]^+$
782.5674	1	PC(34:1)* PC(O-34:2(OH)) PC(P-34:1(OH)) PE(37:1) PE(O-37:2(OH)) PE(P-37:1(OH))	$[M+Na]^+$
810.5988	1	PC(36:1)* PC(O-36:2(OH)) PC(P-36:1(OH)) PE(39:1)	$[M+Na]^+$
All hits are based on database search - LipidMaps[50] * Described in literature[43,45]			

Supplementary Table 2: Database annotations based on human metabolome (HMDB) and LipidMaps database corresponding to MS images shown in Figure 4.

m/z	Δm to database in ppm	Substance	Adduct
786.6006	≤0.1	PC(36:2)[1,2] PC(O-36:3(OH))[1] PC(P-36:2(OH))[1] PE(39:2)[1]	$[M+H]^+$
		PC(36:1(OH))[1] PE(39:1(OH))[1] PS(O-38:1)[1] PS(P-38:0)[1]	$[M+H-H_2O]^+$
		PA(41:3)[1]	$[M+NH_4]^+$
1157.3592	<0.1	Heptasaccharide[3]	$[M-H_2O+Na]^+$
780.5514	<0.1	PC(34:2)[1,2] or PE(37:2)[1,2]	$[M+Na]^+$
[1] LipidMaps[50] [2] Described in literature[43,45] [3] Manually calculated from the sum formula			

Supplementary Table 3: Fragments of PC(36:2) found by MS/MSI.

Ion species	*m/z* experimental	*m/z* theoretical	Δm in ppm
$[M+Na]^+$	808.5823	808.5827	0.49
$[M-C_3H_9N+Na]^+$	749.5086	749.5092	0.80
$[M-C_3H_9N-C_2H_5O_4P]^+$	625.5164	625.5166	0.32
$[M-C_3H_9N-C_2H_4O_4PNa]^+$	603.5345	603.5347	0.33

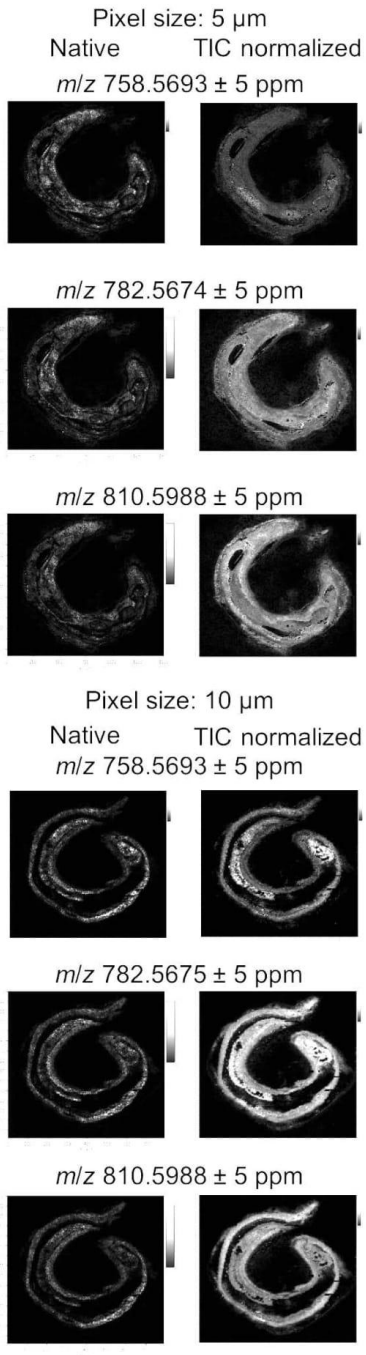

Supplementary Figure 1: Native ion images (left) compared to total-ion-current normalized ion images (right).

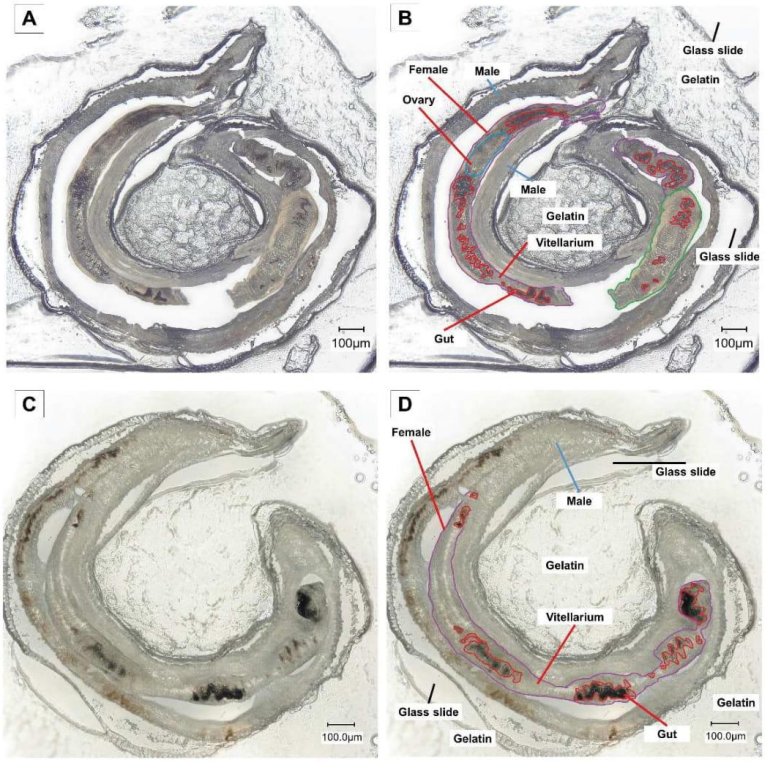

Supplementary Figure 2: Non-processed microscope images (A and C) of two consecutive tissue cryosections of a *Schistosoma mansoni* couple embedded in gelatin (Rx1500). Organs were annotated according to characteristic visual features such as shape and color, female parts marked in red, male parts marked in blue. The tissue fragment marked green in B was lost during matrix application, determined microscopically after MSI (data not shown).

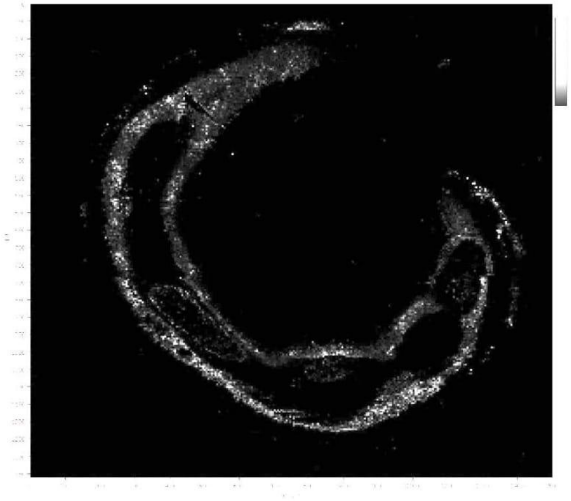

Supplementary Figure 3: Ion channel of *m/z* 995.3063 ± 5 ppm which can be assigned to hexasaccharides as $[M-H_2O+Na]^+$ with Δm= <1 ppm.

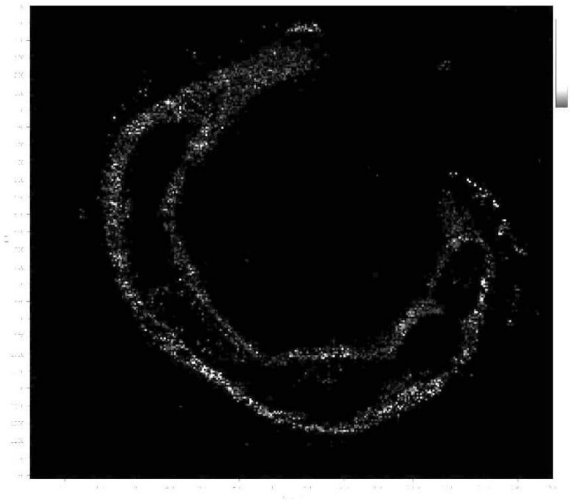

Supplementary Figure 4: Ion channel of *m/z* 1319.4112 ± 5 ppm, which can be assigned to octasaccharides as $[M-H_2O+Na]^+$ with Δm= <1 ppm.

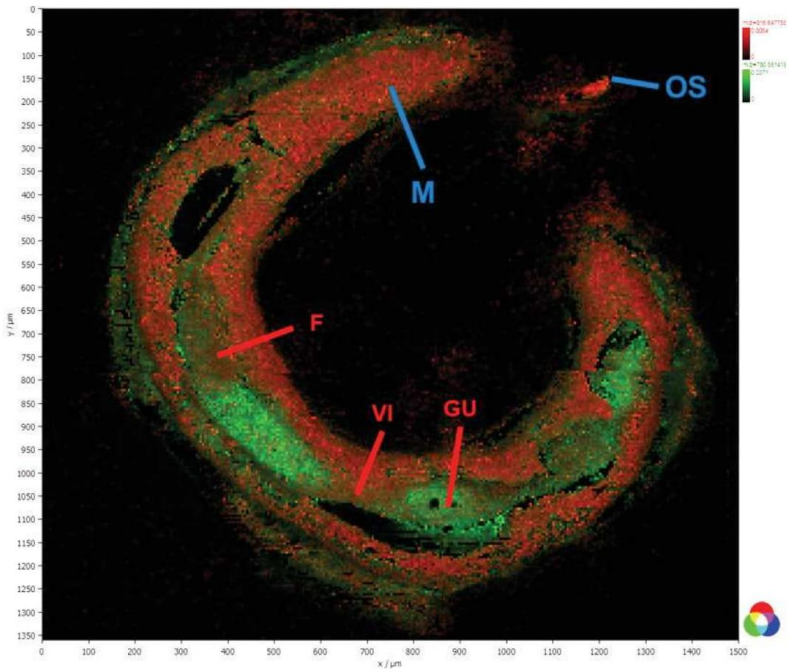

Supplementary Figure 5: AP-SMALDI MS image of a schistosome couple cryosection. Ion signals for red and green channel are different from those in Figure 4. Male (M) with oral sucker (OS) and Female (F) with vitellarium (VI) and gut (GU). Red channel – *m/z* 816.6478 assigned to PC(38:1) as $[M+H]^+$ Δm= <1 ppm.[45] Green channel – *m/z* 780.5514 assigned to PC(34:2) as $[M+Na]^+$ Δm= <1 ppm.[43,45]

Chapter III - Publication 2

Tissue- and sex-specific lipidomic analysis of *Schistosoma mansoni* using high-resolution atmospheric pressure scanning microprobe matrix-assisted laser desorption/ionization mass spectrometry imaging

Kadesch, Patrik*; Quack, Thomas[#]; Gerbig, Stefanie*; Grevelding, Christoph G.[#]; Spengler, Bernhard*

* Institute of Inorganic and Analytical Chemistry, Justus Liebig University Giessen, Giessen, Germany

[#] Institute of Parasitology, Justus Liebig University Giessen, Giessen, Germany

PLOS Neglected Tropical Diseases **2020**, 14(5), e0008145

RESEARCH ARTICLE

Tissue- and sex-specific lipidomic analysis of *Schistosoma mansoni* using high-resolution atmospheric pressure scanning microprobe matrix-assisted laser desorption/ionization mass spectrometry imaging

Patrik Kadesch[1], Thomas Quack[2], Stefanie Gerbig[1], Christoph G. Grevelding[2], Bernhard Spengler[1]*

1 Institute of Inorganic and Analytical Chemistry, Justus Liebig University Giessen, Giessen, Germany, **2** Institute of Parasitology, Justus Liebig University Giessen, Biomedical Research Center Seltersberg (BFS), Giessen, Germany

* Bernhard.spengler@anorg.chemie.uni-giessen.de

OPEN ACCESS

Citation: Kadesch P, Quack T, Gerbig S, Grevelding CG, Spengler B (2020) Tissue- and sex-specific lipidomic analysis of *Schistosoma mansoni* using high-resolution atmospheric pressure scanning microprobe matrix-assisted laser desorption/ionization mass spectrometry imaging. PLoS Negl Trop Dis 14(5): e0008145. https://doi.org/10.1371/journal.pntd.0008145

Editor: Neil David Young, The University of Melbourne, AUSTRALIA

Received: September 27, 2019

Accepted: February 16, 2020

Published: May 13, 2020

Data Availability Statement: All MS image files are available from the Metaspace database (Metaspace2020.eu)

Funding: Financial support by the Deutsche Forschungsgemeinschaft (DFG) under grants Sp314/13-1 and INST 162/500-1 FUGG and by the State of Hesse, LOEWE Center "DRUID", is gratefully acknowledged (all authors). PK received a scholarship by the Promotionskolleg

Abstract

Schistosomes are human pathogens causing the neglected tropical disease schistosomiasis, which occurs worldwide in (sub-)tropical regions. This infectious disease is often associated with poverty, and more than 700 million people are at risk of infection. Exploitation of novel habitats and limited therapeutic options brought schistosomes into research focus. Schistosomes are the only trematodes that have evolved separate sexes. They are covered by their metabolically active tegument, a surface area representing the interface between male and female in their permanent mating contact but also between parasite and host. The tegument comprises, besides others, numerous specific lipid compounds. Limited information is available on the exact lipid composition and its spatial distribution. We used atmospheric-pressure scanning microprobe matrix-assisted laser desorption/ionization (AP-SMALDI) mass spectrometry imaging (MSI) to characterize the *Schistosoma mansoni* tegument surface in comparison to tissue sections of whole worms or couples. We found that phosphatidylcholines (PC) and specific phosphatidylethanolamines (PE) are significantly more abundant inside the worm body compared to the tegument. On the other hand, the latter was found to be enriched in sphingomyelins (SM), phosphatidylserines (PS), lysophosphatidylcholines (LPC), and specific PE species. We further investigated lipid classes concerning number of carbon atoms in fatty acyl chains as well as the degree of unsaturation and found pronounced differences between the tegument and whole-worm body. Furthermore, differences between male and female teguments were found. The lipid composition of *S. mansoni* tissues has been investigated in an untargeted, spatially resolved manner for the first time.

"Bioressourcen und Biotechnologie" of the Technische Hochschule Mittelhessen and by Justus Liebig University. The funders had no role in study design, data collection and analysis, decision to publish, or preparation of the manuscript.

Competing interests: I have read the journal's policy and the authors of this manuscript have the following competing interests: Bernhard Spengler and CGG are consultants of TransMIT GmbH Giessen.

Author summary

WHO-defined Neglected Tropical Diseases, including schistosomiasis, are a burden for a significant part of the human world population. The fight against the diecious trematode *Schistosoma mansoni* can be supported by investigations of the specific molecular communication in male/female and in worm/host interactions. Improving the knowledge about *S. mansoni* is mandatory, since there is justified fear of the possibility of resistance development against the only available drug Praziquantel. We used mass spectrometry imaging as a powerful tool to provide topographic and tissue-specific information on the parasite. We investigated single male and female worms, as well as mating couples, regarding both, their inner tissue, and their intact surfaces, the tegument. We found highly specific lipid species and visualized their local distributions and abundances in high-resolution molecular images. Our findings may help to improve knowledge of the complex life cycles and of molecular communication mechanisms of schistosomes and may help to develop new drugs and strategies for treatment of the infectious disease.

Introduction

Schistosomiasis is a waterborne disease with about 280 million people affected and many more at risk.[1] Untreated, multiple clinical manifestations with potential mortal outcome occur, counting for more than 200,000 deaths per year.[1] Especially in children, severe developmental impairments are observed, estimated to account for millions of disability-adjusted life years.[2] The disease is caused by pathogens of the genus *Schistosoma (S. haematobium*, *S. japonicum*, and *S. mansoni)*. The World Health Organization (WHO) has classified schistosomiasis as one of the neglected tropical diseases due to global spreading and its poverty-related endemicity.[1] With Praziquantel, there is currently only one widely applied drug available, and there is no vaccine yet.

Schistosomes exhibit a complex life cycle. When *S. mansoni* eggs are exposed to water, male and female miracidia hedge, which are infective for intermediate snail hosts of the genus *Biomphalaria*. Within the snail, asexual reproduction occurs, and multiple generations of sporocysts are produced that finally lead to the generation of *cercariae*, which are released to the aqueous environment, being infective for vertebrates such as humans. Upon skin penetration of the final host, *cercariae* lose their tails and transform into schistosomula, which follow the blood stream to the liver while they mature to the adult life-stage. After mating of males and females, the couples migrate to the mesenteric plexus of the gut (or the bladder in case of *S. haematobium*), where they shed approximately 300 eggs daily, many of which leave the body via feces (*S. japonicum*, *S. mansoni*) or urine (*S. haematobium*).

One of the biological peculiarities of schistosomes is that they have evolved separate sexes during evolution, whereas all other trematodes are hermaphrodites. Furthermore, a constant pairing contact is necessary for sexual maturation of the female, which is achieved by pairing-induced mitogenic activity and subsequent differentiation of the gonads. The latter consist of the ovary and the vitellarium.[3]

As trematodes, adult schistosomes exhibit characteristic organs such as oral sucker (OS), required for nutrient uptake, elimination of metabolites and pathogen-host interaction,[4] a ventral sucker (VS) for motility, the gut (GU), testes (TE; in males), ovary (OV) and vitellarium (VI) in females, and the tegument (T), the outer surface structure covering the worm body. The physiologically active tegument is unique to *Neodermata* and exhibits several key

functions, crucial among others for nutrient uptake, host-parasite interaction, and survival.[5–10]

In the past couple of years, lipids have gained research interest not only as membrane components but also as functional constituents involved in cellular communication, key metabolic pathways, and as diagnostic markers.[11, 12] Therefore, various lipidomic studies have been conducted, contributing to our understanding of the characteristic lipid biology of schistosomes, especially in *S. mansoni*. For example, octadecenoic acid with a double bond position at Δ5, odd-chain fatty acyl phospholipid substituents, or long-chain fatty acids have been described.[13–18] Ceramides (Cer), known as signaling molecules, can be converted to sphingomyelins (SM) by addition of phosphocholine to the Cer hydroxyl head-group moiety.[19] By fluorescent lipid analogues, it has been demonstrated that SM of male schistosomes is synthesized from Cer, transported to the tegument and excreted to the medium.[19] Lipid extracts of whole-worms and tegument were analyzed by high performance liquid chromatography (HPLC), coupled to tandem mass spectrometry (MS), and it was shown that the tegument remarkably differs in phosphatidylserine (PS), phosphatidylcholine (PC), and lysophospholipid concentrations, compared to the inner part of the worm.[10] Great emphasis was placed on creating a comprehensive lipid atlas throughout all life stages of *S. mansoni*.[20] These data serve as the fundamental basis to investigate the functional role of specific lipids. The spatial information, which is lost during sample preparation for LC analysis, would strongly aid in understanding biological processes.

MALDI-MSI has been reported to be able to distinguish male and female based on individual *m/z*-signals.[21] However, discrimination was lacking when using unsupervised methods such as principle component analysis (PCA).[22] This was probably due to low spatial and mass resolution and/or topography-related signal intensity artifacts.

Mass spectrometry imaging (MSI)[23] adds valuable semi-quantitative, spatially resolved information to chemical investigations.[24] MSI is of special interest for untargeted metabolomics, because a wide variety of substance classes and valuable structural features can be assessed at once. One of the most advanced techniques with regard to spatial resolution is atmospheric pressure scanning microprobe matrix-assisted laser desorption/ionization (AP-S-MALDI)[25] MSI. It is well suited for lipidomic analysis and capable to achieve high lateral resolution of 5–10 μm pixel size,[25] and 1.4 μm with an experimental setup, respectively.[26] When operating at such high spatial resolution on rough surfaces, topography-related artifacts may occur as the depth of focus is only about 40 μm at 5 μm laser focus diameter.[27] If not corrected, this leads to severe artifacts during the MALDI process, which can be overcome by autofocusing for each pixel. [27]

To investigate the spatial distribution of lipids in paired *S. mansoni* adults, AP-SMALDI MSI has been utilized to compare tegumental surface-associated lipid signals to those present inside the whole-worm body. Lipid signals were annotated based on a combination of Metaspace[28] data repository and a home-built, LC-MS/MS-based database. Elevated signal intensities were observed for sphingomyelins (SM), phosphatidylserines (PS), and lysophosphatidylcholins (LPC) at the tegument surface, as well as phosphatidylcholines (PC) and phosphatidylethanolamines (PE) for the worm body. Differentially abundant fatty acyl substituents were also found when comparing lipid composition of surfaces and sections. Furthermore, data analysis revealed differences between male and female surfaces, an aspect not yet addressed in previous studies on male-female interaction in the biochemical context.

Methods

Quality grades and manufacturers of all chemicals used are shown in S1 Table.

Ethic statement

Animal experiments were performed in accordance with the European Convention for the Protection of Vertebrate Animals used for experimental and other scientific purposes (ETS No 123; revised Appendix A) and were approved by the Regional Council (Regierungspraesidium) Giessen (V54-19 c 20/15 c GI 18/10).

Schistosoma mansoni maintainance

Parasite maintenance was carried out as described elsewhere.[29] In brief, Syrian hamsters (*Mesocricetus auratus*) were infected with *cercariae* of *S. mansoni* (Liberian strain).[29] Worm couples were isolated 46 days post infection by hepatoportal perfusion.[30] Eggs were extracted from the livers of infected hamsters to obtain miracidia for infecting the intermediate snail host *Biomphalaria glabrata*.[29]

Fixation and cryosectioning

Directly after perfusion, schistosome couples were separated by repetitive pipetting to obtain individual worms with known pairing history. The worm samples were prepared as described elsewhere.[31] In brief, worms were fixed in 6.7% glutaraldehyde solution in phosphate-buffered saline and snap-frozen in liquid nitrogen. Cryosections of couples were prepared at 30–40 μm thickness using a cryotome (HM 525, Thermo Fisher Scientific) after micro-embedding in 8% gelatin. Sections were mounted to glass slides (VWR, Radnor, PA, USA) and stored at -80˚C until further analysis.

Lipid extraction

Lipid extraction was carried out using a methyl-tert butylether (MtBE) protocol.[32] 200–500 worms were homogenized in 50 μL ice-cold ammonium acetate (50 mM) in a potter homogenizer (glass). 600 μL methyl-tert butylether (MtBE) and 150 μL methanol were added and shaken at 4˚C for 1 h at 1,000 rpm (Thermomixer, Eppendorf, Hamburg, Germany). 200 μL water were added, shaken for 10 min (aforementioned conditions) and centrifuged at 1,000 x g for 5 min (Centrifuge 5804, Eppendorf). The organic phase was collected, and the aqueous phase was re-extracted with 400 μL MtBE, 120 μL methanol, and 100 μL water for 1 h (aforementioned conditions). After 5 min centrifugation at 1,000 x g, the organic phases were united, and the solvent was evaporated under a gentle stream of nitrogen in an ice bath until dryness. The dry extracts were dissolved in methanol:water 1:9 V/V to yield stock concentrations of 1 g of dried extract per mL and working solutions of 50 ng/μL.

LC-MS analysis

Separation was conducted by ultra-high performance liquid chromatography (UHPLC; "Ultimate3000 RS", Thermo Fisher Scientific, Bremen, Germany). The UHPLC was coupled to a "Q Exactive" orbital trapping mass spectrometer (Thermo Fisher Scientific, Bremen) via a heated electrospray ionization source (HESI II, Thermo Fisher Scientific) allowing data-dependent acquisition (DDA). The LC-MS method development was adapted from literature.[33] All parameters are shown in S2 Table.

AP-SMALDI MS imaging

Intact male or female worms were taken from the freezer and fixed to glass slides by a thin film of gelatin; alternatively, cryosections of couples were used. Digital light microscopic images were recorded with a microscope (VHX5000, Keyence, Osaka, Japan) with 250- to 1000-fold

magnification using a 3D-stitching mode. 2,5-dihydroxybenzoic acid (DHB, 30 mg/mL in acetone:water 1:1 V/V and 0.1% trifluoroacetic acid) was applied by pneumatic spraying of 70 μL of matrix solution at a flow rate of 10 μL/min, using a "SMALDIPrep" matrix preparation system (TransMIT GmbH, Giessen, Germany). The nebulizing nitrogen gas pressure was 1 bar. The sample was rotated with 500 rpm during pneumatic spraying.

For MS imaging, an autofocusing[27] "AP-SMALDI5 AF" ion source (TransMIT GmbH) was operated at 5 μm/pixel. 50 pulses/pixel were applied in positive-ion mode. An orbital trapping mass spectrometer ("Q Exactive HF", Thermo Fisher Scientific, Bremen), was operated in scan mode from m/z 500–2000 at a mass resolution of 240,000 and a typical mass accuracy $\leq$ 3 ppm, using the lock-mass function (m/z 716.12462 = $[5DHB\text{-}4H_2O+NH_4]^+$). The inlet capillary was heated to 250˚C, and a potential of 3 kV was applied between sample holder and inlet capillary. This setup enabled molecular topographic analyses of complex surfaces with high accuracy in mass and space at scan rates of about 1 pixel/s. Image sizes are listed in Table 1.

Data analysis

Data was converted into mzXML or MS2 file formats using Proteowizard[34] (v3.0.11028). The software packages LipidMatch[35] (v2.0.2) and Lipid Data Analyzer[36] (v2.6.2) were used for lipid identification based on fragmentation rules and retention time alignment, respectively. Only annotations found by both software tools were considered for database generation on lipid species level, specifying total fatty acyl chain lengths (or sphingosine base) and the number of double bonds. The data analysis process is visualized in S1 Fig. The database finally comprised triglycerides (TG), diglycerides (DG), sphingomyelins (SM), ceramides (Cer), phosphatidylcholines (PC), lyso-PC (LPC), phosphatidylethanolamines (PE), lyso-PE (LPE), phosphatidylserines (PS), phosphatidylglycerols (PG), and phosphatidylinositoles (PI) and included 469 lipid species in total.

MS imaging data were converted to imzML (imzML-converter v1.3[37]) and uploaded to Metaspace[28] for automated, FDR-controlled annotation using SwissLipids[38] database (data available through https://metaspace2020.eu/project/Kadesch-2019-Smansoni). Annotations were further processed manually for all measurements removing non-reproducible signals found in two or less samples (for graphical illustration see S2 Fig). Comparison with the aforementioned LC-MS database resulted in 227 lipids corresponding to 412 signals. Tissue regions were defined using region-of-interest (RoI) function in Mirion[39] (v3), exporting the mean, total ion current (TIC)-normalized signal intensities per RoI of aforementioned 412 m/z-signals (RoI was saved to imzML file). One RoI per MSI dataset was defined, to yield signal intensities for three biological replicates per class (worm body, male and female surfaces), enabling statistical analysis. For statistical analyses, the data matrix was imported to Perseus[40, 41] (v1.6.1.3), and the classification of lipid marker signals was done by hierarchical clustering (see step-by-step protocol in S3 Fig). MS ion images were visualized through MSiReader[42, 43] (v1) using the TIC normalization feature.

Table 1. MSI image dimensions of acquired data files; 5 μm/pixel, autofocusing mode, positive-ion polarity.

biological replicate number	male surface	female surface	mated couple section
1	280 x 280	400 x 174	340 x 300
2	400 x 300	235 x 275	290 x 265
3	420 x 270	300 x 260	300 x 272

https://doi.org/10.1371/journal.pntd.0008145.t001

Results and discussion

Comparison of surface/tegument versus worm body tissue

Because of the uniqueness of the tegument, knowledge about its lipidome is of high interest. Only very few studies addressed the lipid composition of this highly specialized surface structure by MS.[9, 10, 21] Additionally, MSI studies have been conducted aiming to differentiate strains and sexes by MALDI-TOF (time of flight) MSI at low resolutions in both, mass and space, not ideally suited for untargeted metabolomics analysis.[21, 22] To shed further light onto the lipidome of the schistosome tegument, we performed AP-SMALDI MSI to characterize the surface area in comparison to the whole-body worm tissue at the molecular level. Since the tegument comprises an approximately 17 nm thick heptalaminate outer membrane,[44] it was not possible to discriminate different layers of the tegument and we therefore further refer to the term surface. Each worm was 5–10 mm long and less than 1 mm thick. The focal depth of the AP-SMALDI ion source at 5 μm lateral resolution is in the range of 40 μm, demanding for pixelwise laser focusing to obtain artifact-free MSI analysis.

Prior to data acquisition by MSI, microscope images were taken as shown in Fig 1A (more detailed in S4 Fig). Surface measurements of males (M) and females (F) are shown on the left side of Fig 1A and 1C–1F, while tissue sections of couples in biological triplicates are shown on the right side. The black arrow indicates the anterior end of the worms.

After mass spectrometric data acquisition, hierarchical clustering (HC) was performed based on relative signal intensities averaged over the whole tissue–containing area (Fig 1B). The signals shown in the HC can be separated in three major parts; specific signals for worm body tissue (red box) and surface (male and female; green box) and unspecific signals (blue box). Surface- or tissue-specific signals were obtained, although the number of unspecific signals predominated in this approach. The latter signals were classified as unspecific, because signal intensities varied between the biological replicates in excess of 5%, and/or insignificant differences occurred when comparing biological classes (surface vs tissue of adult worms). HC served as a ranking system for subsequent visualization of corresponding MS ion images by MSiReader (Fig 1C–1F), setting a mass deviation of ± 5 ppm for MS image generation.

Fig 1C shows an ion signal at m/z 742.5381 in blue, which was categorized unspecific by HC. The signal was assigned to protonated PE (36:3) and shows a homogenous distribution throughout all measurements and locations. The red ion channel in Fig 1D shows a signal, which is significantly upregulated inside the worm body. This signal was detected at m/z 786.6007 and was assigned to the protonated molecule of PC (36:2). Signals upregulated at the surface were also found as indicated by m/z 805.6194 in green (Fig 1E), which can be assigned to SM (40:3) as sodiated molecule. Additionally, the tegumental contours of the male and female worms can be observed in the cryosections by the same signal, confirming its higher abundance on the surface. The differential composition between surface and worm-body tissue becomes even more obvious in the red-green-blue overlay (RGB) (Fig 1F). While the whole worms are dominated by green colour, the sections are mostly red/purple. The classification approach by multivariate statistical analysis, particularly HC, was successfully used to classify m/z-signal intensities with respect to localized lipid compositions.

Since ion images of individual lipid species are not representative for the abundance of the entire lipid class, we continued to investigate the signal intensities from worm surface and inner tissue for all lipid classes mentioned. Thereby, a number of marker signals were obtained being characteristic for either worm surface or inner tissue, not necessarily as the most abundant lipid species in the tissues, but rather signals of discrimination. Results are shown as Bar chart in **Fig 2**. A detailed description of all lipids summarized here can be found in S3 Table.

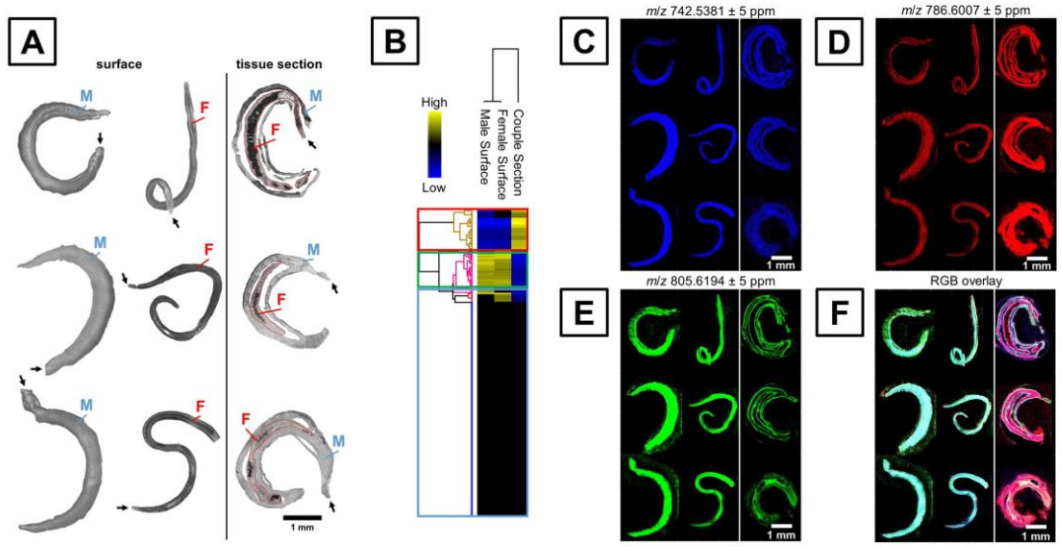

Fig 1. Results of MS imaging analysis conducted in positive-ion mode followed by multivariate statistical analysis. A–Light microscopic images of male (M) and female (F) *S. mansoni* surfaces and cryosections of couples recorded prior to matrix application. Black arrows indicate anterior end. All images are drawn to scale. B–Hierarchical clustering of mean TIC-normalized signal intensities indicating differentially abundant lipids on the surface versus inner tissue. Signals with elevated intensities in worm bodies are marked with a red box, prominent surface signals are boxed in green, and indifferent signals are indicated by a blue box. C–AP-SMALDI MS image of an indifferent signal at *m/z* 742.5381, equally distributed among surface and tissue, which was assigned to PE (36:3) as protonated molecule. D–MS image at *m/z* 786.6007 assigned to $[PC (36:2) + H]^+$, showing increased signal intensities in the worm section. E–MS image at *m/z* 805.6194 assigned to SM (40:3) as sodiated ion, upregulated in the worm surface of males and females. F–Red-green-blue (RGB)-overlay of MS ion channels C to E, depicting the differences between surface and inner tissues. In total, the MS ion images comprised ~840,000 spectra, acquired with a spatial resolution of 5 μm in positive-ion mode.

https://doi.org/10.1371/journal.pntd.0008145.g001

The extensive variation between surface and inner tissue can be recognized easily. The sum composition comprising all entities which passed analysis of variance (ANOVA) testing at a false-discovery-rate (FDR) of 5%, are shown in Fig 2A. Nine lipid classes are included in the diagram. TG, PE and PC formed the largest fractions.

Signals that were highly abundant inside the worm tissue are shown in Fig 2 (section). One significantly enriched species was a LPC, while all other marker signals exclusively belonged to the classes of PE and PC (20 substances per class). PE and PC lipid species can be isobaric and, therefore, are indiscriminable even at a high mass resolution of R = 240,000. However, using LC-MS/MS bulk analysis, we verified that both species were present in the worm although they were not distinguishable in MSI. PE and PC are common membrane constituents that determine membrane stability and rigidity.[45] Since the internal tissue of *S. mansoni* includes several tissue types and organs including the respective membranes, the observed predominance of PC and PE was expected. However, our findings are partially in contrast to previous publications which found a higher abundance of PC lipids in the tegument compared to the inner worm body by multiple-reaction-monitoring MS[10] and indirect quantitation by light scattering.[17] One explanation for this discrepancy might be that in our case, several isobaric lipids might have been analyzed as one signal. On the other hand, we did not take ion suppression effects into account, which can lead to altered signal intensity ratios compared to measurements with preceeding chromatographic separation. Two of the three major lipid

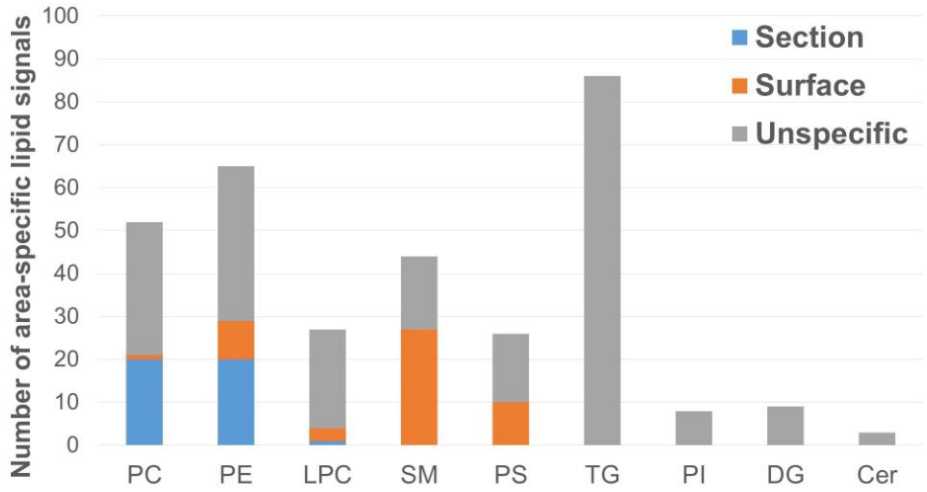

Fig 2. Location-specific lipids according to hierarchical clustering. Hierarchical clustering revealed specific lipid profiles inside the worm tissue (Section), on the worm surface (not discriminating between male and female) (Surface), and unspecific signals (either lacking intra-group reproducibility or significant inter-group differences) (Unspecific). Lipid sub-class abbreviations follow LipidMaps nomenclature.

https://doi.org/10.1371/journal.pntd.0008145.g002

constituents, indeed, show the same trend as described in previous publications (see S5 Fig). Another reason for disagreements is that tegument removal and lipid extraction are indirect methods, with intrinsic potential for artifact formation, compared to direct surface analysis by MSI.

A composition entirely different from the inner tissue was observed for the tegumental surface (Fig 2, in orange colour). The predominant class here was SM, besides PS and PE, and minor groups of LPC and PC. In comparison to the sum composition prior to HC, a relative specificity of SM and PS is obvious for the surface. It was reported previously, that SM accumulates at the *S. mansoni* surface where reversible breakdown to the respective ceramide lipids can occur.[19] The ceramides can enter the worm body freely while sphingomyelin is retained on the tegument.[19] Since these findings were derived from fluorescence microscopy, detailed information about individual lipid species was previously unavailable. Our findings enhance knowledge of SM species on the surface of schistosomes (see S3 Table). An increase in SM abundance is associated with increased membrane thickness and stability and has been well studied in a yeast model system.[45–47] However, the function of individual SM species remains unknown. PS have also been found in systematic studies of the tegument using a shotgun-lipidomics approach.[10] Our findings are well in accordance with this data. *S. mansoni*-derived PS could be of interest as they have been shown to act on toll-like receptor 2 (TLR2) in cell culture *in vitro*, in dependence of the fatty acyl substituents.[48] The binding pocket for PS on TLR2 might thus be a potential target for drug development. Minor signals of LPC and PC were found to be elevated on the surface. From literature it is known that *S. mansoni* has a rapid fatty acid turnover between phospholipid deacylation and reacylation.[17,18] Therefore, unraveling schistosomal PC acylases could be another topic in drug development.

In addition, signals with unspecific distribution were found in the tegument and in body tissue, showing no differential intensities within sample groups (Fig 2, unspecific). The lipid

class composition of these unspecific lipids was similar to the sum composition. It is remarkable that although TG comprise the largest group of lipids before clustering, all TG lipids were classified as unspecific. However, some TGs were in fact specific for male vs female surfaces (see chapter below), and may have been removed during statistical testing, due to lower signal intensities and therefore more unstable signals compared to e.g. PC. Low pH value has been shown for schistosoma tissue. [49] It is therefore reasonable that PC is positively net-charged and readily detectable with high signal intensities under ambient conditions.

PEs appeared as marker signals for both surface and worm tissue. We therefore further investigated the PE lipid class on a more detailed lipid-species level. Fig 3A shows a diagram depicting the fatty acyl chain lengths versus the number of double bonds in detected PE lipids. Signals found with elevated intensities in the worm tissue are shown as blue cross markers, signals elevated in the surface measurements are shown as orange symbols, and unspecific signals as green squares. Signals classified as both specific and -unspecific (e.g. PE (38:2), see Fig 3A) originated from the presence of multiple *m*/*z*-values caused by different adducts formed. While one adduct was detected as specific, another ion of the same lipid stayed below the threshold of being classified as specific.

The PE composition of surface marker signals appears to be systematically different form tissue-specific signals. Therefore, mean values of fatty acyl chain lengths and number of double bonds were calculated for each class (Fig 3B). Error bars represent the standard deviation between the PEs observed in each class. Herein, differences between surface (in orange) and worm body (in blue) with respect to fatty acyl chain lengths were observed. PE with decreased chain length were predominantly detected on the surface compared to the inner tissue. These trends were preserved when removing putative isobaric interferences of PE/PC as shown in S6 Fig. A decrease in length of the fatty acyl substituents might be associated with decreasing gel-to-liquid-crystalline phase transition (T_M), a measure for temperature stability of membranes, and therefore the temperature required to induce a disordered liquid crystalline phase, thus disrupting the ordered gel phase.[45] For *S. mansoni*, this may indicate that the tegument-associated-surface is more fluidic and thus less rigid compared to the inside. The fluidity could be correlated with the flexibility of the tegument needed for e.g. encapsulating the female during pairing and the subsequent migration of the couple as well as for the high metabolic activity of the tegument. Previously, an LC-MS based study found no differences in PE composition between tegument and worm body, most probably due to lacking methodical accuracy (overlapping error bars, lack of statistical significance).[10] In total, 17 PE species, all of which contain even-numbered fatty acid chains and at least one double bond, were found and quantified in their study.[10] Based on LC coupled with highly sensitive, high-resolution mass spectrometry, we were able to identify 42 PEs (see Fig 3A), some of which contained odd-numbered fatty acid chains (see raw data in S7 Fig) or fully saturated species. To verify that the PE assignments were correctly determined and to rule out isobaric bias, plots of *m*/*z* vs signal intensity were exemplarily assessed as shown in S8 Fig. Statistical categorization and assignment of quasi–isobaric PEs were confirmed for those species discriminable by MS. In total, 20 and 9 signals assigned to PEs were found to specifically occur in worm tissue and the tegument, respectively. PE (39:4) was detected as protonated species and as sodium adduct. The protonated ion was found to be specific for the worm surface, while the sodium adduct was found specifically in the inner worm tissue (see S9 Fig). This rare observation might indicate that either the sodium distribution in the worm was uneven or the ion signal intensities were influenced by an unknown isobaric interference.

Modeling the tegumental membrane of schistosomes could help to understand the complex tegumental surface structure in more detail, as well as lipid conversion processes such as PS synthesis.

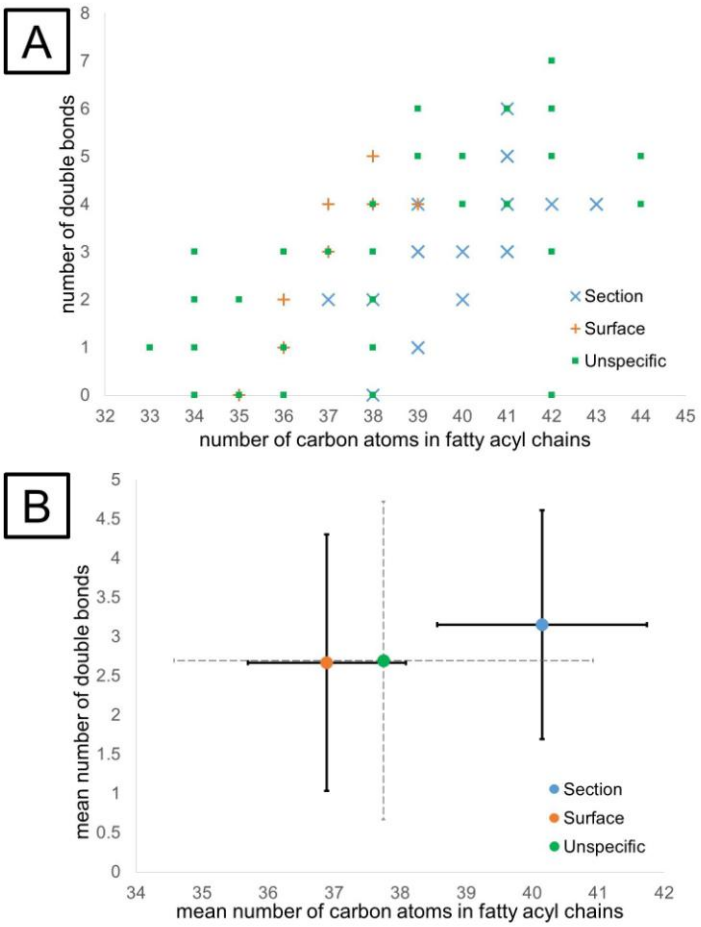

Fig 3. Number of carbon atoms in fatty acyl chains vs number of double bonds in detected phosphatidylethanolamines (PE). A–Worm tissue section-specific signals (blue cross), surface/tegument specific signals (orange +) and unspecific signals (green square). Overlapping indicators are attributed to the presence of several adducts corresponding to one lipid species. B–Arithmetic mean values of fatty acyl chain lengths and double bond numbers for worm tissue sections (blue), surface/tegument (orange) and unspecific signals (green). Error bars show the standard deviation across sections, surfaces and unspecific localizations, respectively.

https://doi.org/10.1371/journal.pntd.0008145.g003

Comparison of tegumental lipid composition of adult male and female *S. mansoni*

Male and female *S. mansoni* worms are morphologically discriminable, as the male contains a gynaecophoric canal and is thicker, due to a higher mass of musculature, but shorter compared to the female. After infection of humans, both sexes occur in identical environments, first the

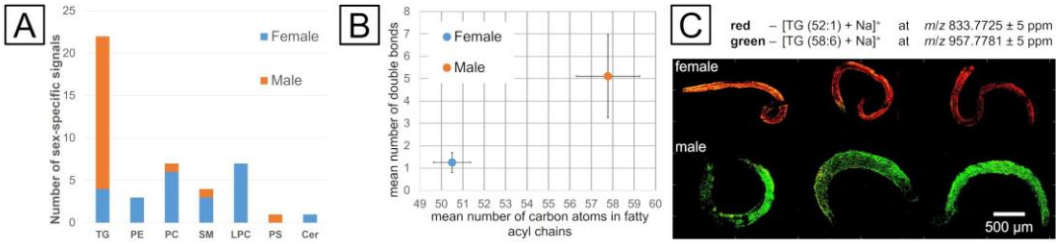

Fig 4. HC of the lipid data set to determine tegumental markers for male and female *S. mansoni*. A–Sum composition prior to statistical analysis (input) and classification based on hierarchical clustering into categories of male- and female-specific signals. B–Differences between male and female in triglyceride composition of the tegument with regard to mean number of carbon atoms in fatty acyl chains and number of double bonds. Error bars represent the standard deviation in each biological class. C–Red-Green (RG)-overlay of marker signals $[TG\ (52:1)+Na]^+$ (red) and $[TG\ (58:6)+Na]^+$ (green) for females (top) and males (bottom).

https://doi.org/10.1371/journal.pntd.0008145.g004

portal vein of the liver and later the mesenteric veins of the gut. The constant pairing contact, however, slightly changes this situation as the proportion of the dorsal surface of the female that is exposed to the host declines, since it is now mainly facing the gynaecophoric canal, the ventral part of the tegument of the male. Previous studies already demonstrated a remarkable consequence of pairing on the transcriptomes and proteomes of schistosome males and females following pairing.[3, 50, 51] Consequently, also differences in the lipid composition on the surface of male and female *S. mansoni* worms were hypothesized. Computational analyses were performed on the basis of the same dataset that was used to compare the lipid composition of *S. mansoni* surface and sections (Fig 1) to unravel sex-specific tegumental lipid-composition. The sum composition is identical to the aforementioned sum composition in Fig 2. Statistical analysis and HC provided differentially abundant signals for male (Fig 4A, in orange colour) and female (Fig 4A, in blue colour) worms. Additionally, composition of unspecific signals was similar to the sum composition. Differences between male and female surfaces seemed to be less pronounced compared to differences between surface and inner tissue. However, the surface of females was significantly enriched in phospholipids (LPC, PC and PE), sphingolipids (Cer and SM) and TG. A more detailed description of all classified lipids can be found in S4 Table. A former MSI study found TGs only in male but not female schistosomes, probably because worm couples were not separated prior to surface analysis.[21]

Especially molecules which can function in upstream signaling cascades are of high interest to gain insights into male-female interaction. Changes in Cer, SM and LPC are known to be strongly involved in signaling pathways and corresponding upstream signaling.[52, 53] However, more data are required to unravel the function of male- and female-specific surface lipids. For males, TG was the predominantly occurring lipid species, while one signal of each PC, PS and SM per class was more abundant when compared to females.

TG lipid species were found to be specific for both the surface of either males or females. For further investigations, the number of carbon atoms in fatty acyl chains was plotted against the number of double bonds in Fig 4B. The error bars represent the standard deviation of all TG species per class. TGs found in females are marked blue, species that were found in males are marked orange. Signals with increased intensities in females comprised shorter fatty acyl substituents and a decreased number of double bonds compared to the TG species in males. A decrease in fatty acyl chain lengths leads to an increase in fluidity, while the fluidity of TGs is proportional to fatty acyl unsaturation. The degree of unsaturation has a larger impact on tegument fluidity compared to the chain length of fatty acids. In sum this leads to increased fluidity

and thus decreased rigidity in TGs on the surface of males. The reason for this difference might be that the males' dorsal and ventral tegumental surfaces are directed towards the host and the female, respectively. Trans–tegumental nutrient uptake has to be performed by the males' dorsal tegument, whereas the ventral tegument is involved in male-female inter-tegumental signal transduction processes, because the ventral male tegument covers the tegumental surface of the female. Alternatively, accumulation of TG containing host-derived LDL-particles can occur,[54] and the tegumental surface of the male, available for binding of lipoprotein particles, is larger compared to the female while mated. Investigations of hamster whole blood by extraction and nESI-MS (data not shown) showed partially the same TG lipid species as obtained by MSI (shown in Fig 4). Therefore, TGs found on the surface might be explained by host-derived lipoprotein particles accumulating on the surface of schistosomes, which have been linked to immune evasion in *S. mansoni*.[9]

Differential lipid compositions between male and female were also visualized through the MS ion images shown in Fig 4C. The red colour channel shows *m/z* 833.7725, which is more abundant in female worms and has been assigned to TG (52:1) as sodiated molecule. The green ion channel represents a signal at *m/z* 957.7781 that was assigned to TG (58:6) found as a surface marker for male worms. The visualization of marker lipids for surfaces of male and female *S. mansoni* via ion images demonstrated that hierarchical clustering is a valuable statistical tool here, allowing for the reliable determination of signals with significantly altered abundance when comparing two or more sample cohorts.

Conclusions

AP-SMALDI MSI was used for spatially resolved investigation of lipids in adult *S. mansoni* couples, supported by lipid identification using LC-MS/MS for more reliable compound annotation. Authentic signal intensities were obtained from complex non-planar topographies, taking advantage of a novel autofocusing technology. The comparison of worm surface and inner tissues unraveled characteristic differences in composition at the lipid-class level. PC and PE were found to be more abundant inside the worms, while higher abundances of SM, PS, PE and LPC were observed at the surface. The number of carbon atoms in fatty acyl chains and the number of double bonds were investigated in detail, because PE lipid species were characteristic for both surface and inner tissue. Fatty acyl chain lengths of PE were found to be decreased at the surface, which may be associated with decreased rigidity.

Differential lipid compositions of male and female surfaces were also analyzed. Several lipids of TG class were found characteristic for the surface of one of the sexes. Decreased fatty acyl chain lengths in females and higher desaturation in males were detected, hinting towards increased membrane fluidity.

The advantage of AP-SMALDI MSI over classical, LC-MS based lipidomic methods is that the spatial distribution of a wide variety of compounds can be determined immediately from the tissue in a semi-quantitative manner. However, some isobaric lipid species like PEs and PCs are not easily discriminated based on MSI data and have to be identified using fragmentation experiments. At high spatial resolution (here 5 μm), the number of generated ions per spot drastically decreases, and fragmentation experiments are often hardly feasible. This might be overcome by further instrumental improvements. LC-based techniques on the other hand require time-consuming extraction methods, considered to be representative for different tissue types but putatively generating a bias. However, a wide variety of compounds and otherwise isobaric species can be separated, quantified, and identified by fragmentation experiments rapidly and in more detail. Therefore, both techniques (LC-MS/MS and MSI) in combination provide a promising platform for a comprehensive analysis.

For the first time, MSI has been used as a tool to characterize *S. mansoni* tegumental surfaces in comparison to whole-worm tissue sections. The suitability of AP-SMALDI MSI was demonstrated to explore locally different lipidomes. Furthermore, this approach allowed to associate specific lipid classes to tissue areas as well as to sex-specific differences at the whole-worm level and thus to testable hypotheses about their potential functions.

Supporting information

S1 Table. Specifications of chemicals used in experimental section.
(DOCX)

S2 Table. UHPLC-MS method for identification of lipids in S. mansoni. Injection volume was 50 μL.
(DOCX)

S3 Table. Detailed lipid annotations of classified lipids from comparison of tegument and inner worm tissue.
(DOCX)

S4 Table. Detailed lipid annotations of classified lipids from comparison of male and female tegument.
(DOCX)

S1 Fig. Graphical illustration of LC-MS^2 data analysis workflow.
(TIF)

S2 Fig. Graphical illustration of the data analysis workflow for MS imaging data. Statistical evaluation work flow was adapted from literature. The statistical analysis comprised five key steps: 1. normalization of one signal to the sum of all signals per measurement, 2. z-score (using median), 3. multiple-class analysis of variance (ANOVA, permutation based false-discovery-rate, FDR, set to 5%, 250 restarts), 4. post-hoc test (5% FDR) and 5. hierarchical clustering (Euclidean distance using average linkage, preprocessing with k-means, maximum 10 iterations, 10 restarts).
(TIF)

S3 Fig. Graphical illustration (from Perseus[41]) of multivariate statistical analysis and categorization of differentially abundant signals from MALDI experiments by hierarchical clustering.
(TIF)

S4 Fig. Digital light microscopic images of male (M) surfaces (left), female (F) surfaces (middle) and cryosections of couples (right). The black arrows indicate the anterior end.
(TIF)

S5 Fig. Distribution of previously reported most abundant lipid species in *S. mansoni* as protonated and sodiated ion species[20] PC (34:1) has been determined in the past to be differentially abundant in whole worm and tegument. [10] However, MS imaging data did not show significant differences based on HC. For PC (36:1) and PC (36:2), however, our findings are well in accordance with previous publications which found higher abundances inside the worm.[10] The same trend is suggested by unsupervised MS imaging data evaluation presented here.
(TIF)

S6 Fig. Number of carbon atoms in fatty acyl chains vs the number of double bonds detected in phosphatidylethanolamines (PE). Isobaric PE/PC interferences were excluded

for surface and section data. A–Comparison of worm-tissue (blue cross) and surface/tegument specific signals vs ions (orange +) with unspecific distribution (green square). Overlapping indicators are attributed to the presence of several adducts corresponding to one lipid species. B–Arithmetic mean fatty acyl and double bond composition for section/inner tissue (blue), surface/tegument (orange) and unspecific signals (green). Error bars show the standard deviation across one location.
(TIF)

S7 Fig. Example for LC-MS/MS based identification of PE (37:4) with MS1 overview spectra and data-dependent MS2 spectra. A–MS1 overview spectrum. B–virtual magnification of mass range m/z 700–800 (from A) showing the mass of PE (37:4) as deprotonated species ($C_{42}H_{75}NO_8P$). C–MS2 spectrum of precursor m/z 752.52 ±0.5 u showing characteristic fragments of PE head group (around m/z 140 and m/z 196), FA (17:0) and FA (20:4). The precursor is not visible in the spectrum and assumedly fragmented quantitatively at NCE = 30. D–virtual magnification of m/z 750–755 (from A) showing mass and isotope ratio of PE 37:4 as ^{12}C, ^{13}C and $^{13}C_2$ isotopologues.
(TIF)

S8 Fig. Example for mass accuracy and resolution obtained in MSI experiments. A–MS ion image of nearly isobaric PE-adduct species $[PE (39:5) + H]^+$ and $[PE (37:2) + Na]^+$ ($\Delta m = 3.1$ ppm) at m/z 780.5537 ± 5 ppm. B–Signal intensity (abundance in NL; normalized level) vs mass deviation in ppm. A double peak can be observed shifted by approximately 1.5 ppm and 2.8 ppm. C–MS ion signal at m/z 780.55254 ± 0.2 ppm showing an increased signal intensity on the worm surface assigned to protonated PE (39:5). D–MS ion at m/z 780.55151 ± 0.2 ppm assigned to PE (37:2) as sodium adduct. By hierarchical clustering, the signal at m/z 780.5537 was determined to be more abundant in the worm body compared to tegumental surface (see Fig 3). The signal was assigned to PE (37:2) as sodiated molecule. The protonated species of PE (39:5), however, was classified as unspecific. The fluctuating signal intensity of the surface measurements putatively led to unspecific classification. This example thus verifies the accuracy and correctness of HC-based classification.
(TIF)

S9 Fig. Putative adducts of PE (39:4) with different distributions. A—Distribution of m/z 782.5694 assigned to $[PE (39:4) + H]^+$. B–distribution of m/z 804.5514 assigned to $[PE (39:4) + Na]^+$. This difference in distribution could be explained by different concentrations of salt in tegument and inner tissue or by isobaric interferences that were not contained in the LC-MS/MS-database.
(TIF)

Author Contributions

Conceptualization: Christoph G. Grevelding, Bernhard Spengler.

Data curation: Patrik Kadesch, Thomas Quack, Stefanie Gerbig.

Formal analysis: Patrik Kadesch, Thomas Quack, Stefanie Gerbig.

Funding acquisition: Christoph G. Grevelding, Bernhard Spengler.

Investigation: Patrik Kadesch, Thomas Quack, Stefanie Gerbig.

Methodology: Thomas Quack, Stefanie Gerbig.

Project administration: Thomas Quack, Stefanie Gerbig.

Resources: Christoph G. Grevelding, Bernhard Spengler.

Supervision: Christoph G. Grevelding, Bernhard Spengler.

Validation: Patrik Kadesch, Thomas Quack, Stefanie Gerbig.

Writing – original draft: Patrik Kadesch, Thomas Quack, Stefanie Gerbig, Christoph G. Grevelding, Bernhard Spengler.

Writing – review & editing: Patrik Kadesch, Thomas Quack, Stefanie Gerbig, Christoph G. Grevelding, Bernhard Spengler.

References

1. World Health Organization. Integrating Neglected Tropical Diseases into Global Health and Development: Fourth WHO report on neglected tropical diseases. Geneva; 2017.
2. McManus DP, Dunne DW, Sacko M, Utzinger J, Vennervald BJ, Zhou X-N. Schistosomiasis. Nat Rev Dis Primers. 2018; 4(1):13. https://doi.org/10.1038/s41572-018-0013-8 PMID: 30093684
3. Lu Z, Sessler F, Holroyd N, Hahnel S, Quack T, Berriman M, et al. Schistosome sex matters: a deep view into gonad-specific and pairing-dependent transcriptomes reveals a complex gender interplay. Sci Rep. 2016; 6:31150. https://doi.org/10.1038/srep31150 PMID: 27499125
4. Skelly PJ, Da'dara AA, Li X-H, Castro-Borges W, Wilson RA. Schistosome feeding and regurgitation. PLoS pathog. 2014; 10(8):e1004246–e. https://doi.org/10.1371/journal.ppat.1004246 PMID: 25121497
5. McLaren DJ, Hockley DJ. Blood flukes have a double outer membrane. Nature. 1977; 269(5624):147–9. https://doi.org/10.1038/269147a0 PMID: 71658
6. Maizels RM, Bundy DA, Selkirk ME, Smith DF, Anderson RM. Immunological modulation and evasion by helminth parasites in human populations. Nature. 1993; 365(6449):797–805. https://doi.org/10.1038/365797a0 PMID: 8413664
7. Pearce EJ, MacDonald AS. The immunobiology of schistosomiasis. Nat Rev Immunol. 2002; 2:499. https://doi.org/10.1038/nri843 PMID: 12094224
8. van der Kleij D, Yazdanbakhsh M. Control of inflammatory diseases by pathogens: lipids and the immune system. Eur J Immunol. 2003; 33(11):2953–63. https://doi.org/10.1002/eji.200324340 PMID: 14579263
9. Van Hellemond JJ, Retra K, Brouwers JFHM, van Balkom BWM, Yazdanbakhsh M, Shoemaker CB, et al. Functions of the tegument of schistosomes: Clues from the proteome and lipidome. Int J Parasitol. 2006; 36(6):691–9. https://doi.org/10.1016/j.ijpara.2006.01.007 PMID: 16545817
10. Retra K, deWalick S, Schmitz M, Yazdanbakhsh M, Tielens AGM, Brouwers JFHM, et al. The tegumental surface membranes of Schistosoma mansoni are enriched in parasite-specific phospholipid species. Int J Parasitol. 2015; 45(9):629–36.
11. Serhan CN, Chiang N, Van Dyke TE. Resolving inflammation: dual anti-inflammatory and pro-resolution lipid mediators. Nat Rev Immunol. 2008; 8:349. https://doi.org/10.1038/nri2294 PMID: 18437155
12. Hannun YA, Obeid LM. Principles of bioactive lipid signalling: lessons from sphingolipids. Nat Rev Mol Cell Bio. 2008; 9:139.
13. Retra K, Bleijerveld OB, van Gestel RA, Tielens AGM, van Hellemond JJ, Brouwers JF. A simple and universal method for the separation and identification of phospholipid molecular species. Rapid Commun Mass Spec. 2008; 22(12):1853–62.
14. Brouwers JF, Versluis C, van Golde LM, Tielens AG. 5-Octadecenoic acid: evidence for a novel type of fatty acid modification in schistosomes. Biochem J. 1998; 334 (Pt 2):315–9.
15. Smith TM, Brooks TJ, White HB. Fatty acid composition of adult Schistosoma mansoni. Lipids. 1969; 4 (1):31–6. https://doi.org/10.1007/BF02531791 PMID: 5766846
16. Meyer F, Meyer H, Bueding E. Lipid metabolism in the parasitic and free-living flatworms, Schistosoma mansoni and Dugesia dorotocephala. BBA—Lipids Lipid Met. 1970; 210(2):257–66.
17. Brouwers JF, Van Hellemond JJ, van Golde LM, Tielens AG. Ether lipids and their possible physiological function in adult Schistosoma mansoni. Mol Biochem Parasitol. 1998; 96(1–2):49–58. https://doi.org/10.1016/s0166-6851(98)00103-0 PMID: 9851606
18. Brouwers JF, Smeenk IM, van Golde LM, Tielens AG. The incorporation, modification and turnover of fatty acids in adult Schistosoma mansoni. Mol Biochem Parasitol. 1997; 88(1–2):175–85. https://doi.org/10.1016/s0166-6851(97)00091-1 PMID: 9274878

19. Redman CA, Kennington S, Spathopoulou T, Kusel JR. Interconversion of sphingomyelin and ceramide in adult Schistosoma mansoni. Mol Biochem Parasitol. 1997; 90(1):145–53. https://doi.org/10.1016/s0166-6851(97)00151-5 PMID: 9497039

20. Giera M, Kaisar MMM, Derks RJE, Steenvoorden E, Kruize YCM, Hokke CH, et al. The Schistosoma mansoni lipidome: Leads for immunomodulation. Anal Chim Acta. 2018; 1037:107–18. https://doi.org/10.1016/j.aca.2017.11.058 PMID: 30292284

21. Ferreira MS, de Oliveira DN, de Oliveira RN, Allegretti SM, Vercesi AE, Catharino RR. Mass spectrometry imaging: a new vision in differentiating Schistosoma mansoni strains. J Mass Spectrom. 2014; 49 (1):86–92. https://doi.org/10.1002/jms.3308 PMID: 24446267

22. Ferreira MS, de Oliveira RN, de Oliveira DN, Esteves CZ, Allegretti SM, Catharino RR. Revealing praziquantel molecular targets using mass spectrometry imaging: an expeditious approach applied to Schistosoma mansoni. Int J Parasitol. 2015; 45(6):385–91. https://doi.org/10.1016/j.ijpara.2014.12.008 PMID: 25812833

23. Spengler B, Hubert M, Kaufmann R. MALDI Ion Imaging and Biological Ion Imaging with a new Scanning UV-Laser Microprobe. 42nd Annual Conf On Mass Spectrom and Allied Topics. Chicago May 29—June 3, 1994, p1041.

24. Spengler B. Mass Spectrometry Imaging of Biomolecular Information. Anal Chem. 2015; 87(1):64–82. https://doi.org/10.1021/ac504543v PMID: 25490190

25. Koestler M, Kirsch D, Hester A, Leisner A, Guenther S, Spengler B. A high-resolution scanning microprobe matrix-assisted laser desorption/ionization ion source for imaging analysis on an ion trap/Fourier transform ion cyclotron resonance mass spectrometer. Rapid commun mass spec. 2008; 22(20):3275–85.

26. Kompauer M, Heiles S, Spengler B. Atmospheric pressure MALDI mass spectrometry imaging of tissues and cells at 1.4-μm lateral resolution. Nat Meth. 2017; 14:90.

27. Kompauer M, Heiles S, Spengler B. Autofocusing MALDI mass spectrometry imaging of tissue sections and 3D chemical topography of nonflat surfaces. Nat Meth. 2017; 14:1156.

28. Palmer A, Phapale P, Chernyavsky I, Lavigne R, Fay D, Tarasov A, et al. FDR-controlled metabolite annotation for high-resolution imaging mass spectrometry. Nature Meth. 2017; 14(1):57–60.

29. Grevelding CG. The female-specific W1 sequence of the Puerto Rican strain of Schistosoma mansoni occurs in both genders of a Liberian strain. Mol Biochem Parasitol. 1995; 71(2):269–72. https://doi.org/10.1016/0166-6851(94)00058-u PMID: 7477111

30. Smithers SR, Terry RJ. The infection of laboratory hosts with cercariae of Schistosoma mansoni and the recovery of the adult worms. Parasitology. 1965; 55(4):695–700. https://doi.org/10.1017/s0031182000086248 PMID: 4957633

31. Kadesch P, Quack T, Gerbig S, Grevelding CG, Spengler B. Lipid Topography in Schistosoma mansoni Cryosections, Revealed by Microembedding and High-Resolution Atmospheric-Pressure Matrix-Assisted Laser Desorption/Ionization (MALDI) Mass Spectrometry Imaging. Anal Chem. 2019; 91(7):4520–8. https://doi.org/10.1021/acs.analchem.8b05440 PMID: 30807108

32. Matyash V, Liebisch G, Kurzchalia TV, Shevchenko A, Schwudke D. Lipid extraction by methyl-tert-butyl ether for high-throughput lipidomics. J Lipid Res. 2008; 49(5):1137–46. https://doi.org/10.1194/jlr.D700041-JLR200 PMID: 18281723

33. Knittelfelder OL, Weberhofer BP, Eichmann TO, Kohlwein SD, Rechberger GN. A versatile ultra-high performance LC-MS method for lipid profiling. J Chromatogr B. 2014;951–952:119–28.

34. Chambers MC, Maclean B, Burke R, Amodei D, Ruderman DL, Neumann S, et al. A cross-platform toolkit for mass spectrometry and proteomics. Nat Biotechnol. 2012; 30:918. https://doi.org/10.1038/nbt.2377 PMID: 23051804

35. Koelmel JP, Kroeger NM, Ulmer CZ, Bowden JA, Patterson RE, Cochran JA, et al. LipidMatch: an automated workflow for rule-based lipid identification using untargeted high-resolution tandem mass spectrometry data. BMC bioinformatics. 2017; 18(1):331–. https://doi.org/10.1186/s12859-017-1744-3 PMID: 28693421

36. Hartler J, Trötzmüller M, Chitraju C, Spener F, Köfeler HC, Thallinger GG. Lipid Data Analyzer: unattended identification and quantitation of lipids in LC-MS data. Bioinformatics. 2011; 27(4):572–7. https://doi.org/10.1093/bioinformatics/btq699 PMID: 21169379

37. Race AM, Styles IB, Bunch J. Inclusive sharing of mass spectrometry imaging data requires a converter for all. J Prot. 2012; 75(16):5111–2.

38. Aimo L, Liechti R, Hyka-Nouspikel N, Niknejad A, Gleizes A, Gotz L, et al. The SwissLipids knowledgebase for lipid biology. Bioinformatics. 2015; 31(17):2860–6. https://doi.org/10.1093/bioinformatics/btv285 PMID: 25943471

39. Paschke C, Leisner A, Hester A, Maass K, Guenther S, Bouschen W, et al. Mirion—a software package for automatic processing of mass spectrometric images. J Am Soc Mass Spectr. 2013; 24(8):1296–306.

40. Cox J, Mann M. 1D and 2D annotation enrichment: a statistical method integrating quantitative proteomics with complementary high-throughput data. BMC bioinformatics. 2012; 13 Suppl 16(Suppl 16): S12–S.

41. Tyanova S, Temu T, Sinitcyn P, Carlson A, Hein MY, Geiger T, et al. The Perseus computational platform for comprehensive analysis of (prote)omics data. Nat Meth. 2016; 13(9):731–40.

42. Robichaud G, Garrard KP, Barry JA, Muddiman DC. MSiReader: An Open-Source Interface to View and Analyze High Resolving Power MS Imaging Files on Matlab Platform. J Am Soc Mass Spectr. 2013; 24(5):718–21.

43. Bokhart MT, Nazari M, Garrard KP, Muddiman DC. MSiReader v1.0: Evolving Open-Source Mass Spectrometry Imaging Software for Targeted and Untargeted Analyses. J Am Soc Mass Spectr. 2018; 29(1):8–16.

44. Hockley DJ, McLaren DJ. Schistosoma mansoni: Changes in the outer membrane of the tegument during development from cercaria to adult worm. Int J Parasitol. 1973; 3(1):13–20. https://doi.org/10.1016/0020-7519(73)90004-0 PMID: 4687430

45. de Kroon AI, Rijken PJ, De Smet CH. Checks and balances in membrane phospholipid class and acyl chain homeostasis, the yeast perspective. Prog lipid res. 2013; 52(4):374–94. https://doi.org/10.1016/j.plipres.2013.04.006 PMID: 23631861

46. Schneiter R, Brugger B, Sandhoff R, Zellnig G, Leber A, Lampl M, et al. Electrospray ionization tandem mass spectrometry (ESI-MS/MS) analysis of the lipid molecular species composition of yeast subcellular membranes reveals acyl chain-based sorting/remodeling of distinct molecular species en route to the plasma membrane. J Cell Biol. 1999; 146(4):741–54. https://doi.org/10.1083/jcb.146.4.741 PMID: 10459010

47. Klemm RW, Ejsing CS, Surma MA, Kaiser HJ, Gerl MJ, Sampaio JL, et al. Segregation of sphingolipids and sterols during formation of secretory vesicles at the trans-Golgi network. J Cell Biol. 2009; 185 (4):601–12. https://doi.org/10.1083/jcb.200901145 PMID: 19433450

48. van der Kleij D, Latz E, Brouwers JFHM, Kruize YCM, Schmitz M, Kurt-Jones EA, et al. A Novel Host-Parasite Lipid Cross-talk: SCHISTOSOMAL LYSO-PHOSPHATIDYLSERINE ACTIVATES TOLL-LIKE RECEPTOR 2 AND AFFECTS IMMUNE POLARIZATION. J Biol Chem. 2002; 277(50):48122–9. https://doi.org/10.1074/jbc.M206941200 PMID: 12359728

49. Faghiri Z, Camargo SMR, Huggel K, Forster IC, Ndegwa D, Verrey F, et al. The Tegument of the Human Parasitic Worm Schistosoma mansoni as an Excretory Organ: The Surface Aquaporin SmAQP Is a Lactate Transporter. PLOS ONE. 2010; 5(5):e10451. https://doi.org/10.1371/journal.pone.0010451 PMID: 20454673

50. Grevelding CG, Sommer G, Kunz W. Female-specific gene expression in Schistosoma mansoni is regulated by pairing. Parasitology. 1997; 115(6):635–40.

51. Cheng G-F, Lin J-J, Feng X-G, Fu Z-Q, Jin Y-M, Yuan C-X, et al. Proteomic analysis of differentially expressed proteins between the male and female worm of Schistosoma japonicum after pairing. Proteomics. 2005; 5(2):511–21. https://doi.org/10.1002/pmic.200400953 PMID: 15700243

52. Meyer zu Heringdorf D, Jakobs KH. Lysophospholipid receptors: Signalling, pharmacology and regulation by lysophospholipid metabolism. BBA Biomembranes. 2007; 1768(4):923–40. https://doi.org/10.1016/j.bbamem.2006.09.026 PMID: 17078925

53. Spiegel S, Foster D, Kolesnick R. Signal transduction through lipid second messengers. Curr Opin Cell Biol. 1996; 8(2):159–67. https://doi.org/10.1016/s0955-0674(96)80061-5 PMID: 8791422

54. Pereira ASA, Padilha RJR, Lima-Filho JL, Chaves MEC. Scanning electron microscopy of the human low-density lipoprotein interaction with the tegument of Schistosoma mansoni. Parasitol Res. 2011; 109 (5):1395–402. https://doi.org/10.1007/s00436-011-2386-4 PMID: 21503638

S1 Table. Specifications of chemicals used in experimental section.

https://doi.org/10.1371/journal.pntd.0008145.s001

Chemical name	Quality grade	Manufacturer
glutaraldehyde	grade I	Sigma-Aldrich, St. Louis, MO, USA
phosphate buffered saline	Gibco	Thermo Fisher Scientific, Bremen, Germany
gelatin	pharm. Eur.	VWR, Radnor, PA, USA
Methyl-tert butylether	for HPLC	Sigma-Aldrich, St. Louis, MO, USA
methanol	LiChroSolv	Merck, Darmstadt, Germany
water	LC-MS grade	VWR, Radnor, PA, USA
formic acid	for mass spectrometry	Honeywell, Morris Plains, NJ, USA
ammonium formate	99.995%	Sigma-Aldrich, St. Louis, MO, USA
2-propanol	for HPLC	VWR, Radnor, PA, USA
ammonium acetate	LC-MS grade	Honeywell, Morris Plains, NJ, USA
2,5-dihydroxy benzoic acid	for synthesis	Merck, Darmstadt, Germany
acetone	Uvasol	Merck, Darmstadt, Germany
trifluoro acetic acid	for spectroscopy	AppliChem, Darmstadt, Germany

S2 Table. UHPLC-MS method for identification of lipids in S. mansoni. Injection volume was 50 µL.

https://doi.org/10.1371/journal.pntd.0008145.s002

UHPLC-method		MS-method	
flow rate in µL/min	90	**MS[1]**	
V(injection) in µL	50		
T(autosampler) in °C	5	*m/z*-range	± 300-1600
T(column oven) in °C	50	automatic gain control	10^6
stationary phase	BEH C18 Acquity (Waters, Milford, MA, USA), 150 x 1 mm, 1.7 µm particle size	Lock-masses (positive polarity only)	*m/z* 391.2843 and *m/z* 610.1842[55]
mobile phase A	water:methanol:2-propanol 6:5:9 v/v/v, 0.1% formic acid and 10 mM ammonium formate	**MS[2]**	
mobile phase B	methanol:2-propanol 1:9 v/v, 0.1% formic acid and 10 mM ammonium formate	fragmentation mechanism	C-trap collisional dissociation (HCD)
t in min	%B	fragmentation energy in normalized collision energy (NCE)	25 (pos.) 30 (neg.)
0	0	*m/z*-selection	ten most intense
1	0	automatic gain control	10^5
31	100	isolation width	± 0.5 Da
41	100	charge inclusion	1 and 2
43	0	isotope exclusion	active
50	0	dynamic exclusion in s	15

S3 Table. Detailed lipid annotations of classified lipids from comparison of tegument and inner worm tissue.

https://doi.org/10.1371/journal.pntd.0008145.s003

					According to SwissLipids database				
Location with increased signal intenisty	Abbreviation	Addukt	Sum formula	mz	Lipid ID	Lipid class	SMILES (pH7.3)	CHEBI	Number of MSI datasets with positive annotation by Metaspace
Worm body tissue	PC(42:9)	M+H	C50H82NO8P	856,585 0596	SLM:0000 56583	SLM:0000 55211	C[N+](C)(C)CCOP([O-])(=O)OCC(COC([*])=O)OC([*])=O	0	9
Worm body tissue	PC(40:6)	M+Na	C48H84NO8P	856,582 6543	SLM:0000 56561	SLM:0000 55211	C[N+](C)(C)CCOP([O-])(=O)OCC(COC([*])=O)OC([*])=O	64431	4
Worm body tissue	PC(40:8)	M+H	C48H80NO8P	830,569 4095	SLM:0000 56563	SLM:0000 55211	C[N+](C)(C)CCOP([O-])(=O)OCC(COC([*])=O)OC([*])=O	0	3
Worm body tissue	PE(41:5)	M+Na	C46H82NO8P	830,567 0042	SLM:0000 57228	SLM:0000 55213	[NH3+]CCOP([O-])(=O)OCC(COC([*])=O)OC([*])=O	0	9
Worm body tissue	PC(42:6)	M+Na	C50H88NO8P	884,613 9544	SLM:0000 56580	SLM:0000 55211	C[N+](C)(C)CCOP([O-])(=O)OCC(COC([*])=O)OC([*])=O	66965	7
Worm body tissue	PC(42:6)	M+H	C50H88NO8P	862,632 0098	SLM:0000 56580	SLM:0000 55211	C[N+](C)(C)CCOP([O-])(=O)OCC(COC([*])=O)OC([*])=O	66965	7
Worm body tissue	PC(40:3)	M+Na	C48H90NO8P	862,629 6045	SLM:0000 56558	SLM:0000 55211	C[N+](C)(C)CCOP([O-])(=O)OCC(COC([*])=O)OC([*])=O	66863	9
Worm body tissue	LPC(20:1)	M+H	C28H56NO7P	550,386 6941	SLM:0000 55329	SLM:0000 55200	C[N+](C)(C)CCOP([O-])(=O)OCC(CO[*])O[*]	67057	9
Worm body tissue	PC(40:6)	M+H	C48H84NO8P	834,600 7096	SLM:0000 56561	SLM:0000 55211	C[N+](C)(C)CCOP([O-])(=O)OCC(COC([*])=O)OC([*])=O	64431	4
Worm body tissue	PE(41:3)	M+Na	C46H86NO8P	834,598 3043	SLM:0000 57226	SLM:0000 55213	[NH3+]CCOP([O-])(=O)OCC(COC([*])=O)OC([*])=O	0	5
Worm body tissue	PE(43:4)	M+H	C48H88NO8P	838,632 0098	SLM:0000 57246	SLM:0000 55213	[NH3+]CCOP([O-])(=O)OCC(COC([*])=O)OC([*])=O	0	5
Worm body tissue	PC(38:1)	M+Na	C46H90NO8P	838,629 6045	SLM:0000 56538	SLM:0000 55211	C[N+](C)(C)CCOP([O-])(=O)OCC(COC([*])=O)OC([*])=O	66860	3
Worm body tissue	PE(41:6)	M+H	C46H80NO8P	806,569 4095	SLM:0000 57229	SLM:0000 55213	[NH3+]CCOP([O-])(=O)OCC(COC([*])=O)OC([*])=O	0	5
Worm body tissue	PE(39:3)	M+Na	C44H82NO8P	806,567 0042	SLM:0000 57208	SLM:0000 55213	[NH3+]CCOP([O-])(=O)OCC(COC([*])=O)OC([*])=O	0	5

Worm body tissue	PE(41:4)	M+H	C46H84NO8P	810,6007096	SLM:0000 57227	SLM:0000 55213	[NH3+]CCOP([O-])(=O)OCC(COC([*])=O)OC([*])=O	0	8
Worm body tissue	PE(39:1)	M+Na	C44H86NO8P	810,5983043	SLM:0000 57206	SLM:0000 55213	[NH3+]CCOP([O-])(=O)OCC(COC([*])=O)OC([*])=O	0	9
Worm body tissue	PE(40:2)	M+H	C45H86NO8P	800,6163597	SLM:0000 57215	SLM:0000 55213	[NH3+]CCOP([O-])(=O)OCC(COC([*])=O)OC([*])=O	71742	7
Worm body tissue	PE(38:2)	M+H	C43H82NO8P	772,5850596	SLM:0000 57197	SLM:0000 55213	[NH3+]CCOP([O-])(=O)OCC(COC([*])=O)OC([*])=O	71735	9
Worm body tissue	PE(41:3)	M+H	C46H86NO8P	812,6163597	SLM:0000 57226	SLM:0000 55213	[NH3+]CCOP([O-])(=O)OCC(COC([*])=O)OC([*])=O	0	5
Worm body tissue	PC(36:0)	M+Na	C44H88NO8P	812,6139544	SLM:0000 56521	SLM:0000 55211	C[N+](C)(C)CCOP([O-])(=O)OCC(COC([*])=O)OC([*])=O	66858	9
Worm body tissue	PE(41:5)	M+H	C46H82NO8P	808,5850596	SLM:0000 57228	SLM:0000 55213	[NH3+]CCOP([O-])(=O)OCC(COC([*])=O)OC([*])=O	0	9
Worm body tissue	PC(36:2)	M+Na	C44H84NO8P	808,5826543	SLM:0000 56523	SLM:0000 55211	C[N+](C)(C)CCOP([O-])(=O)OCC(COC([*])=O)OC([*])=O	64433	9
Worm body tissue	PE(40:3)	M+H	C45H84NO8P	798,6007096	SLM:0000 57216	SLM:0000 55213	[NH3+]CCOP([O-])(=O)OCC(COC([*])=O)OC([*])=O	71743	7
Worm body tissue	PE(38:0)	M+Na	C43H86NO8P	798,5983043	SLM:0000 57195	SLM:0000 55213	[NH3+]CCOP([O-])(=O)OCC(COC([*])=O)OC([*])=O	71733	9
Worm body tissue	PC(40:7)	M+H	C48H82NO8P	832,5850596	SLM:0000 56562	SLM:0000 55211	C[N+](C)(C)CCOP([O-])(=O)OCC(COC([*])=O)OC([*])=O	0	9
Worm body tissue	PE(41:4)	M+Na	C46H84NO8P	832,5826543	SLM:0000 57227	SLM:0000 55213	[NH3+]CCOP([O-])(=O)OCC(COC([*])=O)OC([*])=O	0	8
Worm body tissue	PE(39:4)	M+Na	C44H80NO8P	804,5513541	SLM:0000 57209	SLM:0000 55213	[NH3+]CCOP([O-])(=O)OCC(COC([*])=O)OC([*])=O	0	8
Worm body tissue	PE(42:4)	M+H	C47H86NO8P	824,6163597	SLM:0000 57236	SLM:0000 55213	[NH3+]CCOP([O-])(=O)OCC(COC([*])=O)OC([*])=O	71751	9
Worm body tissue	PC(37:1)	M+Na	C45H88NO8P	824,6139544	SLM:0000 56531	SLM:0000 55211	C[N+](C)(C)CCOP([O-])(=O)OCC(COC([*])=O)OC([*])=O	0	9
Worm body tissue	PE(37:2)	M+H	C42H80NO8P	758,5694095	SLM:0000 57190	SLM:0000 55213	[NH3+]CCOP([O-])(=O)OCC(COC([*])=O)OC([*])=O	0	9
Worm body tissue	PE(39:1)	M+	C44H86	788,616	SLM:0000	SLM:0000	[NH3+]CCOP([O-	0	9

		H	NO8P	3597	57206	55213	])(=O)OCC(COC([*])=O)OC([*])=O		
Worm body tissue	PC(36:2)	M+H	C44H84NO8P	786,6007096	SLM:0000 56523	SLM:0000 55211	C[N+](C)(C)CCOP([O-])(=O)OCC(COC([*])=O)OC([*])=O	64433	9
Worm body tissue	PE(39:3)	M+H	C44H82NO8P	784,5850596	SLM:0000 57208	SLM:0000 55213	[NH3+]CCOP([O-])(=O)OCC(COC([*])=O)OC([*])=O	0	5
Worm body tissue	PC(34:0)	M+Na	C42H84NO8P	784,5826543	SLM:0000 56507	SLM:0000 55211	C[N+](C)(C)CCOP([O-])(=O)OCC(COC([*])=O)OC([*])=O	66855	8
Worm body tissue	PC(40:5)	M+H	C48H86NO8P	836,6163597	SLM:0000 56560	SLM:0000 55211	C[N+](C)(C)CCOP([O-])(=O)OCC(COC([*])=O)OC([*])=O	64524	9
Worm body tissue	PC(38:2)	M+Na	C46H88NO8P	836,6139544	SLM:0000 56539	SLM:0000 55211	C[N+](C)(C)CCOP([O-])(=O)OCC(COC([*])=O)OC([*])=O	66859	5
Worm body tissue	PC(37:1)	M+H	C45H88NO8P	802,6320098	SLM:0000 56531	SLM:0000 55211	C[N+](C)(C)CCOP([O-])(=O)OCC(COC([*])=O)OC([*])=O	0	9
Worm body tissue	PC(40:5)	M+Na	C48H86NO8P	858,5983043	SLM:0000 56560	SLM:0000 55211	C[N+](C)(C)CCOP([O-])(=O)OCC(COC([*])=O)OC([*])=O	64524	9
Worm body tissue	PC(42:8)	M+H	C50H84NO8P	858,6007096	SLM:0000 56582	SLM:0000 55211	C[N+](C)(C)CCOP([O-])(=O)OCC(COC([*])=O)OC([*])=O	0	5
Worm body tissue	PC(42:7)	M+H	C50H86NO8P	860,6163597	SLM:0000 56581	SLM:0000 55211	C[N+](C)(C)CCOP([O-])(=O)OCC(COC([*])=O)OC([*])=O	0	6
Worm body tissue	PE(43:4)	M+Na	C48H88NO8P	860,6139544	SLM:0000 57246	SLM:0000 55213	[NH3+]CCOP([O-])(=O)OCC(COC([*])=O)OC([*])=O	0	5
Unspecific distribution	LPC(22:4)	M+H	C30H54NO7P	572,3710441	SLM:0000 55339	SLM:0000 55200	C[N+](C)(C)CCOP([O-])(=O)OCC(CO[*])O[*]	0	6
Unspecific distribution	LPC(20:1)	M+Na	C28H56NO7P	572,3686387	SLM:0000 55329	SLM:0000 55200	C[N+](C)(C)CCOP([O-])(=O)OCC(CO[*])O[*]	67057	9
Unspecific distribution	LPC(22:5)	M+H	C30H52NO7P	570,355394	SLM:0000 55340	SLM:0000 55200	C[N+](C)(C)CCOP([O-])(=O)OCC(CO[*])O[*]	0	8
Unspecific distribution	LPC(20:2)	M+Na	C28H54NO7P	570,3529887	SLM:0000 55330	SLM:0000 55200	C[N+](C)(C)CCOP([O-])(=O)OCC(CO[*])O[*]	0	9
Worm Surface	SM(d36:1)	M+K	C41H83N2O6P	769,5620112	SLM:0003 90739	SLM:0000 01000	C[N+](C)(C)CCOP([O-])(=O)OC[C@H](NC([*])=O)[C@H](O)[*]	0	9
Worm Surface	SM(d40:2)	M+K	C45H89N2O6P	823,6089614	SLM:0003 90795	SLM:0000 01000	C[N+](C)(C)CCOP([O-])(=O)OC[C@H](NC([*])=O)[C@H](O)[*]	0	8

Worm Surface	SM(d40:3)	M+K	C45H87N2O6P	821,593 3114	SLM:0003 90793	SLM:0000 01000	C[N+](C)(C)CCOP([O-])(=O)OC[C@H](NC([*])=O)[C@H](O)[*]	0	9
Worm Surface	SM(d36:1)	M+Na	C41H83N2O6P	753,588 074	SLM:0003 90739	SLM:0000 01000	C[N+](C)(C)CCOP([O-])(=O)OC[C@H](NC([*])=O)[C@H](O)[*]	0	9
Worm Surface	SM(d42:2)	M+K	C47H93N2O6P	851,640 2616	SLM:0003 90823	SLM:0000 01000	C[N+](C)(C)CCOP([O-])(=O)OC[C@H](NC([*])=O)[C@H](O)[*]	0	8
Worm Surface	SM(d33:1)	M+Na	C38H77N2O6P	711,541 1238	SLM:0003 90704	SLM:0000 01000	C[N+](C)(C)CCOP([O-])(=O)OC[C@H](NC([*])=O)[C@H](O)[*]	0	9
Worm Surface	SM(d39:2)	M+Na	C44H87N2O6P	793,619 3741	SLM:0003 90780	SLM:0000 01000	C[N+](C)(C)CCOP([O-])(=O)OC[C@H](NC([*])=O)[C@H](O)[*]	0	9
Worm Surface	PE(38:5)	M+H	C43H76NO8P	766,538 1094	SLM:0000 57200	SLM:0000 55213	[NH3+]CCOP([O-])(=O)OCC(COC([*])=O)OC([*])=O	71738	9
Worm Surface	PE(36:2)	M+Na	C41H78NO8P	766,535 7041	SLM:0000 57181	SLM:0000 55213	[NH3+]CCOP([O-])(=O)OCC(COC([*])=O)OC([*])=O	71728	9
Worm Surface	SM(d38:2)	M+Na	C43H85N2O6P	779,603 7241	SLM:0003 90765	SLM:0000 01000	C[N+](C)(C)CCOP([O-])(=O)OC[C@H](NC([*])=O)[C@H](O)[*]	0	7
Worm Surface	PS(38:1)	M+K	C44H84NO10P	856,546 4207	SLM:0000 58892	SLM:0000 55218	[NH3+][C@@H](COP([O-])(=O)OCC(COC([*])=O)OC([*])=O)C([O-])=O	72072	8
Worm Surface	PS(40:1)	M+K	C46H88NO10P	884,577 7209	SLM:0000 58909	SLM:0000 55218	[NH3+][C@@H](COP([O-])(=O)OCC(COC([*])=O)OC([*])=O)C([O-])=O	72079	9
Worm Surface	SM(d40:1)	M+Na	C45H91N2O6P	809,650 6743	SLM:0003 90797	SLM:0000 01000	C[N+](C)(C)CCOP([O-])(=O)OC[C@H](NC([*])=O)[C@H](O)[*]	0	9
Worm Surface	PS(34:0)	M+K	C40H78NO10P	802,499 4705	SLM:0000 58861	SLM:0000 55218	[NH3+][C@@H](COP([O-])(=O)OCC(COC([*])=O)OC([*])=O)C([O-])=O	72057	9
Worm Surface	SM(d38:2)	M+K	C43H85N2O6P	795,577 6613	SLM:0003 90765	SLM:0000 01000	C[N+](C)(C)CCOP([O-])(=O)OC[C@H](NC([*])=O)[C@H](O)[*]	0	7
Worm Surface	PE(39:4)	M+H	C44H80NO8P	782,569 4095	SLM:0000 57209	SLM:0000 55213	[NH3+]CCOP([O-])(=O)OCC(COC([*])=O)OC([*])=O	0	8
Worm Surface	PE(37:4)	M+H	C42H76NO8P	754,538 1094	SLM:0000 57192	SLM:0000 55213	[NH3+]CCOP([O-])(=O)OCC(COC([*])=O)OC([*])=O	0	9

Worm Surface	PC(32:1)	M+Na	C40H78NO8P	754,535 7041	SLM:0000 56494	SLM:0000 55211	C[N+](C)(C)CCOP([O-])(=O)OCC(COC([*])=O)OC([*])=O	66849	7
Worm Surface	PS(42:2)	M+K	C48H90NO10P	910,593 3709	SLM:0000 58930	SLM:0000 55218	[NH3+][C@@H](COP([O-])(=O)OCC(COC([*])=O)OC([*])=O)C([O-])=O	72087	5
Worm Surface	PS(42:1)	M+K	C48H92NO10P	912,609 021	SLM:0000 58927	SLM:0000 55218	[NH3+][C@@H](COP([O-])(=O)OCC(COC([*])=O)OC([*])=O)C([O-])=O	72086	9
Worm Surface	SM(d42:2)	M+Na	C47H93N2O6P	835,666 3243	SLM:0003 90823	SLM:0000 01000	C[N+](C)(C)CCOP([O-])(=O)OC[C@H](NC([*])=O)[C@H](O)[*]	0	8
Worm Surface	SM(d40:3)	M+Na	C45H87N2O6P	805,619 3741	SLM:0003 90793	SLM:0000 01000	C[N+](C)(C)CCOP([O-])(=O)OC[C@H](NC([*])=O)[C@H](O)[*]	0	9
Worm Surface	PS(40:2)	M+K	C46H86NO10P	882,562 0708	SLM:0000 58911	SLM:0000 55218	[NH3+][C@@H](COP([O-])(=O)OCC(COC([*])=O)OC([*])=O)C([O-])=O	72080	9
Worm Surface	SM(d37:2)	M+Na	C42H83N2O6P	765,588 074	SLM:0003 90751	SLM:0000 01000	C[N+](C)(C)CCOP([O-])(=O)OC[C@H](NC([*])=O)[C@H](O)[*]	0	7
Worm Surface	PS(36:0)	M+K	C42H82NO10P	830,530 7707	SLM:0000 58875	SLM:0000 55218	[NH3+][C@@H](COP([O-])(=O)OCC(COC([*])=O)OC([*])=O)C([O-])=O	72064	9
Worm Surface	PS(38:0)	M+K	C44H86NO10P	858,562 0708	SLM:0000 58891	SLM:0000 55218	[NH3+][C@@H](COP([O-])(=O)OCC(COC([*])=O)OC([*])=O)C([O-])=O	72071	9
Worm Surface	SM(d33:1)	M+H	C38H77N2O6P	689,559 1792	SLM:0003 90704	SLM:0000 01000	C[N+](C)(C)CCOP([O-])(=O)OC[C@H](NC([*])=O)[C@H](O)[*]	0	9
Worm Surface	SM(d38:1)	M+Na	C43H87N2O6P	781,619 3741	SLM:0003 90767	SLM:0000 01000	C[N+](C)(C)CCOP([O-])(=O)OC[C@H](NC([*])=O)[C@H](O)[*]	0	9
Worm Surface	SM(d37:1)	M+Na	C42H85N2O6P	767,603 7241	SLM:0003 90753	SLM:0000 01000	C[N+](C)(C)CCOP([O-])(=O)OC[C@H](NC([*])=O)[C@H](O)[*]	0	9
Worm Surface	SM(d41:1)	M+Na	C46H93N2O6P	823,666 3243	SLM:0003 90811	SLM:0000 01000	C[N+](C)(C)CCOP([O-])(=O)OC[C@H](NC([*])=O)[C@H](O)[*]	0	9
Worm Surface	SM(d35:1)	M+Na	C40H81N2O6P	739,572 4239	SLM:0003 90726	SLM:0000 01000	C[N+](C)(C)CCOP([O-])(=O)OC[C@H](NC([*])=O)[C@H](O)[*]	0	9

Worm Surface	SM(d36:3)	M+H	C41H79N2O6P	727,574 8292	SLM:0003 90735	SLM:0000 01000	C[N+](C)(C)CCOP([O-])(=O)OC[C@H](NC([*])=O)[C@H](O)[*]	0	7
Worm Surface	SM(d39:1)	M+Na	C44H89N2O6P	795,635 0242	SLM:0003 90782	SLM:0000 01000	C[N+](C)(C)CCOP([O-])(=O)OC[C@H](NC([*])=O)[C@H](O)[*]	0	9
Worm Surface	SM(d42:1)	M+Na	C47H95N2O6P	837,681 9744	SLM:0003 90824	SLM:0000 01000	C[N+](C)(C)CCOP([O-])(=O)OC[C@H](NC([*])=O)[C@H](O)[*]	0	9
Worm Surface	SM(d40:2)	M+Na	C45H89N2O6P	807,635 0242	SLM:0003 90795	SLM:0000 01000	C[N+](C)(C)CCOP([O-])(=O)OC[C@H](NC([*])=O)[C@H](O)[*]	0	8
Worm Surface	LPC(20:3)	M+H	C28H52NO7P	546,355 394	SLM:0000 55331	SLM:0000 55200	C[N+](C)(C)CCOP([O-])(=O)OCC(CO[*])O[*]	0	6
Worm Surface	SM(d39:2)	M+H	C44H87N2O6P	771,637 4295	SLM:0003 90780	SLM:0000 01000	C[N+](C)(C)CCOP([O-])(=O)OC[C@H](NC([*])=O)[C@H](O)[*]	0	9
Worm Surface	PE(36:1)	M+H	C41H80NO8P	746,569 4095	SLM:0000 57180	SLM:0000 55213	[NH3+]CCOP([O-])(=O)OCC(COC([*])=O)OC([*])=O	71727	6
Worm Surface	PE(38:4)	M+H	C43H78NO8P	768,553 7594	SLM:0000 57199	SLM:0000 55213	[NH3+]CCOP([O-])(=O)OCC(COC([*])=O)OC([*])=O	71737	9
Worm Surface	PE(36:1)	M+Na	C41H80NO8P	768,551 3541	SLM:0000 57180	SLM:0000 55213	[NH3+]CCOP([O-])(=O)OCC(COC([*])=O)OC([*])=O	71727	6
Worm Surface	LPC(18:0)	M+Na	C26H54NO7P	546,352 9887	SLM:0000 55322	SLM:0000 55200	C[N+](C)(C)CCOP([O-])(=O)OCC(CO[*])O[*]	64561	9
Worm Surface	SM(d36:2)	M+Na	C41H81N2O6P	751,572 4239	SLM:0003 90737	SLM:0000 01000	C[N+](C)(C)CCOP([O-])(=O)OC[C@H](NC([*])=O)[C@H](O)[*]	0	9
Worm Surface	SM(d44:2)	M+Na	C49H97N2O6P	863,697 6244	SLM:0003 90849	SLM:0000 01000	C[N+](C)(C)CCOP([O-])(=O)OC[C@H](NC([*])=O)[C@H](O)[*]	0	9
Worm Surface	SM(d43:1)	M+Na	C48H97N2O6P	851,697 6244	SLM:0003 90838	SLM:0000 01000	C[N+](C)(C)CCOP([O-])(=O)OC[C@H](NC([*])=O)[C@H](O)[*]	0	3
Worm Surface	PS(34:2)	M+K	C40H74NO10P	798,468 1704	SLM:0000 58863	SLM:0000 55218	[NH3+][C@@H](COP([O-])(=O)OCC(COC([*])=O)OC([*])=O)C([O-])=O	72059	3
Worm Surface	PE(37:3)	M+H	C42H78NO8P	756,553 7594	SLM:0000 57191	SLM:0000 55213	[NH3+]CCOP([O-])(=O)OCC(COC([*])=O)OC([*])=O	0	9
Worm Surface	PE(35:0)	M+Na	C40H80NO8P	756,551 3541	SLM:0000 57172	SLM:0000 55213	[NH3+]CCOP([O-])(=O)OCC(COC([*])=O)OC([*])=O	0	9

Worm Surface	SM(d36:3)	M+Na	C41H79N2O6P	749,556 7739	SLM:0003 90735	SLM:0000 01000	C[N+](C)(C)CCOP([O-])(=O)OC[C@H](NC([*])=O)[C@H](O)[*]	0	7
Worm Surface	PS(35:0)	M+Na	C41H80NO10P	800,541 1834	SLM:0000 58868	SLM:0000 55218	[NH3+][C@@H](COP([O-])(=O)OCC(COC([*])=O)OC([*])=O)C([O-])=O	0	8
Worm Surface	LPC(17:0)	M+Na	C25H52NO7P	532,337 3386	SLM:0000 55321	SLM:0000 55200	C[N+](C)(C)CCOP([O-])(=O)OCC(CO[*])O[*]	0	9
Unspecific distribution	TG(64:8)	M+H	C67H114O6	1015,86 8796	SLM:0003 08472	SLM:0000 00400	[*]C(=O)OCC(COC([*])=O)OC([*])=O	0	4
Unspecific distribution	TG(62:5)	M+Na	C65H116O6	1015,86 6391	SLM:0003 08438	SLM:0000 00400	[*]C(=O)OCC(COC([*])=O)OC([*])=O	0	3
Unspecific distribution	TG(60:7)	M+K	C63H108O6	999,777 7275	SLM:0003 08410	SLM:0000 00400	[*]C(=O)OCC(COC([*])=O)OC([*])=O	0	3
Unspecific distribution	TG(62:7)	M+H	C65H112O6	989,853 1458	SLM:0003 08440	SLM:0000 00400	[*]C(=O)OCC(COC([*])=O)OC([*])=O	0	4
Unspecific distribution	TG(60:4)	M+Na	C63H114O6	989,850 7405	SLM:0003 08407	SLM:0000 00400	[*]C(=O)OCC(COC([*])=O)OC([*])=O	0	7
Unspecific distribution	TG(62:8)	M+H	C65H110O6	987,837 4957	SLM:0003 08441	SLM:0000 00400	[*]C(=O)OCC(COC([*])=O)OC([*])=O	0	4
Unspecific distribution	TG(60:5)	M+Na	C63H112O6	987,835 0904	SLM:0003 08408	SLM:0000 00400	[*]C(=O)OCC(COC([*])=O)OC([*])=O	0	7
Unspecific distribution	TG(62:9)	M+H	C65H108O6	985,821 8457	SLM:0003 08442	SLM:0000 00400	[*]C(=O)OCC(COC([*])=O)OC([*])=O	0	4
Unspecific distribution	TG(60:6)	M+Na	C63H110O6	985,819 4404	SLM:0003 08409	SLM:0000 00400	[*]C(=O)OCC(COC([*])=O)OC([*])=O	0	8
Unspecific distribution	TG(62:10)	M+H	C65H106O6	983,806 1956	SLM:0003 08428	SLM:0000 00400	[*]C(=O)OCC(COC([*])=O)OC([*])=O	0	4
Unspecific distribution	TG(60:7)	M+Na	C63H108O6	983,803 7903	SLM:0003 08410	SLM:0000 00400	[*]C(=O)OCC(COC([*])=O)OC([*])=O	0	3
Unspecific distribution	TG(62:11)	M+H	C65H104O6	981,790 5455	SLM:0003 08429	SLM:0000 00400	[*]C(=O)OCC(COC([*])=O)OC([*])=O	0	8
Unspecific distribution	TG(60:8)	M+Na	C63H106O6	981,788 1402	SLM:0003 08411	SLM:0000 00400	[*]C(=O)OCC(COC([*])=O)OC([*])=O	0	8

Unspecific distribution	TG(62:12)	M+H	C65H102O6	979,774 8955	SLM:0003 08430	SLM:0000 00400	[*]C(=O)OCC(COC([*])=O)OC([*])=O	0	7
Unspecific distribution	TG(60:9)	M+Na	C63H104O6	979,772 4902	SLM:0003 08412	SLM:0000 00400	[*]C(=O)OCC(COC([*])=O)OC([*])=O	0	8
Unspecific distribution	TG(58:4)	M+K	C61H110O6	977,793 3776	SLM:0003 08378	SLM:0000 00400	[*]C(=O)OCC(COC([*])=O)OC([*])=O	0	6
Unspecific distribution	TG(58:10)	M+K	C61H98O6	965,699 4772	SLM:0003 08371	SLM:0000 00400	[*]C(=O)OCC(COC([*])=O)OC([*])=O	0	3
Unspecific distribution	TG(60:6)	M+H	C63H110O6	963,837 4957	SLM:0003 08409	SLM:0000 00400	[*]C(=O)OCC(COC([*])=O)OC([*])=O	0	8
Unspecific distribution	TG(58:3)	M+Na	C61H112O6	963,835 0904	SLM:0003 08377	SLM:0000 00400	[*]C(=O)OCC(COC([*])=O)OC([*])=O	0	8
Unspecific distribution	TG(60:7)	M+H	C63H108O6	961,821 8457	SLM:0003 08410	SLM:0000 00400	[*]C(=O)OCC(COC([*])=O)OC([*])=O	0	3
Unspecific distribution	TG(58:4)	M+Na	C61H110O6	961,819 4404	SLM:0003 08378	SLM:0000 00400	[*]C(=O)OCC(COC([*])=O)OC([*])=O	0	6
Unspecific distribution	TG(60:8)	M+H	C63H106O6	959,806 1956	SLM:0003 08411	SLM:0000 00400	[*]C(=O)OCC(COC([*])=O)OC([*])=O	0	8
Unspecific distribution	TG(58:5)	M+Na	C61H108O6	959,803 7903	SLM:0003 08379	SLM:0000 00400	[*]C(=O)OCC(COC([*])=O)OC([*])=O	0	5
Unspecific distribution	TG(60:9)	M+H	C63H104O6	957,790 5455	SLM:0003 08412	SLM:0000 00400	[*]C(=O)OCC(COC([*])=O)OC([*])=O	0	8
Unspecific distribution	TG(58:6)	M+Na	C61H106O6	957,788 1402	SLM:0003 08380	SLM:0000 00400	[*]C(=O)OCC(COC([*])=O)OC([*])=O	0	5
Unspecific distribution	TG(60:10)	M+H	C63H102O6	955,774 8955	SLM:0003 08399	SLM:0000 00400	[*]C(=O)OCC(COC([*])=O)OC([*])=O	0	6
Unspecific distribution	TG(58:7)	M+Na	C61H104O6	955,772 4902	SLM:0003 08381	SLM:0000 00400	[*]C(=O)OCC(COC([*])=O)OC([*])=O	0	5
Unspecific distribution	TG(60:11)	M+H	C63H100O6	953,759 2454	SLM:0003 08400	SLM:0000 00400	[*]C(=O)OCC(COC([*])=O)OC([*])=O	0	9
Unspecific distribution	TG(58:8)	M+Na	C61H102O6	953,756 8401	SLM:0003 08382	SLM:0000 00400	[*]C(=O)OCC(COC([*])=O)OC([*])=O	0	3
Unspecific distribution	TG(56:3	M+K	C59H108	951,777	SLM:0003	SLM:0000	[*]C(=O)OCC(COC([*])=O)OC([*])=O	0	6

	)		O6	7275	08349	00400			
Unspecific distribution	TG(60:12)	M+H	C63H98O6	951,743 5953	SLM:0003 08401	SLM:0000 00400	[*]C(=O)OCC(COC([*])=O)OC([*])=O	0	7
Unspecific distribution	TG(58:9)	M+Na	C61H100O6	951,741 19	SLM:0003 08383	SLM:0000 00400	[*]C(=O)OCC(COC([*])=O)OC([*])=O	0	8
Unspecific distribution	TG(56:4)	M+K	C59H106O6	949,762 0775	SLM:0003 08350	SLM:0000 00400	[*]C(=O)OCC(COC([*])=O)OC([*])=O	0	6
Unspecific distribution	TG(58:10)	M+Na	C61H98O6	949,725 54	SLM:0003 08371	SLM:0000 00400	[*]C(=O)OCC(COC([*])=O)OC([*])=O	0	3
Unspecific distribution	TG(56:5)	M+K	C59H104O6	947,746 4274	SLM:0003 08351	SLM:0000 00400	[*]C(=O)OCC(COC([*])=O)OC([*])=O	0	6
Unspecific distribution	TG(57:5)	M+Na	C60H106O6	945,788 1402	SLM:0003 08364	SLM:0000 00400	[*]C(=O)OCC(COC([*])=O)OC([*])=O	0	3
Unspecific distribution	TG(56:6)	M+K	C59H102O6	945,730 7773	SLM:0003 08352	SLM:0000 00400	[*]C(=O)OCC(COC([*])=O)OC([*])=O	0	6
Unspecific distribution	TG(57:6)	M+Na	C60H104O6	943,772 4902	SLM:0003 08365	SLM:0000 00400	[*]C(=O)OCC(COC([*])=O)OC([*])=O	0	3
Unspecific distribution	TG(56:8)	M+K	C59H98O6	941,699 4772	SLM:0003 08354	SLM:0000 00400	[*]C(=O)OCC(COC([*])=O)OC([*])=O	0	3
Unspecific distribution	TG(58:4)	M+H	C61H110O6	939,837 4957	SLM:0003 08378	SLM:0000 00400	[*]C(=O)OCC(COC([*])=O)OC([*])=O	0	6
Unspecific distribution	TG(58:5)	M+H	C61H108O6	937,821 8457	SLM:0003 08379	SLM:0000 00400	[*]C(=O)OCC(COC([*])=O)OC([*])=O	0	5
Unspecific distribution	TG(56:2)	M+Na	C59H110O6	937,819 4404	SLM:0003 08348	SLM:0000 00400	[*]C(=O)OCC(COC([*])=O)OC([*])=O	0	8
Unspecific distribution	TG(58:6)	M+H	C61H106O6	935,806 1956	SLM:0003 08380	SLM:0000 00400	[*]C(=O)OCC(COC([*])=O)OC([*])=O	0	5
Unspecific distribution	TG(56:3)	M+Na	C59H108O6	935,803 7903	SLM:0003 08349	SLM:0000 00400	[*]C(=O)OCC(COC([*])=O)OC([*])=O	0	6
Unspecific distribution	TG(58:7)	M+H	C61H104O6	933,790 5455	SLM:0003 08381	SLM:0000 00400	[*]C(=O)OCC(COC([*])=O)OC([*])=O	0	5
Unspecific distribution	TG(56:4)	M+Na	C59H106O6	933,788 1402	SLM:0003 08350	SLM:0000 00400	[*]C(=O)OCC(COC([*])=O)OC([*])=O	0	6

Unspecific distribution	TG(58:8)	M+H	C61H102O6	931,774 8955	SLM:0003 08382	SLM:0000 00400	[*]C(=O)OCC(COC([*])=O)OC([*])=O	0	3
Unspecific distribution	TG(56:5)	M+Na	C59H104O6	931,772 4902	SLM:0003 08351	SLM:0000 00400	[*]C(=O)OCC(COC([*])=O)OC([*])=O	0	6
Unspecific distribution	TG(58:9)	M+H	C61H100O6	929,759 2454	SLM:0003 08383	SLM:0000 00400	[*]C(=O)OCC(COC([*])=O)OC([*])=O	0	8
Unspecific distribution	TG(56:6)	M+Na	C59H102O6	929,756 8401	SLM:0003 08352	SLM:0000 00400	[*]C(=O)OCC(COC([*])=O)OC([*])=O	0	6
Unspecific distribution	TG(58:10)	M+H	C61H98O6	927,743 5953	SLM:0003 08371	SLM:0000 00400	[*]C(=O)OCC(COC([*])=O)OC([*])=O	0	3
Unspecific distribution	TG(56:7)	M+Na	C59H100O6	927,741 19	SLM:0003 08353	SLM:0000 00400	[*]C(=O)OCC(COC([*])=O)OC([*])=O	0	5
Unspecific distribution	TG(54:2)	M+K	C57H106O6	925,762 0775	SLM:0003 08322	SLM:0000 00400	[*]C(=O)OCC(COC([*])=O)OC([*])=O	0	6
Unspecific distribution	TG(58:11)	M+H	C61H96O6	925,727 9453	SLM:0003 08372	SLM:0000 00400	[*]C(=O)OCC(COC([*])=O)OC([*])=O	0	8
Unspecific distribution	TG(56:8)	M+Na	C59H98O6	925,725 54	SLM:0003 08354	SLM:0000 00400	[*]C(=O)OCC(COC([*])=O)OC([*])=O	0	3
Unspecific distribution	PI(38:4)	M+K	C47H83O13P	925,520 2656	SLM:0000 58237	SLM:0000 55216	OC1C(O)C(O)C(OP([O-])(=O)OCC(COC([*])=O)OC([*])=O)C(O)C1O	0	3
Unspecific distribution	TG(56:9)	M+Na	C59H96O6	923,709 8899	SLM:0003 08355	SLM:0000 00400	[*]C(=O)OCC(COC([*])=O)OC([*])=O	0	3
Unspecific distribution	TG(54:5)	M+K	C57H100O6	919,715 1273	SLM:0003 08325	SLM:0000 00400	[*]C(=O)OCC(COC([*])=O)OC([*])=O	0	5
Unspecific distribution	TG(56:3)	M+H	C59H108O6	913,821 8457	SLM:0003 08349	SLM:0000 00400	[*]C(=O)OCC(COC([*])=O)OC([*])=O	0	6
Unspecific distribution	TG(56:5)	M+H	C59H104O6	909,790 5455	SLM:0003 08351	SLM:0000 00400	[*]C(=O)OCC(COC([*])=O)OC([*])=O	0	6
Unspecific distribution	TG(54:2)	M+Na	C57H106O6	909,788 1402	SLM:0003 08322	SLM:0000 00400	[*]C(=O)OCC(COC([*])=O)OC([*])=O	0	6
Unspecific distribution	PI(40:7)	M+H	C49H81O13P	909,548 7336	SLM:0000 58258	SLM:0000 55216	OC1C(O)C(O)C(OP([O-])(=O)OCC(COC([*])=O)OC([*])=O)C(O)C1O	0	4
Unspecific distribution	TG(56:6	M+	C59H102	907,774	SLM:0003	SLM:0000	[*]C(=O)OCC(COC([*])=O)OC([*])=O	0	6

	)	H	O6	8955	08352	00400			
Unspecific distribution	PI(38:5)	M+Na	C47H81O13P	907,530 6783	SLM:0000 58238	SLM:0000 55216	OC1C(O)C(O)C(OP([O-])(=O)OCC(COC([*])=O)OC([*])=O)C(O)C1O	0	4
Unspecific distribution	TG(56:7)	M+H	C59H100O6	905,759 2454	SLM:0003 08353	SLM:0000 00400	[*]C(=O)OCC(COC([*])=O)OC([*])=O	0	5
Unspecific distribution	PS(43:4)	M+Na	C49H88NO10P	904,603 7836	SLM:0000 58942	SLM:0000 55218	[NH3+][C@@H](COP([O-])(=O)OCC(COC([*])=O)OC([*])=O)C([O-])=O	0	9
Unspecific distribution	TG(56:8)	M+H	C59H98O6	903,743 5953	SLM:0003 08354	SLM:0000 00400	[*]C(=O)OCC(COC([*])=O)OC([*])=O	0	3
Unspecific distribution	TG(54:5)	M+Na	C57H100O6	903,741 19	SLM:0003 08325	SLM:0000 00400	[*]C(=O)OCC(COC([*])=O)OC([*])=O	0	5
Unspecific distribution	TG(56:9)	M+H	C59H96O6	901,727 9453	SLM:0003 08355	SLM:0000 00400	[*]C(=O)OCC(COC([*])=O)OC([*])=O	0	3
Unspecific distribution	TG(52:1)	M+K	C55H104O6	899,746 4274	SLM:0003 08296	SLM:0000 00400	[*]C(=O)OCC(COC([*])=O)OC([*])=O	0	5
Unspecific distribution	PC(42:1)	M+Na	C50H98NO8P	894,692 2047	SLM:0000 56573	SLM:0000 55211	C[N+](C)(C)CCOP([O-])(=O)OCC(COC([*])=O)OC([*])=O	669 70	4
Unspecific distribution	PC(44:5)	M+H	C52H94NO8P	892,678 96	SLM:0000 56599	SLM:0000 55211	C[N+](C)(C)CCOP([O-])(=O)OCC(COC([*])=O)OC([*])=O	669 74	3
Unspecific distribution	PC(42:2)	M+Na	C50H96NO8P	892,676 5546	SLM:0000 56576	SLM:0000 55211	C[N+](C)(C)CCOP([O-])(=O)OCC(COC([*])=O)OC([*])=O	669 69	3
Unspecific distribution	PC(44:6)	M+H	C52H92NO8P	890,663 3099	SLM:0000 56600	SLM:0000 55211	C[N+](C)(C)CCOP([O-])(=O)OCC(COC([*])=O)OC([*])=O	669 73	3
Unspecific distribution	PC(42:3)	M+Na	C50H94NO8P	890,660 9046	SLM:0000 56577	SLM:0000 55211	C[N+](C)(C)CCOP([O-])(=O)OCC(COC([*])=O)OC([*])=O	669 68	3
Unspecific distribution	PI(38:4)	M+H	C47H83O13P	887,564 3837	SLM:0000 58237	SLM:0000 55216	OC1C(O)C(O)C(OP([O-])(=O)OCC(COC([*])=O)OC([*])=O)C(O)C1O	0	3
Unspecific distribution	PI(36:1)	M+Na	C45H85O13P	887,561 9784	SLM:0000 58218	SLM:0000 55216	OC1C(O)C(O)C(OP([O-])(=O)OCC(COC([*])=O)OC([*])=O)C(O)C1O	743 71	9
Unspecific distribution	PC(44:8)	M+H	C52H88NO8P	886,632 0098	SLM:0000 56602	SLM:0000 55211	C[N+](C)(C)CCOP([O-])(=O)OCC(COC([*])=O)OC([*])=O	0	4

Unspecific distribution	PC(42:5)	M+Na	C50H90NO8P	886,629 6045	SLM:0000 56579	SLM:0000 55211	C[N+](C)(C)CCOP([O-])(=O)OCC(COC([*])=O)OC([*])=O	669 66	7
Unspecific distribution	TG(52:0)	M+Na	C55H106O6	885,788 1402	SLM:0003 08295	SLM:0000 00400	[*]C(=O)OCC(COC([*])=O)OC([*])=O	0	3
Unspecific distribution	PI(38:5)	M+H	C47H81O13P	885,548 7336	SLM:0000 58238	SLM:0000 55216	OC1C(O)C(O)C(OP([O-])(=O)OCC(COC([*])=O)OC([*])=O)C(O)C1O	0	4
Unspecific distribution	PI(36:2)	M+Na	C45H83O13P	885,546 3283	SLM:0000 58219	SLM:0000 55216	OC1C(O)C(O)C(OP([O-])(=O)OCC(COC([*])=O)OC([*])=O)C(O)C1O	743 72	7
Unspecific distribution	TG(52:1)	M+Na	C55H104O6	883,772 4902	SLM:0003 08296	SLM:0000 00400	[*]C(=O)OCC(COC([*])=O)OC([*])=O	0	5
Unspecific distribution	PI(36:3)	M+Na	C45H81O13P	883,530 6783	SLM:0000 58220	SLM:0000 55216	OC1C(O)C(O)C(OP([O-])(=O)OCC(COC([*])=O)OC([*])=O)C(O)C1O	0	3
Unspecific distribution	TG(54:5)	M+H	C57H100O6	881,759 2454	SLM:0003 08325	SLM:0000 00400	[*]C(=O)OCC(COC([*])=O)OC([*])=O	0	5
Unspecific distribution	TG(52:2)	M+Na	C55H102O6	881,756 8401	SLM:0003 08298	SLM:0000 00400	[*]C(=O)OCC(COC([*])=O)OC([*])=O	0	8
Unspecific distribution	TG(52:3)	M+Na	C55H100O6	879,741 19	SLM:0003 08299	SLM:0000 00400	[*]C(=O)OCC(COC([*])=O)OC([*])=O	0	8
Unspecific distribution	PS(41:3)	M+Na	C47H86NO10P	878,588 1336	SLM:0000 58922	SLM:0000 55218	[NH3+][C@@H](COP([O-])(=O)OCC(COC([*])=O)OC([*])=O)C([O-])=O	0	9
Unspecific distribution	PE(44:4)	M+Na	C49H90NO8P	874,629 6045	SLM:0000 57256	SLM:0000 55213	[NH3+]CCOP([O-])(=O)OCC(COC([*])=O)OC([*])=O	717 58	3
Unspecific distribution	PS(41:5)	M+Na	C47H82NO10P	874,556 8334	SLM:0000 58924	SLM:0000 55218	[NH3+][C@@H](COP([O-])(=O)OCC(COC([*])=O)OC([*])=O)C([O-])=O	0	3
Unspecific distribution	PC(40:6)	M+K	C48H84NO8P	872,556 5915	SLM:0000 56561	SLM:0000 55211	C[N+](C)(C)CCOP([O-])(=O)OCC(COC([*])=O)OC([*])=O	644 31	4
Unspecific distribution	TG(50:1)	M+K	C53H100O6	871,715 1273	SLM:0003 08276	SLM:0000 00400	[*]C(=O)OCC(COC([*])=O)OC([*])=O	0	5
Unspecific distribution	PS(42:3)	M+H	C48H88NO10P	870,621 839	SLM:0000 58931	SLM:0000 55218	[NH3+][C@@H](COP([O-])(=O)OCC(COC([*])=O)OC([*])=O)C([O-])=O	720 88	3

Unspecific distribution	TG(53:4)	M+H	C56H100O6	869,759 2454	SLM:0003 08311	SLM:0000 00400	[*]C(=O)OCC(COC([*])=O)OC([*])=O	0	4
Unspecific distribution	TG(51:1)	M+Na	C54H102O6	869,756 8401	SLM:0003 08286	SLM:0000 00400	[*]C(=O)OCC(COC([*])=O)OC([*])=O	0	4
Unspecific distribution	PC(42:3)	M+H	C50H94NO8P	868,678 96	SLM:0000 56577	SLM:0000 55211	C[N+](C)(C)CCOP([O-])(=O)OCC(COC([*])=O)OC([*])=O	669 68	3
Unspecific distribution	PC(40:0)	M+Na	C48H96NO8P	868,676 5546	SLM:0000 56554	SLM:0000 55211	C[N+](C)(C)CCOP([O-])(=O)OCC(COC([*])=O)OC([*])=O	668 66	6
Unspecific distribution	PS(42:4)	M+H	C48H86NO10P	868,606 1889	SLM:0000 58932	SLM:0000 55218	[NH3+][C@@H](COP([O-])(=O)OCC(COC([*])=O)OC([*])=O)C([O-])=O	720 89	3
Unspecific distribution	PS(40:1)	M+Na	C46H88NO10P	868,603 7836	SLM:0000 58909	SLM:0000 55218	[NH3+][C@@H](COP([O-])(=O)OCC(COC([*])=O)OC([*])=O)C([O-])=O	720 79	9
Unspecific distribution	PC(42:4)	M+H	C50H92NO8P	866,663 3099	SLM:0000 56578	SLM:0000 55211	C[N+](C)(C)CCOP([O-])(=O)OCC(COC([*])=O)OC([*])=O	669 67	4
Unspecific distribution	PC(40:1)	M+Na	C48H94NO8P	866,660 9046	SLM:0000 56555	SLM:0000 55211	C[N+](C)(C)CCOP([O-])(=O)OCC(COC([*])=O)OC([*])=O	668 65	6
Unspecific distribution	PS(40:2)	M+Na	C46H86NO10P	866,588 1336	SLM:0000 58911	SLM:0000 55218	[NH3+][C@@H](COP([O-])(=O)OCC(COC([*])=O)OC([*])=O)C([O-])=O	720 80	9
Unspecific distribution	TG(51:3)	M+Na	C54H98O6	865,725 54	SLM:0003 08288	SLM:0000 00400	[*]C(=O)OCC(COC([*])=O)OC([*])=O	0	3
Unspecific distribution	PC(42:5)	M+H	C50H90NO8P	864,647 6598	SLM:0000 56579	SLM:0000 55211	C[N+](C)(C)CCOP([O-])(=O)OCC(COC([*])=O)OC([*])=O	669 66	7
Unspecific distribution	PC(40:2)	M+Na	C48H92NO8P	864,645 2545	SLM:0000 56557	SLM:0000 55211	C[N+](C)(C)CCOP([O-])(=O)OCC(COC([*])=O)OC([*])=O	668 64	9
Unspecific distribution	PS(40:3)	M+Na	C46H84NO10P	864,572 4835	SLM:0000 58912	SLM:0000 55218	[NH3+][C@@H](COP([O-])(=O)OCC(COC([*])=O)OC([*])=O)C([O-])=O	720 81	3
Unspecific distribution	TG(51:4)	M+Na	C54H96O6	863,709 8899	SLM:0003 08289	SLM:0000 00400	[*]C(=O)OCC(COC([*])=O)OC([*])=O	0	3
Unspecific distribution	TG(52:3	M+	C55H100	857,759	SLM:0003	SLM:0000	[*]C(=O)OCC(COC([*])=O)OC([*])=O	0	8

	)	H	O6	2454	08299	00400			
Unspecific distribution	TG(50:0)	M+Na	C53H102O6	857,7568401	SLM:00030827 5	SLM:0000 00400	[*]C(=O)OCC(COC([*])=O)OC([*])=O	0	6
Unspecific distribution	PS(41:3)	M+H	C47H86NO10P	856,6061889	SLM:0000 58922	SLM:0000 55218	[NH3+][C@@H](COP([O-])(=O)OCC(COC([*])=O)OC([*])=O)C([O-])=O	0	9
Unspecific distribution	TG(50:1)	M+Na	C53H100O6	855,741 19	SLM:00030827 6	SLM:0000 00400	[*]C(=O)OCC(COC([*])=O)OC([*])=O	0	5
Unspecific distribution	PE(42:0)	M+Na	C47H94NO8P	854,6609046	SLM:0000 57230	SLM:0000 55213	[NH3+]CCOP([O-])(=O)OCC(COC([*])=O)OC([*])=O	71747	4
Unspecific distribution	PC(38:1)	M+K	C46H90NO8P	854,6035417	SLM:0000 56538	SLM:0000 55211	C[N+](C)(C)CCOP([O-])(=O)OCC(COC([*])=O)OC([*])=O	66860	3
Unspecific distribution	PS(41:4)	M+H	C47H84NO10P	854,5905389	SLM:0000 58923	SLM:0000 55218	[NH3+][C@@H](COP([O-])(=O)OCC(COC([*])=O)OC([*])=O)C([O-])=O	0	8
Unspecific distribution	PS(39:1)	M+Na	C45H86NO10P	854,5881336	SLM:0000 58902	SLM:0000 55218	[NH3+][C@@H](COP([O-])(=O)OCC(COC([*])=O)OC([*])=O)C([O-])=O	0	8
Unspecific distribution	TG(50:2)	M+Na	C53H98O6	853,72554	SLM:00030827 7	SLM:0000 00400	[*]C(=O)OCC(COC([*])=O)OC([*])=O	0	6
Unspecific distribution	PC(39:1)	M+Na	C47H92NO8P	852,6452545	SLM:0000 56548	SLM:0000 55211	C[N+](C)(C)CCOP([O-])(=O)OCC(COC([*])=O)OC([*])=O	0	3
Unspecific distribution	PC(38:2)	M+K	C46H88NO8P	852,5878916	SLM:0000 56539	SLM:0000 55211	C[N+](C)(C)CCOP([O-])(=O)OCC(COC([*])=O)OC([*])=O	66859	5
Unspecific distribution	PC(40:8)	M+Na	C48H80NO8P	852,5513541	SLM:0000 56563	SLM:0000 55211	C[N+](C)(C)CCOP([O-])(=O)OCC(COC([*])=O)OC([*])=O	0	3
Unspecific distribution	TG(50:3)	M+Na	C53H96O6	851,7098899	SLM:00030827 8	SLM:0000 00400	[*]C(=O)OCC(COC([*])=O)OC([*])=O	0	9
Unspecific distribution	PE(44:5)	M+H	C49H88NO8P	850,6320098	SLM:0000 57257	SLM:0000 55213	[NH3+]CCOP([O-])(=O)OCC(COC([*])=O)OC([*])=O	71759	3
Unspecific distribution	TG(50:4)	M+Na	C53H94O6	849,6942398	SLM:00030827 9	SLM:0000 00400	[*]C(=O)OCC(COC([*])=O)OC([*])=O	0	4
Unspecific distribution	PE(42:3)	M+	C47H88	848,613	SLM:0000	SLM:0000	[NH3+]CCOP([O-	717	5

		Na	NO8P	9544	57235	55213	])(=O)OCC(COC([*])=O)OC([*])=O	50	
Unspecific distribution	PE(41:4)	M+K	C46H84NO8P	848,5565915	SLM:0000 57227	SLM:0000 55213	[NH3+]CCOP([O-])(=O)OCC(COC([*])=O)OC([*])=O	0	8
Unspecific distribution	PC(40:0)	M+H	C48H96NO8P	846,69461	SLM:0000 56554	SLM:0000 55211	C[N+](C)(C)CCOP([O-])(=O)OCC(COC([*])=O)OC([*])=O	66866	6
Unspecific distribution	PS(39:5)	M+Na	C45H78NO10P	846,5255333	SLM:0000 58906	SLM:0000 55218	[NH3+][C@@H](COP([O-])(=O)OCC(COC([*])=O)OC([*])=O)C([O-])=O	0	4
Unspecific distribution	PE(42:5)	M+Na	C47H84NO8P	844,5826543	SLM:0000 57237	SLM:0000 55213	[NH3+]CCOP([O-])(=O)OCC(COC([*])=O)OC([*])=O	71752	3
Unspecific distribution	PE(42:6)	M+Na	C47H82NO8P	842,5670042	SLM:0000 57238	SLM:0000 55213	[NH3+]CCOP([O-])(=O)OCC(COC([*])=O)OC([*])=O	71753	3
Unspecific distribution	SM(d44:2)	M+H	C49H97N2O6P	841,7156798	SLM:00039084 9	SLM:0000 01000	C[N+](C)(C)CCOP([O-])(=O)OC[C@H](NC([*])=O)[C@H](O)[*]	0	9
Unspecific distribution	TG(50:3)	M+H	C53H96O6	829,7279453	SLM:00030827 8	SLM:0000 00400	[*]C(=O)OCC(COC([*])=O)OC([*])=O	0	9
Unspecific distribution	TG(48:0)	M+Na	C51H98O6	829,72554	SLM:00030825 7	SLM:0000 00400	[*]C(=O)OCC(COC([*])=O)OC([*])=O	0	6
Unspecific distribution	SM(d43:1)	M+H	C48H97N2O6P	829,7156798	SLM:00039083 8	SLM:0000 01000	C[N+](C)(C)CCOP([O-])(=O)OC[C@H](NC([*])=O)[C@H](O)[*]	0	3
Unspecific distribution	PE(41:6)	M+Na	C46H80NO8P	828,5513541	SLM:0000 57229	SLM:0000 55213	[NH3+]CCOP([O-])(=O)OCC(COC([*])=O)OC([*])=O	0	5
Unspecific distribution	TG(50:4)	M+H	C53H94O6	827,7122952	SLM:00030827 9	SLM:0000 00400	[*]C(=O)OCC(COC([*])=O)OC([*])=O	0	4
Unspecific distribution	TG(48:1)	M+Na	C51H96O6	827,7098899	SLM:00030825 8	SLM:0000 00400	[*]C(=O)OCC(COC([*])=O)OC([*])=O	0	4
Unspecific distribution	PS(37:1)	M+Na	C43H82NO10P	826,5568334	SLM:0000 58885	SLM:0000 55218	[NH3+][C@@H](COP([O-])(=O)OCC(COC([*])=O)OC([*])=O)C([O-])=O	0	3
Unspecific distribution	PC(36:2)	M+K	C44H84NO8P	824,5565915	SLM:0000 56523	SLM:0000 55211	C[N+](C)(C)CCOP([O-])(=O)OCC(COC([*])=O)OC([*])=O	64433	9
Unspecific distribution	PS(37:4)	M+Na	C43H76NO10P	820,5098832	SLM:0000 58888	SLM:0000 55218	[NH3+][C@@H](COP([O-])(=O)OCC(COC([*])=O)OC([*])=O)C([O-	0	5

							])=O		
Unspecific distribution	PE(42:7)	M+H	C47H80NO8P	818,5694095	SLM:0000057239	SLM:0000055213	[NH3+]CCOP([O-])(=O)OCC(COC([*])=O)OC([*])=O	0	5
Unspecific distribution	PE(40:4)	M+Na	C45H82NO8P	818,5670042	SLM:0000057217	SLM:0000055213	[NH3+]CCOP([O-])(=O)OCC(COC([*])=O)OC([*])=O	71744	9
Unspecific distribution	PC(38:1)	M+H	C46H90NO8P	816,6476598	SLM:0000056538	SLM:0000055211	C[N+](C)(C)CCOP([O-])(=O)OCC(COC([*])=O)OC([*])=O	66860	3
Unspecific distribution	SM(d42:1)	M+H	C47H95N2O6P	815,7000298	SLM:0003090824	SLM:0000001000	C[N+](C)(C)CCOP([O-])(=O)OC[C@H](NC([*])=O)[C@H](O)[*]	0	9
Unspecific distribution	PC(38:2)	M+H	C46H88NO8P	814,6320098	SLM:0000056539	SLM:0000055211	C[N+](C)(C)CCOP([O-])(=O)OCC(COC([*])=O)OC([*])=O	66859	5
Unspecific distribution	PS(38:3)	M+H	C44H80NO10P	814,5592387	SLM:0000058894	SLM:0000055218	[NH3+][C@@H](COP([O-])(=O)OCC(COC([*])=O)OC([*])=O)C([O-])=O	72074	7
Unspecific distribution	PS(36:0)	M+Na	C42H82NO10P	814,5568334	SLM:0000058875	SLM:0000055218	[NH3+][C@@H](COP([O-])(=O)OCC(COC([*])=O)OC([*])=O)C([O-])=O	72064	9
Unspecific distribution	SM(d42:2)	M+H	C47H93N2O6P	813,6843797	SLM:0003090823	SLM:0000001000	C[N+](C)(C)CCOP([O-])(=O)OC[C@H](NC([*])=O)[C@H](O)[*]	0	8
Unspecific distribution	PE(39:5)	M+Na	C44H78NO8P	802,5357041	SLM:0000057210	SLM:0000055213	[NH3+]CCOP([O-])(=O)OCC(COC([*])=O)OC([*])=O	0	3
Unspecific distribution	SM(d41:1)	M+H	C46H93N2O6P	801,6843797	SLM:0003090811	SLM:0000001000	C[N+](C)(C)CCOP([O-])(=O)OC[C@H](NC([*])=O)[C@H](O)[*]	0	9
Unspecific distribution	PC(34:0)	M+K	C42H84NO8P	800,5565915	SLM:0000056507	SLM:0000055211	C[N+](C)(C)CCOP([O-])(=O)OCC(COC([*])=O)OC([*])=O	66855	8
Unspecific distribution	PE(40:5)	M+H	C45H80NO8P	794,5694095	SLM:0000057218	SLM:0000055213	[NH3+]CCOP([O-])(=O)OCC(COC([*])=O)OC([*])=O	71745	9
Unspecific distribution	PE(38:2)	M+Na	C43H82NO8P	794,5670042	SLM:0000057197	SLM:0000055213	[NH3+]CCOP([O-])(=O)OCC(COC([*])=O)OC([*])=O	71735	9
Unspecific distribution	PE(38:3)	M+Na	C43H80NO8P	792,5513541	SLM:0000057198	SLM:0000055213	[NH3+]CCOP([O-])(=O)OCC(COC([*])=O)OC([*])=O	71736	3
Unspecific distribution	PC(36:0)	M+H	C44H88NO8P	790,6320098	SLM:0000056521	SLM:0000055211	C[N+](C)(C)CCOP([O-])(=O)OCC(COC([*])=O)OC([*])=O	66858	9

Unspecific distribution	PE(38:4)	M+Na	C43H78NO8P	790,5357041	SLM:0000057199	SLM:0000055213	[NH3+]CCOP([O-])(=O)OCC(COC([*])=O)OC([*])=O	71737	9
Unspecific distribution	SM(d40:1)	M+H	C45H91N2O6P	787,6687296	SLM:0003090797	SLM:0000001000	C[N+](C)(C)CCOP([O-])(=O)OC[C@H](NC([*])=O)[C@H](O)[*]	0	9
Unspecific distribution	SM(d40:2)	M+H	C45H89N2O6P	785,6530796	SLM:0003090795	SLM:0000001000	C[N+](C)(C)CCOP([O-])(=O)OC[C@H](NC([*])=O)[C@H](O)[*]	0	8
Unspecific distribution	PE(36:1)	M+K	C41H80NO8P	784,5252914	SLM:0000057180	SLM:0000055213	[NH3+]CCOP([O-])(=O)OCC(COC([*])=O)OC([*])=O	71727	6
Unspecific distribution	SM(d40:3)	M+H	C45H87N2O6P	783,6374295	SLM:0003090793	SLM:0000001000	C[N+](C)(C)CCOP([O-])(=O)OC[C@H](NC([*])=O)[C@H](O)[*]	0	9
Unspecific distribution	PE(39:6)	M+H	C44H76NO8P	778,5381094	SLM:0000057211	SLM:0000055213	[NH3+]CCOP([O-])(=O)OCC(COC([*])=O)OC([*])=O	0	3
Unspecific distribution	PE(37:3)	M+Na	C42H78NO8P	778,5357041	SLM:0000057191	SLM:0000055213	[NH3+]CCOP([O-])(=O)OCC(COC([*])=O)OC([*])=O	0	9
Unspecific distribution	PE(38:0)	M+H	C43H86NO8P	776,6163597	SLM:0000057195	SLM:0000055213	[NH3+]CCOP([O-])(=O)OCC(COC([*])=O)OC([*])=O	71733	9
Unspecific distribution	PE(38:1)	M+H	C43H84NO8P	774,6007096	SLM:0000057196	SLM:0000055213	[NH3+]CCOP([O-])(=O)OCC(COC([*])=O)OC([*])=O	71734	4
Unspecific distribution	SM(d39:1)	M+H	C44H89N2O6P	773,6530796	SLM:0003090782	SLM:0000001000	C[N+](C)(C)CCOP([O-])(=O)OC[C@H](NC([*])=O)[C@H](O)[*]	0	9
Unspecific distribution	PE(35:0)	M+K	C40H80NO8P	772,5252914	SLM:0000057172	SLM:0000055213	[NH3+]CCOP([O-])(=O)OCC(COC([*])=O)OC([*])=O	0	9
Unspecific distribution	PE(38:3)	M+H	C43H80NO8P	770,5694095	SLM:0000057198	SLM:0000055213	[NH3+]CCOP([O-])(=O)OCC(COC([*])=O)OC([*])=O	71736	3
Unspecific distribution	PE(36:0)	M+Na	C41H82NO8P	770,5670042	SLM:0000057179	SLM:0000055213	[NH3+]CCOP([O-])(=O)OCC(COC([*])=O)OC([*])=O	71726	9
Unspecific distribution	PC(32:1)	M+K	C40H78NO8P	770,5096413	SLM:0000056494	SLM:0000055211	C[N+](C)(C)CCOP([O-])(=O)OCC(COC([*])=O)OC([*])=O	66849	7
Unspecific distribution	PE(36:3)	M+Na	C41H76NO8P	764,5200054	SLM:0000057182	SLM:0000055213	[NH3+]CCOP([O-])(=O)OCC(COC([*])=O)OC([*])=O	71729	9
Unspecific distribution	PC(34:0)	M+H	C42H84NO8P	762,6007096	SLM:0000056507	SLM:0000055211	C[N+](C)(C)CCOP([O-])(=O)OCC(COC([*])=O)OC([*])=O	66855	8
Unspecific distribution	SM(d38:	M+	C43H87	759,637	SLM:0003	SLM:0000	C[N+](C)(C)CCOP([O-	0	9

	1)	H	N2O6P	4295	90767	01000	])(=O)OC[C@H](NC([*])=O)[C@H](O)[*]		
Unspecific distribution	PE(34:0)	M+K	C39H78NO8P	758,5096413	SLM:00005716	SLM:00005521	[NH3+]CCOP([O-])(=O)OCC(COC([*])=O)OC([*])=O	71718	5
Unspecific distribution	SM(d38:2)	M+H	C43H85N2O6P	757,6217794	SLM:00039076	SLM:00001000	C[N+](C)(C)CCOP([O-])(=O)OC[C@H](NC([*])=O)[C@H](O)[*]	0	7
Unspecific distribution	PE(35:2)	M+Na	C40H76NO8P	752,5200054	SLM:00005717	SLM:00005521	[NH3+]CCOP([O-])(=O)OCC(COC([*])=O)OC([*])=O	0	6
Unspecific distribution	PE(36:0)	M+H	C41H82NO8P	748,5850596	SLM:00005717	SLM:00005521	[NH3+]CCOP([O-])(=O)OCC(COC([*])=O)OC([*])=O	71726	9
Unspecific distribution	SM(d37:1)	M+H	C42H85N2O6P	745,6217794	SLM:00039075	SLM:00001000	C[N+](C)(C)CCOP([O-])(=O)OC[C@H](NC([*])=O)[C@H](O)[*]	0	9
Unspecific distribution	SM(d37:2)	M+H	C42H83N2O6P	743,6061294	SLM:00039075	SLM:00001000	C[N+](C)(C)CCOP([O-])(=O)OC[C@H](NC([*])=O)[C@H](O)[*]	0	7
Unspecific distribution	PE(36:3)	M+H	C41H76NO8P	742,5381094	SLM:00005718	SLM:00005521	[NH3+]CCOP([O-])(=O)OCC(COC([*])=O)OC([*])=O	71729	9
Unspecific distribution	PE(34:0)	M+Na	C39H78NO8P	742,5357041	SLM:00005716	SLM:00005521	[NH3+]CCOP([O-])(=O)OCC(COC([*])=O)OC([*])=O	71718	5
Unspecific distribution	PE(34:1)	M+Na	C39H76NO8P	740,5200054	SLM:00005716	SLM:00005521	[NH3+]CCOP([O-])(=O)OCC(COC([*])=O)OC([*])=O	71720	4
Unspecific distribution	PE(34:2)	M+Na	C39H74NO8P	738,5044039	SLM:00005716	SLM:00005521	[NH3+]CCOP([O-])(=O)OCC(COC([*])=O)OC([*])=O	71721	5
Unspecific distribution	PE(34:3)	M+Na	C39H72NO8P	736,4887539	SLM:00005716	SLM:00005521	[NH3+]CCOP([O-])(=O)OCC(COC([*])=O)OC([*])=O	71722	3
Unspecific distribution	PC(32:1)	M+H	C40H78NO8P	732,5537594	SLM:00005649	SLM:00005521	C[N+](C)(C)CCOP([O-])(=O)OCC(COC([*])=O)OC([*])=O	66849	7
Unspecific distribution	SM(d36:1)	M+H	C41H83N2O6P	731,6061294	SLM:00039073	SLM:00001000	C[N+](C)(C)CCOP([O-])(=O)OC[C@H](NC([*])=O)[C@H](O)[*]	0	9
Unspecific distribution	PE(35:2)	M+H	C40H76NO8P	730,5381094	SLM:00005717	SLM:00005521	[NH3+]CCOP([O-])(=O)OCC(COC([*])=O)OC([*])=O	0	6
Unspecific distribution	SM(d36:2)	M+H	C41H81N2O6P	729,5904793	SLM:00039073	SLM:00001000	C[N+](C)(C)CCOP([O-])(=O)OC[C@H](NC([*])=O)[C@H](O)[*]	0	9
Unspecific distribution	PC(30:0)	M+Na	C38H76NO8P	728,5200054	SLM:00005647	SLM:00005521	C[N+](C)(C)CCOP([O-])(=O)OCC(COC([*])=O)OC([*])=O	65303	9

Unspecific distribution	SM(d33:1)	M+K	C38H77N2O6P	727,5150061	SLM:00039070	SLM:00001000	C[N+](C)(C)CCOP([O-])(=O)OC[C@H](NC([*])=O)[C@H](O)[*]	0	9
Unspecific distribution	PE(33:1)	M+Na	C38H74NO8P	726,5044039	SLM:00005715	SLM:00005521	[NH3+]CCOP([O-])(=O)OCC(COC([*])=O)OC([*])=O	0	8
Unspecific distribution	PE(34:1)	M+H	C39H76NO8P	718,5381094	SLM:00005716	SLM:00005521	[NH3+]CCOP([O-])(=O)OCC(COC([*])=O)OC([*])=O	71720	4
Unspecific distribution	SM(d35:1)	M+H	C40H81N2O6P	717,5904793	SLM:00039072	SLM:00001000	C[N+](C)(C)CCOP([O-])(=O)OC[C@H](NC([*])=O)[C@H](O)[*]	0	9
Unspecific distribution	PE(34:2)	M+H	C39H74NO8P	716,5224593	SLM:00005716	SLM:00005521	[NH3+]CCOP([O-])(=O)OCC(COC([*])=O)OC([*])=O	71721	5
Unspecific distribution	PC(30:0)	M+H	C38H76NO8P	706,5381094	SLM:00005647	SLM:00005521	C[N+](C)(C)CCOP([O-])(=O)OCC(COC([*])=O)OC([*])=O	65303	9
Unspecific distribution	PC(28:0)	M+Na	C36H72NO8P	700,4887539	SLM:00005646	SLM:00005521	C[N+](C)(C)CCOP([O-])(=O)OCC(COC([*])=O)OC([*])=O	65294	3
Unspecific distribution	PC(28:0)	M+H	C36H72NO8P	678,5068092	SLM:00005646	SLM:00005521	C[N+](C)(C)CCOP([O-])(=O)OCC(COC([*])=O)OC([*])=O	65294	3
Unspecific distribution	DG(40:4)	M+H	C43H76O5	673,57653	SLM:00037449	SLM:00000401	[*]OCC(CO[*])O[*]	0	3
Unspecific distribution	DG(40:5)	M+H	C43H74O5	671,56088	SLM:00037450	SLM:00000401	[*]OCC(CO[*])O[*]	0	3
Unspecific distribution	DG(38:2)	M+Na	C41H76O5	671,5584746	SLM:00037429	SLM:00000401	[*]OCC(CO[*])O[*]	0	3
Unspecific distribution	DG(38:4)	M+Na	C41H72O5	667,5271745	SLM:00037431	SLM:00000401	[*]OCC(CO[*])O[*]	0	3
Unspecific distribution	DG(38:4)	M+H	C41H72O5	645,5452299	SLM:00037431	SLM:00000401	[*]OCC(CO[*])O[*]	0	3
Unspecific distribution	DG(36:1)	M+Na	C39H74O5	645,5428246	SLM:00037412	SLM:00000401	[*]OCC(CO[*])O[*]	0	3
Unspecific distribution	LPC(24:1)	M+Na	C32H64NO7P	628,4312239	SLM:00005534	SLM:00005520	C[N+](C)(C)CCOP([O-])(=O)OCC(CO[*])O[*]	74471	5
Unspecific distribution	DG(36:3)	M+H	C39H70O5	619,5295798	SLM:00037414	SLM:00000401	[*]OCC(CO[*])O[*]	0	4
Unspecific distribution	DG(34:1	M+	C37H70	617,511	SLM:0003	SLM:0000	[*]OCC(CO[*])O[*]	0	3

	)	Na	O5	5245	07398	00401			
Unspecific distribution	DG(34:2)	M+Na	C37H68O5	615,4958744	SLM:00007399	SLM:0000 00401	[*]OCC(CO[*])O[*]	0	3
Unspecific distribution	LPC(22:6)	M+K	C30H50NO7P	606,2956258	SLM:0000 55341	SLM:0000 55200	C[N+](C)(C)CCOP([O-])(=O)OCC(CO[*])O[*]	0	6
Unspecific distribution	LPC(22:4)	M+Na	C30H54NO7P	594,3529887	SLM:0000 55339	SLM:0000 55200	C[N+](C)(C)CCOP([O-])(=O)OCC(CO[*])O[*]	0	6
Unspecific distribution	LPC(22:0)	M+H	C30H62NO7P	580,4336443	SLM:0000 55335	SLM:0000 55200	C[N+](C)(C)CCOP([O-])(=O)OCC(CO[*])O[*]	67061	3
Unspecific distribution	LPC(22:1)	M+H	C30H60NO7P	578,4179942	SLM:0000 55336	SLM:0000 55200	C[N+](C)(C)CCOP([O-])(=O)OCC(CO[*])O[*]	67060	4
Unspecific distribution	LPC(20:0)	M+Na	C28H58NO7P	574,3842888	SLM:0000 55328	SLM:0000 55200	C[N+](C)(C)CCOP([O-])(=O)OCC(CO[*])O[*]	67058	4
Unspecific distribution	LPC(22:6)	M+H	C30H50NO7P	568,3397439	SLM:0000 55341	SLM:0000 55200	C[N+](C)(C)CCOP([O-])(=O)OCC(CO[*])O[*]	0	6
Unspecific distribution	Cer(d36:1)	M+H	C36H71NO3	566,5506496	SLM:0003 91261	SLM:0003 99814	OC[C@H](NC([*])=O)[C@H](O)[*]	0	3
Unspecific distribution	LPC(18:0)	M+K	C26H54NO7P	562,3269259	SLM:0000 55322	SLM:0000 55200	C[N+](C)(C)CCOP([O-])(=O)OCC(CO[*])O[*]	64561	9
Unspecific distribution	Cer(d34:1)	M+Na	C34H67NO3	560,5012941	SLM:0003 91236	SLM:0003 99814	OC[C@H](NC([*])=O)[C@H](O)[*]	0	3
Unspecific distribution	LPC(20:2)	M+H	C28H54NO7P	548,3710441	SLM:0000 55330	SLM:0000 55200	C[N+](C)(C)CCOP([O-])(=O)OCC(CO[*])O[*]	0	9
Unspecific distribution	LPC(20:4)	M+H	C28H50NO7P	544,3397439	SLM:0000 55332	SLM:0000 55200	C[N+](C)(C)CCOP([O-])(=O)OCC(CO[*])O[*]	0	7
Unspecific distribution	LPC(18:1)	M+Na	C26H52NO7P	544,3373386	SLM:0000 55323	SLM:0000 55200	C[N+](C)(C)CCOP([O-])(=O)OCC(CO[*])O[*]	64566	9
Unspecific distribution	LPC(18:2)	M+Na	C26H50NO7P	542,3216886	SLM:0000 55324	SLM:0000 55200	C[N+](C)(C)CCOP([O-])(=O)OCC(CO[*])O[*]	0	9
Unspecific distribution	Cer(d34:1)	M+H	C34H67NO3	538,5193495	SLM:0003 91236	SLM:0003 99814	OC[C@H](NC([*])=O)[C@H](O)[*]	0	3
Unspecific distribution	LPC(19:0)	M+H	C27H56NO7P	538,3866941	SLM:0000 55327	SLM:0000 55200	C[N+](C)(C)CCOP([O-])(=O)OCC(CO[*])O[*]	0	6

Unspecific distribution	LPC(16:0)	M+K	C24H50NO7P	534,2956258	SLM:0000 55318	SLM:0000 55200	C[N+](C)(C)CCOP([O-])(=O)OCC(CO[*])O[*]	64563	9
Unspecific distribution	LPC(18:0)	M+H	C26H54NO7P	524,3710441	SLM:0000 55322	SLM:0000 55200	C[N+](C)(C)CCOP([O-])(=O)OCC(CO[*])O[*]	64561	9
Unspecific distribution	LPC(18:2)	M+H	C26H50NO7P	520,3397439	SLM:0000 55324	SLM:0000 55200	C[N+](C)(C)CCOP([O-])(=O)OCC(CO[*])O[*]	0	9
Unspecific distribution	LPC(16:0)	M+Na	C24H50NO7P	518,3216886	SLM:0000 55318	SLM:0000 55200	C[N+](C)(C)CCOP([O-])(=O)OCC(CO[*])O[*]	64563	9
Unspecific distribution	LPC(15:0)	M+Na	C23H48NO7P	504,3060385	SLM:0000 55317	SLM:0000 55200	C[N+](C)(C)CCOP([O-])(=O)OCC(CO[*])O[*]	0	4
Unspecific distribution	LPC(17:0)	M+H	C25H52NO7P	510,3553940	SLM:0000 55321	SLM:0000 55200	C[N+](C)(C)CCOP([O-])(=O)OCC(CO[*])O[*]	0	9

S4 Table. Detailed lipid annotations of classified lipids from comparison of male and female tegument.

https://doi.org/10.1371/journal.pntd.0008145.s004

					According to SwissLipids database				
Location with increased signal intenisty	Abbreviation	Adduct	formula	mz	Lipid ID	Lipid class	SMILES (pH7.3)	CHEBI	Number of MSI datasets with positive annotation by Metaspace
Female	TG(52:1)	M+Na	C55H104O6	883,7724902	SLM:000308296	SLM:000000400	[*]C(=O)OCC(COC([*])=O)OC([*])=O	0	5
Female	PC(40:6)	M+H	C48H84NO8P	834,6007096	SLM:000056561	SLM:000055211	C[N+](C)(C)CCOP([O-])(=O)OCC(COC([*])=O)OC([*])=O	64431	4
Female	PE(41:3)	M+Na	C46H86NO8P	834,5983043	SLM:000057226	SLM:000055213	[NH3+]CCOP([O-])(=O)OCC(COC([*])=O)OC([*])=O	0	5
Female	SM(d36:1)	M+K	C41H83N2O6P	769,5620112	SLM:000390739	SLM:000001000	C[N+](C)(C)CCOP([O-])(=O)OC[C@H](NC([*])=O)[C@H](O)[*]	0	9
Female	PC(42:9)	M+H	C50H82NO8P	856,5850596	SLM:000056583	SLM:000055211	C[N+](C)(C)CCOP([O-])(=O)OCC(COC([*])=O)OC([*])=O	0	9
Female	PC(40:6)	M+Na	C48H84NO8P	856,5826543	SLM:000056561	SLM:000055211	C[N+](C)(C)CCOP([O-])(=O)OCC(COC([*])=O)OC([*])=O	64431	4
Female	TG(50:1)	M+K	C53H100O6	871,7151273	SLM:000308276	SLM:000000400	[*]C(=O)OCC(COC([*])=O)OC([*])=O	0	5
Female	SM(d43:1)	M+H	C48H97N2O6P	829,7156798	SLM:000390838	SLM:000001000	C[N+](C)(C)CCOP([O-])(=O)OC[C@H](NC([*])=O)[C@H](O)[*]	0	3
Female	PC(40:7)	M+H	C48H82NO8P	832,5850596	SLM:000056562	SLM:000055211	C[N+](C)(C)CCOP([O-])(=O)OCC(COC([*])=O)OC([*])=O	0	9
Female	PE(41:4)	M+Na	C46H84NO8P	832,5826543	SLM:000057227	SLM:000055213	[NH3+]CCOP([O-])(=O)OCC(COC([*])=O)OC([*])=O	0	8
Female	LPC(20:1)	M+H	C28H56NO7P	550,3866941	SLM:000055329	SLM:000055200	C[N+](C)(C)CCOP([O-])(=O)OCC(CO[*])O[*]	67057	9
Female	PC(42:7)	M+H	C50H86NO8P	860,6163597	SLM:000056581	SLM:000055211	C[N+](C)(C)CCOP([O-])(=O)OCC(COC([*])=O)OC([*])=O	0	6
Female	PE(43:4)	M+Na	C48H88NO8P	860,6139544	SLM:000057246	SLM:000055213	[NH3+]CCOP([O-])(=O)OCC(COC([*])=O)OC([*])=O	0	5
Female	TG(50:1)	M+Na	C53H100O6	855,74119	SLM:000308276	SLM:000000400	[*]C(=O)OCC(COC([*])=O)OC([*])=O	0	5
Female	TG(50:2)	M+Na	C53H98O6	853,72554	SLM:000308277	SLM:000000400	[*]C(=O)OCC(COC([*])=O)OC([*])=O	0	6
Female	LPC(20:2)	M+H	C28H54NO7P	548,371044	SLM:00005533	SLM:00005520	C[N+](C)(C)CCOP([O-	0	9

				1	0	0	])(=O)OCC(CO[*])O[*]		
Female	PC(36:0)	M+H	C44H88NO8P	790,6320098	SLM:000056521	SLM:000055211	C[N+](C)(C)CCOP([O-])(=O)OCC(COC([*])=O)OC([*])=O	66858	9
Female	LPC(22:4)	M+H	C30H54NO7P	572,3710441	SLM:000055339	SLM:000055200	C[N+](C)(C)CCOP([O-])(=O)OCC(CO[*])O[*]	0	6
Female	LPC(20:1)	M+Na	C28H56NO7P	572,3686387	SLM:000055329	SLM:000055200	C[N+](C)(C)CCOP([O-])(=O)OCC(CO[*])O[*]	67057	9
Female	LPC(18:2)	M+Na	C26H50NO7P	542,3216886	SLM:000055324	SLM:000055200	C[N+](C)(C)CCOP([O-])(=O)OCC(CO[*])O[*]	0	9
Female	SM(d43:1)	M+Na	C48H97N2O6P	851,6976244	SLM:000390838	SLM:000001000	C[N+](C)(C)CCOP([O-])(=O)OC[C@H](NC([*])=O)[C@H](O)[*]	0	3
Female	LPC(22:5)	M+H	C30H52NO7P	570,355394	SLM:000055340	SLM:000055200	C[N+](C)(C)CCOP([O-])(=O)OCC(CO[*])O[*]	0	8
Female	LPC(20:2)	M+Na	C28H54NO7P	570,3529887	SLM:000055330	SLM:000055200	C[N+](C)(C)CCOP([O-])(=O)OCC(CO[*])O[*]	0	9
Female	Cer(d34:1)	M+H	C34H67NO3	538,5193495	SLM:000391236	SLM:000399814	OC[C@H](NC([*])=O)[C@H](O)[*]	0	3
Male	TG(60:7)	M+H	C63H108O6	961,8218457	SLM:000308410	SLM:000000400	[*]C(=O)OCC(COC([*])=O)OC([*])=O	0	3
Male	TG(58:4)	M+Na	C61H110O6	961,8194404	SLM:000308378	SLM:000000400	[*]C(=O)OCC(COC([*])=O)OC([*])=O	0	6
Male	TG(58:7)	M+H	C61H104O6	933,7905455	SLM:000308381	SLM:000000400	[*]C(=O)OCC(COC([*])=O)OC([*])=O	0	5
Male	TG(56:4)	M+Na	C59H106O6	933,7881402	SLM:000308350	SLM:000000400	[*]C(=O)OCC(COC([*])=O)OC([*])=O	0	6
Male	TG(58:5)	M+H	C61H108O6	937,8218457	SLM:000308379	SLM:000000400	[*]C(=O)OCC(COC([*])=O)OC([*])=O	0	5
Male	TG(56:2)	M+Na	C59H110O6	937,8194404	SLM:000308348	SLM:000000400	[*]C(=O)OCC(COC([*])=O)OC([*])=O	0	8
Male	TG(58:3)	M+Na	C61H112O6	963,8350904	SLM:000308377	SLM:000000400	[*]C(=O)OCC(COC([*])=O)OC([*])=O	0	8
Male	TG(60:6)	M+H	C63H110O6	963,8374957	SLM:000308409	SLM:000000400	[*]C(=O)OCC(COC([*])=O)OC([*])=O	0	8
Male	TG(58:6)	M+H	C61H106O6	935,8061956	SLM:000308380	SLM:000000400	[*]C(=O)OCC(COC([*])=O)OC([*])=O	0	5
Male	TG(56:3)	M+Na	C59H108O6	935,803790	SLM:00030834	SLM:00000040	[*]C(=O)OCC(COC([*])=O)OC([*])=O	0	6

				3	9	0			
Male	TG(60:8)	M+H	C63H106O6	959,8061956	SLM:000308411	SLM:000000400	[*]C(=O)OCC(COC([*])=O)OC([*])=O	0	8
Male	TG(58:5)	M+Na	C61H108O6	959,8037903	SLM:000308379	SLM:000000400	[*]C(=O)OCC(COC([*])=O)OC([*])=O	0	5
Male	SM(d38:2)	M+Na	C43H85N2O6P	779,6037241	SLM:000390765	SLM:000001000	C[N+](C)(C)CCOP([O-])(=O)OC[C@H](NC([*])=O)[C@H](O)[*]	0	7
Male	TG(60:9)	M+H	C63H104O6	957,7905455	SLM:000308412	SLM:000000400	[*]C(=O)OCC(COC([*])=O)OC([*])=O	0	8
Male	TG(58:6)	M+Na	C61H106O6	957,7881402	SLM:000308380	SLM:000000400	[*]C(=O)OCC(COC([*])=O)OC([*])=O	0	5
Male	PS(38:1)	M+K	C44H84NO10P	856,5464207	SLM:000058892	SLM:000055218	[NH3+][C@@H](COP([O-])(=O)OCC(COC([*])=O)OC([*])=O)C([O-])=O	72072	8
Male	PC(30:0)	M+H	C38H76NO8P	706,5381094	SLM:000056479	SLM:000055211	C[N+](C)(C)CCOP([O-])(=O)OCC(COC([*])=O)OC([*])=O	65303	9
Male	TG(56:4)	M+K	C59H106O6	949,7620775	SLM:000308350	SLM:000000400	[*]C(=O)OCC(COC([*])=O)OC([*])=O	0	6
Male	TG(56:6)	M+H	C59H102O6	907,7748955	SLM:000308352	SLM:000000400	[*]C(=O)OCC(COC([*])=O)OC([*])=O	0	6
Male	TG(56:3)	M+K	C59H108O6	951,7777275	SLM:000308349	SLM:000000400	[*]C(=O)OCC(COC([*])=O)OC([*])=O	0	6
Male	TG(58:4)	M+K	C61H110O6	977,7933776	SLM:000308378	SLM:000000400	[*]C(=O)OCC(COC([*])=O)OC([*])=O	0	6
Unspecific	TG(64:8)	M+H	C67H114O6	1015,868796	SLM:000308472	SLM:000000400	[*]C(=O)OCC(COC([*])=O)OC([*])=O	0	4
Unspecific	TG(62:5)	M+Na	C65H116O6	1015,866391	SLM:000308438	SLM:000000400	[*]C(=O)OCC(COC([*])=O)OC([*])=O	0	3
Unspecific	TG(60:7)	M+K	C63H108O6	999,7772275	SLM:000308410	SLM:000000400	[*]C(=O)OCC(COC([*])=O)OC([*])=O	0	3
Unspecific	TG(62:7)	M+H	C65H112O6	989,8531458	SLM:000308440	SLM:000000400	[*]C(=O)OCC(COC([*])=O)OC([*])=O	0	4
Unspecific	TG(60:4)	M+Na	C63H114O6	989,8507405	SLM:000308407	SLM:000000400	[*]C(=O)OCC(COC([*])=O)OC([*])=O	0	7
Unspecific	TG(62:8)	M+H	C65H110O6	987,8374957	SLM:000308441	SLM:000000400	[*]C(=O)OCC(COC([*])=O)OC([*])=O	0	4

Unspecific	TG(60:5)	M+Na	C63H112O6	987,8350904	SLM:00030840 8	SLM:00000040 0	[*]C(=O)OCC(COC([*])=O)OC([*])=O	0	7
Unspecific	TG(62:9)	M+H	C65H108O6	985,8218457	SLM:00030844 2	SLM:00000040 0	[*]C(=O)OCC(COC([*])=O)OC([*])=O	0	4
Unspecific	TG(60:6)	M+Na	C63H110O6	985,8194404	SLM:00030840 9	SLM:00000040 0	[*]C(=O)OCC(COC([*])=O)OC([*])=O	0	8
Unspecific	TG(62:10)	M+H	C65H106O6	983,8061956	SLM:00030842 8	SLM:00000040 0	[*]C(=O)OCC(COC([*])=O)OC([*])=O	0	4
Unspecific	TG(60:7)	M+Na	C63H108O6	983,8037903	SLM:00030841 0	SLM:00000040 0	[*]C(=O)OCC(COC([*])=O)OC([*])=O	0	3
Unspecific	TG(62:11)	M+H	C65H104O6	981,7905455	SLM:00030842 9	SLM:00000040 0	[*]C(=O)OCC(COC([*])=O)OC([*])=O	0	8
Unspecific	TG(60:8)	M+Na	C63H106O6	981,7881402	SLM:00030841 1	SLM:00000040 0	[*]C(=O)OCC(COC([*])=O)OC([*])=O	0	8
Unspecific	TG(62:12)	M+H	C65H102O6	979,7748955	SLM:00030843 0	SLM:00000040 0	[*]C(=O)OCC(COC([*])=O)OC([*])=O	0	7
Unspecific	TG(60:9)	M+Na	C63H104O6	979,7724902	SLM:00030841 2	SLM:00000040 0	[*]C(=O)OCC(COC([*])=O)OC([*])=O	0	8
Unspecific	TG(58:10)	M+K	C61H98O6	965,6994772	SLM:00030837 1	SLM:00000040 0	[*]C(=O)OCC(COC([*])=O)OC([*])=O	0	3
Unspecific	TG(60:10)	M+H	C63H102O6	955,7748955	SLM:00030839 9	SLM:00000040 0	[*]C(=O)OCC(COC([*])=O)OC([*])=O	0	6
Unspecific	TG(58:7)	M+Na	C61H104O6	955,7724902	SLM:00030838 1	SLM:00000040 0	[*]C(=O)OCC(COC([*])=O)OC([*])=O	0	5
Unspecific	TG(60:11)	M+H	C63H100O6	953,7592454	SLM:00030840 0	SLM:00000040 0	[*]C(=O)OCC(COC([*])=O)OC([*])=O	0	9
Unspecific	TG(58:8)	M+Na	C61H102O6	953,7568401	SLM:00030838 2	SLM:00000040 0	[*]C(=O)OCC(COC([*])=O)OC([*])=O	0	3
Unspecific	TG(60:12)	M+H	C63H98O6	951,7435953	SLM:00030840 1	SLM:00000040 0	[*]C(=O)OCC(COC([*])=O)OC([*])=O	0	7
Unspecific	TG(58:9)	M+Na	C61H100O6	951,74119	SLM:00030838 3	SLM:00000040 0	[*]C(=O)OCC(COC([*])=O)OC([*])=O	0	8
Unspecific	TG(58:10)	M+Na	C61H98O6	949,72554	SLM:00030837 1	SLM:00000040 0	[*]C(=O)OCC(COC([*])=O)OC([*])=O	0	3
Unspecific	TG(56:5)	M+K	C59H104O6	947,7464274	SLM:00030835 1	SLM:00000040 0	[*]C(=O)OCC(COC([*])=O)OC([*])=O	0	6

Unspecific	TG(57:5)	M+Na	C60H106O6	945,7881402	SLM:00030836 4	SLM:00000040 0	[*]C(=O)OCC(COC([*])=O)OC([*])=O	0	3
Unspecific	TG(56:6)	M+K	C59H102O6	945,7307773	SLM:00030835 2	SLM:00000040 0	[*]C(=O)OCC(COC([*])=O)OC([*])=O	0	6
Unspecific	TG(57:6)	M+Na	C60H104O6	943,7724902	SLM:00030836 5	SLM:00000040 0	[*]C(=O)OCC(COC([*])=O)OC([*])=O	0	3
Unspecific	TG(56:8)	M+K	C59H98O6	941,6994772	SLM:00030835 4	SLM:00000040 0	[*]C(=O)OCC(COC([*])=O)OC([*])=O	0	3
Unspecific	TG(58:4)	M+H	C61H110O6	939,8374957	SLM:00030837 8	SLM:00000040 0	[*]C(=O)OCC(COC([*])=O)OC([*])=O	0	6
Unspecific	TG(58:8)	M+H	C61H102O6	931,7748955	SLM:00030838 2	SLM:00000040 0	[*]C(=O)OCC(COC([*])=O)OC([*])=O	0	3
Unspecific	TG(56:5)	M+Na	C59H104O6	931,7724902	SLM:00030835 1	SLM:00000040 0	[*]C(=O)OCC(COC([*])=O)OC([*])=O	0	6
Unspecific	TG(58:9)	M+H	C61H100O6	929,7592454	SLM:00030838 3	SLM:00000040 0	[*]C(=O)OCC(COC([*])=O)OC([*])=O	0	8
Unspecific	TG(56:6)	M+Na	C59H102O6	929,7568401	SLM:00030835 2	SLM:00000040 0	[*]C(=O)OCC(COC([*])=O)OC([*])=O	0	6
Unspecific	TG(58:10)	M+H	C61H98O6	927,7435953	SLM:00030837 1	SLM:00000040 0	[*]C(=O)OCC(COC([*])=O)OC([*])=O	0	3
Unspecific	TG(56:7)	M+Na	C59H100O6	927,74119	SLM:00030835 3	SLM:00000040 0	[*]C(=O)OCC(COC([*])=O)OC([*])=O	0	5
Unspecific	TG(54:2)	M+K	C57H106O6	925,7620775	SLM:00030832 2	SLM:00000040 0	[*]C(=O)OCC(COC([*])=O)OC([*])=O	0	6
Unspecific	TG(58:11)	M+H	C61H96O6	925,7279453	SLM:00030837 2	SLM:00000040 0	[*]C(=O)OCC(COC([*])=O)OC([*])=O	0	8
Unspecific	TG(56:8)	M+Na	C59H98O6	925,72554	SLM:00030835 4	SLM:00000040 0	[*]C(=O)OCC(COC([*])=O)OC([*])=O	0	3
Unspecific	PI(38:4)	M+K	C47H83O13P	925,5202656	SLM:00005823 7	SLM:00005521 6	OC1C(O)C(O)C(OP([O-])(=O)OCC(COC([*])=O)OC([*])=O)C(O)C1O	0	3
Unspecific	TG(56:9)	M+Na	C59H96O6	923,7098899	SLM:00030835 5	SLM:00000040 0	[*]C(=O)OCC(COC([*])=O)OC([*])=O	0	3
Unspecific	TG(54:5)	M+K	C57H100O6	919,7151273	SLM:00030832 5	SLM:00000040 0	[*]C(=O)OCC(COC([*])=O)OC([*])=O	0	5
Unspecific	TG(56:3)	M+H	C59H108O6	913,821845	SLM:00030834	SLM:00000040	[*]C(=O)OCC(COC([*])=O)OC([*])=O	0	6

				7	9	0			
Unspecific	PS(42:1)	M+K	C48H92NO10P	912,609021	SLM:00005892 7	SLM:00005521 8	[NH3+][C@@H](COP([O-])(=O)OCC(COC([*])=O)OC([*])=O)C([O-])=O	72086	9
Unspecific	PS(42:2)	M+K	C48H90NO10P	910,593370 9	SLM:00005893 0	SLM:00005521 8	[NH3+][C@@H](COP([O-])(=O)OCC(COC([*])=O)OC([*])=O)C([O-])=O	72087	5
Unspecific	TG(56:5)	M+H	C59H104O6	909,790545 5	SLM:00030835 1	SLM:00000040 0	[*]C(=O)OCC(COC([*])=O)OC([*])=O	0	6
Unspecific	TG(54:2)	M+Na	C57H106O6	909,788140 2	SLM:00030832 2	SLM:00000040 0	[*]C(=O)OCC(COC([*])=O)OC([*])=O	0	6
Unspecific	PI(40:7)	M+H	C49H81O13P	909,548733 6	SLM:00005825 8	SLM:00005521 6	OC1C(O)C(O)C(OP([O-])(=O)OCC(COC([*])=O)OC([*])=O)C(O)C1O	0	4
Unspecific	PI(38:5)	M+Na	C47H81O13P	907,530678 3	SLM:00005823 8	SLM:00005521 6	OC1C(O)C(O)C(OP([O-])(=O)OCC(COC([*])=O)OC([*])=O)C(O)C1O	0	4
Unspecific	TG(56:7)	M+H	C59H100O6	905,759245 4	SLM:00030835 3	SLM:00000040 0	[*]C(=O)OCC(COC([*])=O)OC([*])=O	0	5
Unspecific	PS(43:4)	M+Na	C49H88NO10P	904,603783 6	SLM:00005894 2	SLM:00005521 8	[NH3+][C@@H](COP([O-])(=O)OCC(COC([*])=O)OC([*])=O)C([O-])=O	0	9
Unspecific	TG(56:8)	M+H	C59H98O6	903,743595 3	SLM:00030835 4	SLM:00000040 0	[*]C(=O)OCC(COC([*])=O)OC([*])=O	0	3
Unspecific	TG(54:5)	M+Na	C57H100O6	903,74119	SLM:00030832 5	SLM:00000040 0	[*]C(=O)OCC(COC([*])=O)OC([*])=O	0	5
Unspecific	TG(56:9)	M+H	C59H96O6	901,727945 3	SLM:00030835 5	SLM:00000040 0	[*]C(=O)OCC(COC([*])=O)OC([*])=O	0	3
Unspecific	TG(52:1)	M+K	C55H104O6	899,746427 4	SLM:00030829 6	SLM:00000040 0	[*]C(=O)OCC(COC([*])=O)OC([*])=O	0	5
Unspecific	PC(42:1)	M+Na	C50H98NO8P	894,692204 7	SLM:00005657 3	SLM:00005521 1	C[N+](C)(C)CCOP([O-])(=O)OCC(COC([*])=O)OC([*])=O	66970	4
Unspecific	PC(44:5)	M+H	C52H94NO8P	892,67896	SLM:00005659 9	SLM:00005521 1	C[N+](C)(C)CCOP([O-])(=O)OCC(COC([*])=O)OC([*])=O	66974	3
Unspecific	PC(42:2)	M+Na	C50H96NO8P	892,676554 6	SLM:00005657 6	SLM:00005521 1	C[N+](C)(C)CCOP([O-])(=O)OCC(COC([*])=O)OC([*])=O	66969	3
Unspecific	PC(44:6)	M+H	C52H92NO8P	890,663309 9	SLM:00005660 0	SLM:00005521 1	C[N+](C)(C)CCOP([O-])(=O)OCC(COC([*])=O)OC([*])=O	66973	3
Unspecific	PC(42:3)	M+Na	C50H94NO8P	890,660904 6	SLM:00005657 7	SLM:00005521 1	C[N+](C)(C)CCOP([O-])(=O)OCC(COC([*])=O)OC([*])=O	66968	3
Unspecific	PI(38:4)	M+H	C47H83O13P	887,564383 7	SLM:00005823 7	SLM:00005521 6	OC1C(O)C(O)C(OP([O-])(=O)OCC(COC([*])=O)OC([*])=O)C(O)C1O	0	3
Unspecific	PI(36:1)	M+Na	C45H85O13P	887,561978 4	SLM:00005821 8	SLM:00005521 6	OC1C(O)C(O)C(OP([O-])(=O)OCC(COC([*])=O)OC([*])=O)C(O)C1O	74371	9
Unspecific	PC(44:8)	M+H	C52H88NO8P	886,632009 8	SLM:00005660 2	SLM:00005521 1	C[N+](C)(C)CCOP([O-])(=O)OCC(COC([*])=O)OC([*])=O	0	4
Unspecific	PC(42:5)	M+Na	C50H90NO8P	886,629604 5	SLM:00005657 9	SLM:00005521 1	C[N+](C)(C)CCOP([O-])(=O)OCC(COC([*])=O)OC([*])=O	66966	7
Unspecific	TG(52:0)	M+Na	C55H106O6	885,788140 2	SLM:00030829 5	SLM:00000040 0	[*]C(=O)OCC(COC([*])=O)OC([*])=O	0	3
Unspecific	PI(38:5)	M+H	C47H81O13P	885,548733 6	SLM:00005823 8	SLM:00005521 6	OC1C(O)C(O)C(OP([O-])(=O)OCC(COC([*])=O)OC([*])=O)C(O)C1O	0	4
Unspecific	PI(36:2)	M+Na	C45H83O13P	885,546328 3	SLM:00005821 9	SLM:00005521 6	OC1C(O)C(O)C(OP([O-])(=O)OCC(COC([*])=O)OC([*])=O)C(O)C1O	74372	7
Unspecific	PC(42:6)	M+Na	C50H88NO8P	884,613954 4	SLM:00005658 0	SLM:00005521 1	C[N+](C)(C)CCOP([O-])(=O)OCC(COC([*])=O)OC([*])=O	66965	7
Unspecific	PS(40:1)	M+K	C46H88NO10P	884,577720 9	SLM:00005890 9	SLM:00005521 8	[NH3+][C@@H](COP([O-])(=O)OCC(COC([*])=O)OC([*])=O)C([O-])=O	72079	9
Unspecific	PI(36:3)	M+Na	C45H81O13P	883,530678 3	SLM:00005822 0	SLM:00005521 6	OC1C(O)C(O)C(OP([O-])(=O)OCC(COC([*])=O)OC([*])=O)C(O)C1O	0	3
Unspecific	PS(40:2)	M+K	C46H86NO10P	882,562070 8	SLM:00005891 1	SLM:00005521 8	[NH3+][C@@H](COP([O-])(=O)OCC(COC([*])=O)OC([*])=O)C([O-])=O	72080	9
Unspecific	TG(54:5)	M+H	C57H100O6	881,759245 4	SLM:00030832 5	SLM:00000040 0	[*]C(=O)OCC(COC([*])=O)OC([*])=O	0	5
Unspecific	TG(52:2)	M+Na	C55H102O6	881,756840	SLM:00030829	SLM:00000040	[*]C(=O)OCC(COC([*])=O)OC([*])=O	0	8

				1	8	0			
Unspecific	TG(52:3)	M+Na	C55H100O6	879,74119	SLM:000308299	SLM:000000400	[*]C(=O)OCC(COC([*])=O)OC([*])=O	0	8
Unspecific	PS(41:3)	M+Na	C47H86NO10P	878,5881336	SLM:000058922	SLM:000055218	[NH3+][C@@H](COP([O-])(=O)OCC(COC([*])=O)OC([*])=O)C([O-])=O	0	9
Unspecific	PE(44:4)	M+Na	C49H90NO8P	874,6296045	SLM:000057256	SLM:000055213	[NH3+]CCOP([O-])(=O)OCC(COC([*])=O)OC([*])=O	71758	3
Unspecific	PS(41:5)	M+Na	C47H82NO10P	874,5568334	SLM:000058924	SLM:000055218	[NH3+][C@@H](COP([O-])(=O)OCC(COC([*])=O)OC([*])=O)C([O-])=O	0	3
Unspecific	PC(40:6)	M+K	C48H84NO8P	872,5565915	SLM:000056561	SLM:000055211	C[N+](C)(C)CCOP([O-])(=O)OCC(COC([*])=O)OC([*])=O	64431	4
Unspecific	PS(42:3)	M+H	C48H88NO10P	870,6218391	SLM:000058931	SLM:000055218	[NH3+][C@@H](COP([O-])(=O)OCC(COC([*])=O)OC([*])=O)C([O-])=O	72088	3
Unspecific	TG(53:4)	M+H	C56H100O6	869,7592454	SLM:000308311	SLM:000000400	[*]C(=O)OCC(COC([*])=O)OC([*])=O	0	4
Unspecific	TG(51:1)	M+Na	C54H102O6	869,7568401	SLM:000308286	SLM:000000400	[*]C(=O)OCC(COC([*])=O)OC([*])=O	0	4
Unspecific	PC(42:3)	M+H	C50H94NO8P	868,67896	SLM:000056577	SLM:000055211	C[N+](C)(C)CCOP([O-])(=O)OCC(COC([*])=O)OC([*])=O	66968	3
Unspecific	PC(40:0)	M+Na	C48H96NO8P	868,6765546	SLM:000056554	SLM:000055211	C[N+](C)(C)CCOP([O-])(=O)OCC(COC([*])=O)OC([*])=O	66866	6
Unspecific	PS(42:4)	M+H	C48H86NO10P	868,6061889	SLM:000058932	SLM:000055218	[NH3+][C@@H](COP([O-])(=O)OCC(COC([*])=O)OC([*])=O)C([O-])=O	72089	3
Unspecific	PS(40:1)	M+Na	C46H88NO10P	868,6037836	SLM:000058909	SLM:000055218	[NH3+][C@@H](COP([O-])(=O)OCC(COC([*])=O)OC([*])=O)C([O-])=O	72079	9
Unspecific	PC(42:4)	M+H	C50H92NO8P	866,6633099	SLM:000056578	SLM:000055211	C[N+](C)(C)CCOP([O-])(=O)OCC(COC([*])=O)OC([*])=O	66967	4
Unspecific	PC(40:1)	M+Na	C48H94NO8P	866,6609046	SLM:000056555	SLM:000055211	C[N+](C)(C)CCOP([O-])(=O)OCC(COC([*])=O)OC([*])=O	66865	6
Unspecific	PS(40:2)	M+Na	C46H86NO10P	866,5881336	SLM:000058911	SLM:000055218	[NH3+][C@@H](COP([O-])(=O)OCC(COC([*])=O)OC([*])=O)C([O-	72080	9

							])=O		
Unspecific	TG(51:3)	M+Na	C54H98O6	865,72554	SLM:000308288	SLM:000000400	[*]C(=O)OCC(COC([*])=O)OC([*])=O	0	3
Unspecific	PC(42:5)	M+H	C50H90NO8P	864,6476598	SLM:000056579	SLM:000055211	C[N+](C)(C)CCOP([O-])(=O)OCC(COC([*])=O)OC([*])=O	66966	7
Unspecific	PC(40:2)	M+Na	C48H92NO8P	864,6452545	SLM:000056557	SLM:000055211	C[N+](C)(C)CCOP([O-])(=O)OCC(COC([*])=O)OC([*])=O	66864	9
Unspecific	PS(40:3)	M+Na	C46H84NO10P	864,5724835	SLM:000058912	SLM:000055218	[NH3+][C@@H](COP([O-])(=O)OCC(COC([*])=O)OC([*])=O)C([O-])=O	72081	3
Unspecific	TG(51:4)	M+Na	C54H96O6	863,7098899	SLM:000308289	SLM:000000400	[*]C(=O)OCC(COC([*])=O)OC([*])=O	0	3
Unspecific	SM(d44:2)	M+Na	C49H97N2O6P	863,6976244	SLM:000390849	SLM:000001000	C[N+](C)(C)CCOP([O-])(=O)OC[C@H](NC([*])=O)[C@H](O)[*]	0	9
Unspecific	PC(42:6)	M+H	C50H88NO8P	862,6320098	SLM:000056580	SLM:000055211	C[N+](C)(C)CCOP([O-])(=O)OCC(COC([*])=O)OC([*])=O	66965	7
Unspecific	PC(40:3)	M+Na	C48H90NO8P	862,6296045	SLM:000056558	SLM:000055211	C[N+](C)(C)CCOP([O-])(=O)OCC(COC([*])=O)OC([*])=O	66863	9
Unspecific	PC(42:8)	M+H	C50H84NO8P	858,6007096	SLM:000056582	SLM:000055211	C[N+](C)(C)CCOP([O-])(=O)OCC(COC([*])=O)OC([*])=O	0	5
Unspecific	PC(40:5)	M+Na	C48H86NO8P	858,5983043	SLM:000056560	SLM:000055211	C[N+](C)(C)CCOP([O-])(=O)OCC(COC([*])=O)OC([*])=O	64524	9
Unspecific	PS(38:0)	M+K	C44H86NO10P	858,5620708	SLM:000058891	SLM:000055218	[NH3+][C@@H](COP([O-])(=O)OCC(COC([*])=O)OC([*])=O)C([O-])=O	72071	9
Unspecific	TG(52:3)	M+H	C55H100O6	857,7592454	SLM:000308299	SLM:000000400	[*]C(=O)OCC(COC([*])=O)OC([*])=O	0	8
Unspecific	TG(50:0)	M+Na	C53H102O6	857,7568401	SLM:000308275	SLM:000000400	[*]C(=O)OCC(COC([*])=O)OC([*])=O	0	6
Unspecific	PS(41:3)	M+H	C47H86NO10P	856,6061889	SLM:000058922	SLM:000055218	[NH3+][C@@H](COP([O-])(=O)OCC(COC([*])=O)OC([*])=O)C([O-])=O	0	9
Unspecific	PE(42:0)	M+Na	C47H94NO8P	854,6609046	SLM:000057230	SLM:000055213	[NH3+]CCOP([O-])(=O)OCC(COC([*])=O)OC([*])=O	71747	4
Unspecific	PC(38:1)	M+K	C46H90NO8P	854,6035417	SLM:000056538	SLM:000055211	C[N+](C)(C)CCOP([O-])(=O)OCC(COC([*])=O)OC([*])=O	66860	3

Unspecific	PS(41:4)	M+H	C47H84NO10P	854,5905389	SLM:000058923	SLM:000055218	[NH3+][C@@H](COP([O-])(=O)OCC(COC([*])=O)OC([*])=O)C([O-])=O	0	8
Unspecific	PS(39:1)	M+Na	C45H86NO10P	854,5881336	SLM:000058902	SLM:000055218	[NH3+][C@@H](COP([O-])(=O)OCC(COC([*])=O)OC([*])=O)C([O-])=O	0	8
Unspecific	PC(39:1)	M+Na	C47H92NO8P	852,6452545	SLM:000056548	SLM:000055211	C[N+](C)(C)CCOP([O-])(=O)OCC(COC([*])=O)OC([*])=O	0	3
Unspecific	PC(38:2)	M+K	C46H88NO8P	852,5878916	SLM:000056539	SLM:000055211	C[N+](C)(C)CCOP([O-])(=O)OCC(COC([*])=O)OC([*])=O	66859	5
Unspecific	PC(40:8)	M+Na	C48H80NO8P	852,5513541	SLM:000056563	SLM:000055211	C[N+](C)(C)CCOP([O-])(=O)OCC(COC([*])=O)OC([*])=O	0	3
Unspecific	TG(50:3)	M+Na	C53H96O6	851,7098899	SLM:000308278	SLM:000000400	[*]C(=O)OCC(COC([*])=O)OC([*])=O	0	9
Unspecific	SM(d42:2)	M+K	C47H93N2O6P	851,6402616	SLM:000390823	SLM:000001000	C[N+](C)(C)CCOP([O-])(=O)OC[C@H](NC([*])=O)[C@H](O)[*]	0	8
Unspecific	PE(44:5)	M+H	C49H88NO8P	850,6320098	SLM:000057257	SLM:000055213	[NH3+]CCOP([O-])(=O)OCC(COC([*])=O)OC([*])=O	71759	3
Unspecific	TG(50:4)	M+Na	C53H94O6	849,6942398	SLM:000308279	SLM:000000400	[*]C(=O)OCC(COC([*])=O)OC([*])=O	0	4
Unspecific	PE(42:3)	M+Na	C47H88NO8P	848,6139544	SLM:000057235	SLM:000055213	[NH3+]CCOP([O-])(=O)OCC(COC([*])=O)OC([*])=O	71750	5
Unspecific	PE(41:4)	M+K	C46H84NO8P	848,5565915	SLM:000057227	SLM:000055213	[NH3+]CCOP([O-])(=O)OCC(COC([*])=O)OC([*])=O	0	8
Unspecific	PC(40:0)	M+H	C48H96NO8P	846,69461	SLM:000056554	SLM:000055211	C[N+](C)(C)CCOP([O-])(=O)OCC(COC([*])=O)OC([*])=O	66866	6
Unspecific	PS(39:5)	M+Na	C45H78NO10P	846,5255333	SLM:000058906	SLM:000055218	[NH3+][C@@H](COP([O-])(=O)OCC(COC([*])=O)OC([*])=O)C([O-])=O	0	4
Unspecific	PE(42:5)	M+Na	C47H84NO8P	844,5826543	SLM:000057237	SLM:000055213	[NH3+]CCOP([O-])(=O)OCC(COC([*])=O)OC([*])=O	71752	3
Unspecific	PE(42:6)	M+Na	C47H82NO8P	842,5670042	SLM:000057238	SLM:000055213	[NH3+]CCOP([O-])(=O)OCC(COC([*])=O)OC([*])=O	71753	3
Unspecific	SM(d44:2)	M+H	C49H97N2O6P	841,7156798	SLM:000390849	SLM:000001000	C[N+](C)(C)CCOP([O-])(=O)OC[C@H](NC([*])=O)[C@H](O)[*]	0	9
Unspecific	PE(43:4)	M+H	C48H88NO8P	838,632009	SLM:000057249	SLM:000055213	[NH3+]CCOP([O-	0	5

				8	6	3	])(=O)OCC(COC([*])=O)OC([*])=O		
Unspecific	PC(38:1)	M+Na	C46H90NO8P	838,6296045	SLM:000056538	SLM:000055211	C[N+](C)(C)CCOP([O-])(=O)OCC(COC([*])=O)OC([*])=O	66860	3
Unspecific	SM(d42:1)	M+Na	C47H95N2O6P	837,6819744	SLM:000390824	SLM:000001000	C[N+](C)(C)CCOP([O-])(=O)OC[C@H](NC([*])=O)[C@H](O)[*]	0	9
Unspecific	PC(40:5)	M+H	C48H86NO8P	836,6163597	SLM:000056560	SLM:000055211	C[N+](C)(C)CCOP([O-])(=O)OCC(COC([*])=O)OC([*])=O	64524	9
Unspecific	PC(38:2)	M+Na	C46H88NO8P	836,6139544	SLM:000056539	SLM:000055211	C[N+](C)(C)CCOP([O-])(=O)OCC(COC([*])=O)OC([*])=O	66859	5
Unspecific	SM(d42:2)	M+Na	C47H93N2O6P	835,6663243	SLM:000390823	SLM:000001000	C[N+](C)(C)CCOP([O-])(=O)OC[C@H](NC([*])=O)[C@H](O)[*]	0	8
Unspecific	PC(40:8)	M+H	C48H80NO8P	830,5694095	SLM:000056563	SLM:000055211	C[N+](C)(C)CCOP([O-])(=O)OCC(COC([*])=O)OC([*])=O	0	3
Unspecific	PE(41:5)	M+Na	C46H82NO8P	830,5670042	SLM:000057228	SLM:000055213	[NH3+]CCOP([O-])(=O)OCC(COC([*])=O)OC([*])=O	0	9
Unspecific	PS(36:0)	M+K	C42H82NO10P	830,5307707	SLM:000058875	SLM:000055218	[NH3+][C@@H](COP([O-])(=O)OCC(COC([*])=O)OC([*])=O)C([O-])=O	72064	9
Unspecific	TG(50:3)	M+H	C53H96O6	829,7279453	SLM:000308278	SLM:000000400	[*]C(=O)OCC(COC([*])=O)OC([*])=O	0	9
Unspecific	TG(48:0)	M+Na	C51H98O6	829,72554	SLM:000308257	SLM:000000400	[*]C(=O)OCC(COC([*])=O)OC([*])=O	0	6
Unspecific	PE(41:6)	M+Na	C46H80NO8P	828,5513541	SLM:000057229	SLM:000055213	[NH3+]CCOP([O-])(=O)OCC(COC([*])=O)OC([*])=O	0	5
Unspecific	TG(50:4)	M+H	C53H94O6	827,7122952	SLM:000308279	SLM:000000400	[*]C(=O)OCC(COC([*])=O)OC([*])=O	0	4
Unspecific	TG(48:1)	M+Na	C51H96O6	827,7098899	SLM:000308258	SLM:000000400	[*]C(=O)OCC(COC([*])=O)OC([*])=O	0	4
Unspecific	PS(37:1)	M+Na	C43H82NO10P	826,5568334	SLM:000058885	SLM:000055218	[NH3+][C@@H](COP([O-])(=O)OCC(COC([*])=O)OC([*])=O)C([O-])=O	0	3
Unspecific	PE(42:4)	M+H	C47H86NO8P	824,6163597	SLM:000057236	SLM:000055213	[NH3+]CCOP([O-])(=O)OCC(COC([*])=O)OC([*])=O	71751	9
Unspecific	PC(37:1)	M+Na	C45H88NO8P	824,6139544	SLM:000056531	SLM:000055211	C[N+](C)(C)CCOP([O-])(=O)OCC(COC([*])=O)OC([*])=O	0	9
Unspecific	PC(36:2)	M+K	C44H84NO8P	824,556591	SLM:000056522	SLM:000055211	C[N+](C)(C)CCOP([O-	6443	9

				5	3	1	])(=O)OCC(COC([*])=O)OC([*])=O	3	
Unspecific	SM(d41:1)	M+Na	C46H93N2O6P	823,6663243	SLM:000390811	SLM:000001000	C[N+](C)(C)CCOP([O-])(=O)OC[C@H](NC([*])=O)[C@H](O)[*]	0	9
Unspecific	SM(d40:2)	M+K	C45H89N2O6P	823,6089614	SLM:000390795	SLM:000001000	C[N+](C)(C)CCOP([O-])(=O)OC[C@H](NC([*])=O)[C@H](O)[*]	0	8
Unspecific	SM(d40:3)	M+K	C45H87N2O6P	821,5931114	SLM:000390793	SLM:000001000	C[N+](C)(C)CCOP([O-])(=O)OC[C@H](NC([*])=O)[C@H](O)[*]	0	9
Unspecific	PS(37:4)	M+Na	C43H76NO10P	820,5098832	SLM:000058888	SLM:000055218	[NH3+][C@@H](COP([O-])(=O)OCC(COC([*])=O)OC([*])=O)C([O-])=O	0	5
Unspecific	PE(42:7)	M+H	C47H80NO8P	818,5694095	SLM:000057239	SLM:000055213	[NH3+]CCOP([O-])(=O)OCC(COC([*])=O)OC([*])=O	0	5
Unspecific	PE(40:4)	M+Na	C45H82NO8P	818,5670042	SLM:000057217	SLM:000055213	[NH3+]CCOP([O-])(=O)OCC(COC([*])=O)OC([*])=O	71744	9
Unspecific	PC(38:1)	M+H	C46H90NO8P	816,6476598	SLM:000056538	SLM:000055211	C[N+](C)(C)CCOP([O-])(=O)OCC(COC([*])=O)OC([*])=O	66860	3
Unspecific	SM(d42:1)	M+H	C47H95N2O6P	815,7002298	SLM:000390824	SLM:000001000	C[N+](C)(C)CCOP([O-])(=O)OC[C@H](NC([*])=O)[C@H](O)[*]	0	9
Unspecific	PC(38:2)	M+H	C46H88NO8P	814,6320098	SLM:000056539	SLM:000055211	C[N+](C)(C)CCOP([O-])(=O)OCC(COC([*])=O)OC([*])=O	66859	5
Unspecific	PS(38:3)	M+H	C44H80NO10P	814,5592387	SLM:000058894	SLM:000055218	[NH3+][C@@H](COP([O-])(=O)OCC(COC([*])=O)OC([*])=O)C([O-])=O	72074	7
Unspecific	PS(36:0)	M+Na	C42H82NO10P	814,5568334	SLM:000058875	SLM:000055218	[NH3+][C@@H](COP([O-])(=O)OCC(COC([*])=O)OC([*])=O)C([O-])=O	72064	9
Unspecific	SM(d42:2)	M+H	C47H93N2O6P	813,6843797	SLM:000390823	SLM:000001000	C[N+](C)(C)CCOP([O-])(=O)OC[C@H](NC([*])=O)[C@H](O)[*]	0	8
Unspecific	PE(41:3)	M+H	C46H86NO8P	812,6163597	SLM:000057226	SLM:000055213	[NH3+]CCOP([O-])(=O)OCC(COC([*])=O)OC([*])=O	0	5
Unspecific	PC(36:0)	M+Na	C44H88NO8P	812,6139544	SLM:000056521	SLM:000055211	C[N+](C)(C)CCOP([O-])(=O)OCC(COC([*])=O)OC([*])=O	66858	9
Unspecific	PE(41:4)	M+H	C46H84NO8P	810,6007096	SLM:000057227	SLM:000055213	[NH3+]CCOP([O-])(=O)OCC(COC([*])=O)OC([*])=O	0	8
Unspecific	PE(39:1)	M+Na	C44H86NO8P	810,5983043	SLM:000057206	SLM:000055213	[NH3+]CCOP([O-])(=O)OCC(COC([*])=O)OC([*])=O	0	9

Unspecific	SM(d40:1)	M+Na	C45H91N2O6P	809,6506743	SLM:000390797	SLM:000001000	C[N+](C)(C)CCOP([O-])(=O)OC[C@H](NC([*])=O)[C@H](O)[*]	0	9
Unspecific	PE(41:5)	M+H	C46H82NO8P	808,5850596	SLM:000057228	SLM:000055213	[NH3+]CCOP([O-])(=O)OCC(COC([*])=O)OC([*])=O	0	9
Unspecific	PC(36:2)	M+Na	C44H84NO8P	808,5826543	SLM:000056523	SLM:000055211	C[N+](C)(C)CCOP([O-])(=O)OCC(COC([*])=O)OC([*])=O	64433	9
Unspecific	SM(d40:2)	M+Na	C45H89N2O6P	807,6350242	SLM:000390795	SLM:000001000	C[N+](C)(C)CCOP([O-])(=O)OC[C@H](NC([*])=O)[C@H](O)[*]	0	8
Unspecific	PE(41:6)	M+H	C46H80NO8P	806,5694095	SLM:000057229	SLM:000055213	[NH3+]CCOP([O-])(=O)OCC(COC([*])=O)OC([*])=O	0	5
Unspecific	PE(39:3)	M+Na	C44H82NO8P	806,5670042	SLM:000057208	SLM:000055213	[NH3+]CCOP([O-])(=O)OCC(COC([*])=O)OC([*])=O	0	5
Unspecific	SM(d40:3)	M+Na	C45H87N2O6P	805,6193741	SLM:000390793	SLM:000001000	C[N+](C)(C)CCOP([O-])(=O)OC[C@H](NC([*])=O)[C@H](O)[*]	0	9
Unspecific	PE(39:4)	M+Na	C44H80NO8P	804,5513541	SLM:000057209	SLM:000055213	[NH3+]CCOP([O-])(=O)OCC(COC([*])=O)OC([*])=O	0	8
Unspecific	PC(37:1)	M+H	C45H88NO8P	802,6320098	SLM:000056531	SLM:000055211	C[N+](C)(C)CCOP([O-])(=O)OCC(COC([*])=O)OC([*])=O	0	9
Unspecific	PE(39:5)	M+Na	C44H78NO8P	802,5357041	SLM:000057210	SLM:000055213	[NH3+]CCOP([O-])(=O)OCC(COC([*])=O)OC([*])=O	0	3
Unspecific	PS(34:0)	M+K	C40H78NO10P	802,4994705	SLM:000058861	SLM:000055218	[NH3+][C@@H](COP([O-])(=O)OCC(COC([*])=O)OC([*])=O)C([O-])=O	72057	9
Unspecific	SM(d41:1)	M+H	C46H93N2O6P	801,6843797	SLM:000390811	SLM:000001000	C[N+](C)(C)CCOP([O-])(=O)OC[C@H](NC([*])=O)[C@H](O)[*]	0	9
Unspecific	PE(40:2)	M+H	C45H86NO8P	800,6163597	SLM:000057215	SLM:000055213	[NH3+]CCOP([O-])(=O)OCC(COC([*])=O)OC([*])=O	71742	7
Unspecific	PC(34:0)	M+K	C42H84NO8P	800,5565915	SLM:000056507	SLM:000055211	C[N+](C)(C)CCOP([O-])(=O)OCC(COC([*])=O)OC([*])=O	66855	8
Unspecific	PS(35:0)	M+Na	C41H80NO10P	800,5411834	SLM:000058868	SLM:000055218	[NH3+][C@@H](COP([O-])(=O)OCC(COC([*])=O)OC([*])=O)C([O-])=O	0	8
Unspecific	PE(40:3)	M+H	C45H84NO8P	798,6007096	SLM:000057216	SLM:000055213	[NH3+]CCOP([O-])(=O)OCC(COC([*])=O)OC([*])=O	71743	7
Unspecific	PE(38:0)	M+Na	C43H86NO8P	798,5983043	SLM:000057195	SLM:000055213	[NH3+]CCOP([O-])(=O)OCC(COC([*])=O)OC([*])=O	71733	9

Unspecific	PS(34:2)	M+K	C40H74NO10P	798,4681704	SLM:000058863	SLM:00005521	[NH3+][C@@H](COP([O-])(=O)OCC(COC([*])=O)OC([*])=O)C([O-])=O	720559	3
Unspecific	SM(d39:1)	M+Na	C44H89N2O6P	795,6350242	SLM:000390782	SLM:00000100	C[N+](C)(C)CCOP([O-])(=O)OC[C@H](NC([*])=O)[C@H](O)[*]	0	9
Unspecific	SM(d38:2)	M+K	C43H85N2O6P	795,5776613	SLM:000390765	SLM:00000100	C[N+](C)(C)CCOP([O-])(=O)OC[C@H](NC([*])=O)[C@H](O)[*]	0	7
Unspecific	PE(40:5)	M+H	C45H80NO8P	794,5694095	SLM:000057218	SLM:00005521	[NH3+]CCOP([O-])(=O)OCC(COC([*])=O)OC([*])=O	717455	9
Unspecific	PE(38:2)	M+Na	C43H82NO8P	794,5670042	SLM:000057197	SLM:00005521	[NH3+]CCOP([O-])(=O)OCC(COC([*])=O)OC([*])=O	717355	9
Unspecific	SM(d39:2)	M+Na	C44H87N2O6P	793,6193741	SLM:000390781	SLM:00000100	C[N+](C)(C)CCOP([O-])(=O)OC[C@H](NC([*])=O)[C@H](O)[*]	0	9
Unspecific	PE(38:3)	M+Na	C43H80NO8P	792,5513541	SLM:000057198	SLM:00005521	[NH3+]CCOP([O-])(=O)OCC(COC([*])=O)OC([*])=O	717366	3
Unspecific	PE(38:4)	M+Na	C43H78NO8P	790,5357041	SLM:000057199	SLM:00005521	[NH3+]CCOP([O-])(=O)OCC(COC([*])=O)OC([*])=O	717377	9
Unspecific	PE(39:1)	M+H	C44H86NO8P	788,6163597	SLM:000057206	SLM:00005521	[NH3+]CCOP([O-])(=O)OCC(COC([*])=O)OC([*])=O	0	9
Unspecific	SM(d40:1)	M+H	C45H91N2O6P	787,6687296	SLM:000390797	SLM:00000100	C[N+](C)(C)CCOP([O-])(=O)OC[C@H](NC([*])=O)[C@H](O)[*]	0	9
Unspecific	PC(36:2)	M+H	C44H84NO8P	786,6007096	SLM:000056523	SLM:00005521	C[N+](C)(C)CCOP([O-])(=O)OCC(COC([*])=O)OC([*])=O	644333	9
Unspecific	SM(d40:2)	M+H	C45H89N2O6P	785,6530796	SLM:000390795	SLM:00000100	C[N+](C)(C)CCOP([O-])(=O)OC[C@H](NC([*])=O)[C@H](O)[*]	0	8
Unspecific	PE(39:3)	M+H	C44H82NO8P	784,5850596	SLM:000057208	SLM:00005521	[NH3+]CCOP([O-])(=O)OCC(COC([*])=O)OC([*])=O	0	5
Unspecific	PC(34:0)	M+Na	C42H84NO8P	784,5826543	SLM:000056507	SLM:00005521	C[N+](C)(C)CCOP([O-])(=O)OCC(COC([*])=O)OC([*])=O	668555	8
Unspecific	PE(36:1)	M+K	C41H80NO8P	784,5252914	SLM:000057180	SLM:00005521	[NH3+]CCOP([O-])(=O)OCC(COC([*])=O)OC([*])=O	717277	6
Unspecific	SM(d40:3)	M+H	C45H87N2O6P	783,6374295	SLM:000390793	SLM:00000100	C[N+](C)(C)CCOP([O-])(=O)OC[C@H](NC([*])=O)[C@H](O)[*]	0	9
Unspecific	PE(39:4)	M+H	C44H80NO8P	782,5694095	SLM:000057209	SLM:00005521	[NH3+]CCOP([O-])(=O)OCC(COC([*])=O)OC([*])=O	0	8
Unspecific	SM(d38:1)	M+Na	C43H87N2O6	781,619374	SLM:00039076	SLM:00000100	C[N+](C)(C)CCOP([O-	0	9

			P	1	7	0	])(=O)OC[C@H](NC([*])=O)[C@H](O)[*]		
Unspecific	PE(39:6)	M+H	C44H76NO8P	778,5381094	SLM:000057211	SLM:00005521	[NH3+]CCOP([O-])(=O)OCC(COC([*])=O)OC([*])=O	0	3
Unspecific	PE(37:3)	M+Na	C42H78NO8P	778,5357041	SLM:000057191	SLM:00005521	[NH3+]CCOP([O-])(=O)OCC(COC([*])=O)OC([*])=O	0	9
Unspecific	PE(38:0)	M+H	C43H86NO8P	776,6163597	SLM:000057195	SLM:00005521	[NH3+]CCOP([O-])(=O)OCC(COC([*])=O)OC([*])=O	717333	9
Unspecific	PE(38:1)	M+H	C43H84NO8P	774,6007096	SLM:000057196	SLM:00005521	[NH3+]CCOP([O-])(=O)OCC(COC([*])=O)OC([*])=O	717344	4
Unspecific	SM(d39:1)	M+H	C44H89N2O6P	773,6530796	SLM:000390782	SLM:00000100	C[N+](C)(C)CCOP([O-])(=O)OC[C@H](NC([*])=O)[C@H](O)[*]	0	9
Unspecific	PE(38:2)	M+H	C43H82NO8P	772,5850596	SLM:000057197	SLM:00005521	[NH3+]CCOP([O-])(=O)OCC(COC([*])=O)OC([*])=O	717355	9
Unspecific	PE(35:0)	M+K	C40H80NO8P	772,5252914	SLM:000057172	SLM:00005521	[NH3+]CCOP([O-])(=O)OCC(COC([*])=O)OC([*])=O	0	9
Unspecific	SM(d39:2)	M+H	C44H87N2O6P	771,6374295	SLM:000390780	SLM:00000100	C[N+](C)(C)CCOP([O-])(=O)OC[C@H](NC([*])=O)[C@H](O)[*]	0	9
Unspecific	PE(38:3)	M+H	C43H80NO8P	770,5694095	SLM:000057198	SLM:00005521	[NH3+]CCOP([O-])(=O)OCC(COC([*])=O)OC([*])=O	717366	3
Unspecific	PE(36:0)	M+Na	C41H82NO8P	770,5670042	SLM:000057179	SLM:00005521	[NH3+]CCOP([O-])(=O)OCC(COC([*])=O)OC([*])=O	717266	9
Unspecific	PC(32:1)	M+K	C40H78NO8P	770,5096413	SLM:000056494	SLM:00005521	C[N+](C)(C)CCOP([O-])(=O)OCC(COC([*])=O)OC([*])=O	668497	7
Unspecific	PE(38:4)	M+H	C43H78NO8P	768,5537594	SLM:000057199	SLM:00005521	[NH3+]CCOP([O-])(=O)OCC(COC([*])=O)OC([*])=O	717377	9
Unspecific	PE(36:1)	M+Na	C41H80NO8P	768,5513541	SLM:000057180	SLM:00005521	[NH3+]CCOP([O-])(=O)OCC(COC([*])=O)OC([*])=O	717277	6
Unspecific	SM(d37:1)	M+Na	C42H85N2O6P	767,6037241	SLM:000390753	SLM:00000100	C[N+](C)(C)CCOP([O-])(=O)OC[C@H](NC([*])=O)[C@H](O)[*]	0	9
Unspecific	PE(38:5)	M+H	C43H76NO8P	766,5381094	SLM:000057200	SLM:00005521	[NH3+]CCOP([O-])(=O)OCC(COC([*])=O)OC([*])=O	717388	9
Unspecific	PE(36:2)	M+Na	C41H78NO8P	766,5357041	SLM:000057181	SLM:00005521	[NH3+]CCOP([O-])(=O)OCC(COC([*])=O)OC([*])=O	717288	9
Unspecific	SM(d37:2)	M+Na	C42H83N2O6P	765,588074	SLM:000390751	SLM:00000100	C[N+](C)(C)CCOP([O-])(=O)OC[C@H](NC([*])=O)[C@H](O)[*]	0	7
Unspecific	PE(36:3)	M+Na	C41H76NO8P	764,520054	SLM:00005718	SLM:00005521	[NH3+]CCOP([O-	7172	9

					2	3	])(=O)OCC(COC([*])=O)OC([*])=O	9	
Unspecific	PC(34:0)	M+H	C42H84NO8P	762,6007096	SLM:000056507	SLM:000055211	C[N+](C)(C)CCOP([O-])(=O)OCC(COC([*])=O)OC([*])=O	66855	8
Unspecific	SM(d38:1)	M+H	C43H87N2O6P	759,6374295	SLM:000390767	SLM:000001000	C[N+](C)(C)CCOP([O-])(=O)OC[C@H](NC([*])=O)[C@H](O)[*]	0	9
Unspecific	PE(37:2)	M+H	C42H80NO8P	758,5694095	SLM:000057190	SLM:000055213	[NH3+]CCOP([O-])(=O)OCC(COC([*])=O)OC([*])=O	0	9
Unspecific	PE(34:0)	M+K	C39H78NO8P	758,5096413	SLM:000057165	SLM:000055213	[NH3+]CCOP([O-])(=O)OCC(COC([*])=O)OC([*])=O	71718	5
Unspecific	SM(d38:2)	M+H	C43H85N2O6P	757,6217794	SLM:000390765	SLM:000001000	C[N+](C)(C)CCOP([O-])(=O)OC[C@H](NC([*])=O)[C@H](O)[*]	0	7
Unspecific	PE(37:3)	M+H	C42H78NO8P	756,5537594	SLM:000057191	SLM:000055213	[NH3+]CCOP([O-])(=O)OCC(COC([*])=O)OC([*])=O	0	9
Unspecific	PE(35:0)	M+Na	C40H80NO8P	756,5513541	SLM:000057172	SLM:000055213	[NH3+]CCOP([O-])(=O)OCC(COC([*])=O)OC([*])=O	0	9
Unspecific	PE(37:4)	M+H	C42H76NO8P	754,5381094	SLM:000057192	SLM:000055213	[NH3+]CCOP([O-])(=O)OCC(COC([*])=O)OC([*])=O	0	9
Unspecific	PC(32:1)	M+Na	C40H78NO8P	754,5357041	SLM:000056494	SLM:000055211	C[N+](C)(C)CCOP([O-])(=O)OCC(COC([*])=O)OC([*])=O	66849	7
Unspecific	SM(d36:1)	M+Na	C41H83N2O6P	753,588074	SLM:000390739	SLM:000001000	C[N+](C)(C)CCOP([O-])(=O)OC[C@H](NC([*])=O)[C@H](O)[*]	0	9
Unspecific	PE(35:2)	M+Na	C40H76NO8P	752,520054	SLM:000057174	SLM:000055213	[NH3+]CCOP([O-])(=O)OCC(COC([*])=O)OC([*])=O	0	6
Unspecific	SM(d36:2)	M+Na	C41H81N2O6P	751,5724239	SLM:000390737	SLM:000001000	C[N+](C)(C)CCOP([O-])(=O)OC[C@H](NC([*])=O)[C@H](O)[*]	0	9
Unspecific	SM(d36:3)	M+Na	C41H79N2O6P	749,5567739	SLM:000390735	SLM:000001000	C[N+](C)(C)CCOP([O-])(=O)OC[C@H](NC([*])=O)[C@H](O)[*]	0	7
Unspecific	PE(36:0)	M+H	C41H82NO8P	748,5850596	SLM:000057179	SLM:000055213	[NH3+]CCOP([O-])(=O)OCC(COC([*])=O)OC([*])=O	71726	9
Unspecific	PE(36:1)	M+H	C41H80NO8P	746,5694095	SLM:000057180	SLM:000055213	[NH3+]CCOP([O-])(=O)OCC(COC([*])=O)OC([*])=O	71727	6
Unspecific	SM(d37:1)	M+H	C42H85N2O6P	745,6217794	SLM:000390753	SLM:000001000	C[N+](C)(C)CCOP([O-])(=O)OC[C@H](NC([*])=O)[C@H](O)[*]	0	9
Unspecific	SM(d37:2)	M+H	C42H83N2O6P	743,6061294	SLM:000390751	SLM:000001000	C[N+](C)(C)CCOP([O-])(=O)OC[C@H](NC([*])=O)[C@H](O)[*]	0	7
Unspecific	PE(36:3)	M+H	C41H76NO8P	742,538109	SLM:000057186	SLM:000055213	[NH3+]CCOP([O-	7172	9

				4	2	3	])(=O)OCC(COC([*])=O)OC([*])=O	9	
Unspecific	PE(34:0)	M+Na	C39H78NO8P	742,5357041	SLM:000057165	SLM:000055213	[NH3+]CCOP([O-])(=O)OCC(COC([*])=O)OC([*])=O	71718	5
Unspecific	PE(34:1)	M+Na	C39H76NO8P	740,520054	SLM:000057166	SLM:000055213	[NH3+]CCOP([O-])(=O)OCC(COC([*])=O)OC([*])=O	71720	4
Unspecific	SM(d35:1)	M+Na	C40H81N2O6P	739,5724239	SLM:000390726	SLM:000001000	C[N+](C)(C)CCOP([O-])(=O)OC[C@H](NC([*])=O)[C@H](O)[*]	0	9
Unspecific	PE(34:2)	M+Na	C39H74NO8P	738,5044039	SLM:000057167	SLM:000055213	[NH3+]CCOP([O-])(=O)OCC(COC([*])=O)OC([*])=O	71721	5
Unspecific	PE(34:3)	M+Na	C39H72NO8P	736,4887539	SLM:000057168	SLM:000055213	[NH3+]CCOP([O-])(=O)OCC(COC([*])=O)OC([*])=O	71722	3
Unspecific	PC(32:1)	M+H	C40H78NO8P	732,5537594	SLM:000056494	SLM:000055211	C[N+](C)(C)CCOP([O-])(=O)OCC(COC([*])=O)OC([*])=O	66849	7
Unspecific	SM(d36:1)	M+H	C41H83N2O6P	731,6061294	SLM:000390739	SLM:000001000	C[N+](C)(C)CCOP([O-])(=O)OC[C@H](NC([*])=O)[C@H](O)[*]	0	9
Unspecific	PE(35:2)	M+H	C40H76NO8P	730,5381094	SLM:000057174	SLM:000055213	[NH3+]CCOP([O-])(=O)OCC(COC([*])=O)OC([*])=O	0	6
Unspecific	SM(d36:2)	M+H	C41H81N2O6P	729,5902793	SLM:000390737	SLM:000001000	C[N+](C)(C)CCOP([O-])(=O)OC[C@H](NC([*])=O)[C@H](O)[*]	0	9
Unspecific	PC(30:0)	M+Na	C38H76NO8P	728,520054	SLM:000056479	SLM:000055211	C[N+](C)(C)CCOP([O-])(=O)OCC(COC([*])=O)OC([*])=O	65303	9
Unspecific	SM(d36:3)	M+H	C41H79N2O6P	727,5748292	SLM:000390735	SLM:000001000	C[N+](C)(C)CCOP([O-])(=O)OC[C@H](NC([*])=O)[C@H](O)[*]	0	7
Unspecific	SM(d33:1)	M+K	C38H77N2O6P	727,515061	SLM:000390704	SLM:000001000	C[N+](C)(C)CCOP([O-])(=O)OC[C@H](NC([*])=O)[C@H](O)[*]	0	9
Unspecific	PE(33:1)	M+Na	C38H74NO8P	726,5044039	SLM:000057159	SLM:000055213	[NH3+]CCOP([O-])(=O)OCC(COC([*])=O)OC([*])=O	0	8
Unspecific	PE(34:1)	M+H	C39H76NO8P	718,5381094	SLM:000057166	SLM:000055213	[NH3+]CCOP([O-])(=O)OCC(COC([*])=O)OC([*])=O	71720	4
Unspecific	SM(d35:1)	M+H	C40H81N2O6P	717,5902793	SLM:000390726	SLM:000001000	C[N+](C)(C)CCOP([O-])(=O)OC[C@H](NC([*])=O)[C@H](O)[*]	0	9
Unspecific	PE(34:2)	M+H	C39H74NO8P	716,5224593	SLM:000057167	SLM:000055213	[NH3+]CCOP([O-])(=O)OCC(COC([*])=O)OC([*])=O	71721	5
Unspecific	SM(d33:1)	M+Na	C38H77N2O6P	711,5411238	SLM:000390704	SLM:000001000	C[N+](C)(C)CCOP([O-])(=O)OC[C@H](NC([*])=O)[C@H](O)[*]	0	9
Unspecific	PC(28:0)	M+Na	C36H72NO8P	700,488753	SLM:000056466	SLM:000055211	C[N+](C)(C)CCOP([O-	6529	3

				9	6	1	])(=O)OCC(COC([*])=O)OC([*])=O	4	
Unspecific	SM(d33:1)	M+H	C38H77N2O6P	689,5591792	SLM:000390704	SLM:000001000	C[N+](C)(C)CCOP([O-])(=O)OC[C@H](NC([*])=O)[C@H](O)[*]	0	9
Unspecific	PC(28:0)	M+H	C36H72NO8P	678,5068092	SLM:000056466	SLM:000055211	C[N+](C)(C)CCOP([O-])(=O)OCC(COC([*])=O)OC([*])=O	65294	3
Unspecific	DG(40:4)	M+H	C43H76O5	673,57653	SLM:000307449	SLM:000000401	[*]OCC(CO[*])O[*]	0	3
Unspecific	DG(40:5)	M+H	C43H74O5	671,56088	SLM:000307450	SLM:000000401	[*]OCC(CO[*])O[*]	0	3
Unspecific	DG(38:2)	M+Na	C41H76O5	671,5584746	SLM:000307429	SLM:000000401	[*]OCC(CO[*])O[*]	0	3
Unspecific	DG(38:4)	M+Na	C41H72O5	667,5271745	SLM:000307431	SLM:000000401	[*]OCC(CO[*])O[*]	0	3
Unspecific	DG(38:4)	M+H	C41H72O5	645,5452299	SLM:000307431	SLM:000000401	[*]OCC(CO[*])O[*]	0	3
Unspecific	DG(36:1)	M+Na	C39H74O5	645,5428246	SLM:000307412	SLM:000000401	[*]OCC(CO[*])O[*]	0	3
Unspecific	LPC(24:1)	M+Na	C32H64NO7P	628,431239	SLM:000055343	SLM:000055200	C[N+](C)(C)CCOP([O-])(=O)OCC(CO[*])O[*]	74471	5
Unspecific	DG(36:3)	M+H	C39H70O5	619,5295798	SLM:000307414	SLM:000000401	[*]OCC(CO[*])O[*]	0	4
Unspecific	DG(34:1)	M+Na	C37H70O5	617,5115245	SLM:000307398	SLM:000000401	[*]OCC(CO[*])O[*]	0	3
Unspecific	DG(34:2)	M+Na	C37H68O5	615,4958744	SLM:000307399	SLM:000000401	[*]OCC(CO[*])O[*]	0	3
Unspecific	LPC(22:6)	M+K	C30H50NO7P	606,2956258	SLM:000055341	SLM:000055200	C[N+](C)(C)CCOP([O-])(=O)OCC(CO[*])O[*]	0	6
Unspecific	LPC(22:4)	M+Na	C30H54NO7P	594,3529887	SLM:000055339	SLM:000055200	C[N+](C)(C)CCOP([O-])(=O)OCC(CO[*])O[*]	0	6
Unspecific	LPC(22:0)	M+H	C30H62NO7P	580,4336443	SLM:000055335	SLM:000055200	C[N+](C)(C)CCOP([O-])(=O)OCC(CO[*])O[*]	67061	3
Unspecific	LPC(22:1)	M+H	C30H60NO7P	578,4179942	SLM:000055336	SLM:000055200	C[N+](C)(C)CCOP([O-])(=O)OCC(CO[*])O[*]	67060	4
Unspecific	LPC(20:0)	M+Na	C28H58NO7P	574,3842888	SLM:000055328	SLM:000055200	C[N+](C)(C)CCOP([O-])(=O)OCC(CO[*])O[*]	67058	4
Unspecific	LPC(22:6)	M+H	C30H50NO7P	568,339743	SLM:00005534	SLM:00005520	C[N+](C)(C)CCOP([O-	0	6

				9	1	0	])(=O)OCC(CO[*])O[*]		
Unspecific	Cer(d36:1)	M+H	C36H71NO3	566,5506496	SLM:000391261	SLM:000399814	OC[C@H](NC([*])=O)[C@H](O)[*]	0	3
Unspecific	LPC(18:0)	M+K	C26H54NO7P	562,3269259	SLM:000055322	SLM:000055200	C[N+](C)(C)CCOP([O-])(=O)OCC(CO[*])O[*]	64561	9
Unspecific	Cer(d34:1)	M+Na	C34H67NO3	560,5012941	SLM:000391236	SLM:000399814	OC[C@H](NC([*])=O)[C@H](O)[*]	0	3
Unspecific	LPC(20:3)	M+H	C28H52NO7P	546,355394	SLM:000055331	SLM:000055200	C[N+](C)(C)CCOP([O-])(=O)OCC(CO[*])O[*]	0	6
Unspecific	LPC(18:0)	M+Na	C26H54NO7P	546,352988	SLM:000055322	SLM:000055200	C[N+](C)(C)CCOP([O-])(=O)OCC(CO[*])O[*]	64561	9
Unspecific	LPC(20:4)	M+H	C28H50NO7P	544,3397439	SLM:000055332	SLM:000055200	C[N+](C)(C)CCOP([O-])(=O)OCC(CO[*])O[*]	0	7
Unspecific	LPC(18:1)	M+Na	C26H52NO7P	544,3373386	SLM:000055323	SLM:000055200	C[N+](C)(C)CCOP([O-])(=O)OCC(CO[*])O[*]	64566	9
Unspecific	LPC(19:0)	M+H	C27H56NO7P	538,3866941	SLM:000055327	SLM:000055200	C[N+](C)(C)CCOP([O-])(=O)OCC(CO[*])O[*]	0	6
Unspecific	LPC(16:0)	M+K	C24H50NO7P	534,2956258	SLM:000055318	SLM:000055200	C[N+](C)(C)CCOP([O-])(=O)OCC(CO[*])O[*]	64563	9
Unspecific	LPC(17:0)	M+Na	C25H52NO7P	532,3373386	SLM:000055321	SLM:000055200	C[N+](C)(C)CCOP([O-])(=O)OCC(CO[*])O[*]	0	9
Unspecific	LPC(18:0)	M+H	C26H54NO7P	524,3710441	SLM:000055322	SLM:000055200	C[N+](C)(C)CCOP([O-])(=O)OCC(CO[*])O[*]	64561	9
Unspecific	LPC(18:2)	M+H	C26H50NO7P	520,3397439	SLM:000055324	SLM:000055200	C[N+](C)(C)CCOP([O-])(=O)OCC(CO[*])O[*]	0	9
Unspecific	LPC(16:0)	M+Na	C24H50NO7P	518,3216886	SLM:000055318	SLM:000055200	C[N+](C)(C)CCOP([O-])(=O)OCC(CO[*])O[*]	64563	9
Unspecific	LPC(15:0)	M+Na	C23H48NO7P	504,3060385	SLM:000055317	SLM:000055200	C[N+](C)(C)CCOP([O-])(=O)OCC(CO[*])O[*]	0	4
Unspecific	LPC(17:0)	M+H	C25H52NO7P	510,355394	SLM:000055321	SLM:000055200	C[N+](C)(C)CCOP([O-])(=O)OCC(CO[*])O[*]	0	9

S1 Fig. Graphical illustration of LC-MS^2 data analysis workflow.

https://doi.org/10.1371/journal.pntd.0008145.s005

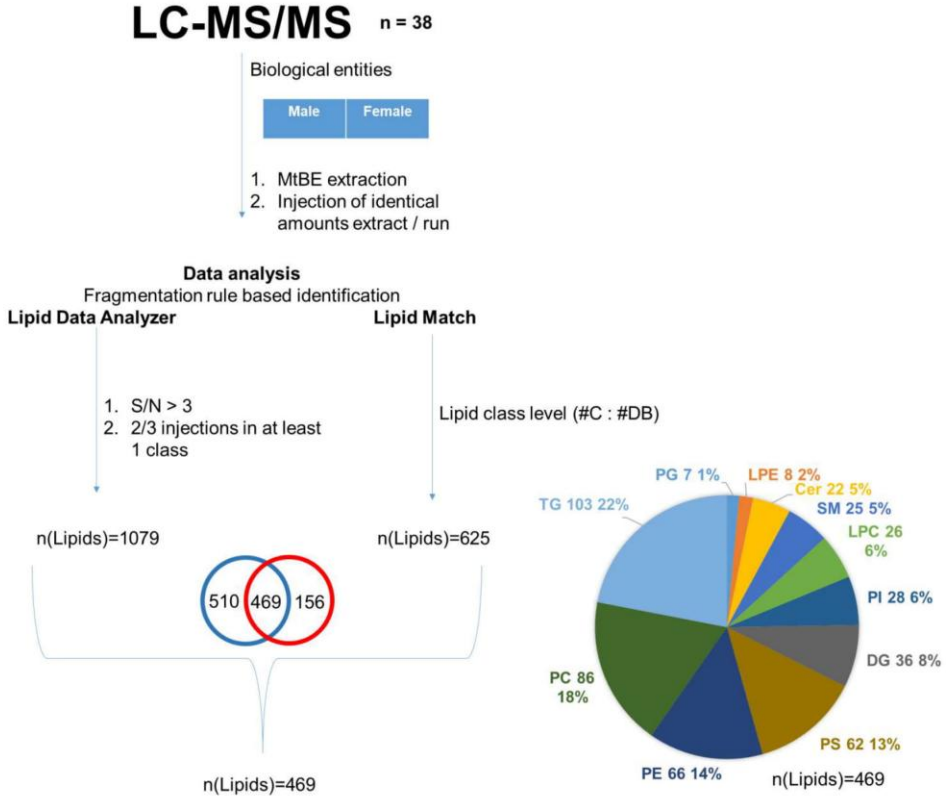

S2 Fig. Graphical illustration of the data analysis workflow for MS imaging data.

Statistical evaluation work flow was adapted from literature. The statistical analysis comprised five key steps: 1. normalization of one signal to the sum of all signals per measurement, 2. z-score (using median), 3. multiple-class analysis of variance (ANOVA, permutation based false-discovery-rate, FDR, set to 5%, 250 restarts), 4. post-hoc test (5% FDR) and 5. hierarchical clustering (Euclidean distance using average linkage, preprocessing with k-means, maximum 10 iterations, 10 restarts).

https://doi.org/10.1371/journal.pntd.0008145.s006

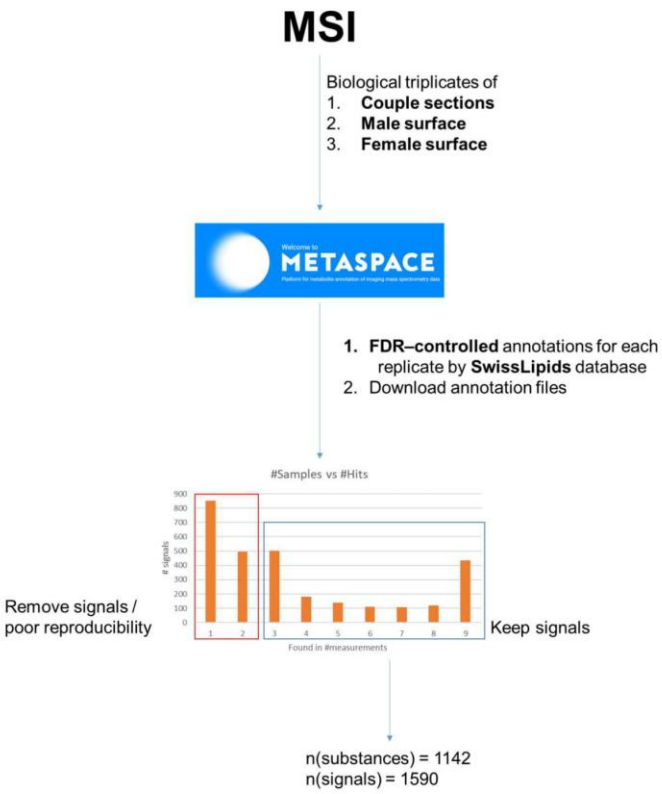

S3 Fig. Graphical illustration (from Perseus[41]) of multivariate statistical analysis and categorization of differentially abundant signals from MALDI experiments by hierarchical clustering.

https://doi.org/10.1371/journal.pntd.0008145.s007

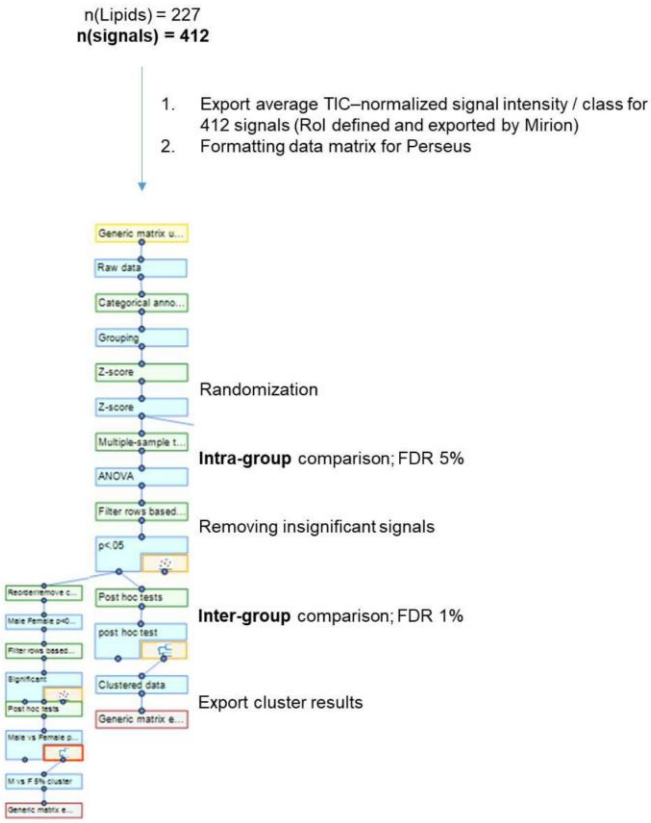

S4 Fig. Digital light microscopic images of male (M) surfaces (left), female (F) surfaces (middle) and cryosections of couples (right). The black arrows indicate the anterior end.

https://doi.org/10.1371/journal.pntd.0008145.s008

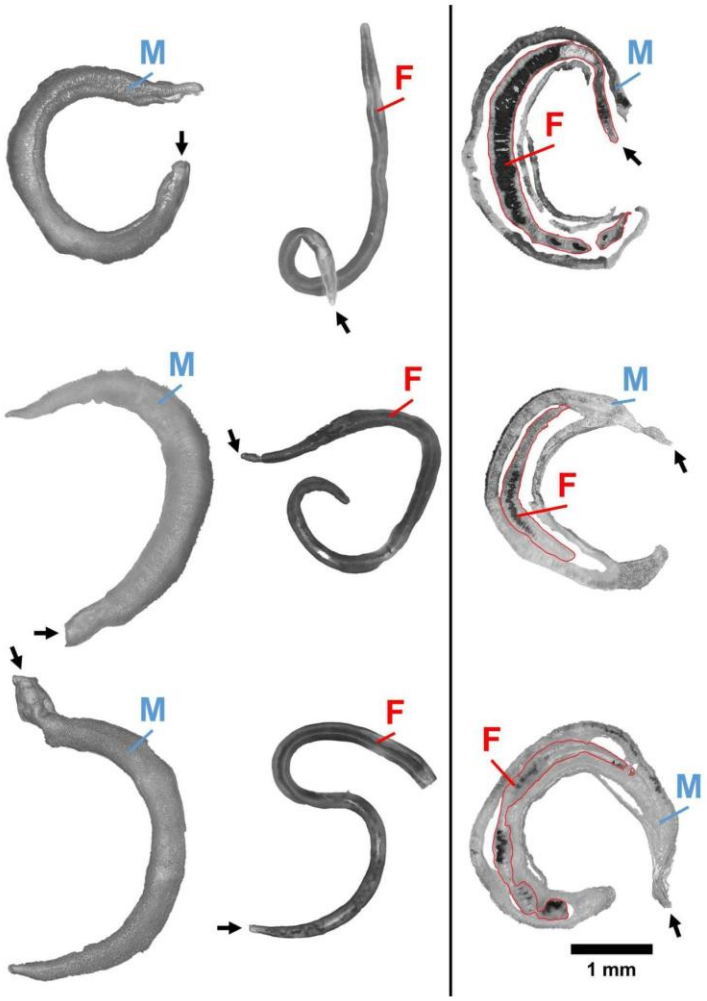

S5 Fig. Distribution of previously reported most abundant lipid species in S. mansoni as protonated and sodiated ion species[20] PC (34:1) has been determined in the past to be differentially abundant in whole worm and tegument.

[10] However, MS imaging data did not show significant differences based on HC. For PC (36:1) and PC (36:2), however, our findings are well in accordance with previous publications which found higher abundances inside the worm.[10] The same trend is suggested by unsupervised MS imaging data evaluation presented here.

https://doi.org/10.1371/journal.pntd.0008145.s009

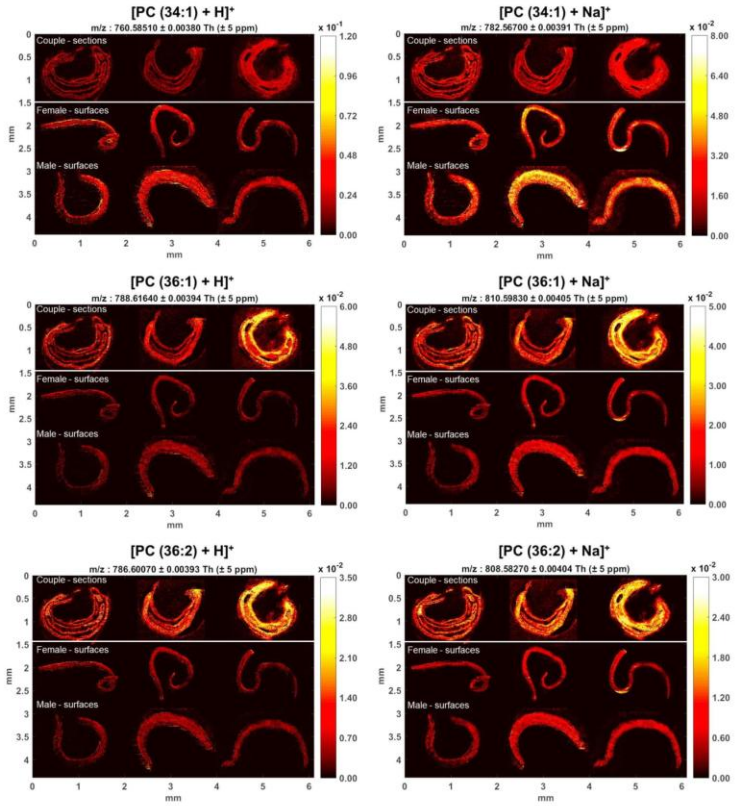

S6 Fig. Number of carbon atoms in fatty acyl chains vs the number of double bonds detected in phosphatidylethanolamines (PE).

Isobaric PE/PC interferences were excluded for surface and section data. A–Comparison of worm-tissue (blue cross) and surface/tegument specific signals vs ions (orange +) with unspecific distribution (green square). Overlapping indicators are attributed to the presence of several adducts corresponding to one lipid species. B–Arithmetic mean fatty acyl and double bond composition for section/inner tissue (blue), surface/tegument (orange) and unspecific signals (green). Error bars show the standard deviation across one location.

https://doi.org/10.1371/journal.pntd.0008145.s010

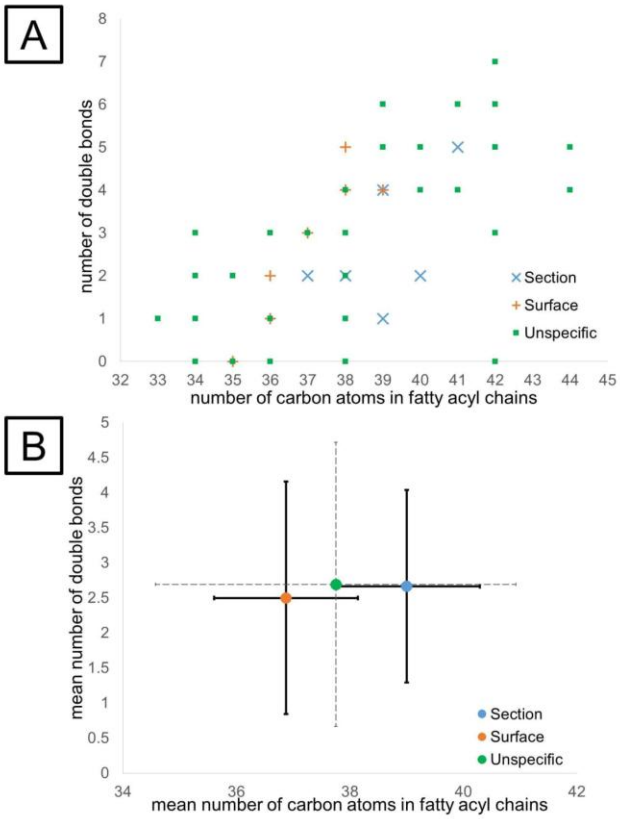

S7 Fig. Example for LC-MS/MS based identification of PE (37:4) with MS1 overview spectra and data-dependent MS2 spectra.

A–MS1 overview spectrum. B–virtual magnification of mass range m/z 700–800 (from A) showing the mass of PE (37:4) as deprotonated species (C42H75NO8P). C–MS2 spectrum of precursor m/z 752.52 ±0.5 u showing characteristic fragments of PE head group (around m/z 140 and m/z 196), FA (17:0) and FA (20:4). The precursor is not visible in the spectrum and assumedly fragmented quantitatively at NCE = 30. D–virtual magnification of m/z 750–755 (from A) showing mass and isotope ratio of PE 37:4 as 12C, 13C and 13C2 isotopologues.

https://doi.org/10.1371/journal.pntd.0008145.s011

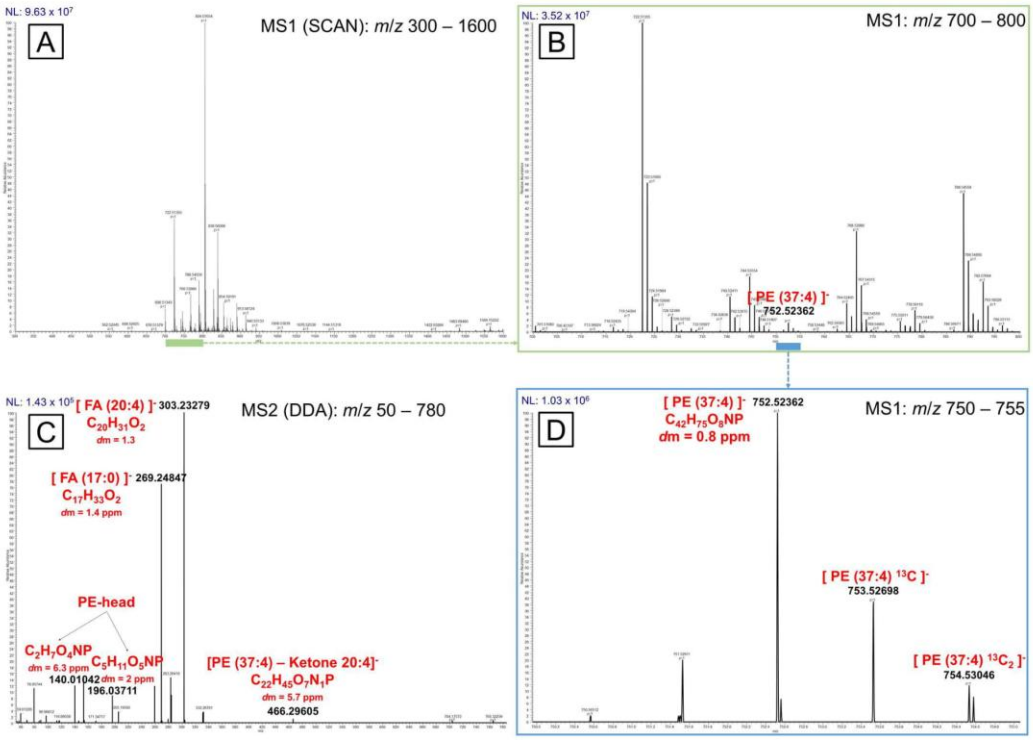

S8 Fig. Example for mass accuracy and resolution obtained in MSI experiments.

A–MS ion image of nearly isobaric PE-adduct species [PE (39:5) + H]+ and [PE (37:2) + Na]+ (Δm = 3.1 ppm) at m/z 780.5537 ± 5 ppm. B–Signal intensity (abundance in NL; normalized level) vs mass deviation in ppm. A double peak can be observed shifted by approximately 1.5 ppm and 2.8 ppm. C–MS ion signal at m/z 780.55254 ± 0.2 ppm showing an increased signal intensity on the worm surface assigned to protonated PE (39:5). D–MS ion at m/z 780.55151 ± 0.2 ppm assigned to PE (37:2) as sodium adduct. By hierarchical clustering, the signal at m/z 780.5537 was determined to be more abundant in the worm body compared to tegumental surface (see Fig 3). The signal was assigned to PE (37:2) as sodiated molecule. The protonated species of PE (39:5), however, was classified as unspecific. The fluctuating signal intensity of the surface measurements putatively led to unspecific classification. This example thus verifies the accuracy and correctness of HC-based classification.

https://doi.org/10.1371/journal.pntd.0008145.s012

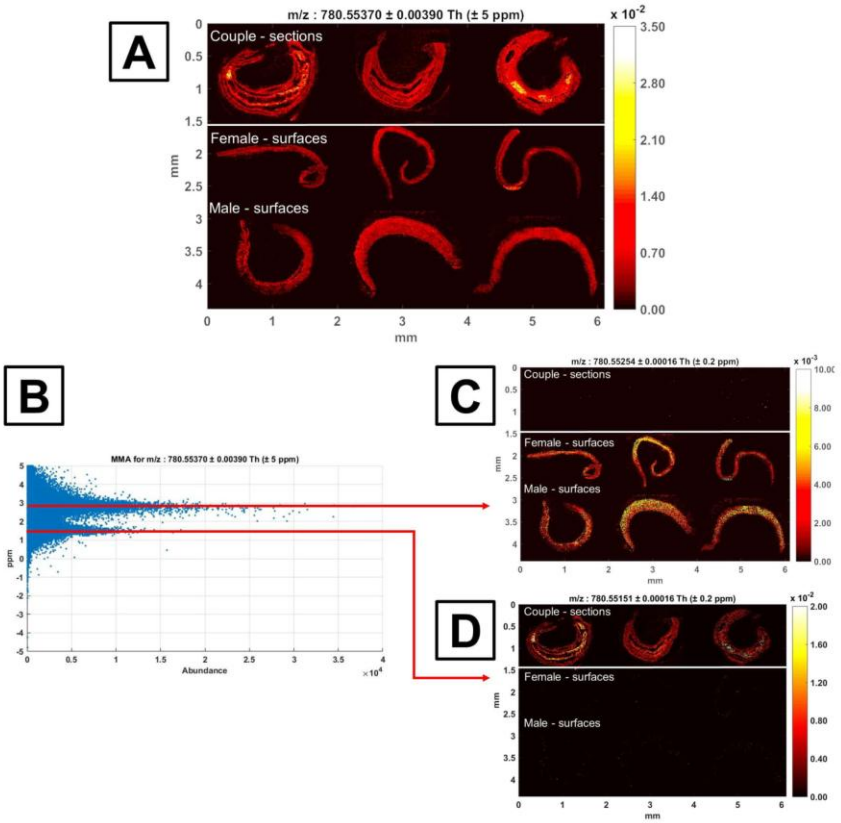

S9 Fig. Putative adducts of PE (39:4) with different distributions.

A—Distribution of m/z 782.5694 assigned to [PE (39:4) + H]+. B–distribution of m/z 804.5514 assigned to [PE (39:4) + Na]+. This difference in distribution could be explained by different concentrations of salt in tegument and inner tissue or by isobaric interferences that were not contained in the LC-MS/MS-database.

https://doi.org/10.1371/journal.pntd.0008145.s013

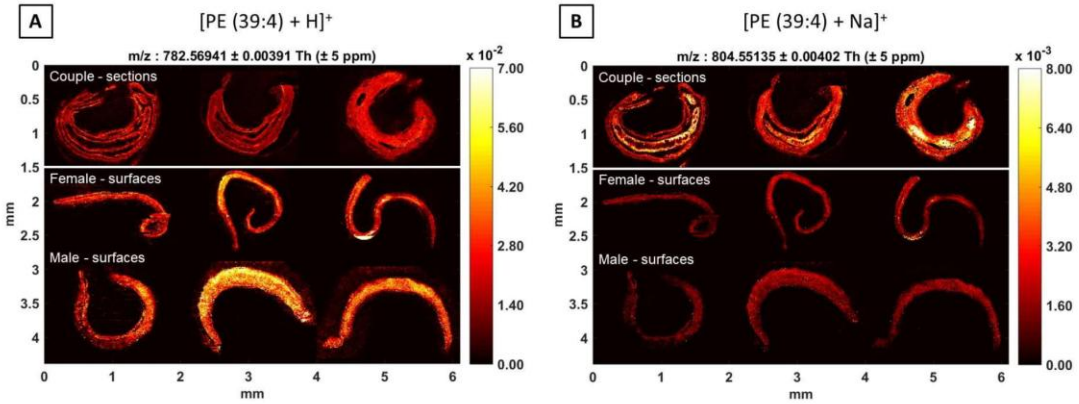

Curriculum vitae

The curriculum vitae was removed from the electronic version of the paper.

The curriculum vitae was removed from the electronic version of the paper.

Acknowledgements

First, I would like to thank Prof. Dr. Bernhard Spengler for giving me the opportunity to work in his research group and for the proposal of such an interesting research project. I enjoyed working with you a lot. Thank you also for hosting such an international research group in Giessen and for your constant support travelling to national and international conferences and giving me the opportunity to represent our group in front of other, internationally recognized scientists. Thank you for your trust.

I would like to thank Dr. Stefanie Gerbig for the supervision of my scientific work and especially for guiding me through the projects. Thank you for always being there. You have taught me how to become a better scientist.

I am very grateful to Prof. Dr. Christoph C. Grevelding and Dr. Thomas Quack for their ideas, fruitful discussions and constant scientific input. Thank you for being the enthusiastic parasitologists and researchers you are.

Thank you to all members of the analytical chemistry department. I really enjoyed the time at and off work, being it scientific conferences or yearly excursions to the Kleinwalsertal, or only brief chats in the coffee kitchen. It was a pleasure to work with you. I would also like to thank the groups of Prof. Grevelding and Prof. Taubert for their valuable scientific input and for helping me out in the labs. This project would not have been possible without your efforts.

I would like to thank my family for their unconditional love and support throughout my studies. I especially thank Johanna for everything she did to support me as well as my dogs Frido and Logan.

Finally, I would like to thank everyone who contributed to the success of my doctoral thesis and, in favor of your valuable life time, did not mention individually.